



Provided by the author(s) and University of Galway in accordance with publisher policies. Please cite the published version when available.

Title	The role of Eya1 in otic neurogenesis in <i>Xenopus laevis</i>
Author(s)	Almasoudi, Suad
Publication Date	2021-07-26
Publisher	NUI Galway
Item record	<a href="http://hdl.handle.net/10379/16879">http://hdl.handle.net/10379/16879</a>

Downloaded 2024-04-26T18:01:32Z

Some rights reserved. For more information, please see the item record link above.





NUI Galway  
OÉ Gaillimh

# **The role of *Eya1* in otic neurogenesis in *Xenopus laevis***

A thesis submitted in partial fulfilment of the requirements of the  
National University of Ireland, Galway for the degree of Doctor of  
Philosophy

Author: Suad Hamdan Almasoudi

Supervisor: Dr. Gerhard Schlosser

School of Natural Sciences

Zoology

National University of Ireland Galway

Submission: June 2021

## Contents

Acknowledgements .....	4
List of abbreviations .....	5
Abstract.....	7
Declaration of Contribution.....	9
Chapter-1 Introduction .....	10
1.1 Cranial placodes.....	11
1.1.1 Origin of cranial sensory placodes .....	12
1.1.2 Neurogenic placodes .....	15
1.1.3 Eyes absent homolog1 (Eya1).....	20
1.2 Neurogenesis.....	23
1.2.1 From progenitor cells to neuronal differentiation .....	23
1.2.2 Neuronal migration through the basal lamina .....	27
1.2.3 Otic neurogenesis .....	28
1.3 Proteins involved in apicobasal (ab) cell polarity .....	34
1.3.1 Functions of apicobasal cell polarity .....	35
1.3.2 Establishment of cell polarity .....	38
1.3.3 Role of apicobasal cell polarity in vertebrate neurogenesis .....	39
1.4 Aims of the project.....	40
Chapter-2 Material and Methods.....	42
2.1 Animal Housing.....	42
2.2 Embryo Incubation and Microinjection .....	42
2.2.1 Human Chorionic Gonadotropic (HCG) Hormones Injection and Egg Collection .....	42
2.2.2 Microelectrode Needle Puller.....	42
2.2.3 <i>In Vitro</i> Fertilization (IVF) of <i>Xenopus laevis</i> Embryos .....	43
2.2.4 mRNA Synthesis for Microinjection .....	43
2.2.5 Microinjection of Morpholino Antisense Oligonucleotides (MO) or mRNAs .....	45
2.3 Immunohistochemistry .....	46
2.3.1 Fixation .....	46
2.3.2 Cryosections.....	46
2.3.3 Immunohistochemistry on cryosections.....	47

2.3.4 Immunohistochemistry on sections with Tyramide Signal Amplification .....	49
2.3.5 Microwave treatment and multiplex immunostaining on section with Tyramide Signal Amplification .....	51
2.3.6 Peptide Competition Assay (PSA) .....	53
2.3.7 EdU (5-ethynyl-20-deoxyuridine) labelling and detection.....	53
2.4.1 Microscopy .....	54
2.4.2 Confocal Microscopy .....	55
2.5 In situ hybridization .....	55
2.5.1 Synthesis of mRNA Probes for in situ hybridization.....	55
2.5.2 Whole mount in situ hybridization.....	56
2.5.3 Vibratome sections.....	58
2.6 Generating a construct with a hormone- inducible dominant- negative from of Six1 (GR-EnR-Six1).....	59
2.6.1 Sub-Cloning of Hormone Inducible Gene (GR) to pCS2--EnR-Six1 Plasmid.....	59
2.6.2 Restriction enzyme digest of insert and plasmid.....	59
2.6.3 Gel electrophoresis and DNA purification by Gel Extraction .....	60
2.6.4 Ligation.....	61
2.6.5 Transformation and plating of bacteria.....	61
2.6.7 Restriction test digest and Midiprep .....	63
2.7 Western Blot.....	63
2.7.1 <i>In vitro</i> Transcription and Translation .....	64
2.7.2 PAGE (Polyacrylamide Gel Electrophoresis).....	64
2.7.3 Protein extraction protocol .....	64
2.7.4 Preparing the PAGE samples .....	65
2.7.5 Blotting.....	65
Chapter-3 Neurogenesis in the otic placode .....	67
3.1 Time course of neurogenesis and neuronal delamination .....	68
3.2 The otic epithelium as a pseudostratified epithelium with apical-basal cell polarity.....	71
3.3 Proliferating and non-proliferating progenitor cells in the otic vesicle .....	80
3.4 Neuronal and sensory differentiation in the otic vesicle.....	87
3.5 Summary.....	91
4.1 Eya1 antibody specificity.....	92
4.2 Eya1 distribution in the developing otic vesicle .....	95



4.3 Subcellular localization of Eya1 .....	101
4.4 Eya1 distribution in relation to Sox3-immunopositive progenitor cells .....	106
4.5 Eya1 distribution in other placodes.....	108
4.6 Summary.....	112
Chapter-5 The function of <i>Eya1</i> in otic neurogenesis.....	113
5.1 Efficacy and specificity of Eya1 Morpholinos .....	113
5.2 Role of Eya1 for progenitor formation and neuronal differentiation in the otic vesicle .....	116
5.2.1 The effect of Eya1 knockdown on otic neurogenesis .....	116
5.2.2 The effect of <i>Eya1</i> overexpression on otic neurogenesis.....	123
5.3 Role of Eya1 for apicobasal cell polarity in the otic vesicle.....	125
5.3.1 The effect of Eya1 knockdown on cell polarity proteins .....	126
5.3.2 The effect of <i>Eya1</i> overexpression on cell polarity proteins .....	131
5.4 Summary.....	134
Chapter-6 Discussion.....	135
6.1 Time course of otic vesicle development .....	135
6.2 The otic epithelium as a pseudostratified epithelium with apicobasal polarity .....	139
6.3 Distribution of Eya1 during development of the otic vesicle in <i>Xenopus</i> .....	143
6.3.1 Distribution of Eya1 in different cranial placodes .....	143
6.3.2 Distribution of Eya1 in the developing otic vesicle .....	145
6.4 Otic neurogenesis in <i>Xenopus</i> .....	146
6.5 Early development of sensory areas in the otic vesicle in <i>Xenopus</i> .....	150
6.6 Role of Eya1 in otic neurogenesis in <i>Xenopus</i> .....	153
6.6.1 Role of Eya1 for proliferation, progenitor maintenance and neuronal differentiation.....	153
6.6.2 Role of Eya1 for apicobasal cell polarity .....	156
6.7 Outlook .....	159
References.....	160
Appendix A: Solutions and buffers .....	196
Appendix B: Specificity of Eya1 antibodies.....	208
Appendix C: Eya1 distribution in cranial placodes.....	209

## Acknowledgements

I would like to express my special appreciation and thanks to my advisor Dr. Gerhard Schlosser: you have been a tremendous mentor for me. I would like to thank you for encouraging my research and for allowing me to grow as a research scientist. Your advice on both research as well as on my career has been priceless. The countless hours spent discussing matters both theoretical and technical in your office will be much missed and have been a source of great inspiration.

I also would like to thank my sponsor, Umm Al Qura University for giving me this chance and the Saudi Arabian Cultural Bureau in Ireland for their advice and help. It has also been an absolute pleasure to work so closely with Santosh Maharana over the first year and later with both Bertrand Hutlet, and Mohamed El-Amri. Your kindness, selflessness and general merriment made the long days in the lab fly by, and my time in Galway that much more enjoyable. Haris Bin Fida, Merin Lawrence, I've really enjoyed the opportunity to get to work closely with you in the past few months. Bahareh Estiri, it was lovely meeting you in the lab.

A special thanks also to a great husband Meteb Almajnoni and my daughter Rodyna. Also, I would like to give a big thank to my family in Saudi Arabia, none of this would have been possible without your love and support. Words cannot express how grateful I am to my mother (Nawal Faloudah), my mother in law, father (Hamdan) and my father in law (may God rest his soul in peace) for all the sacrifices that you've made on my behalf. Your prayer for me was what sustained me thus far. I only hope I can pay it back in kind. In addition, I want to thank my brothers (Mohammed and Faisal) and my sisters (Reem, Haneen and Ghaday) for help and encouragement.

Finally, to all other friends I've made in Galway, thank you for making my time here so memorable.

## List of abbreviations

• <b>AH</b>	Adenohypophyseal
• <b>aPKC</b>	Aprotein kinase C
• <b>bHIH</b>	Basic helix loop helix
• <b>BSA-</b>	Bovine Serum Albumin
• <b>CLSM</b>	Confocal Laser Scanning Microscopy
• <b>DAPI</b>	4',6-diamidino-2-phenylindole
• <b>DMSO</b>	Dimethyl sulfoxide
• <b>EB</b>	Epibranchial placodes
• <b>EdU</b>	5-Ethynyl-2'-deoxyuridine
• <b>eO1</b>	Olfactory epithelium
• <b>epIX</b>	Glossopharyngeal placode
• <b>epVII</b>	Facial epibranchial placode
• <b>epX1</b>	First vagal placode
• <b>gPr</b>	Profundal ganglion
• <b>gV</b>	Trigeminal ganglion
• <b>HCG</b>	Human Chorionic Gonadotropic Hormones
• <b>hp2</b>	Hypobranchial placode
• <b>HRP</b>	Horseradish peroxidase
• <b>Io</b>	Infraorbital
• <b>m</b>	Middle trunk line
• <b>mGFP</b>	Membrane green fluorescent protein
• <b>MLC</b>	Myosin light chain
• <b>MO</b>	Morpholino Antisense Oligonucleotides
• <b>ov</b>	Optic vesicle
• <b>pAD</b>	Anterodorsal placode
• <b>PAR</b>	Partitioning defective
• <b>PAR3</b>	Partitioning defective 3 homolog
• <b>pAV</b>	Anteroventral lateral lineplacode
• <b>PB</b>	Phosphate buffer
• <b>PBS</b>	Phosphate buffer saline
• <b>PCNA</b>	Proliferating cell nuclear antigen
• <b>PFA</b>	Paraformaldehyde
• <b>pH3</b>	Phosphorylated histone H3
• <b>pHA</b>	Adenohypophyseal placode
• <b>php</b>	Pharyngeal pouch
• <b>pM</b>	Middle lateral line placode
• <b>pO1</b>	Olfactory placode
• <b>pOt</b>	Otic placode

- **pP**                   Posterior poster placode
- **pPa**                Posterior placodal area
- **PPE**                Preplacodal ectoderm
- **pPr**                Profundal placode
- **pST**                Supratemporal placode
- **Pv**                 Trigeminal placode
- **RT**                 Room temperature
- **so**                 Supraorbital
- **som**                Somites
- **TNT**                Transcription and translation
- **v**                  Ventral trunk line
- **VCG**               Vestibulocochlear ganglion
- **vOt**                Otic vesicle

## Abstract

Cranial placodes are specialized areas of thickening of the early embryonic ectoderm at the head and give rise to sensory organs and ganglia. In vertebrates, the inner ear is derived from one of these placodes, the otic placode. All cranial placodes arise from a common region of origin, the preplacodal ectoderm (PPE), determined by the expression of *Eya1* and *Six1* genes. *Eya1* and *Six1* were previously shown to play a crucial role both for the maintenance of proliferating progenitors and for neuronal differentiation in cranial placodes including the otic placode, but the mechanisms are still obscure.

The main aim of this study is to elucidate the role of *Eya1* during neurogenesis in the developing inner ear (otic vesicle) of *Xenopus laevis* with a particular focus on the role of *Eya1* for cell proliferation, the formation of progenitors and differentiating neurons as well as for the distribution of cell polarity proteins during otic vesicle development.

Since otic neurogenesis in *Xenopus* has not yet been studied in any detail, the first part of this study uses immunostaining and confocal microscopy to provide a detailed description of otic neurogenesis in *Xenopus*. It is shown that the otic vesicle of *Xenopus* comprises a pseudostratified epithelium with apicobasal polarity (apical enrichment of Par3, aPKC, phosphorylated Myosin light chain, N-cadherin) and interkinetic nuclear migration (apical localization of mitotic, pH3-positive cells). A Sox3-immunopositive neurosensory area in the ventromedial otic vesicle gives rise to neuroblasts, which delaminate through breaches in the basal lamina between stages 27 and 39. Delaminated cells congregate to form the vestibulocochlear ganglion, whose peripheral cells continue to proliferate (incorporate EdU), while central cells differentiate into Islet1/2-immunopositive neurons (stage 29) and send out neurites (stage 31). The central part of the neurosensory area retains Sox3 but stops proliferating from stage 33, forming the first sensory areas (utricle/sacculus maculae).

Since only the expression of *Eya1* mRNA but not of Eya1 protein has been previously analysed, the second part of the study then provides a detailed analysis of the subcellular distribution of Eya1 protein during development of the otic vesicle and its distribution in relation to markers of proliferation, progenitors and differentiating neurons using a *Xenopus*-specific Eya1 antibody, double-immunostaining with other antibodies and confocal microscopy. Eya1 protein localizes to both nuclei and cytoplasm in the otic epithelium, with levels of nuclear Eya1 declining in differentiating (Islet1/2+) ganglion neurons and in the developing sensory areas. The distribution of Eya1 in other cranial placodes throughout embryonic development is also characterized.

Finally, in the third part of the study Eya1 and Six1 gain and loss of function experiments demonstrated that Eya1 and Six1 are essential for cell proliferation, progenitor maintenance and neuronal differentiation in the epithelium of the developing otic vesicle. Eya1 is also required to establish a proper apical distribution of cell polarity proteins and of N-cadherin in the otic epithelium. This suggests that Eya1 plays an important role for maintenance of epithelial cells with apicobasal polarity during otic neurogenesis. Further studies are needed to elucidate whether and how this role is linked to Eya1's function in progenitor proliferation and neuronal differentiation.

## Declaration of Contribution

I declare that this thesis is all my own work and not submitted to any other university for any other degree other than only at the National University of Ireland Galway, Republic of Ireland.

All my project work was fully funded by Um Alqura university, the Kingdom of Saudi Arabia

Signed \_\_\_\_\_  \_\_\_\_\_

(Almasoudi, Suad Hamdan)

## Chapter-1 Introduction

The vertebrates are a huge taxon and consist of all animals that have backbones. Currently, 54,807 species are described (Table 1). The evolutionary success of vertebrates as evident from this large diversity has been attributed to the evolution of a “New Head” with new sense organs (eyes, ears, nose) and a protective skull by vertebrate ancestors (Northcutt and Gans, 1983). However, despite their central importance for vertebrate evolution, the development of many vertebrate-specific sense organs is still poorly understood. This project focusses on the development of the inner ear. This will be studied in frogs, which are the most diverse group of amphibians (Pyron and Wiens, 2011) and are particularly well suited for embryological studies.

In the last century, most embryological studies were done on the common frog *Rana* (Eriksson, 2019). However, since the 1950s, most experiments focused on another frog that is *Xenopus laevis* (South African Clawed Toad). Scientists shifted to study *Xenopus laevis* for several reasons. First, *Xenopus laevis* is aquatic and a very suitable animal to breed, which can live for more than 10 years in the laboratory. Secondly, a small dose of gonadotropic hormone is enough to induce spawning, as was discovered in the 1930's. Thirdly, development can be followed because *Xenopus* embryos develop externally. Fourthly, each ovulation can generate hundreds of eggs. Fifth, *Xenopus laevis* is considered as very good model for different study purposes such as molecular studies and experimental embryology (Amaya et al., 1998; Kay and Peng, 1992; Khokha et al., 2002; Pike et al 2019).

Here, I will use embryos of *Xenopus laevis* to address the development of the sensory neurons of the inner ear from the otic placode.



**Table 1.1.** The number of vertebrates described and evaluated by 2021 (IUCN RED list, 2021).

	Estimated Number of described species	Number of species evaluated by 2021 (IUCN Red List version 2021-1)	% of described species evaluated by 2021 (IUCN Red List version 2021-1)
<b>VERTEBRATES</b>			
Mammals	6,513	5,940	91%
Birds	11,158	11,158	100%
Reptiles	11,341	8,492	75%
Amphibians	8,309	7,212	87%
Fishes	35,797	22,005	61%
<b>Subtotal</b>	<b>73,118</b>	<b>54,807</b>	<b>75%</b>

### 1.1 Cranial placodes

The so-called “New Head” hypothesis, which proposes that the vertebrates head is unique and distinguished from other Chordata was published nearly three decades ago. Northcutt and Gans (1983) first pointed out that the vertebrate head is an evolutionary novelty with many structures developing from two novel embryonic tissues that are the neural crest and the neurogenic placodes (Baker and Bronner-Fraser, 2001; Diogo et al., 2015; Northcutt and Gans,1983; Schlosser and Northcutt, 2000; Schlosser, 2014). When the neural tube is closed, neural crest cells emerge from the ectoderm at the border of the neural plate. Neural crest cells produce bone, cartilages, secretory cells, pigment cells, glia cells and sensory neurons. Also, it is associated with connective tissues. Thickenings of the embryonic ectoderm region are termed the cranial sensory placodes and they give rise to different types of cells such as sensory neurons and associated sensory receptors cells. Both neural crest and cranial placodes are very important tissues to build a vertebrate head (Diogo et al., 2015; Graham and Begbie, 2000; Manni et al., 2004; Schlosser, 2014; Sullivan et al., 2019).

Cranial placodes are specialized areas of the early embryonic ectoderm and often characterized as a distinct thickening. After neural tube closure, cranial placodes invaginate and give rise to the paired sensory organs of the vertebrate head and contribute to cranial ganglia and the pituitary gland (Adenohypophysis). Also, all placodes give rise to many non-epidermal cell types such as secretory cells, neurons and glia (Bailey and Streit, 2005; Baker and Bronner-Fraser, 2001; von Kupffer, 1895; McCabe and Bronner-Fraser, 2009; Pieper et al., 2011; Saint-Jeannet and Moody, 2014; Schlosser and Ahrens, 2004; Schlosser and Northcutt, 2000; Schlosser, 2002 a, 2003, 2010, 2014; Van Wijhe, 1883). Previous studies used the thickened area of the embryonic ectoderm and interruptions of the basement membrane as guides to identify the cranial placodes (Pieper et al., 2011; Schlosser and Northcutt, 2000; Schlosser, 2006).

### **1.1.1 Origin of cranial sensory placodes**

Fate maps in teleost (Dutta et al., 2005; Kozłowski et al., 1997), amphibian (Eagleson et al., 1995; Carpenter, 1937; Pieper et al., 2011; Schlosser, 2006, 2010) and amniote embryos (Streit, 2002; Xu et al., 2008) confirmed that all cranial placodes have a common origin from a crescent-shaped area that surrounds the anterior neural plate and is distinguished by *Six1* and *Eya1* genes, which is called pre-placodal ectoderm (PPE) or panplacodal primordium region (PPR) in the early stages (Fig. 1.1) (Schlosser, 2006, 2010).

During subsequent embryonic development, the PPE breaks up into distinct placodes. In *Xenopus laevis*, the cranial placodes comprise the following types: olfactory placode, lens placode, otic placode, Adenohypophyseal placode, profundal placode, trigeminal placode, epibranchial placodes, hypobranchial placodes, and lateral line placodes (Ahrens and Schlosser, 2005; Baker and Bronner-Fraser, 2001; McCabe and Fraser, 2009; Pieper et al., 2011; Saint-Jeannet and Moody, 2014; Schlosser and Northcutt, 2000; Schlosser and Ahrens, 2004; Schlosser, 2002 a,b, 2003, 2006, 2010; Schlosser et al., 2008;). In amniotes, the

profundal placode is known as the ophthalmic placode and the trigeminal placode as the maxillomandibular placode of the trigeminal nerve (Schlosser and Northcutt, 2000; Schlosser and Ahrens, 2004) (Fig. 1.2).

Whereas cranial placodes originate from a deep layer of precursor cells, other types of placodes emerge from the superficial ectodermal layer, such as hairs, feathers, scales, and teeth in chick (Biggs and Mikkola, 2014; Dhouailly, 2009; Mikkola, 2007) and cement and hatching glands in amphibian (Schlosser, 2010; Sive and Bradley, 1996).

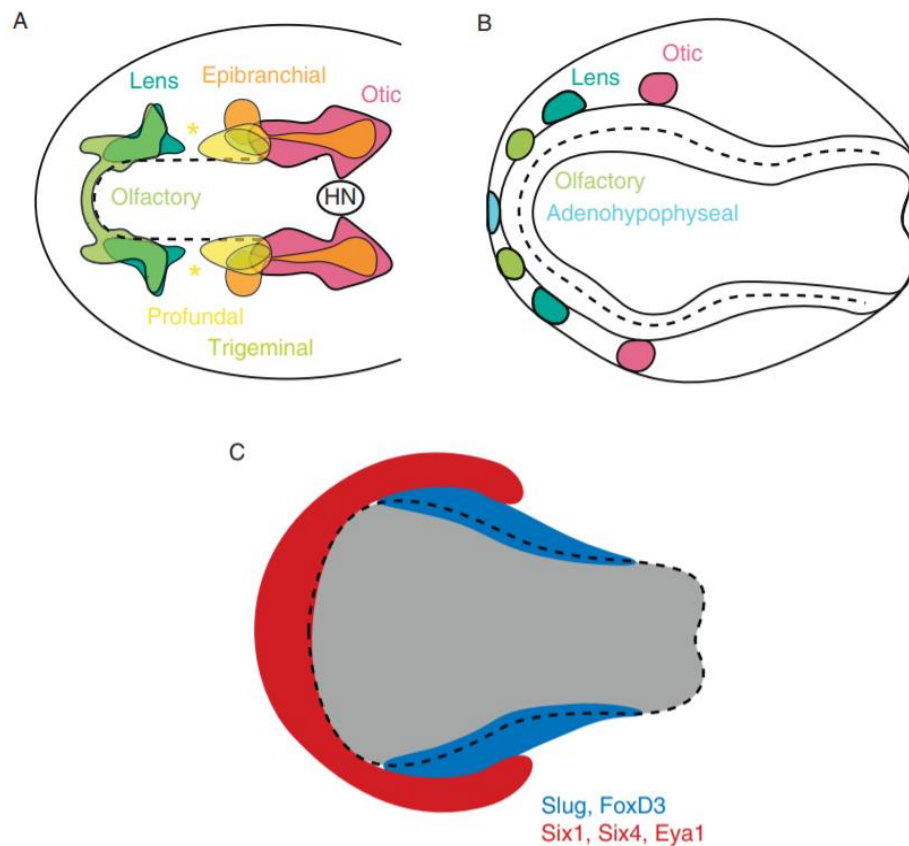


**Fig. 1.1. Fate maps showing the origin of cranial placodes from panplacodal ectoderm (PPE).** Border of the neural tube is indicated by broken line. (A): Chick embryo at 0-1 somite stage. (B): Salamander embryo. (C): Preplacodal ectoderm (red) is distinguished by Six1, Six4 and Eya1 expression and the neural crest by Slug, FoxD3 expression (reproduced from Schlosser, 2010).

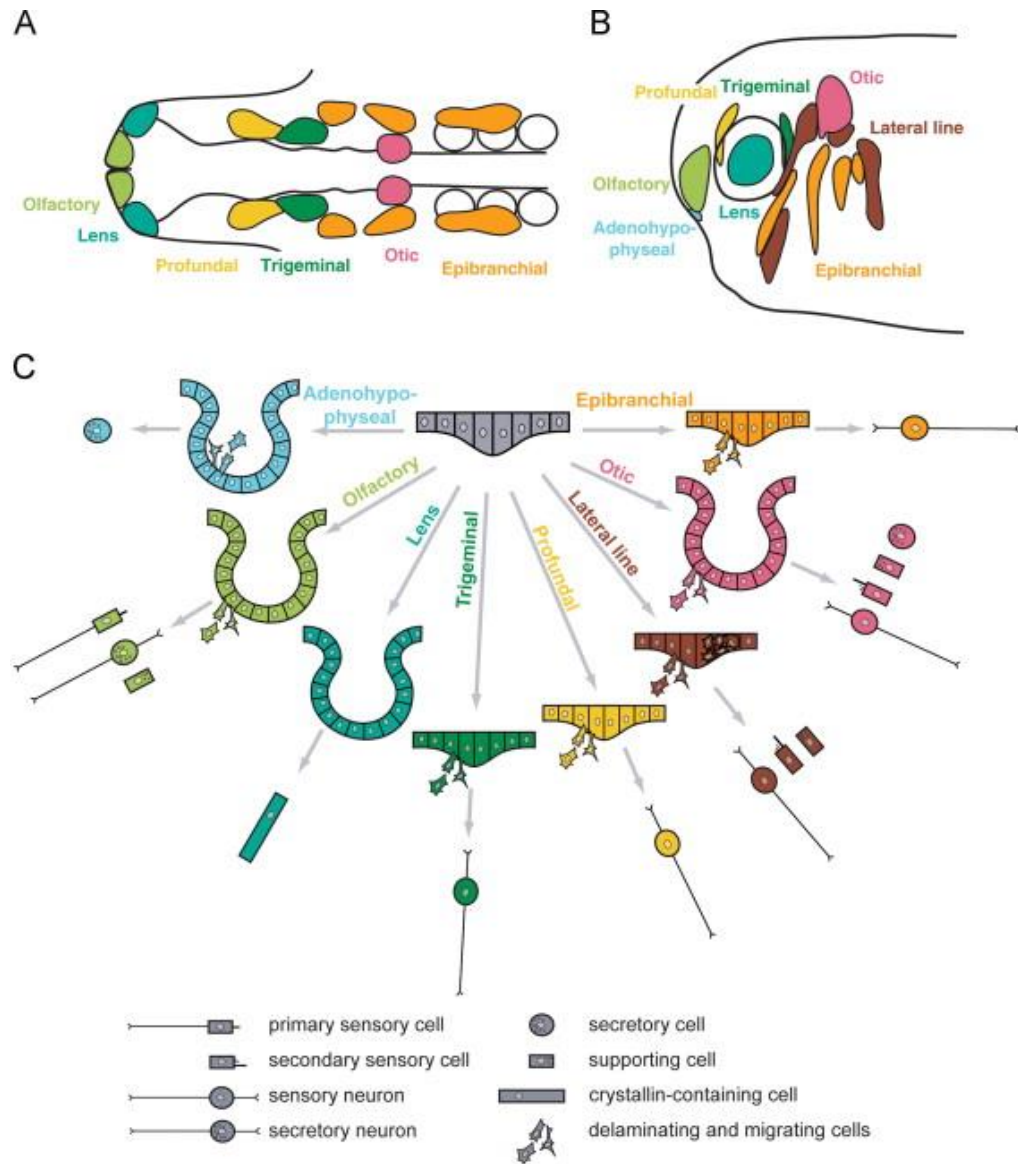


**Fig. 1.2. Origin of cranial placode from PPE in Chick and *Xenopus*.** (A, B; Chick, *Xenopus*, respectively): Different types of cranial placode at stage 10-13 (Chick embryo) and at tailbud stage (*Xenopus* embryo). (C): Different cranial placode give rise to various cell types (reproduced from Schlosser, 2010).

### 1.1.2 Neurogenic placodes

The ectodermal regions, which give rise to sensory neurons, glial cells and ciliated sensory receptor and nonepidermal cell types are called neurogenic placodes (Baker and Bronner-Fraser 2001; Northcutt, 1996; Schlosser, 2003). To identify neurogenic cranial placodes specifically, different genes involved in the regulation of neurogenesis can be used, including *Eya1*, *Six1*, *Neurog1*, *Neurog2*, *NeuroD1*, *MyT1*, and *Delta-1* (Brugmann et al., 2004; Nieber, et al., 2009; Pandur and Moody, 2000; Schlosser and Northcutt, 2000; Schlosser, 2006, 2014; Schlosser, et al., 2008).

In *Xenopus laevis*, neurogenic placodes comprise the olfactory placode, profundal and trigeminal placodes, otic placode, epibranchial placode, hypobranchial placode, and lateral line placode, i.e. all cranial placodes excluding lens and Adenohypophyseal placode (Ahrens and Schlosser, 2005; Baker and Bronner-Fraser 2001; Pieper et al., 2011; Schlosser and Northcutt, 2000; Schlosser, 2003, 2010, 2014). In most vertebrates, most of these cranial placodes are present but there are differences between groups in the number of epibranchial and lateral line placodes (Schlosser and Northcutt, 2000; Schlosser, 2002b; 2006).

The development of neurogenic placodes was studied in detail and their positions determined from the time of neural tube closure to larval stages in *Xenopus laevis* (Schlosser and Northcutt, 2000).

The olfactory placode in *Xenopus laevis* is found in the rostral side of the head and located anterior to the optic vesicle and lateral to the Adenohypophyseal placode. In the early stage (stage 14), the olfactory placode is recognized by *Neurog2* (= *X-NGNR-1*) expression and individualized clearly at stage 24. During stage 24 to 40, the olfactory placode size and position are maintained (Brugmann and Moody, 2005; Saint-Jeannet and Moody, 2014; Klein and Graziadei, 1983; Pieper et al., 2011; Schlosser and Northcutt, 2000; Schlosser, 2014). The olfactory placode gives

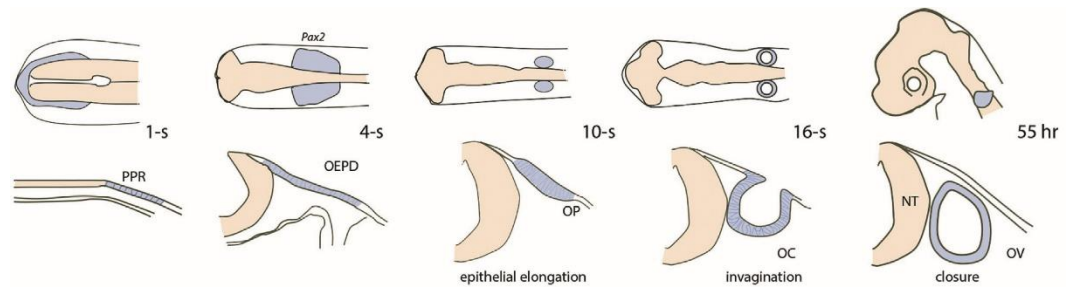
rise to olfactory and vomeronasal sensory neurons that populate the epithelium of the nose, which are important to detect odors and pheromones, respectively. Also, olfactory placodes generate a number of additional cell types, for instance supporting cells, mucus-producing cells and migratory cells, which migrate into the forebrain and form the ganglion of the terminal nerve and produce gonadotropin-releasing hormone GnRH (Baker and Bronner-Fraser, 2001; Bailey and Streit, 2005; Brugmann and Moody, 2005; Fornaro et al., 2001; Klein and Graziadei, 1983; Saint-Jeannet and Moody, 2014; Schlosser and Northcutt, 2000; Schlosser, 2010; Whitlock et al., 2006).

The profundal and trigeminal placodes are recognized at an early stage (stage 21) with the profundal (or ophthalmic) placode localizing dorsally of the optic vesicle, whereas the trigeminal (or maxillomandibular) placode is found posterior to the optic vesicle in *Xenopus laevis* (Fig. 1.2 B) (Baker and Bronner-Fraser, 2001; Davies et al., 1982; Pieper et al., 2011; Schlosser and Northcutt, 2000; Schlosser, 2006, 2010, 2014). The profundal and trigeminal placodes generate neurons, which form the profundal and trigeminal ganglions and give rise to the profundal and trigeminal nerves (Andermann et al., 2002; Brugmann and Moody, 2005; Graham and Begbie, 2000; Northcutt and Brändle, 1995; Schlosser and Northcutt, 2000; Schlosser and Ahrens, 2004; Schlosser, 2006, 2010, 2014).

The otic placode is derived from the posterior placodal area (also known as otic-epibranchial placodal precursor domain) and is located posterior to the trigeminal placode and adjacent to the central hindbrain in all vertebrates (Alsina et al., 2009; Baker and Bronner-Fraser, 2001; Bailey and Streit, 2005; Gallagher et al., 1996; Graham and Begbie, 2000; Northcutt et al., 1994, 1995; Northcutt and Brändle, 1995; Northcutt, 1996; Schlosser and Northcutt, 2000; Solomon et al., 2003). During development of the inner ear of most vertebrate species, the first morphologically visible structure is the otic placode, which emerges from a thickening of embryonic ectoderm. Subsequently, the otic placode invaginates to form the otic cup, which invaginates completely from the ectoderm to form the otic

vesicle (Figs. 1.3, 1.4). From the otic vesicle originate different types of cells, including the epithelial supporting cells, endolymph-secreting cells as well as the mechanosensory hair cells, which are secondary sensory cells (without an axon) (Fig. 1.4). In addition, the sensory neurons delaminate from the medial region of the otic vesicle to form the vestibulocochlear ganglion of the eighth cranial nerve and innervate the hair cells (Fig.1.4). The inner ear is very important for vertebrates and it is responsible for hearing and balance (Alsina and Whitfield, 2017; Baker and Bronner-Fraser, 2001; Brugmann and Moody, 2005; Freter et al., 2008; Groves and Branner Fraster, 2000; Gallagher et al., 1996; Maroon et al., 2002; Northcutt et al., 1994, 1995; Northcutt and Brändle, 1995; Sánchez-Guardado et al., 2014; Schlosser and Northcutt, 2000; Schlosser, 2010, 2014; Schwarzer et al., 2017; Solomon et al., 2003; Wright and Mansour, 2003).

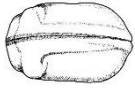


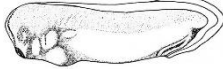



The lateral line placodes are sensory placodes that are originally part of the posterior placodal area, which gives rise to several lateral line placodes, including the anterodorsal, anteroventral, middle and posterior lateral line placode (Van Wijhe, 1883). A fifth lateral line placode, the supratemporal lateral line placode develops in *Xenopus laevis* at later stages (Fig. 1.2 B). (Schlosser and Northcutt, 2000, Schlosser, 2006, 2010, 2014; Winklbauer and Hausen, 1983). All lateral line placodes form ganglion cells in the early stages. In later stages, lateral line placodes give rise to the sensory ridges or migratory primordia. Then, the lateral line ganglion sends out neurites, which associate with both sensory ridges and migratory primordia. They elongate or migrate in limited ways in the head and trunk of the embryo to form sensory organs, which are the neuromasts or ampullary or tuberos organs. These organs comprise secondary sensory cells (hair cells) and supporting cells. Neuromasts are s very important for detecting water movements while ampullary or tuberos organs detect electric fields (Gompel et al., 2001; Metcalfe, 1989; Northcutt, 1992, 1997; Schlosser, 2002a; Schlosser, 2006, 2010, 2014; Winklbauer, 1989). In vertebrates the number of lateral lines is different between families and they are lost in amniotes (Baker et al., 2008; Raible and Krust, 2000; Schlosser, 2002b, 2014; Schlosser and Northcutt, 2000).



**Fig. 1.3. Early development of the chick inner ear.** Formation of the otic vesicle from thickened otic placodes. Preplacodal region (PPR-blue) expresses Pax2 and gives rise to the oticepibranchial placode domain (OEPD) at 4 somite stage. At 10 somites stage, the epibranchial placode precursor cells are separated from otic placode precursor cells. Next, the otic placode invaginates to give rise to the otic vesicle at the 16 somites stage (reproduced from Alsina and Whitfield, 2017).

Epibranchial and hypobranchial placodes are the last group of placodes originating from the posterior placodal area. In *Xenopus laevis* there are five epibranchial placodes- the facial epibranchial placode, the glossopharyngeal epibranchial placode, and three vagal epibranchial placodes - and two hypobranchial placodes (Schlosser and Northcutt, 2000; Schlosser, 2002a, 2003, 2006, 2010, 2014). Epibranchial and hypobranchial placodes are related to pharyngeal pouches and their location is determined dorsally and ventrally to pharyngeal pouches (Fig. 1.2 B). All epibranchial placodes give rise to viscerosensory neurons and ganglia of the branchiomeric cranial nerves (Fig. 1.2 B) (Baker et al., 2008; Northcutt, 2004; Schlosser et al., 1999; Schlosser and Northcutt, 2000; Schlosser, 2002a; Schlosser, 2010, 2014).



	Stage 21	Stage 23/24	Stage 27	Stage 29/30	Stage 33/34	Stage 35/38	Stage 40
<i>Xenopus</i>							
	Otic placode	Otic cup	Otic vesicle  Delamination of vestibulocochlear neurons starts	Otic vesicle fully invaginated	First neurites in vestibulocochlear ganglion (st 32)  First hair cells (st 31)  Separation of sensory areas start	Ongoing delamination of vestibulocochlear neurons	End of otic neurogenesis

**Fig.1.4. Scheme of embryonic development in *Xenopus*.** Main events of otic development as described in the present study are indicated. Drawings and stages are based on Nieuwkoop and Faber (1967).

### 1.1.3 Eyes absent homolog1 (*Eya1*)

The *Drosophila* eyes absent gene *Eya* participates in the formation of the regulatory network (Six-Eya-Dach-Pax), which is necessary for the development of normal eyes in *Drosophila* (Kumar, 2009; Schlosser, 2006; Silver et al., 2003). *Eya* has homologous genes in many species of invertebrates and vertebrates. While a single *Eya* gene is recognized in most invertebrates, four different types of *Eya* are present (*Eya1-4*) in vertebrates. All *Eya* proteins are characterized by a highly conserved, 271 amino acid *Eya* domain on the C-terminus (Abdelhak et al., 1997a, b; Borsani et al., 1999; Kalatzis et al., 1998; Xu et al., 1997a; Zimmerman et al., 1997). In addition, *Eya* proteins have a N-terminal domain, which is important for transactivation coupled with the C-terminal *Eya* domain (phosphatase activity localization) (Li et al., 2003; Li et al., 2010; Ohto et al., 1999; Schlosser, 2010; Silver et al., 2003). *Eya1* acts both a transcriptional coactivator of the transcription factor *Six1* and as a phosphatase (Li et al., 2003; Schlosser, 2010, 2014; Silver and Rebay, 2005; Xu, 2013). The interaction between *Eya* and *Six* proteins is essential for the recruitment of *Eya* to the nucleus (Ohto et al., 1999; Schlosser, 2010; Zhang et al., 2004).

*Eya1* plays an important role in the embryonic development of cranial placodes and other tissues for instance the eye (in invertebrates), ear, kidney, heart, branchial arches, muscles, secretory cells, and trunk skeleton. Furthermore, interactions between *Eya1* and *Six1* are required to regulate cell fate specification (proliferation or differentiation) and maintaining the balance between the proliferation of progenitor cells and differentiation of neurons (Ahmed et al., 2012a, b; Pieper et al., 2012; Schlosser et al., 2008; Schlosser, 2010, 2014; Wong et al., 2013; Wu et al., 2015; Xu, 2013; Xu et al., 1999; Zou et al., 2004). *Eya1* expression is found initially throughout the preplacodal ectoderm (PPE) at neural plate stage (Fig. 1.1) and is maintained in placodes during neural fold stages and organogenesis (Abdelhak et al., 1997b; Ahmed et al., 2012b; Baker and Bronner-Fraser, 2001; David et al., 2001; Ishihara et al., 2008; Xu et al., 1997b). Although *Eya* genes are

present in all vertebrates including *Xenopus*, zebrafish and mammals, patterns of *Eya* expression in placode derivatives are different from one species to another. In *Xenopus laevis*, *Eya1* is present in all neurogenic placodes, but it is absent in the profundal and trigeminal placode of zebrafish and mouse. In turn, the *Eya2* gene expressed in the trigeminal and in the epibranchial ganglia of mouse (Abdelhak et al., 1997a, b; Ahmed et al., 2012a; David et al., 2001; Ishihara et al., 2008; Sahly et al., 1999; Schlosser and Ahrens, 2004; Schlosser et al., 2008; Xu, 2013; Xu et al., 1997a; Xu et al., 1999; Zou et al., 2004).

*Eya1* knockdown in *Drosophila* causes absent of eyes, while ectopic retinal development is induced by *Eya1* misexpression (Bonini et al., 1993; Chen et al., 1997; Pappu and Mardon, 2004; Punzo et al., 2001). In *Xenopus laevis*, *Six1* and *Eya1* knockdown leads to defects in ear development, such as a reduction in its size. In addition, *NeuroD1* gene expression (a neuronal differentiation marker) was reduced by *Eya1* mutation in neurogenic placodes (Li et al., 2010; Schlosser et al., 2008; Schlosser, 2010). Similarly, in mouse and zebrafish *Eya1* loss- function causes a reduction in expression of neuronal determination and differentiation genes and a reduction in proliferation in the olfactory, epibranchial, and otic placode (Ahmed et al., 2012b; Kozłowski et al., 2005; Whitfield, 2002; Zou et al., 2004, 2008). In addition, *Eya1* mutants present defects in Adenohypophysis development of zebrafish (Nica et al., 2006). Additionally, delay of myogenesis and poor muscle development in mice are a result of *Eya1* mutation (Grifone et al., 2007). Moreover, *Eya1* mutation leads to renal abnormalities, loss of hearing and thyroid hypoplasia or thyroid dysgenesis which is distinguished by a reduction of thyroid lobe size and parafollicular cells (Wong et al., 2013; Xu et al., 1999,2002; Xu, 2013).

In human patients, *Eya1* mutation causes different diseases in the developing embryo, for example, branchio-oto (BO) and branchio-oto-renal syndrome (BOR) including deafness, renal malformations and many defects in the nose and eye lens (Abdelhak et al., 1997b; Ishihara et al., 2008; Li et al., 2010; Musharraf et al., 2014;

Orten et al., 2008; Schlosser et al., 2008; Xu et al., 1999; Xu et al., 2002). Additionally, otofaciocervical (OFCS) syndrome symptoms include facial problems, ear defects and mild intellectual disability (Pohl et al., 2013). In humans, *Eya1* mutation is common in BOR syndrome and more than 80 mutations have been documented (Orent et al., 2008).

Taken together, these previous studies show clearly that *Eya1* is required for progenitor proliferation and neuronal differentiation in placodes, but the underlying mechanisms are poorly understood. Since *Eya1* together with *Six1* promotes both cell proliferation and neuronal differentiation in placodes of *Xenopus laevis* in a dosage-dependent way, it appears to be able to regulate the balance between progenitors and differentiating neurons in placodes (Schlosser et al., 2008; Riddiford et al., 2017). Previous studies have suggested that this may involve the direct transcriptional regulation of two sets of target genes, those promoting progenitor maintenance and proliferation (e.g. *Sox2/3*, *Hes5*) as well as those promoting neuronal or sensory differentiation (e.g. *Neurog1/2*, *Atoh1*, *POU4f1*, *Islet2*) (Ahmed et al., 2012 a, b; Riddiford et al., 2016; Li et al., 2020). However, *Eya1* has also been shown to directly dephosphorylate cell polarity proteins such as atypical protein kinase C (aPKC) in the cerebellum, thereby affecting apicobasal cell polarity (see section 1.3) and changing the balance between proliferating and differentiating cells by controlling the proportion between symmetric and asymmetric cell divisions (Merk et al., 2019). Another study (El Hashash et al., 2011) reported a similar role of *Eya1* in the lung epithelium but was subsequently retracted (El Hashash et al., 2017). To test, whether *Eya1* may fulfill its function in the inner ear by similar mechanisms, I have investigated in this study the role of *Eya1* for cell proliferation, the formation of progenitors and differentiating neurons as well as for the distribution of cell polarity proteins during otic vesicle development in *Xenopus laevis*.

## 1.2 Neurogenesis

In vertebrates, neurons are produced in three ways: from the neuroepithelium of the neural tube, from the neural crest and from ectodermal cranial placodes. The neurogenic cranial placodes are specific epithelial cells, which contain neural progenitor cells and give rise to the sensory neurons of the peripheral nervous system (Freter et al., 2013; Graham et al., 2007; Lassiter et al., 2014). Different sensory cell types are generated from each placode, for instance, the olfactory placode gives rise to the primary sensory cells (with an axon) and otic and lateral line placodes produce secondary sensory cells (without an axon) and sensory neurons. Likewise, the profundal/trigeminal and epibranchial placodes give rise to sensory neurons but not sensory cells (Andermann et al., 2002; Barber, 1982; Cau et al., 2002; Dhallan et al., 1990; Fritsch et al., 2002; Schlosser, 2006, 2010, 2014). Overall, the process of neurogenesis in placodes, neural crest and central nervous system is regulated by similar mechanisms, which I will briefly review in the following section.

### 1.2.1 From progenitor cells to neuronal differentiation

There are a huge number of neurons involved in the functioning of the nervous system (Baker and Brown, 2018; White, et al., 1986). Several genes are involved in regulating specification and differentiation of neurons and sensory cells during embryonic development. These genes encode transcription factors including members of the SoxB1 group and proneural basic Helix-Loop-Helix (bHLH) transcription factors. The bHLH gene family in vertebrates comprises *Ascl1*, *Atoh1* and *Neurogenins* (*Neurogs*) related to the *Drosophila* proneural genes (*achaete-scute* and *atonal*) which are expressed in proliferating progenitor cells and induce the expression of another bHLH gene, *NeuroD1*, in differentiating neurons (Andermann et al. 2002; Baker and Brown, 2018; Cau et al., 2002; Chen et al., 2008; Kamachi and Kondoh, 2013; Sarkar and Hochedlinger, 2013; Schlosser et al., 2008; Schlosser, 2010). In addition, neuronal differentiation of neurogenic

placodes is regulated by *Eya1* and *Six1* in a concentration dependent way (Christophorou et al., 2009; Schlosser et al., 2008; Schlosser, 2010; Zheng et al., 2003; Zou et al., 2004).

The Sox gene family encodes a large number of transcription factors that contain a highly conserved High Mobility Group (HMG) domain and are related to the testis determining gene *Sry*. The SoxB1 subfamily includes *Sox1*, *Sox2* and *Sox3* (and *Sox19*, which was found in fish species only). The three SoxB1 genes were found to have overlapping functions with some expression differences between vertebrate groups (Collignon et al., 1996; Jiang et al., 2019; Kishi et al., 2000; Laudet et al., 1993; Rogers et al., 2008; Sarkar and Hochedlinger, 2013; Wegner, 1999; Zaouter, 2017).

Previous studies provided evidence that Sox1, Sox2 and Sox3 are expressed in neurogenic and non-neurogenic cranial placodes at the early stages of many vertebrate embryos (Schlosser and Ahrens, 2004; Meulemans and Bronner-Fraser, 2007). In addition, Sox2 and Sox3 expression were found co-expressed in neural progenitor cells and Sox3 misexpression leads to ectopic expression of Pax6 and *Eya1* and induces Sox2 expression in non-neurogenic domain of otic placode as well as a defect in the sensory organ (Abelló, 2010; Abu-Elmagd, 2001; Collignon et al., 1996; Kishi et al., 2000 and Köster et al., 2000). This suggests that *Sox3* plays a central role in the otic neural fate decisions and sensory organ development.

SoxB1 factors play a crucial role in neural and neurogenic and non-neurogenic placodes development. First, they act to maintain progenitor cells in the proliferative state and keep them undifferentiated (Bylund et al., 2003; Graham et al., 2003). And second, they control terminal differentiation and bias the development of cells into neurons or sensory cells (Abu-Elmagd et al., 2001; Dvorakova et al., 2019; Panaliappan et al., 2018; Pevny and Placzek, 2005; Schlosser and Ahrens, 2004; Schlosser et al., 2008; Wegner and Stolt, 2005; Wegner, 2010).

SoxB1 genes directly activate the Notch signaling pathway in CNS and placodes which is important for the maintenance of undifferentiated neural precursors cells at early stages (Cau et al., 2002; Holmberg et al., 2008; Panaliappan et al., 2018). In addition, in order to block neuronal differentiation in Notch-independent pathways, SoxB1 activates many genes involved in progenitor maintenance and signaling pathways such as the hedgehog and the epidermal growth factor (EGF) pathway (Favaro et al., 2009; Holmberg et al., 2008).

SoxB1 (Sox1, Sox2, and Sox3) transcription factors promote neuronal and sensory cell development, directly and indirectly. SoxB1 maintains progenitor cells in an undifferentiated state directly by reducing proneural bHLH neuronal transcription factors activity (Neurog1, Neurog2, NeuroD1) or indirectly by modulating the activity of signaling pathways (Holmberg et al., 2008; Kamachi and Kondoh, 2013; Kuwabara et al., 2009; Ross et al., 2003; Zhou et al., 2016).

Downstream of SoxB1, neuronal differentiation is determined by proneural bHLH genes in *Drosophila* and vertebrates. Proneural bHLH transcription factors are essential to promote cells to leave cell cycle during neurogenesis and to activate the expression of neuronal genes in the central and peripheral nervous system and cranial placodes (Bertrand et al., 2002; Holmberg et al., 2008). Proneural bHLH proteins are divided into two major groups: the Achaete-Scute related proteins (e.g. Ascl1) and the Atonal related proteins (ARPs), which include Atonal (Atoh1), the Neurogenin group (Neurog1/Neurog2) and NeuroD-like proteins (NeuroD1) (Andermann et al., 2002; Baker and Brown, 2018; Cau et al., 2002).

The expression of proneural bHLH proteins is found in several placodes in different patterns (dependent on species) (Cau et al., 2002; Schlosser and Northcutt, 2000). The production of neurons or sensory neurons is inhibited after knockdown mutations of proneural genes. For example, *Neurog2* (*Atoh4*) mutation led to an absence of sensory ganglia and eliminated *NeuroD1* expression in placodal cells

(Cau et al., 2002; Fode et al., 1998). Also, a loss of function of *Mash1* and *Neurog1* in mice resulted in a reduction of the generation of the olfactory sensory neurons (Cau et al., 2002; Fode et al., 1998). In addition, injection of morpholino oligonucleotides for *Neurog1* in zebrafish blocked the differentiation of all cranial ganglia, which derived from the trigeminal, lateral line, epibranchial and otic placodes (Andermann et al., 2002). In contrast, overexpression of proneural bHLH genes induces ectopic neurons and activates Notch signaling (Cau et al., 2002). In the brains of mice, activation of the expression of *Ascl1* and *Neurog2* converts astrocytes into neurons (Masserdotti et al., 2015). In the mammalian auditory system, overexpression of *Atoh1* converts non-sensory cells (supporting cells) into sensory hair cells (Izumikawa et al., 2005; Walters et al., 2017). Interestingly, there are complex mechanisms by which proneural genes promote the transition between progenitors and neuronal differentiation. For instances, dephosphorylation of *Ascl1* (proneural transcription factor) decreases the cyclin dependent kinases (CDK) activity, then promotes neuronal differentiation in *Xenopus* embryos. By contrast, a highly phosphorylated form of *Ascl1* by CDK maintains proneural proteins in progenitor cells (Ali et al., 2011, 2014).

In the cranial placodes, both *SoxB1* and proneural bHLH genes are regulated by the transcription factor *Six1* and its cofactor *Eya1* (Ahmed et al., 2012a, b; Baker and Brown, 2018; Zou et al., 2004). A previous study suggested that *Six1* and *Eya1* are direct regulators to *SoxB1* genes (*Sox2*, *Sox3*) and proneural genes (*Atoh1*, *Neurog1*) to induce neuronal or sensory differentiation in *Xenopus laevis* embryos (Riddiford and Schlosser, 2016). In addition, in mice *Six1* and *Eya1* together with *Sox2* were shown to directly activate *Atoh1* during hair cell formation (Ahmed et al., 2012a). On the other hand, *Six1* and *Eya1* mutations compromise *Neurog1* and *NeuroD1* expression, which can lead to loss of sensory neurons in the otic vesicle of mice (Zou et al., 2004).



### **1.2.2 Neuronal migration through the basal lamina**

The basal lamina is a thin layer of extracellular matrix generated by epithelial cells. It is located on the basal surface of the epithelial cells in front of the basement membrane. It comprises two layers fibronectin (basal) and laminin (apical). Generally, the role of basal lamina is to support and regulate the interaction between cells in the tissues during embryonic development and it helps to maintain the final form of organs (Brownell and Slavkin, 1980; Carlsson et al., 1981; Slavkin et al., 1983).

Neuronal migration through the basal lamina is documented in a number of previous studies using immunostaining to trace the basal lamina during the migration of neurons. In the early chick embryo, the neurons of the cochlea-vestibular ganglion (CVG) migrate from the ventral region of the otocyst epithelium (Whitehead and Morest 1985 a, b). When CVG migration is complete, ganglion cells send their axons to innervate the receptor hair cells. However, the basal lamina has appeared before CVG cell migration with two basal lamina associated glycoproteins (fibronectin and laminin) completely surrounding the otic vesicle adjacent to the neural tube (Hemond and Morest, 1991). In the epibranchial placodes, laminin was then shown to be downregulated in the region underlying neuroblast migration region similar to what was observed during neural crest delamination (Graham et al., 2007). This result suggests that the basal lamina was broken down at the region of the neuronal migration from the epithelium.

There is no evidence to suggest that basal lamina is interrupted before CVG migrations, but immunostaining showed that several fragments of basal lamina are pushed out by cell migrations (Hemond and Morest, 1991). However, it is not known if cell migration forces are coming from epithelial cells or the migrating cells itself (Hemond and Morest, 1991). Many mechanisms were implicated in the neuronal migration from otic epithelium through the basal lamina. Probably, there is chemical degradation of the basal lamina by mesenchymal cells which are located

outside of the otocyst and causes weakening of the basal lamina barrier (Hemond and Morest, 1991). In addition, Carney and Silver (1983) suggested that the disruption of the basal lamina in otic epithelium of mice is due to different enzymes released from the epithelial cells of the otic vesicle. The third mechanism may involve epithelial cells that produce a force that helps the CVG cells to migrate outside the otic epithelium (Hemond and Morest, 1991). For example, increased numbers of mitotic cells lead to increasing pressure in one zone (physical force) (Hemond and Morest, 1991).

On the other hand, changes in the basal lamina may also affect other processes beyond cell migration. Local reductions in the basal lamina location were also seen to be correlated with increased mitotic activity of adjacent otic epithelial cells suggesting the possibility that reductions in basal lamina stimulate mitoses in this region (Graziadei and Graziadei, 1979; Hemond and Morest, 1991). However, this speculation needs to be further tested.

### **1.2.3 Otic neurogenesis**

The generation of the vestibulocochlear ganglion of the eighth cranial nerve from the otic vesicle in vertebrates is already briefly described above (1.1.2). Otic neurogenesis initiates by generating a division in the otic vesicle between a neurosensory domain, which generates neurons of the VIIIth ganglion and sensory hair cells and a non-neurosensory domain (Andermann et al., 2002; Maier et al., 2014). In order to distinguish between non-neurosensory and neurosensory domains in otic placodes, several mechanisms interact (Fig. 1.5) (Maier et al., 2014). In otic placodes of chicks and mice, the non-neurosensory domain is located posteriorly and the neurosensory domain is anterior (Fig.1.6) (Gálvez et al., 2017; Raft et al., 2007; Maier et al., 2014; Neves et al., 2013). However, sensory hair cells were generated in both anterior and posterior domains of the otic vesicle in fish (Haddon and Lewis, 1996).

Tbx1 is a transcription factor, which is expressed in the non-neurosensory domain and which plays a very important role to control the extent of the neurosensory domain characterized by SoxB1 expression. *Tbx1* mutation causes extension of the neurosensory domain in the mouse (Raft et al., 2004). The *Hes1* (Hairy and enhancer of split 1) gene encodes a transcription factor which is co-expressed with Tbx1 and also expands the neurosensory domain when mutated (Radosevic et al., 2011). Later, *Tbx1* plays a role in sensory cell development (crisetae, cochlea) and in the otic vesicle, *Tbx1* expression is complementary to *Neurog1* (Raft et al., 2004). Another transcription factor, which plays a role in restricting the neurosensory domain to the anterior otic vesicle, is Lmx1b, which is located in the ectoderm adjacent to neural tube and its expression is induced in the dorsal-medial and posterior regions of the otic vesicle (Abelló et al., 2007, 2010; Jidigam et al., 2015).

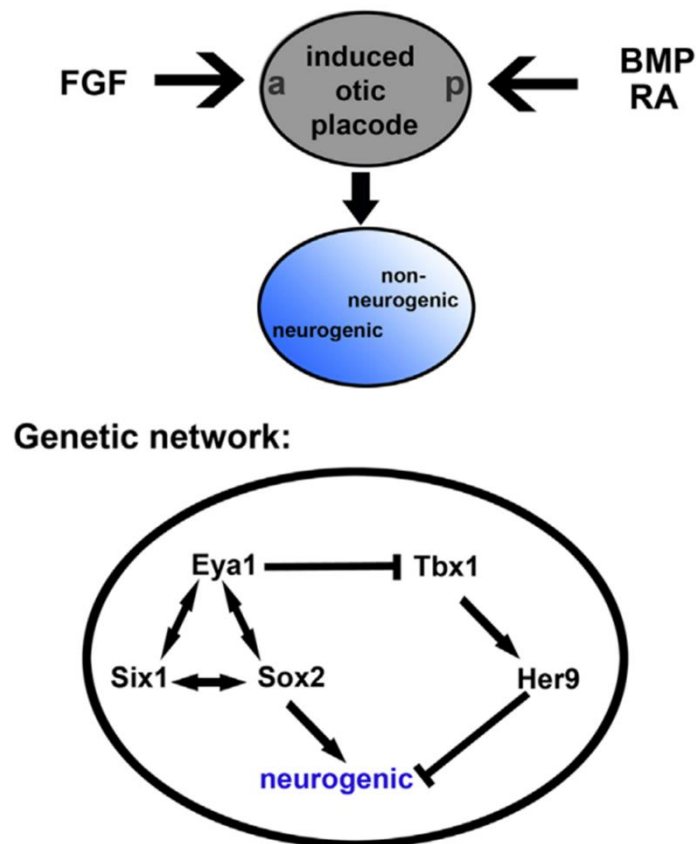


**Fig. 1.5. Signaling pathways and gene regulatory networks participating in the establishment of the neurosensory (=neurogenic) domain in the otic placode. a: anterior, p: posterior. (reproduced from Maier et al., 2014).**

In addition to these transcription factors, there are several signaling pathways that play an important role to regulate the boundaries between non-neurosensory and neurosensory domains in the otic placode such as retinoic acid (RA) which acts on the anterior-posterior axis of the otic vesicle and is released from the mesoderm around otic vesicle. Also, RA plays a role in regulating Tbx1 expression in otic placode (Bok et al., 2011). Additionally, Hedgehog (Hh) signaling regulates Tbx1 expression, with overexpression of Hh leading to the repression of Tbx1 and Hh inhibition inducing Tbx1 in zebrafish (Hammond et al., 2010; Radosevic et al., 2011).

During inner ear development, neurosensory progenitors generate neuronal or sensory precursors. Once neurons have delaminated from neurosensory epithelium, hair cells and supporting cells develop from the progenitor cells that remain in the epithelium (Fig. 1.6) (Gálvez et al., 2017). Notch signaling plays important roles in these two sequential decisions by two different mechanisms that are lateral inhibition and lateral induction. Lateral induction is associated with prosensory specification and lateral inhibition is essential to determine hair cells (Fig. 1.6) (Gálvez et al., 2017; Hartman et al., 2010). In mammals, there are four Notch receptors (Notch1-4) and five Notch ligands (Delta1,3,4 and Jagged1,2) (Kiernan, 2013). These ligands are membrane bound proteins which interact with the Notch trans-membrane receptor on the surface of neighbouring cells. This interaction leads to proteolytic cleavage of Notch allowing the intercellular domain (NICD) to move to the nucleus and bind with RBP-JK family proteins to form a transcriptional activator.

Two basic Helix-loop-Helix (bHLH) proteins are important to regulate the differentiation of neurons and hair cells; these are Neurog1 and Atoh1, respectively (Fig. 1.6) (Gálvez et al., 2017). In the inner ear, Sox3 and Sox2 activate Neurog1 to show positive signal in neurosensory domain of otic vesicle. These cells subsequently delaminate and upregulate NeuroD1 and other neuronal differentiation genes (Fig. 1.6) (Gálvez et al., 2017; Fritzsche et al., 2010; Raft et al.,

2007). In the neurosensory domain of the otic vesicle, the *Neurog1* positive domain becomes reduced, while *Atoh1* is upregulated in a complementary domain, which will form the sensory patches of the inner ear (Raft et al., 2007). Otic neurogenesis in mammalian and zebrafish embryos is known to be determined by the proneural gene *Neurog1* (Ma et al., 1998; Andermann et al., 2002; Cau et al., 2002). Similarly, in *Xenopus laevis*, *Neurog1* but not the *Neurog2* orthologue *Xngnr1* is expressed in the otic and lateral line placodes (Schlosser and Northcutt, 2000; Nieber et al., 2009).

Proneural genes activate the expression of Notch ligands such as *Delta1* resulting in lateral inhibition. During lateral inhibition, Notch signalling activates target genes such as *Hes1* and *Hes5* in adjacent cells, which repress the transcription of *Ascl1*, *Neurog1/2* or other proneural genes and then inhibits the differentiation of neuronal cells. Importantly, this lateral inhibition process is important to prevent the differentiation and maintain a progenitor state in adjacent cells (Liu et al., 2014; Petrovic et al., 2014).

Notch mediated lateral inhibition is also involved to decide between hair cells and supporting cells. In terminal mitosis, prosensory cells initiate *Atoh1* expression that promotes the formation of hair cells. After expression of *Atoh1*, *Jagged2* and *Delta1* that are members of Notch pathway initiates in hair cells, they interact with the Notch receptor to activate Notch signaling. As a result, *Hes1* and *Hes5* is expressed in adjacent cells which will form supporting cells (Lanford et al., 2000; Liu et al., 2014).

Those cells, in which Notch signaling is inhibited escape lateral inhibition and initiate neuronal differentiation. In chicks, differentiation of neurons starts in cells expressing high levels of *Neurog1* and *Delta1*, which subsequently activate *NeuroDI* and *NeuroM* (Bell et al., 2008). *NeuroDI* is a neuronal differentiation gene and plays a role in neuronal formation and differentiation (Bell et al., 2008). In *Xenopus*, *NeuroDI* is expressed in scattered cells that stopped division within

the inner ectodermal layer and is seen in all of placode-derived ganglion cells as well as in cells that migrate away from the placode (Brugmann and Moody, 2005; Schlosser and Northcutt, 2000; Schlosser et al., 2008). Similarly, in mouse *NeuroD1* expression was found in cells that have stopped division and migrated to form neurons in different placodes, including olfactory, epibranchial and otic placodes (Bell et al., 2008; Fode et al., 1998; Suzuki et al., 2003).

In addition to SoxB1 and bHLH transcription factors, there are several transcription factors expressed strongly in otic placode or vesicle of *Xenopus laevis*, including Six1, Six4 and Eya1 which play a role in otic neurogenesis (Schlosser and Ahrens, 2004). Previous studies confirmed that *Eya1* and *Six1* play important roles in otic neurogenesis by regulating the expression of SoxB1 genes as well as neuronal differentiation (Zou et al., 2004; Schlosser et al., 2008; Ahmed et al., 2012b; Riddiford et al., 2016, 2017; Xu et al., 2021).

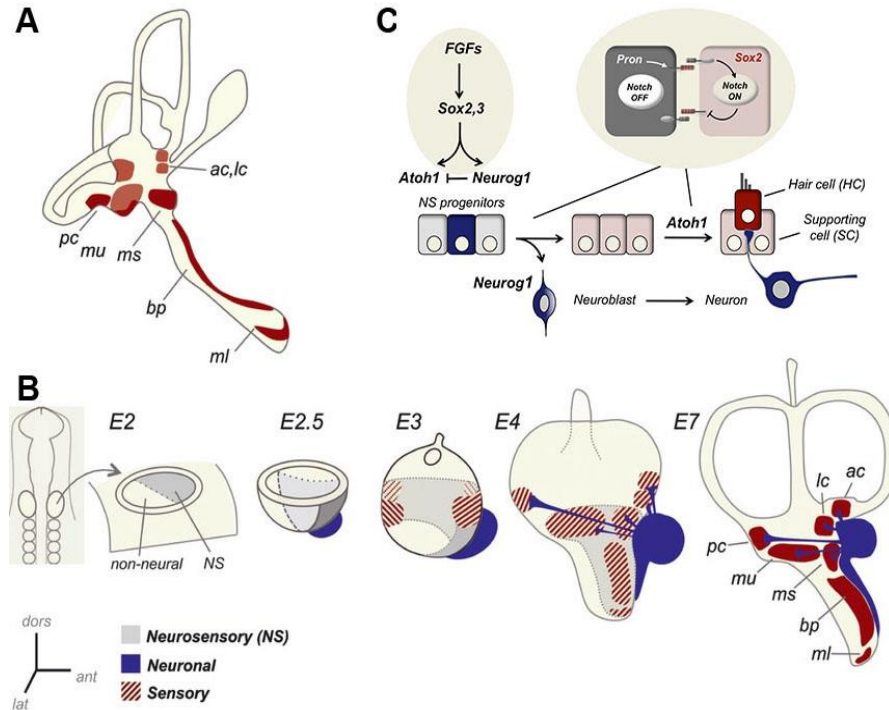


**Fig. 1.6. Development of neurons and sensory cells in the inner ear. A:** Diagram of chick inner ear with sensory patches indicated in red: ac: anterior crista; bp: basilar papilla; lc: lateral crista; ml: lagenar macula; ms: saccular macula; mu: utricular macula; pc: posterior crista. **B:** Development of the inner ear in the chick from embryonic days (E) 2–7. The neurosensory (NS) domain is established early, before invagination. It subsequently gives rise to the hair cells and supporting cells of the sensory patches (red) and the neurons of the vestibulocochlear ganglion (blue). **C:** Specification of neurons (blue) and hair cells (red) during inner ear development. After induction by FGF, Sox2 and Sox3 in the neurosensory (NS) domain promote expression of both Atoh1 and Neurog1. Subsequently, neurons (specified by Neurog1) differentiate first and delaminate from the neurosensory domain, followed by the differentiation of hair cells (specified by Atoh1). During both steps, cells expressing the proneural gene (Pron) – *Neurog1* or *Atoh1* - repress differentiation in adjacent cells via Notch mediated lateral inhibition (insert). This allows, first, to single out neuronal precursors from cells remaining in the neurosensory domain and, second, to decide between hair cells and supporting cells. **A, B:** Reprinted from Neves et al. 2013. **C:** Reprinted from Gálvez et al., 2017

### 1.3 Proteins involved in apicobasal (ab) cell polarity

Epithelial cells have an intrinsic asymmetry in their structures and shapes which is referred to as apicobasal cell polarity. Cell polarity is important for several cellular functions and is based on the specific distribution of several molecules such as phospholipids and protein complexes to apical, basal and lateral regions of the plasma membrane (Knoblich, 2010; Martin-Belmonte and Perez-Moreno, 2012; Noatynska et al., 2013). In both vertebrates and invertebrates, a conserved set of polarity proteins including Partition defective 3 (PAR3) (= Bazooka in *Drosophila*), PAR6, aPKC, Dlg, Scrib, Lgl, and PAR1 are involved in controlling epithelial cell polarity (Chen and Zhang, 2013). The PAR3/PAR6/aPKC complex together with its interacting proteins has the most central role in epithelial cell polarity. Previous studies demonstrated that PAR3, PAR6 and aPKC are required to establish anterior-posterior polarity and regulate different development stages of polarization in *C. elegans* and *Drosophila* embryos (Kemphues et al., 2000; Tabuse et al., 1998). In addition, the PAR3/PAR6/aPKC complex plays an important role in regulating asymmetric cell division of *Drosophila* neuroblast and establishment of the axon-dendrite polarity of neurons (Shi et al., 2003; Wodarz et al., 1999).

Additional proteins that affect apical-basal polarity in epithelia are myosin light chain and N-cadherin. Myosin light chain (MLC) is a motor protein and plays a very important role in many processes including apical cell contraction and cell division. It also regulates the polarity of epithelial cells, cell migration, protrusion formation and adherens maturation (Gutjahr et al., 2005; Vicente-Manzanares and Horwitz, 2010).

Finally, cadherins are a large family of glycoproteins which are essential for the calcium-dependent cell-cell adhesion mechanism and are often distributed in a polarized manner. They are divided into subclasses such as E-, C-, N-cadherins (Takeichi et al., 1988). N-cadherin, which is concentrated in adherens junctions, is a cell adhesion protein implicated in the maintenance of cell polarity in the neural



tube and in polarizing migrating neurons (Jossin and Cooper, 2011; Miyamoto et al., 2015; Lele et al., 2002; Rouso et al., 2012).

### **1.3.1 Functions of apicobasal cell polarity**

Different regions can be recognized in the plasma membrane of epithelial cells including an apical region that faces the external environment, a lateral region adjacent to neighboring cells and a basal region adjacent to the extracellular matrix (ECM). The lateral and basal membranes together are referred to as basolateral membrane. In *Drosophila*, the lateral region of plasma membrane contains septate junctions (SJ) and adherens junctions (AJ), while the lateral region of plasma membrane in vertebrate contains tight junctions (TJ) and adherens junctions (AJ). Tight junctions involve the localization of proteins in a region of contact between adjacent cells (tight junctions) where they prevent transmembrane diffusion (Assémat et al., 2008; Coopman and Djiane., 2016; Johnston and Ahringer, 2010; Noatynska et al., 2013). Tight junctions, thus, act as barrier to control the passage of ions and molecules between neighboring epithelial cells, while adherens junctions initiate cell-cell contacts and maintain the contact between neighboring cells (Hartsock and Nelson, 2008) (Fig. 1.7). In addition, the polarized distribution of molecules in the plasma membrane of epithelial cells allows them to adopt different shapes (Harris & Tepass 2010; Tepass, 2012; Nance & Zallen 2011). Polarity proteins in the plasma membrane of epithelial cells are kept in place by cytoskeletal proteins and are transferred from incorrect positions on the plasma membrane to the right location by vesicles (Coopman and Djiane., 2016. Johnston and Ahringer, 2010).

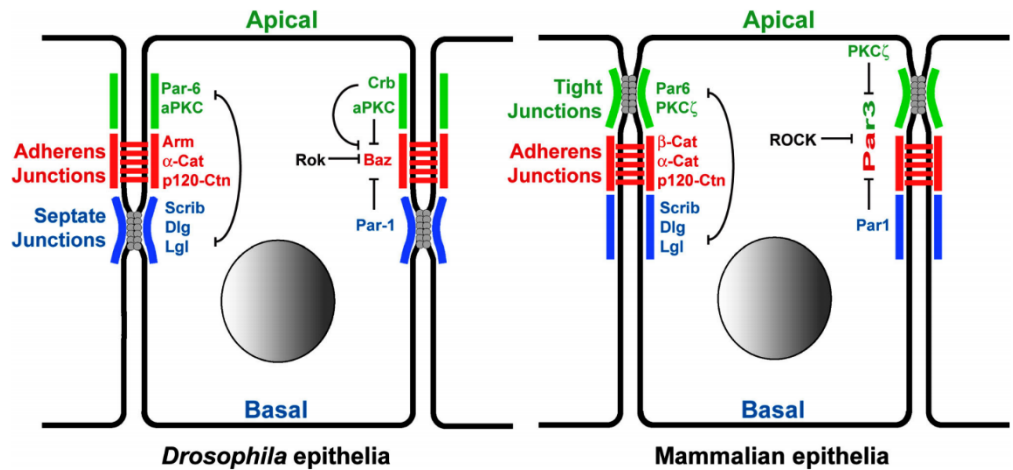


**Fig. 1.7. Polarization of the *Drosophila* and Mammalian Epithelial Cell.** Adherens junctions, (shown in red) are localized between the apical and basal membranous domains characterized by two different protein complexes, the apical PAR6/PKC $\zeta$  (green), and the baso-lateral Dlg/Lgl/Scrib/PAR1 (blue) complex (reproduced from Coopman and Djiane., 2016).

Apicobasal cell polarity is also important during cell division to regulate the balance between the proliferating and differentiating cells in many tissues by either producing similar daughters (symmetric cell division; often resulting in two progenitor cells) or daughters with different fates (asymmetric cell division; often resulting in one progenitor and one differentiating cell) (Vorhagen and Niessen, 2014; Noatynska et al., 2013).

Asymmetric cell division requires the asymmetric segregation of cell fate determinants into the two daughter cells driven by the polarized distribution of cell fate determinants in the cell and the orientation of the mitotic spindle along the apico-basal axis (Charville and Rando, 2013). This has been studied in great detail in the *Drosophila* neuroblast, which divides to generate another neuroblast (progenitor cell) from the apical position and a ganglion mother cell (small cells) from the basal position that produces neuron or glia (Goodman and Doe, 1993; Knoblich, 2010) (Fig. 1.8). During delamination of the neuroblast, the Baz/PAR3–

PAR6–aPKC proteins localizes apically in the neuroblast (Petronczki and Knoblich, 2001; Rolls et al., 2003). The apical aPKC/PAR3/PAR6 complex then recruits adapter proteins (Inscuteable (Insc) and LGN together with G $\alpha$ i to the apical cortex. LGN then binds to Mud/mNuMA, which helps to align the spindle position along the apico–basal axis. In addition, phosphorylation of Miranda (adapter protein) and the cell fate determinant Numb (a Notch inhibitor) by aPKC changes their localization to the basolateral membrane. As a consequence, the differentiation promoting Numb protein is only inherited by the basal daughter cell, while the apical daughter cell will be devoid of Numb and retain progenitor status (reviewed in Chen and Zhang; 2013; Knoblich, 2010; Tepass, 2012).

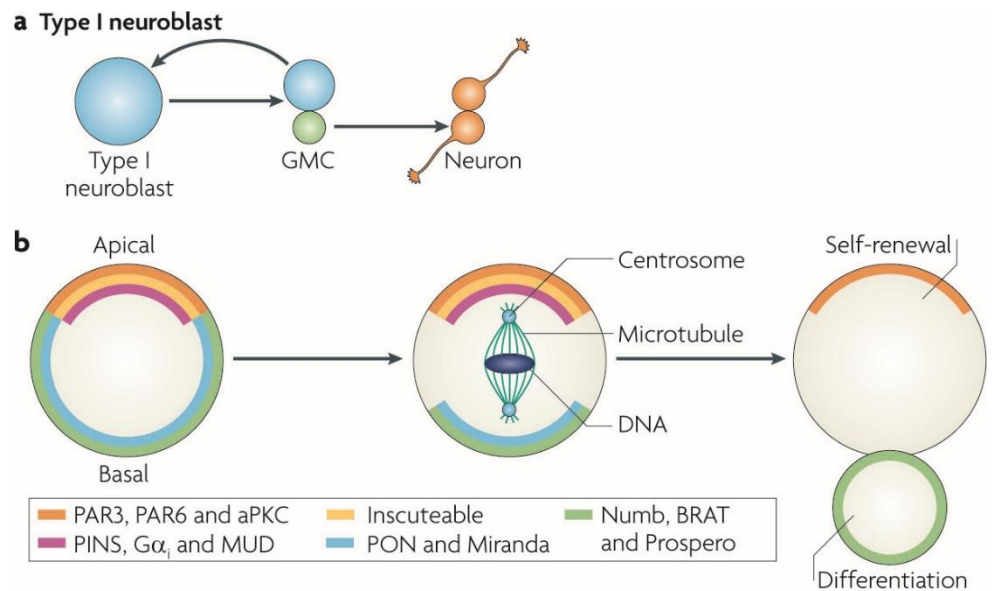


**Fig.1.8. Models for asymmetric cell division.** (a): *Drosophila* neuroblast divides asymmetrically into one neuroblast (progenitor cell) from the apical position and a ganglion mother cell (GMC) in basal position that produces neuron. (b): After mitosis, Numb and other molecular act together to prevent self-renewal and segregated into one of daughter cells (reproduced from Knoblich, 2010).

### 1.3.2 Establishment of cell polarity

The apico-basal epithelial cell polarity in *Drosophila* is established by the interaction of several proteins, in particular PAR1, PAR2, PAR3 (known as Bazooka – Baz – in *Drosophila*), PAR6 and atypical protein kinase C (aPKC) (Benton and Johnston, 2003; Doe and Bowerman, 2001; Nance and Zallen, 2011). The proteins PAR3, PAR6 and aPKC are all bound to each other. PAR3 is found in the adherens junction below PAR6 and aPKC, which expand into the apical surface (Harris and Reifer, 2004) (Fig. 1.7). This interaction between PAR6, aPKC and PAR3 is important to form the PAR complex and is required to establish the recruitment of PAR6/aPKC to the apical membrane (Horikoshi et al. 2009). In the PAR complex, PAR6 acts to control aPKC activity and its position in the apical membrane (Atwood et al. 2007). While, the interaction between PAR6 and active (GTP-loaded) Cdc42 is also important to apical recruitment and function of PAR6, it is not known how Cdc42 is recruited at the apical membrane of the epithelial cell (Atwood et al. 2007, Hutterer et al. 2004). In order to place PAR3 at the adherens junction and PAR6/aPKC on the apical membrane, the PAR complex must be dissolved by the phosphorylation of PAR3 by aPKC (Chen and Zhang, 2013; Horikoshi et al. 2009). In addition, the interaction between PAR6 and Crumb enhances the apical recruitment of PAR6/aPKC (Morais-de-Sa et al. 2010; Chen and Zhang, 2013). Crumb proteins (CRB) are located on the apical region and regulate the expansion of the apical-lateral surface (Macara, 2004). Crumb mutants lead to loss of apical membrane indicating that they are required to form the apical domain (Wodarz et al. 1993).

Another protein complex with an important role for apicobasal polarity is Lgl/Scrib/Dlg, which is located on the basolateral side and conserved between nematodes, flies, and mammals (Chen and Zhang, 2013). Apical polarity proteins of the PAR complex play an important role to exclude basolateral proteins from the apical domain such as Scribble (Scrib) (Bilder et al. 2003). In epithelial cells, aPKC

phosphorylates many target proteins relating to polarity (Suzuki et al. 2004). Previous studies demonstrated that both the basolateral proteins Lgl and PAR1 are phosphorylated by aPKC to prevent them from associating with the apical membrane (Suzuki et al. 2004; Tepass, 2012). Conversely, PAR1 phosphorylates PAR3 to prevent the PAR3/PAR6/aPKC complex from accumulating at the basolateral side of the epithelial cell.

### **1.3.3 Role of apicobasal cell polarity in vertebrate neurogenesis**

The PAR protein complex including PAR3, PAR6 and aPKC plays a crucial role in generating the polarity of neuronal cells in vertebrates like in *Drosophila* (Chen et al., 2013; Goldstein and Macara, de Matos Simões et al., 2010; Kempfues, 2000; Shi et al., 2003) (Fig. 1.7). In vitro, knockout of *PAR3* led to deficient polarity of hippocampal neurons (Chen et al., 2013; Hapak et al., 2018). In addition, mammalian PAR3 and PAR6 are found polarized in a new axon and are considered as regulators of the actin cytoskeleton in this future axon (Zhang and Macara, 2008). Furthermore, mammalian PAR3 and PAR6 are involved in the regulation of microtubule dynamics in neurons and future axons (Chen et al., 2013). Defects in the localization of PAR3 or PAR6 disrupted the stability of microtubules, neuronal polarization and axon specification (Chen et al., 2013; Shi et al., 2003). Cell polarity proteins are also necessary in CNS development, for example during neurogenesis of specialized neuroepithelia and neurite outgrowth (Chalmers et al., 2005; Sabherwal et al., 2009; Solecki et al., 2006). Also, polarity proteins play important roles in formation of synaptic contacts and during neuronal migration (Solecki et al., 2006). Finally, like in *Drosophila*, the PAR complex and other proteins involved in apicobasal cell polarity are also involved in the regulation of asymmetric cell division in the vertebrate CNS, thereby affecting the balance between progenitor proliferation and neuronal differentiation (e.g. Costa et al., 2008; Farkas and Huttner, 2008; Bultje et al., 2009; Alexandre et al., 2010; Willardsen and Link, 2011).

The role of cell polarity proteins during early neurogenesis has been particularly well studied in *Xenopus*. In *Xenopus* neurogenesis, superficial layer cells are polarized and remain as progenitor cells (Davidson and Keller, 1999), while deep layer cells are not polarized and generate the primary neurons and precursors of secondary neurons (Sabherwal et al., 2009). A previous study has shown that aPKC is localized on the apical side of the membrane of superficial layer cells and Lgl2 is localised to the basolateral side (Chalmers et al., 2005). However, there is no distribution of aPKC and Lgl2 in the membrane of deep layer cells (Sabherwal et al., 2009). In order to examine the effect of cell polarity proteins on cell fate, *aPKC* overexpression was examined in deep cells of *Xenopus* ectoderm. Overexpression of a membrane-tethered form of aPKC induced the proliferation of cells and inhibited the generation of primary neurons (Sabherwal et al., 2009). Conversely, loss-of-function experiments by using aPKC morpholinos or other means of inhibiting aPKC promoted the differentiation of primary neurons (Sabherwal et al., 2009). Taken together, these results demonstrated that activation of aPKC in progenitor cells reduced differentiation of neurons in *Xenopus*, although details of the mechanism involved remain unclear.

#### **1.4 Aims of the project**

The main aim of this Ph.D. project is to study the role of *Eya1* during neurogenesis in the otic vesicle of *Xenopus laevis* with a particular focus on the role of Eya1 for cell proliferation, the formation of progenitors and differentiating neurons as well as for the distribution of cell polarity proteins during otic vesicle development. This project is divided into three parts.

Since otic neurogenesis in *Xenopus* has not yet been studied in any detail, the first part of the project aims to provide a detailed description of this process, elucidating (a) the spatiotemporal pattern of otic neurogenesis as judged by the delamination of neuroblasts through gaps in the basal lamina; (b) the organization of the neurogenic otic epithelium including the subcellular distribution of cell polarity

proteins; and (c) the changing distribution of cell proliferation, neurosensory progenitors, and differentiating neurons during development of the otic vesicle. Immunostaining with different antibodies was used in combination with confocal microscopy to determine the distribution of basal lamina (laminin), cell polarity proteins (aPKC, PAR3, MLC and N-cadherin), cell proliferation (pH3 and EdU incorporation) and the localization of progenitor cells (Sox3) and differentiating neurons (Islet1/2, acetylated tubulin). In order to demonstrate the distribution of proteins in relation to the cell membrane more precisely, immunostaining was performed in embryos that had been injected with membrane-bound GFP at the 2-cell stage.

The second part of the project seeks to characterize the localization of *Eya1* protein during different stages in *Xenopus laevis*. because only the distribution of *Eya1* mRNA has been previously described (David et al., 2001). The specificity of the *Eya1* antibodies used was confirmed by using a Western blot experiment and a peptide competition assay. The subcellular distribution of *Eya1* protein during development of the otic vesicle and its distribution in relation to markers of proliferation, progenitors and differentiating neurons was then characterized by double-immunostaining and confocal microscopy. The distribution of *Eya1* protein was also clarified for all other cranial placodes of *Xenopus laevis* from early embryonic stages (stage 15) to early larval stages (stage 40).

The third and final part of this study aims to understand the role of *Eya1* for cell proliferation, progenitor formation, neuronal differentiation as well as for the proper distribution of cell polarity proteins in the otic vesicle using gain or loss of function experiments. At the 2-cell stage, embryos were injected with *Eya1* antisense morpholino oligonucleotide, a dominant-negative Six1 construct or with *Eya1* and Six1 mRNAs. Subsequently, the otic vesicle was analyzed by immunostaining for the various markers mentioned above.

## **Chapter-2 Material and Methods**

### **2.1 Animal Housing**

The African clawed frog *Xenopus laevis* was used as a model organism in this project. *Xenopus laevis* frogs were imported from Nasco (Fort Atkinson, WI, USA). Irish and European legislation was followed on all experimental processes that were performed and covered under the project license (AE19125/P019) to Dr. Gerhard Schlosser. Furthermore, all experiments have been approved by the NUI Galway Animal Care Research Ethics Committee (ACREC: 14/Dec/01).

### **2.2 Embryo Incubation and Microinjection**

#### **2.2.1 Human Chorionic Gonadotropic (HCG) Hormones Injection and Egg Collection**

HCG hormone was used to induce egg laying in female *Xenopus laevis*. One week prior to egg collection for *in vitro* fertilization, two female frogs were injected with 50 units HCG each into dorsal lymph sac (Hrynyk et al.,2018). One day before egg collection, injection was repeated for each primed female frog with 750 units HCG. Frogs injected with HCG were kept in 18 °C incubator overnight, before the *in vitro* fertilization experiment.

#### **2.2.2 Microelectrode Needle Puller**

A Narishige electrode puller (Cat. No. PN-31) was used to produce long, sharp microcapillary needles for microinjection. Needle puller machine was adjusted to standard work conditions (Heat 98.1 °C, sub magnet 22.0, main magnet 94.1) for the pulling. Then glass capillary (Narishige Cat. No. GD-1) was inserted and melted by the electrically heated platinum heater. Finally, the glass capillary is pulled by



electromagnetic force to produce a micropipette. After pulling, the tip of the micropipette was broken to approximately 10-15  $\mu\text{m}$  inner tip diameter.

### **2.2.3 *In Vitro* Fertilization (IVF) of *Xenopus laevis* Embryos**

For *in vitro* fertilization day, female frogs were transferred from 18 °C to room temperature (RT) and placed into 1x MBSH (Appendix. A.1). Frogs were kept in a quiet place. Subsequently, an adult male frog was anaesthetized in 0.1% MS 222 (Tricaine methane sulfonate) in tap water with a pH 7.4. After 15-30 minutes, testes were removed by microdissection. The testes were transferred to a small petri dish with 1x MBSH and stored at 4°C.

Every hour, eggs were collected by plastic transfer pipette and placed in a big petri dish. IVF was initiated by adding a small piece of macerated testis using two forceps. In each dish, 300 to 500 eggs were taken to fertilization. The Fertilization was activated by 0.1x MBS hypotonic solution (Appendix. A.1) at RT. After 20 min. the buffer was discarded and replaced by 2% Cysteine in tap H<sub>2</sub>O with a pH=8 (see Appendix A.1) for dejelling. After completion of dejelling (7-10 min.), embryos were rinsed with 0.1X MBS for 4 times and kept on a 14°C cold plate. After one to two hours, 2- or 4-cell stage embryos were taken for microinjection of various constructs (MO, GR-mRNA injection).

### **2.2.4 mRNA Synthesis for Microinjection**

The synthesis of mRNA was done using the Ambion mMessenger Machine Kit (Ambion, Cat. No.- AM1340). This mRNA was used for the microinjection into *Xenopus* embryos. Before mRNA synthesis, the target plasmid was linearized by the appropriate restriction enzymes.

To linearize plasmids for mRNA synthesis, 10  $\mu\text{g}$  plasmid (e.g. 10  $\mu\text{l}$  for 1  $\mu\text{g}/\mu\text{l}$ ) and 5  $\mu\text{l}$  restriction enzyme were added into an Eppendorf tube. For some restriction

enzymes, 0.5 µl BSA was added to the enhancement of the restriction enzyme digestion process. Also, 5 µl of restriction buffer was added and 40 µl of dH<sub>2</sub>O with mixing the mixture well by pipetting up and down. The mixture was incubated overnight at 37° C. Once the restriction enzyme digestion was over, the linear plasmid was purified by RT-PCR purification using the protocol described in 2.6.2).

mRNA was then synthesized using the Ambion mMessage Machine kit. A 20 µl reaction mixture was prepared for 1 µg of linearized plasmid by the following steps in a new Eppendorf tube, 3 µl linearized and purified plasmid (0.33 µg/µl) was added to 3 µl nuclease free H<sub>2</sub>O, 2 µl 10x transcription buffer, 10 µl 2xNTP and 2 µl RNA polymerase (SP6). The reaction mixture was mixed well by pipetting up and down, and also spun briefly. Then, the mixture was incubated for 15 min at 37° C.

Using the RNeasy Qiagen Kit (Qiagen, Cat. N0. - 74104) the mRNA was purified. In order to bring the volume of the mRNA synthesis mixture to 100 µl, nuclease free H<sub>2</sub>O was added. Before adding 250 µl of 100 % EtOH, 350 µl of buffer RLT was added into the mixture and mixed well by pipetting. Next, the reaction mixture was applied to the RNeasy column, spun for 15 seconds and the flow through was discarded. The column was transferred to a new collection tube, 500 µl of buffer RPE was added, and centrifuged again for another 15 seconds and the flow through was discarded. Again, 500 µl of buffer RPE was added and spun for 2 min, the flow through was discarded. The column was transferred again to a new collection tube and centrifuged for 1 min, discarding the flow through and the collection tube. For the final elution, the column was transferred to a collection tube. Elution was done with up to 30 µl RNase free water by spinning for 1 min. To get a high concentration of mRNA, the volume of RNase free water used ranged from 15 -30 µl. The concentration of the collected samples was measured by using a Nano Drop ND1000.

### 2.2.5 Microinjection of Morpholino Antisense Oligonucleotides (MO) or mRNAs

Embryos were injected with 5 nl of the following mRNAs at different concentrations: *mGFP*: 50 ng/ $\mu$ l (250 pg); *GR-EnR-Six1*: 100 ng/ $\mu$ l (500 pg); *Eya1-myc*: 100 ng/ $\mu$ l (500 pg); *Eya1-GR*: 100 ng/ $\mu$ l (500 pg); and *Eya1*-MO1+MO2 (*Eya1* MO1: 5'-TACTATGTGGACTGGTTAGATCCTG-3; *Eya1* MO2: 5'-ATATTTGTTCTGTCAGTGGCAAGTC-3; Schlosser et al., 2008) were injected in conc. 25  $\mu$ M (1 ng), 50  $\mu$ M (2 ng), and 250  $\mu$ M (10 ng). For control experiment, a standard control MO (5'-CCTCTTACCTCAGTTACAATTTATA-3', Schlosser et al., 2008) was used in conc. 50  $\mu$ M (2 ng). *mGFP* 50 ng/ $\mu$ l (250 pg) were co-injected for lineage tracing.

For microinjection of probes, embryos were placed into 4% agar dishes along with 5% Ficoll in 0.1x MBS. The microelectrodes (10-15  $\mu$ m) were connected to a microinjector (Narishige; cat no.: IM-300) for microinjections. The size of the droplet injected was calibrated to 5 nl by injecting water into oil on top of a micro-ruler.

Injected embryos were kept in 5% Ficoll for the quick healing from microinjection. After completing the injection, embryos were transferred to a petri dish containing 4% ficoll. Cold plate temperature was set at 14C<sup>0</sup> to culture the embryos overnight. The following day, the Ficoll solution was changed to 0.1x MBS and dead embryos were removed immediately. Stages were determined according to Nieuwkoop and Faber, 1967.

## **2.3 Immunohistochemistry**

All immunohistochemical experiments were done in at least five embryos per marker analysed; functional studies followed by immunostaining were done in at least three embryos per marker analysed.

### **2.3.1 Fixation**

Embryos were fixed by using 4% paraformaldehyde (PFA) in phosphate buffer (PB) (Appendix. A.1) for overnight at 4<sup>0</sup>C. On the next day, embryos were rinsed in PB twice for 10 minutes, and 50 % EtOH one time for 5 minutes. Embryos were stored in 70 % EtOH at 4<sup>0</sup>C.

Some embryos were fixed in Dent's fixative for immunohistochemistry (N-Cadherin antibody) experiments. Dent's fixative was made by adding 80% methanol and 20% dimethyl sulfoxide (DMSO).

### **2.3.2 Cryosections**

Before cryo-sectioning, embryos were re-hydrated one times for 10 min in 50% EtOH, then PB. Thereafter, embryos were incubated in 20% sucrose (in PB). Finally, prior liquid was removed and replaced by 20% sucrose for overnight at 4<sup>0</sup>C. Next day, embryos were embedded in mounting medium (O.C.T. compound, VWR) for cryotomy that was added to rubber forms. Embryos were oriented to get transverse sections and shock frozen in 2-methylbutane cooled with liquid nitrogen. Rubber forms were kept in cryostat at least 20 min before cutting and cooled forceps, different sizes of brushes, and razor blades were also cooled to the same temperature as the cryostat (LEICA, CM1850). The blocks were initially cut at 20 µm thickness, the angle of the knife was adjusted to zero degree and the temperature was reduced to -19<sup>0</sup>C. Once the sample was reached, the thickness was changed to 10 µm. Sections were picked up by using Super frost slides (Thermo scientific). In

preparation for immunostaining, slides were labelled by marker pen (Super PAP Pen) (Daido Sangyo Co., Ltd, Tokyo, Japan) to prevent running off the solution. Slides were dried at least 30-40 min at room temperature or overnight before continuing with immunostaining.

### **2.3.3 Immunohistochemistry on cryosections**

Proteins were visualized and analyzed by using antibodies as follows. On the first day, sections were washed three times for 10 minutes each by phosphate buffer saline (PBS) (Appendix. A.1). To prevent the interaction between the specific antibody and unspecific proteins, 3% Bovine Serum Albumin (BSA) (blocking buffer) in PBS (Sigma) was added for one hour at room temperature. This was followed by another blocking buffer to make sure nonspecific binding sites are blocked by Normal goat serum (Sigma). For each slide, 250  $\mu$ l was added (5  $\mu$ l Normal goat serum in 245  $\mu$ l PBS). The primary antibody was diluted in PBS/BSA with 5% dimethylsulfoxide (DMSO) (Fisher Scientific). To each slide, 100  $\mu$ l of primary antibody was added and the slide was then covered by a coverslip and incubated overnight in wet chamber at room temperature. The primary antibodies used are listed in Table 2.1.

On the second day, slides were washed with PBS for 10 minutes three times before incubating the slides with secondary antibody diluted in PBS with 5% DMSO and 4',6-diamidino-2-phenylindole (DAPI, 100-500 ng/ $\mu$ l diluted from stock of 100  $\mu$ g/ml). For each slide, 100  $\mu$ l of secondary antibody (1:500) was added using either Alexa488-conjugated anti-mouse antibody (Molecular Probes: Product number: A11001); Alexa594-conjugated anti-mouse antibody (Molecular Probes: Product number: A11005); Alexa488-conjugated anti-rabbit antibody (Invitrogen: Product number: A11008); Alexa594-conjugated anti-rabbit antibody (Invitrogen: Product number: A11012). The slides were covered by coverslips and incubated in a dark wet chamber at room temperature for at least 2 hours. To remove the cover glass and secondary antibody, slides were washed three times with PBS for 10 minutes

each. Finally, three drops of Fluoroshield (Sigma: F6182) were used to cover the slide with a coverslip leaving it to harden between 1-2 days in dark room at room temperature. Finally, the coverslip was sealed with transparent nail polish.

**Table 2.1. Antibody table.** Details of sources and concentrations of antibodies that were used for Immunohistochemistry in this study.

<b>Antibody</b>	<b>Supplier, Product number</b>	<b>Species</b>	<b>Dilution</b>
<b>Laminin</b>	Sigma, L9393	Rabbit-Polyclonal	1:25
<b>Phospho Histone 3 (pH3)</b>	Merck, 06-570	Rabbit-Polyclonal	1:100
<b>GFP</b>	Santa Crus Biotechnology, NC, sc-8334	Rabbit-Polyclonal	1:1000
<b>GFP</b>	Abcam, 9F9.F9	Mouse-Monoclonal	1:1000
<b>Tubulin, Acetylated</b>	Sigma, T6793	Mouse-Monoclonal	1:1000
<b>N-cadherin (CDH2)</b>	Abnova, PAB7876	Mouse-Monoclonal	1:200
<b>Myosin light chain (phosph S20)</b>	Abcam, ab2480	Rabbit-Polyclonal	1:200
<b>Atypical protein kinase (aPKC)</b>	Santa Crus Biotechnology, sc-216	Rabbit-Polyclonal	1:200
<b>Partitioning-defective 3 (PAR3)</b>	M Millipore: o7-330	Rabbit-Polyclonal	1:200
<b>Eya1</b>	(Ahrens and Schlosser, 2005)	Guinea pig-Polyclonal	1:50
<b>Sox3</b>	(Zhang et al., 2004)	Rabbit-Polyclonal	1:250
<b>Islet-1/2</b>	DSHB, 39,4D5	Mouse-Monoclonal	1:200

### **2.3.4 Immunohistochemistry on sections with Tyramide Signal Amplification**

Tyramide Signal Amplification (TSA) is a technique using a biotinylated tyramine to detect specific proteins, where tyramide, a phenolic compound, has the ability to bind to the electron rich surface of targets. In this technique, immunostaining is performed with antibodies coupled with horseradish peroxidase (HRP), an enzyme that catalyzes the covalent reaction of tyramine to tyrosine residues. The reaction with fluorescent tyramide causes large numbers of fluorescent dye molecules to be deposited in the vicinity of the antibody, generating a higher density of a target protein compared to conventional immunofluorescence which allows to increase the signal-background ratio (Fig. 2.1).

This is a two-day experiment, using the TSA plus Cyanine 3/Fluorescein System kit (Perkin Elmer- Cat. No. NEI753001kT). On the first day, slides were incubated in 3% Hydrogen peroxide (H<sub>2</sub>O<sub>2</sub>) in PBS for 30 minutes to quench endogenous peroxidase activity. Then slides were washed three times with PBS for 10 min each. Furthermore, 3% Bovine serum albumin was prepared in PBS and slides were incubated for one hour followed by incubation in normal goat serum (20 µl /ml) for 30 minutes. The primary antibodies (PAR3, aPKC, MLC, Eya1, Islet1/2) were diluted in PBS/PSA with 5% DMSO and 100 µl was added for each slide and covered by coverslip. Slides were incubated overnight in a humidified chamber. There are different antibodies that were used with TSA (Table 2.1).

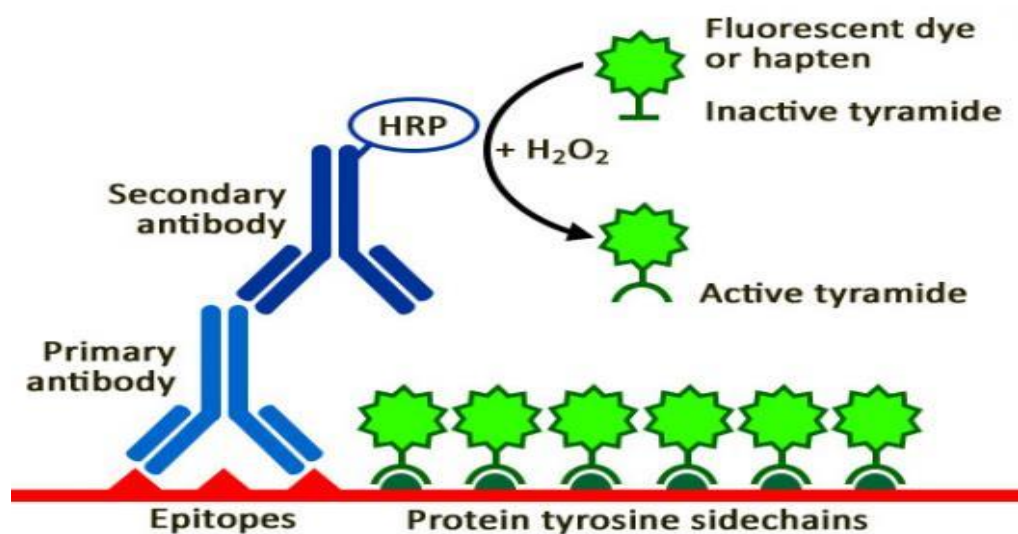


**Fig 2.1. Schematic presentation of tyramide signal amplification (TSA)**  
(reproduced from Biotium Glowing products for science).

On the second day, slides were washed by using PBS three times for 10 minutes each. TNB blocking solution (1.5 %, Perkin-Elmer) was added to prevent nonspecific background for 30 minutes and 250  $\mu$ l for each slide. Then the blocking buffer was removed and slides were incubated with the following secondary antibodies: HRP-coupled goat anti-rabbit antibody (Invitrogen, Product number: G56120, 1:500); HRP-coupled goat anti-guinea pig (Abcam, 6771,1:500) and diluted in PBS with 5% DMSO and 4',6-diamidino-2-phenylindole (DAPI, 100-500 ng/ $\mu$ l diluted from stock of 100  $\mu$ g/ml). Each slide was incubated with 100  $\mu$ l of antibody solution and covered by coverslip overnight in wet and dark chamber. On the next day, the secondary antibody and coverslip were removed, and slides were washed by PBS buffer three time for 10 minutes each. Fluoroshield (Sigma: F6182) was added and slides were covered by coverslip. Slides were left for two days and sealed with transparent nail polish.



### **2.3.5 Microwave treatment and multiplex immunostaining on section with Tyramide Signal Amplification**

This method has two main advantages. First, by using multiplexed antibodies from the same host or different host, multiple antigens can be detected in the same tissue sections. Second, this method can reduce the background from antibody cross-reactivity. Because this process depends on signal amplification in first staining, slides were stained with the first primary antibody on the first day followed by horseradish peroxidase enzyme HRP-coupled secondary antibody and tyramid signaling amplification on the second day. Then, slides were immersed in a microwaved boiling sodium citrate buffer for 8 minutes to strip the antibodies used to detect the first antigen, while the insoluble fluorophore-tyramide deposition is retained on the tissue. This allows to stain the slides with antibodies directed against another antigen in a second step (Francisco-Cruz et al., 2020; Lyu et al., 2020; Toth and Mezey, 2007).

For staining with the first antibody, slides were placed in a Coplin glass jar (115 mm x 90 mm) and filled with 70 ml of boiling sodium citrate buffer (10 mM, pH 6.0) for 2.5 minutes. Then the jar was covered with a lid and microwaved for an additional 8 minutes in a 700 W microwave oven. The lid was removed to allow slides to cool down in the buffer at room temperature for 25 minutes. Next, sodium citrate solution was replaced by 3% hydrogen peroxide (H<sub>2</sub>O<sub>2</sub>) in PBS for 30 minutes to quench endogenous peroxidase activity. Subsequently, slides were washed with phosphate buffer saline (PBS) for 10 minutes three times (Appendix. A.1). and stored between 1 to 2 days at 4° C. Slides were then incubated in a 3% Bovine Serum Albumin (BSA) (blocking reagent) in PBS (Sigma) and stored at 4 C° for 2 days. Slides were then incubated with the first primary antibody, anti-Eya1 GP1 (1:50, anti guinea pig polyclonal; Ahrens and Schlosser, 2005) diluted in PBS/BSA with 1% Triton X100 (Sigma) for 1 day in a humidified chamber the next morning slides were rinsed three times by PBS for 10 minutes each in order to prevent nonspecific background. Sections were then incubated in TNB blocking

solution (1.5 %, Perkin-Elmer) for 30 minutes and 250  $\mu$ l for each slide. For 2 hours, slides were incubated with secondary antibody: horseradish peroxidase enzyme HRP-coupled goat anti-guinea pig (Abcam, 6771,1:500) and diluted in PBS with 1% Triton X100 (Sigma) and 4',6-diamidino-2-phenylindole (DAPI, 100-500 ng/ $\mu$ l diluted from stock of 100  $\mu$ g/ml). Each slide was incubated with 100  $\mu$ l of antibody solution and covered by coverslip for 2 hours in a wet and dark chamber. Then coverslips and secondary antibody were removed by immersion in PBS and slides were rinsed by PBS buffer three time for 10 minutes each. The fluorophore–tyramide was diluted in its buffer (1:50) according to the manufacturer's instructions (PerkinElmer kit) and 100  $\mu$ l was added to each slide with coverslip for 1 hour in humidified and dark chamber. Slides were rinsed three times for 10 minutes each by PBS and kept at 4 C<sup>o</sup> between 2 to 3 days before moving to next step.

The second step required stripping the first antibody by using heating so, slides again were placed in a Coplin glass jar (115 mm x 90 mm) filled with 70 ml of boiling sodium citrate buffer (10 mM, pH 6.0) for 2.5 minutes. Then slides were immersed in this buffer solution with a lid and microwaved between 6 to 8 minutes in a 700 W microwave oven. The lid was then removed to cool down the solution at RT for 25 minutes. Next, sodium citrate solution was replaced by phosphate buffer saline (PBS) (Appendix. A.1) and slides were rinsed three times for 10 minutes each. At the same step, slides with PBS were kept in a glass jar at 4 C<sup>o</sup> for 2 days. Subsequently slides were incubated in a 3% Bovine Serum Albumin (BSA) (blocking reagent) in PBS (Sigma) and stored at 4 C<sup>o</sup> for 1 day. For each slide, 250  $\mu$ l was added (5  $\mu$ l Normal goat serum in 250  $\mu$ l PBS). The second primary antibody, Sox3 was diluted to 1: 100 (rabbit polyclonal; Zhang et al., 2003) in PBS/BSA with 1% Triton X100 (Sigma). To each slide, 100  $\mu$ l of primary antibody was added and the slide was then covered by a coverslip and incubated 2 days in wet chamber at room temperature. After that slides were rinsed three times for 10 minutes each. Slides were incubated with secondary anti body (1:500, Alexa594-conjugated anti-rabbit antibody; Invitrogen: Product number: A11012) and the

biotinylated secondary antibody was diluted in PBS/BSA with 1% Triton X100 (Sigma) for 2 hours at RT in a humidified and a dark chamber. Slides were transferred to a Coplin jar containing PBS and washed three times with PBS for 10 minutes each. Fluoroshield (Sigma: F6182) was added and slides were covered by coverslips. Slides were left for one day and sealed with transparent nail polish.

### **2.3.6 Peptide Competition Assay (PSA)**

The peptide competition assay was done with guinea pig anti-*Eya1* antibodies to confirm their specific binding in immunohistochemistry. The specific *Eya1* peptide against which these antibodies were originally raised was synthesized (RLSGSGDPSGTGLDNSHINSC, Eurogentec: product number: LAB2032) and co-incubated with the antibodies.

To prepare the blocking peptide solution, 1 mg of peptide was diluted in 1 ml PBS. Three tubes for each *Eya1* antibody were then prepared. The first tube contained only the antibody not pre-incubated with peptide and in the two other tubes the antibody was pre-incubated with peptide solution at two different ratios (5:1 & 10:1). Tubes were mixed gently and incubated at 4°C overnight. Immunohistochemistry was then performed using tyramide signal amplification. Finally, the staining pattern was compared between the blocked and unblocked antibody.

### **2.3.7 EdU (5-ethynyl-20-deoxyuridine) labelling and detection**

Cell proliferation is very important for normal tissue development. In this study, the thymidine analog 5-ethynyl-2'-deoxyuridine (EdU) was used to label cell proliferation cells. EdU can be incorporated into DNA during different stages of the cell cycle (including the S phase (Gorsuch et al., 2017; Okada and Shi, 2017)). In addition, EdU can be combined with other methods of staining such as immunohistochemistry and in situ hybridization (Okada and Shi, 2017).

The stock solutions were prepared according to Click-iT Plus EdU Alexa Fluor 594 and 488 Imaging Kit (Thermo Fisher Scientific). A 10 mM stock solution of Edu was prepared by adding 800  $\mu$ l 0.1 MBS solution to 5 mg of Edu powder and mixing well until the Edu was fully dissolved. Between 25 to 30 embryos were incubated in a 48-well plate with 500  $\mu$ l of Edu working dilution (200  $\mu$ l stock solution of Edu and 300  $\mu$ l of 0.1 MBS) for 16 hours on cold plate at 15° C prior to fixation at stages 26, 28, 29 and 35. For double immunostaining with EdU, first embryos were cryosectioned and immunostained with membrane GFP or Sox3 antibodies (see sections 2.3.2 and 2.3.3) (Table 2.1) before starting the EdU reaction. After incubating slides with secondary antibody for 2 hours, each slide was washed twice with 300  $\mu$ l of 3% BSA in PBS for 30 minutes at RT. The wash solution was removed to incubate each slide in permeabilization buffer; 500  $\mu$ l of 0.5% Triton X-100 in PBS for 20 minutes at RT. After removing of permeabilization buffer, slides washed twice with 300  $\mu$ l of 3% BSA in PBS for 20 minutes at RT. Click it reaction cocktail was prepared according to the Click-iT Plus EdU Alexa Fluor 594 and 488 Imaging Kit (Thermo Fisher Scientific). Then the wash solution was removed and incubated with 250  $\mu$ l of Click –IT reaction cocktail in each slide for 30 minutes at RT in dark chamber. Next, Click –IT reaction cocktail was removed and sections were incubated once with 300  $\mu$ l of 3% BSA in PBS for 30 minutes at RT for washing. For nuclear staining, DNA staining was proceeded by removing the wash solution and adding each slide 250  $\mu$ l of DAPI that was diluted in PBS (1:200). Each slide was washed three times for 10 minutes with 300  $\mu$ l of PBS. Fluoroshield (Sigma: F6182) was added and slides were covered by coverslip. Slides were left for one day and sealed with transparent nail polish.

## **2.4 Imaging and Data Analysis**

### **2.4.1 Microscopy**

An Olympus SZX7 stereomicroscope was used to determine the quality and stage of embryos. However, embryos that were injected by mGFP were checked for fluorescence using an Olympus SZX16 microscope equipped with a DP71 camera. Some images were taken using an Olympus BX51 compound microscope equipped with different fluorescent filters. The Olympus Cell D software package was used to adjust light balance and scale bar.

### **2.4.2 Confocal Microscopy**

Images were taken using an Olympus Fluoview 1000 Confocal Microscope to visualize fluorescence using two or three Diode lasers control d lasers lines that are 405 nm (blue), 448 nm or 473 nm (green), 559 nm or 635 nm (red). Two different oil immersion objectives were used (20x Fluor 0.85 NA working distance 2.0 mm and 60x Fluor 1.35 NA working distance 2.0 mm). For visual observation transmitted light observation was used at Olympus software (Olympus Fluoview FV1000). The brightness and contrast in every channel were adjusted as appropriate. The distribution of immunostained proteins was also followed by using z-stack technique. Images were scanned along the z-axis using a step size between 0.1  $\mu\text{m}$  to 1  $\mu\text{m}$ . The images were saved in TIF and JPG files. Finally, orientation, brightness and contrast were adjusted by importing the images into Photoshop CS5 (Adobe).

## **2.5 In situ hybridization**

Three embryos were analyzed in sections after in situ hybridization for *Neurog1*.

### **2.5.1 Synthesis of mRNA Probes for in situ hybridization**

Antisense oligonucleotide probes for in situ hybridization experiments were synthesized from 1  $\mu\text{g}$  of a PCR-product amplified from a plasmid, which has the gene of interest, *Neurog1*, inserted (Table 2.3). The antisense RNA probe was

synthesized using the DIG RNA Labelling Kit according to manufacturer's instructions (Roche; cat no.: 11175025910). In a 1.5 ml Eppendorf cup, 3  $\mu$ l linearized and purified plasmid (0.33  $\mu$ g/ $\mu$ l), 10  $\mu$ l DEPC-H<sub>2</sub>O, 2  $\mu$ l 10x NTP labeling mixture, 2  $\mu$ l 10x transcription buffer, 1  $\mu$ l RNase inhibitor (RNAsin) and 2  $\mu$ l RNA polymerase (T7) were added, mixed well and spun briefly. Then the reaction mixture was incubated for 2 hrs at 37° C. 2  $\mu$ l DNaseI (kit) was added after 2 hrs of incubation to remove the linear plasmid and was incubated for 15min at 37° C.

Synthesized probes were purified using the RNeasy kit according to the manufacturer's instructions (Qiagen, Cat. NO. - 74104) and diluted to a final concentration of 100 ng/ $\mu$ l with hybridization buffer and stored at -20° C (Table 2.3). The quantity and quality was tested using the NanoDrop ND100 machine.

**Table 2.3.** Vector and probe synthesis information for constructs used

Gene	Vector	Linearize	probe	source
<i>Neurog1</i>	pCS2+	PCR from pCS2+	T7	Nieber et al., 2009

### 2.5.2 Whole mount in situ hybridization

All the information on solution and buffers used in in situ experiments are given in Appendix. A.2.

In order to avoid RNase contamination, in-situ-hybridization experiment was conducted under carefully controlled conditions (gloves, use of DEPC-treated and autoclaved solutions until end of hybridization). PFA-fixed embryos, which had been transferred to 70% EtOH for long term storage were rehydrated in 50% EtOH

and 30% EtOH (made up with DEPC-H<sub>2</sub>O) for 5 minutes each, and washed three times for 5 minutes in Ptw (1x PBS + 0.1% Tween-20). Then the embryos were treated with Proteinase K for 4 minutes and washed two times in 0.1 M TEA (last step in 4 ml) for 5 minutes each. Then embryos were rinsed again twice for 5 minutes each with 0.5 ml TEA/acetic anhydride (250 µl acetic anhydride in 10 ml 0.1 M TEA). This was followed by washing two times in Ptw for 5 minutes each and fixation in MEMFA for 20 minutes at RT because embryos are fragile after Proteinase K treatment and have to be post-fixed. The embryos were 5 times washed with Ptw for 5 min each time and transferred to screw-capped tubes with 1 ml Ptw, during last wash. In each tube, 250 µl hybridization buffer was added and was removed when all embryos were settled in the tube bottom. Then a further 250 µl hybridization buffer was added and incubated for 10 minutes at 60° C. The hybridization buffer was again removed and each tube was then incubated for 6 hours in 250 µl of fresh hybridization buffer at 60° C. Hybridization buffer was then replaced by the 250 µl of digoxigenin-labelled RNA probes diluted 1:100 in hybridization buffer and returned to 60°C overnight.

After overnight incubation, the probe was replaced with 200 µl hybridization buffer, and embryos were incubated at 60°C for 10 minutes before washing each vial with 1 ml 2x SSC three times for 20 minutes at 60° C. The embryos were incubated for 30 minutes at 37° C with freshly prepared 2x SSC + RNase A (10 µl of 2 mg/ml stock) + 0.1 µl RNase T1. Embryos were then washed with 1 ml of 2xSSC for 10 min at RT, twice in 0.2x SSC at 60° C for 30 minutes each and twice in MAB for 10 minutes total at RT. Embryos were then pre-incubated in MAB + 2% BBR for 1 hr at RT and then in MAB + 2% BBR + 20% HIGS for 1 hour. Finally, the embryos were incubated overnight in MAB + 2% BBR + 20% HIGS with 1:1000 AP-coupled, anti-digoxigenin antibody (Roche) in the dark at 4° C (0.5 ml/vial).

On the 3rd day, the antibody solution was removed, and embryos were washed with 1x MAB five times for 1 hour each at RT. The embryos were again washed two

times in freshly prepared AP buffer for 5 minutes each. The embryos were then incubated in 0.5 ml NBT/BCIP-solution (AP buffer + NBT (4.5 µl [100 mg/ml] in 10 ml AP buffer) + BCIP (35 µl [50 mg/ml] in 10 ml AP buffer) and incubated at RT in the dark until the staining was apparent. Once the embryos were well stained, embryos were washed by 1x MAB for 3 times, 5 min each, at RT to stop the reaction. Finally, Embryos were re-fixed overnight in Bouin solution without picric acid at 4° C (2.5 ml Formaldehyde; 0.5 ml glacial acetic acid; 7.0 ml dH<sub>2</sub>O).

On the fourth day, background staining was removed by washing in 100% EtOH two times for 30 minutes each, and 70% EtOH, 50% EtOH for 5 minutes each. To remove pigmentation, embryos were bleached in bleaching solution at RT for overnight. Finally, embryos were washed in 1x SSC for 5 min, and then in 50 % EtOH for 5 min each and stored at 4° C in 70% EtOH.

### **2.5.3 Vibratome sections**

To prepare the specimens for sectioning, 4% Agar was dissolved in 100 ml of phosphate buffer (PB) (Appendix A.3) using machine hot plate to bring Agar to boiling point. The Agar was then left slightly to cool again before pouring into weighing boats. During the time, embryos were rehydrated from 70 % EtOH, via 50 % EtOH for 10 minutes and incubated in PB for 30 minutes. Carefully, each embryo was dried with a tissue paper and then embedded in the warm agar for 20 minutes.

After the agar solidified, it was trimmed and cut at 20-50 µm with the vibratome. Sections were collected on super frosted slides. Sections were left to dry 2 hours and cover slipped with Fluoroshield (Sigma: F6182) and coverslipped. Each side of the cover slip was fixed with nail polish to protect the embryo.



## **2.6 Generating a construct with a hormone- inducible dominant- negative from of Six1 (GR-EnR-Six1)**

### **2.6.1 Sub-Cloning of Hormone Inducible Gene (GR) to pCS2--EnR-Six1 Plasmid**

In the sub cloning process, the hormone inducible glucocorticoid receptor (GR) was removed from the pCS2- GR-Sox3-GFP plasmid (Zhang and Klymkowsky, 2007) by restriction digestion with with HindIII and ClaI and was sub-cloned into the corresponding sites of the expression vector pCS2-EnR-Six1 plasmid (Brugmann et al., 2004), which contains the Engrailed repressor domain (EnR) and the Six1 DNA-binding domain.

### **2.6.2 Restriction enzyme digest of insert and plasmid**

In order to avoid enzyme incompatibility in the digestion process, single restriction enzymes were used for the restriction digestion followed by another enzyme. When the restriction digestion reaction was completed, the digested plasmid and inserts were taken into purification using the RT-PCR purification Qiagen kit to clean the reaction mixture. After second restriction digestion, the restriction digestion was confirmed by running 1 % agarose gel electrophoresis. Once the restriction digestion was confirmed, the plasmid and insert were taken into the ligation reaction. On the first day, the standard 50 µl units of the reaction mixture were prepared by adding 10 µl plasmid/inserts (of 1 µg/µl) into 30 µl H<sub>2</sub>O and then adding 5 µl of restriction enzyme A for both plasmid/insert (HindIII), 5µl of restriction buffer A (10X R Buffer) After mixing, the reaction mixture was left at 37° C for overnight.

On the second day, the digested DNA was purified using the RT-PCR purification kit (Qiagen). 250 µl buffer PB was added to 50 µl restriction reaction and transferred to a column that was applied to a new Eppendorf tube. Then column was spun at maximal speed

(12,000rpm) and the flow through was removed. The column was put back in same tube, and was spun again at max speed (12,000rpm) and the flow through was removed, 750 µl PE buffer was added. Again, column was put back and spun another time, removing the flow through. The column was then transferred to a collection tube and DNA was eluted with 40µl buffer EB (10mM Tris, pH 8.5).

Next, a 50 µl reaction was prepared by adding 5µl restriction enzyme B (Bsu 151- ClaI) and 5µl restriction buffer B (10X Buffer Tango) to the 40 µl elute. The reaction mixture was mixed and left at 37° C for overnight.

### **2.6.3 Gel electrophoresis and DNA purification by Gel Extraction**

On the third day, the restriction reaction was run on a large 1% Agarose gel. The 1% Agarose gel was prepared in 1x TAE buffer (0.8 ml 50x TAE or 1.6 ml for Fisher minichambers) (Appendix. A.4) with 2 µl SybrSafe (10000x; Invitrogen) added at approximately 50°C. The gel was left to cool in-chamber for around 30 minutes. Then 1x TAE was added into chamber and comb was removed. Gel was loaded with DNA (1 µl loading buffer + 10 µl DNA; 3 µl 1kb DNA ladder (Fisher, Cat.No-5M0311)). Gels were run at 90 V for approximately 45 minutes (or until lower blue bands approached the end of the gel).

A gel extraction kit (Qiagen, Cat. No.-28706) was used for DNA extraction. The proper bands were cut out (GR insert region and EnR-Six1 plasmid) from the gel slab and taken into Eppendorf tubes. The bands were then weighed (weight in mg = approx. volume in µl). Three volumes of buffer QG was added to gel bands and heated at 50° C for 10 min until the gel was dissolved by shaking it every 2 min. Then one volume of isopropanol was added and mixed. After applying the mixture to Qiagen quick spin column, it was centrifuged at 10,000 rpm for 1 min and the flow through was discarded and then 0.5 ml of buffer QG was added and then centrifuged again at 10,000 rpm for 1min. To wash the spin column, 0.75 ml buffer PE was added and incubated for three minutes and then centrifuged at 10,000 rpm

for 1 min. To remove all the rest of PE buffer, the flow through was discarded, centrifuged again at 10,000 rpm for 1min. 30 µl nuclease free water was added in the spin column for elution and incubated for 1 min and then centrifuged at 10,000 rpm for 1min. NanoDrop ND1000 was used to check the sample quality and quantity and the sample was then stored at -20° C.

#### **2.6.4 Ligation**

The insert of interest (GR) was ligated or joined to the HindIII and ClaI digested pCS2-EnR-Six1 plasmid using the T4 ligase enzyme (NEB, Cat. No.-M0202S). The insert of interest was used at approximately 1 to 6x times the concentration than the plasmid (e.g. 10 ng insert with 50 ng plasmid in a 10 µl reaction). The ligation reaction mixture was prepared by adding 1 µl eluate of target and then 14 µl eluate of insert was added. Finally, 0.4 µl T4 ligase and 2 µl T4 buffer were added followed by adding 2.6 µl with dH<sub>2</sub>O. Then the reaction mixture was incubated for overnight at 37° C.

#### **2.6.5 Transformation and plating of bacteria**

2.5% Luria Broth (LB) was prepared in distilled H<sub>2</sub>O (dH<sub>2</sub>O) in 100 ml Erlenmeyer flasks, sealed with aluminium foil and autoclaved. 9.25 g LB agar was added in 250 ml dH<sub>2</sub>O, and supplemented with an appropriate antibiotic (e.g. ampicillin 100 µg/ml) then was taken for autoclaving. When LB agar was cold enough to touch, LB agar was poured in agar plates up to cool at RT and plates were stored upside down at 4°C. XL1-Blue competent *E. coli* cells (Agilent; cat no.: 200249) were thawed on ice and transformed according to manufacturer's instructions. 100 µl XL1-Blue competent cells were aliquoted into sterile Eppendorf cups and 1.7 µl of 1.42 M β-mercaptoethanol (kit; toxic! fume hood) was added to 100 µl bacteria for 10 minutes incubation. Then 2.5 µl of ligated plasmid was added for 30 minutes on ice. Heat shock was given to the bacteria for 45 seconds at 42° C using a preheated thermal block and they were then transferred to the ice for 2 min. After

heat-shocking the bacteria, 900 µl LB medium was added and bacteria were left to recover at 37°C for one hour. Two plates were prepared for each plasmid, 100 µl of recovered bacteria were added onto the first plate and spread with a sterile tool. The remaining 900 µl of recovered bacteria were centrifuged for 8' at 6000 rpm and the upper 800 µl LB media were removed, the bacteria re-suspended in the remaining 100 µl, and plated on the second agar plate by spreading with a sterile tool. Plates were incubated upside down at 37° C overnight. Once the colonies were grown on the next day, they were taken into Mini Prep or Midi Prep.

### **2.6.6 Plasmid Extraction from Bacteria by Mini Prep Protocol**

The TELT Mini Prep protocols was used for small quantity DNA material, while for larger quantity, the Macherey Nagel NucleoBond Midi Prep Kit (Cat No – 740410.10) were used (see 2.6.7).

A single colony was picked with a sterile pipette tip (only touched with sterilized forceps that has been dipped into 70% EtOH and flamed) inoculating 10 ml LB containing the antibiotic ampicillin (final conc. of 100 µg/ml). The bacteria were cultured at 37 °C overnight on shaker. 1.5 ml of this bacteria culture were taken and centrifuged for 5 min at 5000 rpm. The supernatant was removed.

The pellets were re-suspended in the 100 µl TELT buffer (Appendix. A.5) and vortexed for mixing and 10 µl lysozyme (10 mg/ml) was added to the pellet and incubated for 10 min at RT. At 100 °C (heating block or water bath), the pellets with lysozyme were boiled for two minutes in a Eppendorf cup with a perforated lid, then they were kept on ice for 2 min for cooling. Next, the pellets were centrifuged for 10 min at maximum speed of 13,000 rpm. The supernatants were transferred into a new reaction tube and the pellets removed with a sterile toothpick. 100 µl isopropanol was added to the supernatant and incubated for 10 min at RT and then, the supernatant was centrifuged for 10 min at maximum speed to precipitate the DNA pellet and the supernatant was discarded. The DNA pellets

were washed in 0.5 ml 70 % EtOH and again centrifuged for 5 min at max speed. The supernatant was removed and the DNA pellets were dried inside a fume hood. Finally, the pellets were re-suspended in 50 µl DEPC-H<sub>2</sub>O. the pellets were confirmed by running a 1% 1x TAE agarose gel for the DNA quality. The quantification and quality control was done using a NanoDrop ND100.

### **2.6.7 Restriction test digest and Midiprep**

The presence of an insert of the proper length was confirmed by preparing a 10 µl restriction reaction (double digest) for 5 µl product from Minipreps (four samples) adding 1 µl restriction enzyme A (HindIII), 1 µl restriction enzyme B (ClaI), 1 µl restriction buffer (10X Buffer Tango) and 2 µl dH<sub>2</sub>O. This was left at 37° C for several hours or overnight and analyzed by gel electrophoresis.

Minipreps confirmed by restriction digestion colonies were then used to inoculate Erlenmeyer flasks containing 100 ml LB supplemented with the appropriate antibiotic (ampicillin; 100 µg/ml). Bacteria were cultured overnight shaking (250 rpm) at 37° C. Plasmids were extracted using the NucleoBond® Xtra Midi Kit according to the manufacturer's instructions (Macherey-Nagel; cat no.: 740410.10) . Pelleted DNA was dissolved in 100 µl H<sub>2</sub>O and transferred to labelled Eppendorf tubes.

The sub-cloned plasmids were confirmed by sequencing by LGC Genomics (<http://www.lgcgroup.com/our-science/genomicsolutions/> - VsHh58c3RtI). The sequences were analysed using the Geneious Software 59).

## **2.7 Western Blot**

Western blot analysis allows to confirm the presence or absence of an individual protein and its expression level by using an antibody. Furthermore, from many

thousands of proteins, western blot can identify a single protein within a cell or tissue lysate.

### **2.7.1 *In vitro* Transcription and Translation**

A Promega TNT coupled reticulocyte lysate kit (Cat. No. L4600) was used. The following solutions were mixed to prepare the reactions: 12.5  $\mu$ l, TNT buffer 1  $\mu$ l, RNA polymerase (SP6) 0.5  $\mu$ l, amino acid mix-methionin 0.25  $\mu$ l, amino acid-leucin 0.25  $\mu$ l, RNAsin 0.5  $\mu$ l. 2  $\mu$ g pCS2-Eya1 alpha in DEPC-H<sub>2</sub>O (Appendix. A.2). Reaction solution was spun briefly, and incubated for 2 hours at 30°C. Finally, synthesized RNA was stored at -20°C.

### **2.7.2 PAGE (Polyacrylamide Gel Electrophoresis)**

PAGE (catalogue number: PCG2017-10EA) was performed by first building up the vertical gel chamber. Then electrode buffer (Appendix. A.6) was filled in, and comb was removed. Finally, samples were prepared from TNT reactions as follows: 2  $\mu$ l TNT reaction were mixed with 2  $\mu$ l 20% SDS (20g of SDS was dissolved into 80 ml of dH<sub>2</sub>O by stirring) (sodium dodecyl sulfate, Fisher Scientific, Product number: BP166-500) and 4  $\mu$ l Sol E (2x) (Appendix. A.2). Furthermore, 1  $\mu$ l length marker and 7  $\mu$ l Sol E (2x) were used for protein length marker. Sample and length marker solution were denatured for 5 minutes at 99°C and centrifuged for 1 minute at 10,000 rpm. Gel was loaded in first run at 20mA, approx. 20'. Then gel was run at 30 mA (20-40 mA will work) until blue band has reached bottom (approx. 1 hour).

### **2.7.3 Protein extraction protocol**

Twenty embryos were injected (5 nl) with Eya1 (100 ng/ $\mu$ l) and Histone H2B-GFP mRNAs (50 ng/ $\mu$ l) at the two-cell stage. Twenty additional embryos were injected with Eya1 (100 ng/ $\mu$ l) and Histone H2B-GFP mRNAs (50 ng/ $\mu$ l) as well as Eya1

MOs (Eya1-MO1 and Eya1-MO2) at concentration 25  $\mu$ M each. After completion of gastrulation, embryos were frozen at -80 °C. In order to extract the proteins, in each tube of twenty embryos 100  $\mu$ l extraction buffer (Appendix A.6) were added and pipetted until the mixture was homogeneous. 100  $\mu$ l Freon was added, vortexed and centrifuged three minutes at full speed. The protein was extracted from the upper phase, avoiding the dark interface between the two phases.

#### **2.7.4 Preparing the PAGE samples**

In each tube the following solutions were added: 10.4  $\mu$ l of protein extract, 4  $\mu$ l of LDS sample buffer 4x and 1.6  $\mu$ l of DTT 10x. The mixture was heated for 10 minutes at 70° for one minutes, and then centrifuged for 1 minute 10,000 rpm. Finally, it was loaded in the gel.

#### **2.7.5 Blotting**

When PAGE was run, a blotting chamber was prepared and approximately 3 l 1x borate transfer buffer (BTB) were prepared (Appendix. A.6). A PVDF membrane was immersed in 100% methanol to activate it for 30 seconds and stored in 1x BTB. A sandwich of 3 layers of filter paper (Whatman 3mm), the PAGE gel, the PVDF membrane and another 3 layers filter paper was made and wetted with BTB. Gently, air bubbles were removed by rolling of glass pipette. Afterwards, the sandwich was inserted into the blotting chamber, which was filled with 1x BTB. Proteins run towards positive pole. The following settings and were used at maximal voltage: 20 minutes at 200 m, 20 minutes at 300 mA, 20 minutes at 400 mA, 60 minutes at 530 mA. Blotting was done at 4° C. The PVDF membrane was then removed and stained by using Coomassie solution (Appendix. A.6) for 1 minute. PVDF membrane was transferred to differentiating solution (Appendix. A.6) between 20-45 minutes until the bands were visualized. By using a pencil, lanes and bands were marked and membrane was left to dry for 20 minutes and scanned in.

The membrane was then washed with PBST (Appendix. A.6) three times for 10 minutes each. For TNT reactions, primary antibodies (a polyclonal guinea pig 1 or 2 anti-*Eya1* antibody) were prepared and diluted 1:1000 in PBST adding some milk powder. For embryo extracts, the primary antibody (a polyclonal guinea pig anti-*Eya1* antibody) was prepared and diluted 1:500 in PBST adding some milk powder. Membranes were then sealed into plastic bags together with primary antibody solution using 10 ml solution/blot. For overnight incubation at 4<sup>0</sup> C, the plastic bag was placed on a shaker and rocked gently. Subsequently, the membrane was washed three times for 10 minutes each. Secondary antibody used was HRP-coupled goat anti guinea pig-antibody (Abcam, 6771). This antibody was diluted 1:5000 in PBST with some of milk powder using 10 ml solution/blot. Again, it was washed by using PBST three times for 10 minutes each. Chemiluminescence substrate was then prepared (Perbio or Transcend; Promega) by adding 0.75 ml solution A to 0.75 ml solution B. The blot was incubated in this solution for 1-5 minutes and sealed into transparent plastic foil. It was then photographed in the dark in the sensitive gel documentation unit (Appendix. A.6).



### Chapter-3 Neurogenesis in the otic placode

In *Xenopus*, the otic vesicle begins to form by invagination from the posterior placodal area at stage 22/23. At stage 28, the otic vesicle has completely separated from the ectoderm and differentiating neurons start to leave the ventromedial otic vesicle to form vestibulocochlear ganglion cells (Sadaghiani and Thiébaud, 1986; Schlosser and Northcutt, 2000; Schlosser and Ahrens, 2004; Schlosser et al., 2008; Sullivan et al., 2019). After formation of the otic vesicle, neuroblasts delaminate and migrate from the otic vesicle to form the vestibulocochlear ganglion (VCG). The VCG contains afferent neurons, which innervate the mechanosensory hair cells of the membranous labyrinth and transmit the information to the brainstem (Alsina et al., 2009; Barald and Kelley, 2004; Freyer and Morrow, 2010; Hemond and Morest, 1991; Ma et al., 2000; Nornes et al., 1990; Schlosser, 2006, 2010 and Schlosser and Northcutt, 2000).

The neurogenic region of the otic vesicle, which generates the sensory neurons of the VCG as well as secondary sensory cells, is characterized by a network of genes including *SoxB1* family genes (*Sox1*, *Sox2* and *Sox3*). These genes maintain cells in a proliferating progenitor state and must be downregulated to permit neuronal differentiation. A number of other transcription factors encoded by basic helix loop helix (bHLH) family genes then act as proneural genes which initiate neuronal differentiation (Baker and Brown, 2018; Fritzsche et al, 2006; Schlosser, 2010, 2006). Proneural genes (bHLH) can be categorized into many subfamilies that act differently during neurogenesis, neuronal differentiation and gliogenesis. For example, *Neurog1* is a neuronal determination (proneural) gene and expressed in progenitor cells of sensory neurons that are still mitotically active while *NeuroD1* is a neuronal differentiation gene and expressed later in postmitotic cells downstream of *Neurog1*. Both *Neurog1* and *NeuroD1* have been shown to overlap with *Sox2* and/or *Sox3* expression in the otic vesicle and elsewhere and are activated by these *SoxB1* transcription factors (Alsina et al., 2009; Baker and Brown, 2018; Gou et al., 2018; Pozzoli et al., 2001; Schlosser et al., 2008).

### 3.1 Time course of neurogenesis and neuronal delamination

To determine the time course of neuronal delamination from the otic vesicle, in the present study particular attention has been directed to the basal lamina, which has been mostly ignored in previous studies. Basal lamina and neurites were marked by using antibodies for laminin and acetylated tubulin antibody, respectively. Additionally, embryos injected with membrane green fluorescent protein (mGFP) were used to label membranes of the epithelial cells of the otic epithelium (Figs. 3.1 A-B-C-J).

At stage 26 the otic vesicle has largely invaginated and the basal lamina surrounded the entire basal surface of the otic vesicle (Fig. 3.1 A). Reorganization of the basal lamina takes place where otic epithelia are in the process of fusion laterally and separate from overlaying ectoderm (Fig. 3.1 A-B). In addition, in some embryos the basal lamina can be seen disrupted on the medial side of the otic vesicle already at stage 26 and such disruptions are frequently seen at stage 28 (Fig. 3.1 B-D). At the same time the basal lamina continues to reorganize laterally (Fig. 3.1 B-D). mGFP staining suggests that labeled epithelial cells begin to migrate out of the medial side of the otic vesicle at stage 28 (Fig. 3.1 B). In order to understand more about the cell shapes, these were reconstructed from mGFP staining of a z-stack and are shown in a schematic diagram (Fig. 3.1 B). The epithelial cells of the otic vesicle are of overall columnar shape and extend all the way from lumen to basal lamina comprising a single layer (blue and purple cells) (Fig. 3.1 B-C). However, the nuclei of neighboring cells were positioned at different levels giving the appearance of more than one layer (Fig. 3.1 B, D). The features described demonstrate that the otic vesicle epithelium is a pseudostratified columnar epithelium. The apical to basal lengths of the epithelial cells are shorter on the lateral sides of the otic vesicle than on its dorsal and ventromedial sides measuring approximately  $44.93 \pm 7.47 \mu\text{m}$  (10 cells) on the dorsal and ventromedial side of the otic vesicle and  $24.28 \pm 3.29 \mu\text{m}$  (10 cells) on the lateral sides (Fig. 3.1 B). At higher magnification superimposition of cell outlines on laminin staining shows

that the basal lamina is displaced on the medial side of the otic vesicle by lamellipodia which protrude from cells probably migrating out of the epithelium of the otic vesicle (Fig. 3.1 C-D). Furthermore, some cells form blob-like protrusions through gaps in the basal lamina (Fig. 3.1 C-D).

At stages 32, 33/34 and 35, the basal lamina continues to be disrupted and cells continue to delaminate in this central portion of the medial otic epithelium., Delaminated cells congregate to form the vestibulocochlear ganglion between the dorsal half of the otic vesicle and the hindbrain (Fig. 1 E-I). In the present study, double staining of acetylated tubulin with laminin was used to study the formation of neurites from differentiated neurons originating from the developing otic vesicle (stage 25-39). At stage 25, the acetylated tubulin antibody only stains cilia on the apical surface of otic epithelial cells but no neurites are evident in the vicinity of the otic vesicle (not shown). During the progress of development, the acetylated tubulin antibody labels some neurites in the vestibulocochlear ganglion (VCG) from stage 32 on, which suggests that delaminating neurons have begun to send out neurites, and the number of acetylated tubulin labeled neurites are increased in later stages (Fig. 3.1 G, J).

At later stages (stages 32-35), the basal lamina surrounding the epithelial cells of otic vesicle continues to show breaks on the ventromedial side of otic vesicle, from where epithelial cells migrated to the site of the VCG and axons of the vestibulocochlear nerve can be recognized between the otic vesicle and the hindbrain (Fig. 3.1 E-J). While the medial gaps are still clear in the basal lamina next to the ganglion at stages 32-35 (Fig. 3.1 E-I), they have closed by stage 39 in a maximum intensity projection image (Fig. 3.1 J). At stages 32-39, cells and acetylated tubulin stained axons are seen sandwiched between the otic epithelium and the basal lamina on the ventromedial side of the otic vesicle (Fig. 3.1 E-J), suggesting that cells delaminating on the ventral side of the otic vesicle migrate dorsally on the inside of the basal lamina before joining the ganglion. At stage 39,

the acetylated tubulin labelled axons emanating from the VCG can be seen to course towards the brainstem (Fig. 3.1 J).

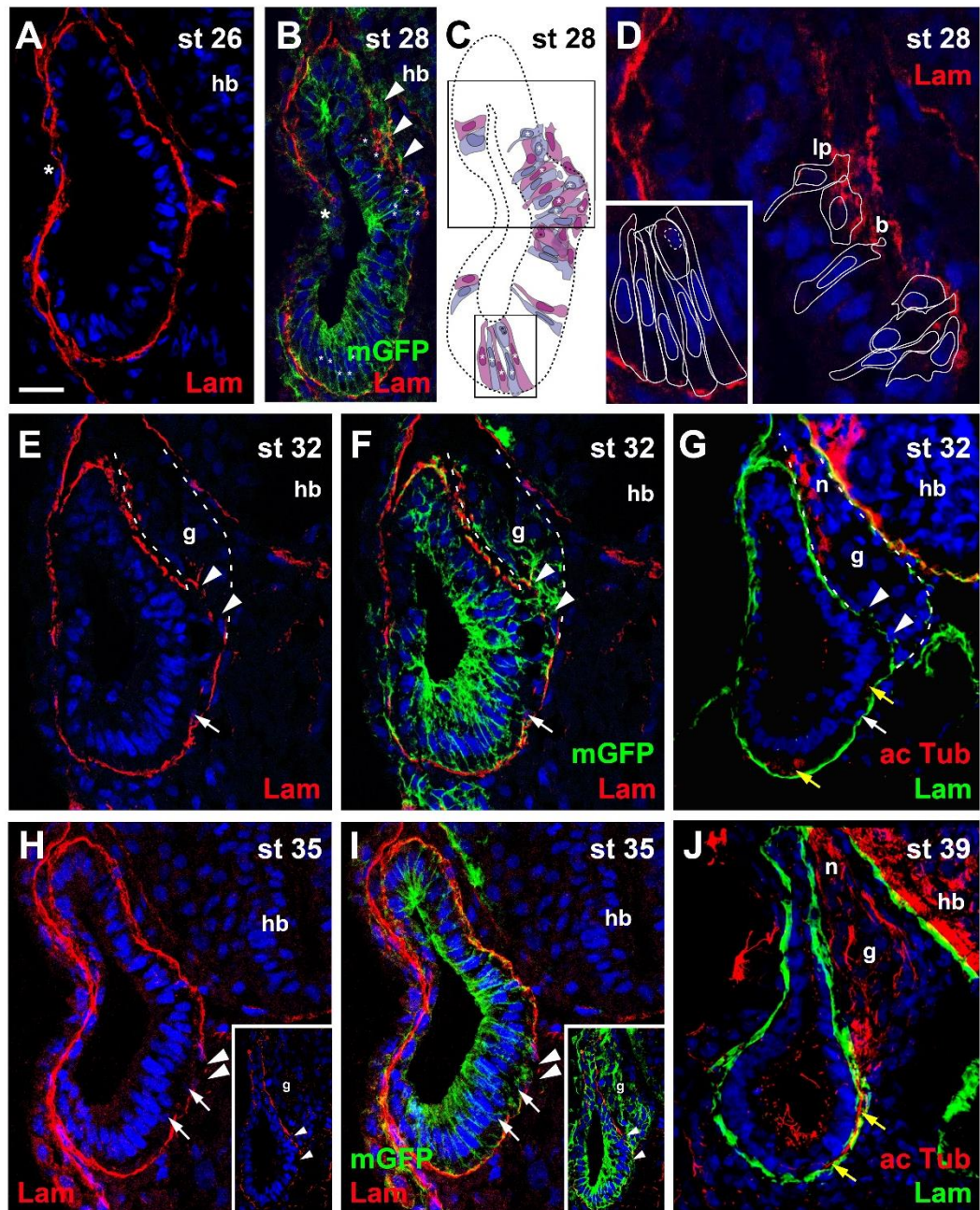


**Fig. 3.1. Time course of neurogenesis and neuronal migration in the otic vesicle.** Immunostaining for laminin (Lam) in transverse sections through the center of the left otic vesicle of *Xenopus* embryos from stage 26 to 39 analyzed in single confocal planes (A-G) or maximum intensity projections of z-stacks (H-J) (dorsal to the top, medial to the right). Some sections have also been immunostained for acetylated tubulin (G, J) or a membrane bound form of GFP (mGFP) following mGFP mRNA injection (B, F, I). DAPI was used to label nuclei. Different channels of same section shown in E, F and in

**H, I**). Arrowheads indicate breaches in the basal lamina. **b**: blob; **g**: vestibulocochlear ganglion; **hb**: hindbrain; **lp**: lamellipodium; **n**: vestibulocochlear nerve. **A**: At stage 26 the otic vesicle has largely invaginated and is surrounded by a basal lamina. Reorganization of the basal lamina takes place where otic epithelia are in the process of fusion laterally (asterisk). **B-D**: At stage 28 the first breaches appear in the basal lamina on the medial side of the otic vesicle (arrowheads), whereas reorganization of the basal lamina continues laterally (asterisk). **C** shows cell shapes reconstructed from mGFP staining of a z-stack, from which **B** was taken. Cells are shown in alternating blue and purple colors for clarity. They form a single-layered, pseudostratified epithelium. Outlines of cells marked with asterisks in the black boxes in **C** are shown at higher magnification in **D** superimposed on laminin staining. Laminin is displaced where lamellipodia protrude from cells which probably migrate out of the otic vesicle. Some cells form blob-like protrusions through gaps in the basal lamina. **E-J**: At later stages (stages 32-39) the ganglion (**g**; outlined with white hatched line in **E-G**) and axons of the vestibulocochlear nerve (**n**) can be recognized between the otic vesicle and the hindbrain. **H** and **I** show a section through the stage 35 otic vesicle immediately posterior to the main body of the ganglion, while a section through another otic vesicle at the center of the ganglion is shown in insets. At stages 32 (**E-G**) and 35 (**H, I**) there are still medial gaps in the basal lamina next to the ganglion, but these have closed by stage 39 (**J**). Cells on the ventromedial side of the otic vesicle (white arrows) and acetylated tubulin stained axons (yellow arrows) located between the otic epithelium and the basal lamina are indicated. Scale bar in **A**: 25  $\mu\text{m}$  (for all panels).

### **3.2 The otic epithelium as a pseudostratified epithelium with apical-basal cell polarity**

In my study, mitotic cells were identified using an antibody recognizing phosphorylated histone H3 (pH3) in stages 26.

Observation by confocal microscopy showed that pH3 antibody revealed mitotic cells throughout the entire otic epithelium at lateral, medial and ventral side in stages 26 (Fig. 3.2 A-C). Mitotic nuclei were typically located near the apical surface of neighboring otic epithelial cells, close to the lumen of the otic vesicle). This suggests that the otic epithelium is polarized along the apicobasal axis and that nuclei in the *Xenopus* otic epithelium probably undergo interkinetic nuclear migration from an apical position at mitosis to a more basal position during the S-phase of the cell cycle and back as described for the neuroepithelium and some placodes in other vertebrates (Sauer, 1936; Spear and Erickson, 2012; Alsina and Whitfield, 2017).

Apical-basal polarity is a fundamental property of epithelial cells and helps to determine the specialized functions of epithelial cells, including the formation of a permeability barrier between adjacent cells. In addition, apical-basal polarity is important during development where it may regulate asymmetric cell divisions thereby affecting cell lineage decisions and the balance between progenitor and differentiating cells (Krahn et al, 2009; Petronczki and Knoblich, 2001; Zhong and Chia, 2008).

To characterize the apical-basal polarization of the otic epithelium, I investigated the spatial distribution of the cell polarity proteins PAR3, aPKC, phosphorylated Myosin light chain (MLC) and of N-cadherin in the *Xenopus* otic vesicle. Also, mGFP was used to label the plasma membrane of the cells comprising the otic epithelium and helps to confirm protein distributions in epithelial cells. To visualize the cell membrane embryos were injected with membrane-bound GFP at the two-cell stage and then analyzed at stages 26-40 (Figs. 3.2 E-F, G-H-I-K-L and N-O).

At stage 26, when the otic vesicle has almost fully invaginated, mGFP staining shows that otic epithelial cells are elongated, columnar cells (Figs. 3.2 A-O and 3.3 A). However, the positions of the nuclei varied give the epithelium a stratified (multilayered) appearance (Figs. 3.2 E-F, G-H-I-K-L and N-O).

The Par3 antibody revealed enrichment of Par3 at the luminal margin of the epithelial cells of the otic vesicle, that is on the apical surface of epithelial cells (Fig. 3.2 D-F). Additionally, PAR3 was also seen apicolaterally and there were many PAR3 spots distributed in nuclei (Figs. 3.2 D-F and 3.3 A-C). Par3-immunopositive spots were also found attached to the outside of many nuclei (perinuclear staining) and these were often closely associated with separate spots of Par3 in the adjacent cell membrane (Fig. 3.3A, D-E). Furthermore, single spots and big clusters of Par3 distribution were observed in cytoplasmic regions of the otic vesicle epithelium (Fig. 3.3 A-C).



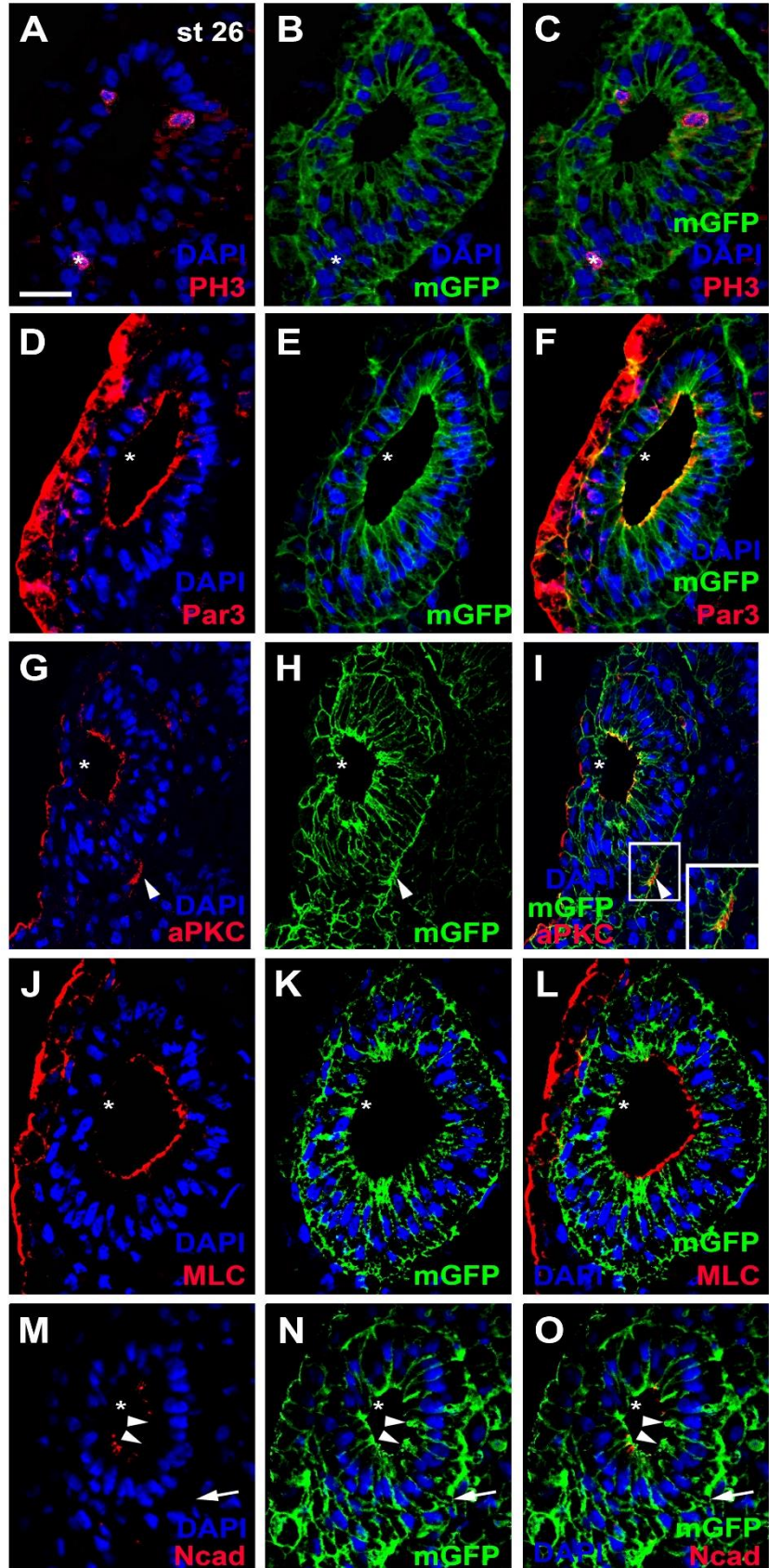


**Fig. 3.2. Distribution of mitoses and apico-basal markers in the otic epithelium at stage 26.** Transverse sections through the center of the left otic vesicle of *Xenopus* embryos at stage 26 analyzed in single confocal planes (dorsal to the top, medial to the right). Sections have also been immunostained for membrane GFP (mGFP) following mGFP mRNA injection. DAPI was used to label nuclei. Different channels of same section shown in **A-C**; **D-F**; **G-I**; **J-L**; **M-O**. **A-C**: Mitotic, pH3 positive cells in the otic epithelium (asterisks) are located near the apical (luminal) surface. **D-O**: Immunostaining for cell polarity proteins Par3 (**D-F**), aPKC (**G-I**), MLC (**J-L**) and N-cadherin (Ncad; **M-O**). Note the prevalence of apical and/or apicolateral staining. Apical PAR3, aPKC, MLC, and N-cadherin staining is notably absent from the lateral domain of the otic epithelium, where invaginating epithelia fuse (asterisk). In addition to its distribution on the apical side of the otic vesicle, aPKC is localized to basal protrusions on the ventromedial side of the otic epithelium (white arrowheads in **G-I**). White boxed area in **I** is shown at higher magnification in insets. Ncad-staining is also absent from the medial and ventromedial otic epithelium (arrowheads), where cells begin to form basal protrusions (arrow). Scale bar in **A**: 25  $\mu\text{m}$  (for all panels).

Interestingly, antibodies to aPKC and MLC showed a relatively similar distribution to the PAR3 protein on the apical side of medial otic epithelium (Figs. 3.2 G-L and 3.3 F-I), although apical staining of aPKC and MLC is stronger and more homogeneous (Figs. 3.2 G-L and 3.3 F-G, H-I). MLC and aPKC were also highly enriched on the apicolateral side of otic epithelial cells (Figs. 3.2 G-L and 3.3 F-G, H-I).

Similar to Par3, MLC expression and aPKC were also found in cytoplasm and were associated with some nuclei (perinuclear) (Fig. 3.3 F-I). aPKC also showed staining of cell membranes adjacent to perinuclear staining (Fig. 3.3 F-I).

Interestingly, in some sections of stage 26 embryos, there were protrusions from some epithelial cells on the basal side of the epithelium. aPKC-immunostaining was found in the cell membrane of such protrusions marking presumably the



leading edge of cells starting to delaminate from the otic vesicle to form the vestibulocochlear ganglion (Fig. 3.2 G-I).

Because Dent's fixative had to be used for immunostaining of N-cadherin, shrinkage and tissue shape were different from the PFA fixed embryos used for immunostaining of aPKC, Par3 and MLC and the otic vesicle appeared more circular (Fig. 3.2 M-O). At stage 26, N-cadherin is weakly expressed on the apical side of the epithelial cells in some sections but is always strongly expressed on the apicolateral side, probably localizing to adherens junctions (Figs. 3.2 M-O and 3.3 J-K). I examined N-cadherin distribution in epithelial cells more closely at higher magnification to show N-cadherin distribution in small clusters at apicolateral side of otic epithelium (Figs. 3.2 M-O and 3.3 J-K).

Once cells have started to delaminate from the otic epithelium, there are some notable changes in the distribution of cell polarity proteins. At stage 35, the otic vesicle has grown in size and the dorsal zone has extended and narrowed (Figs. 3.4, A, D, I-K). The kidney shape with indentation of the lateral side, which is observed in PFA-fixed embryos (immunostained for Par3, aPKC and MLC) is not present in Dent- or Bouin-fixed embryos (immunostained for N-cadherin or PCNA; see below) suggesting that it represents an artefact of PFA fixation.

At stage 35, PAR3 could no longer be detected on the apical or apicolateral side of otic epithelial cells (Fig. 3.4 A-G). However, strong and irregular distribution of PAR3 was observed in vestibulocochlear ganglion cells. Remarkably, PAR3 distribution was found throughout the cell membrane of vestibulocochlear ganglion cells including their leading edge (axon forming) and trailing edge (dendrite forming) (Fig. 3.4 A-H). MLC has become strongly reduced on the apical and apicolateral side of otic epithelial cells (Fig. 3.5 A-G). There was a weak distribution of MLC in the cytoplasm of vestibulocochlear ganglion cells (Fig. 3.5 A-G). In contrast, aPKC expression was still concentrated in apical and apicolateral sides of the otic epithelial cells similar to the previous stage (stage 26) (Fig. 3.5 I-

P). In addition, aPKC expression was found in neurons of the vestibulocochlear ganglion adjacent to the otic vesicle (Fig. 3.4 I-P). By following z-stack images, aPKC distribution was found to be enriched in membranes of the leading and trailing edge of delaminating ganglion cells (Fig. 3.4 M-P). There are no major changes in the distribution of N-cadherin at stage 35 (not shown).

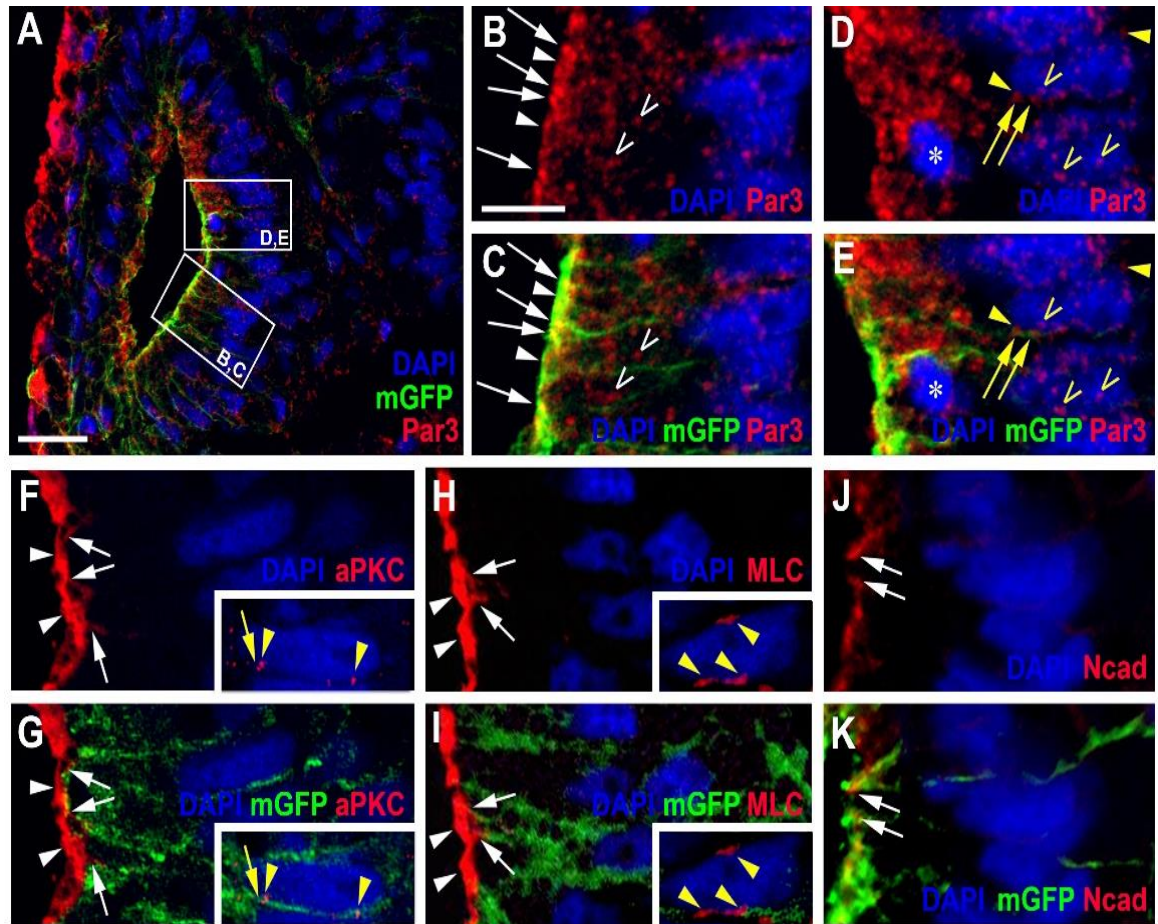


**Fig. 3.3. Apico-basal polarity in the pseudostratified otic epithelium at stage 26.** Immunostaining for the cell polarity proteins Par3, aPKC, MLC and N-cadherin (Ncad) in transverse sections through the center of the left otic vesicle of *Xenopus* embryos at stage 26 analyzed in single confocal planes (dorsal to the top, medial to the right). Sections have also been immunostained for membrane GFP (mGFP) following mGFP mRNA injection. Distribution of cell polarity proteins in medial otic epithelium as indicated in overview (A; Par3) and higher magnified views of Par3 (lower and upper box in A shown in B, C and D, E, respectively), aPKC (F, G), MLC (H, I) and N-cadherin (J, K). DAPI was used to label nuclei. Different channels of same region shown in B, C; D, E; F, G; H, I; J, K. Inserts in F-I show nuclei from adjacent cells in medial otic epithelium, which show clear perinuclear and membrane staining. All proteins are localized to the apical (Par3, aPKC, MLC) and/or apicolateral (Par3, aPKC, MLC, Ncad) surface of cells. In addition, Par3 is localized to some cytoplasmic regions and nuclei and Par3, aPKC and MLC show staining of membranes and perinuclear staining associated with some nuclei. White arrowheads indicate apical staining; white arrows: apicolateral (junctional) staining; white open arrowheads: cytoplasmic staining; yellow arrows: membrane staining next to nuclei; yellow arrowheads: perinuclear staining; yellow open arrowheads: nuclear staining; asterisk in D, E: dividing nuclei. Scale bars: A: 25  $\mu\text{m}$ ; B: 10  $\mu\text{m}$  (for B-K).

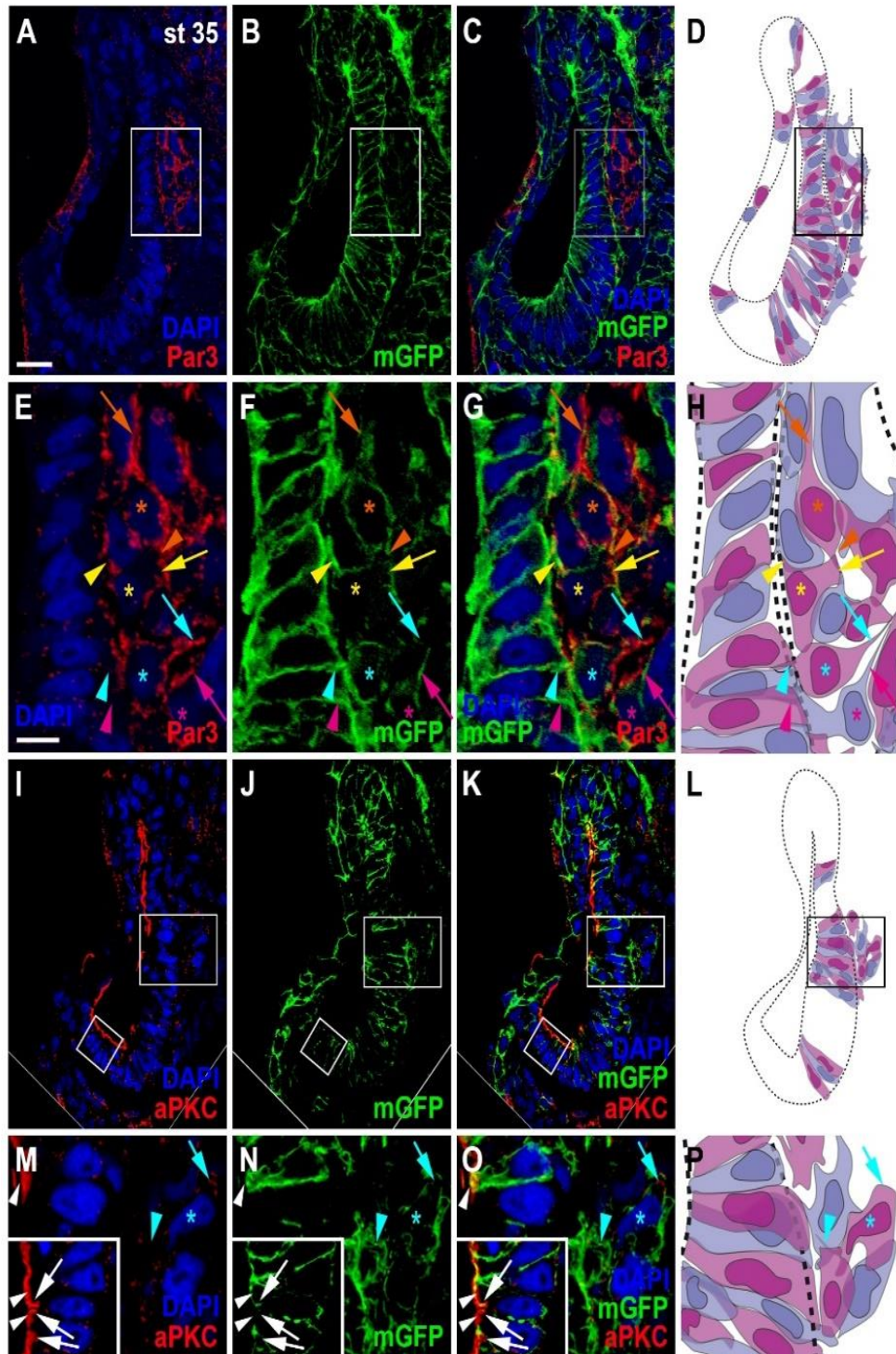


**Fig. 3.4. Distribution of apico-basal polarity markers Par3 and aPKC in otic vesicle and vestibulocochlear ganglion at stage 35.** Immunostaining for the cell polarity proteins Par3 (A-C, E-G) and aPKC (I-K, M-O) in transverse sections through the



center of the left otic vesicle of *Xenopus* embryos at stage 35 analyzed in single confocal planes (dorsal to the top, medial to the right). Sections have also been immunostained for membrane GFP (mGFP) following *mGFP* mRNA injection. Different channels of same section and cell shapes (shown in alternating blue and purple colors for clarity) reconstructed from mGFP staining of a z-stack are shown in **A-D** and **I-L** with boxed regions shown magnified in **E-H** and **M-P**. **A-H**: Par3 staining at stage 35 is strongly reduced in the otic epithelium and is mostly found localized to the membranes of vestibulocochlear ganglion cells. **I-O**: aPKC is still localized to the apical side of the otic epithelium at stage 35, but is also enriched in membranes of the leading edge of delaminating ganglion cells. White arrows indicate apical staining; white arrowheads: apicolateral (junctional) staining; colored arrows: leading edge (axon forming) of vestibulocochlear ganglion cells; colored arrowheads: trailing edge (dendrite forming) of vestibulocochlear ganglion cells; colored asterisks: nuclei. Individual cells are indicated by different colors. Scale bars: A: 25  $\mu\text{m}$  (for **A-D**, **I-L**); E: 10  $\mu\text{m}$  (for **E-G**, **M-O**).

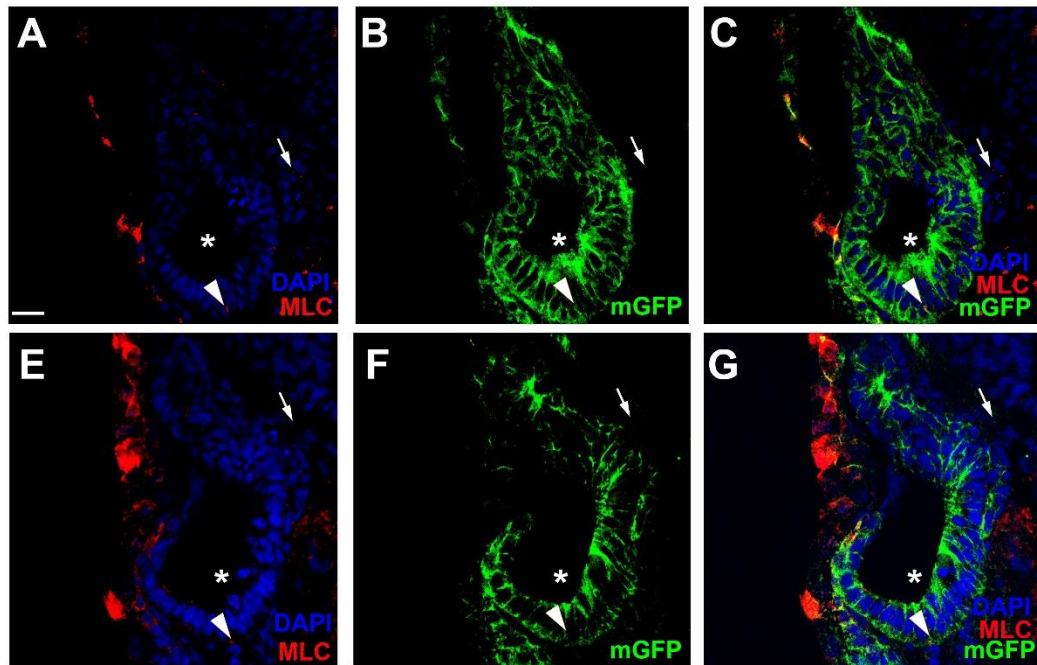


**Fig. 3.5. Distribution of apico-basal polarity marker phosphorylated Myosin light chain (MLC) in otic vesicle and vestibulocochlear ganglion at stage 35.** Immunostaining for MLC (**A-C**) in transverse sections through the center of the left otic vesicle of *Xenopus* embryos at stage 35 analyzed in single confocal planes (dorsal to the top, medial to the right) and a maximum intensity projection taken from a z-stack (**E-G**). Sections have also been immunostained for membrane GFP (mGFP) following *mGFP* mRNA injection. Different channels of same section are shown. MLC staining at stage 35 is strongly reduced in apical and apicolateral regions of the otic epithelium (asterisks); some residual staining is found in basolateral cell membranes (arrowhead) and in the cytoplasm of vestibulocochlear ganglion cells (arrow). Scale bars: A: 25  $\mu\text{m}$  (for **A-G**).

### 3.3 Proliferating and non-proliferating progenitor cells in the otic vesicle

The labeling, detection, and quantification of proliferating and non-proliferating progenitor cells is important for our understanding of organ homeostasis and normal tissue development (Zeng et al., 2010; Buck et al., 2008). To gain insights into the spatiotemporal pattern of proliferation during otic neurogenesis, I analysed the distribution of cell proliferation in the developing otic vesicle.

First, the percentage of mitotic cells in the epithelium of otic vesicle was counted by determining the proportion of DAPI –positive nuclei that also are immunostained by the pH3 antibody at stage 26 and stage 35 (Table 3.1). At stage 26, pH3-positive nuclei comprised  $1.63 \pm 0.51$  % of otic epithelial nuclei with a slight but not quite significant increase to  $2.6 \pm 0.39$  % at stage 35 ( $p = 0.057$ , t-test, Table 3.1).

**Table 3.1: Percentage of mitotic (pH3 positive nuclei) during otice vesicle development.**

	Embryos	DAPI nuclei	pH3	%
Stage 26	1	317	7	0.02208
	2	358	5	0.01396
	3	466	6	0.0128
Stage 35	1	798	22	0.02756
	2	727	21	0.02888
	3	741	16	0.02159

Second, the thymidine analog 5-ethynyl-2'-deoxyuridine (EdU), which is incorporated into cellular DNA during active DNA synthesis (i.e., during S phase of the cell cycle), was used in this study to visualize proliferating cells. To label the entire population of proliferating cells, I sacrificed embryos immediately after a 16 hours incubation in EdU. Since EdU-staining is compatible with other staining methods, such as immunohistochemistry (Zeng et al., 2010), the present study combines the detection of proliferating cells using EdU with immunohistochemical detection of the progenitor marker Sox3 during development of the otic vesicle (stages 26–35).

Both EdU and Sox3 staining show nuclear distribution in all stages analyzed (Fig. 3.6 A-I). At early embryonic stages (stage 26), Sox3 expression was found in a small group of cells on the ventromedial side of the otic vesicle and is located within a broader domain of EdU staining. Most Sox3-immunopositive cells are also labelled with EdU (Fig.3.6 A-C). Also, there was co-localization between Sox3 and EdU in the ventricular zone of the hindbrain, where proliferating neuronal progenitors are known to be localized, in all stages from stage 26 to 35 (Figs. 3.6 A-I, 3.8, A-L).

At stages 29 and 35, when the otic vesicle has extended along the dorsoventral axis, Sox3 expression is still confined mostly to cells of the ventromedial region of the otic vesicle, but the majority of these are no longer proliferative as indicated by lack of EdU staining (Fig. 3.6 D-I). Remarkably, there are a few cells at the upper and lower border of this domain, which remain positive for both EdU and Sox3 staining (Fig. 3.6 D-I). Reduction of EdU in the ventromedial zone of the otic epithelium suggests that cells have left the cell cycle in this area and possibly have started sensory differentiation (see section 3.4 below). In the vestibulocochlear ganglion, EdU positive cells (proliferative cells) are confined to the periphery of the ganglion (Fig. 3.6 D-I).

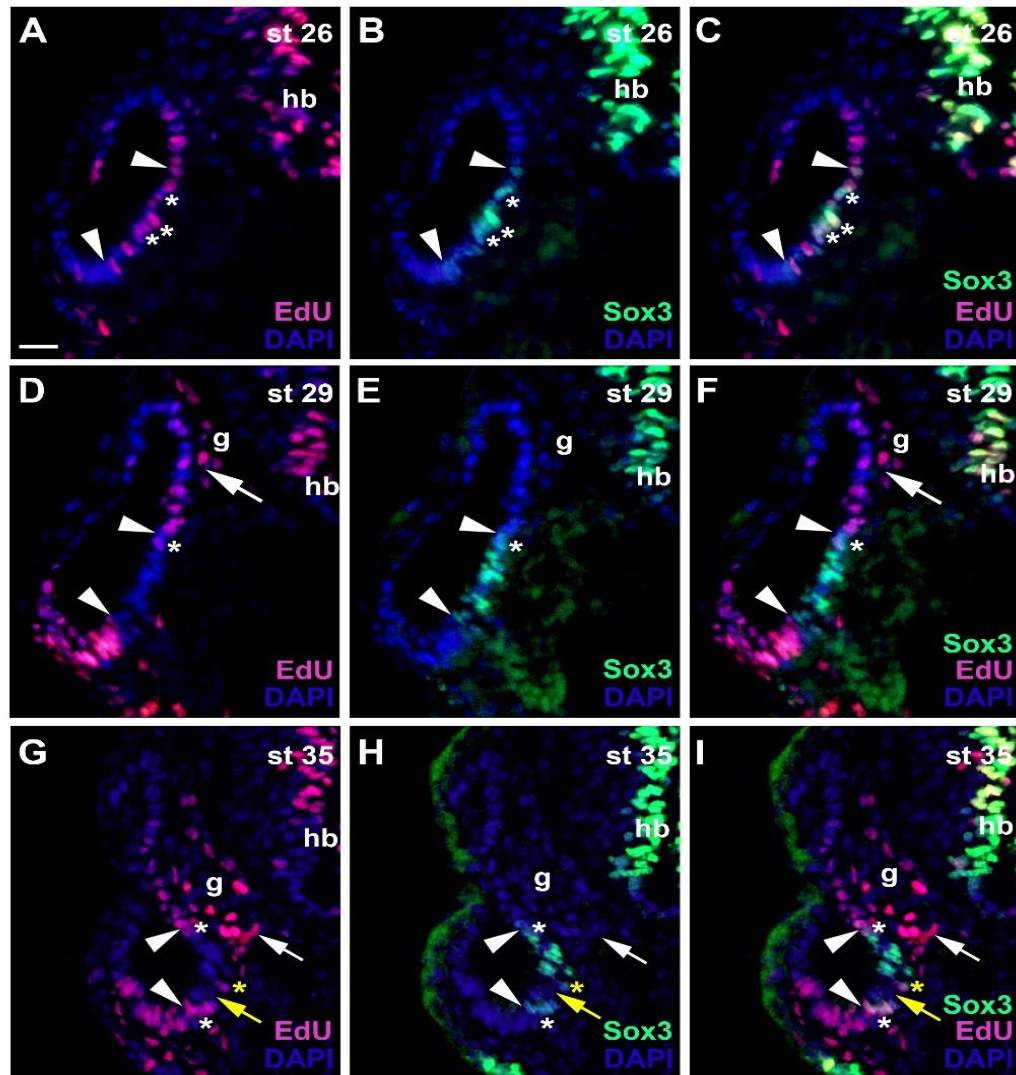


**Fig. 3.6. Changing distribution of proliferative and non-proliferative progenitors during development of the otic vesicle.** Distribution of proliferative (EdU-positive) cells and Sox3-immunopositive sensorineural progenitors in transverse sections through the center of the left otic vesicle of *Xenopus* embryos from stage 26 to 35 (dorsal to the top, medial to the right). Different channels of same section shown in **A-C**; **D-F**; and **G-I**. **G**: vestibulocochlear ganglion; hb: hindbrain. At stage 26 (**A-C**), Sox3-immunopositive cells are confined to the ventromedial part of the otic vesicle (between arrowheads), located within a broader domain of EdU staining. All Sox3-immunopositive cells are also labelled with EdU (asterisks indicate double-labeled cells). At stages 29 (**D-F**) and 35 (**G-I**), most cells in the ventromedial region are immunopositive for Sox3 (region between arrowheads) but are no longer proliferative as indicated by lack of EdU staining. A few cells, which are both EdU- and Sox3-positive remain at the upper and lower border of this domain (white asterisks). From stage 35 on, a region of Sox3-immunonegative nuclei (yellow arrows) separates a dorsal from a ventral domain of Sox3-positive cells within the ventromedial domain. Occasional EdU-positive cells are found in this intervening domain (yellow asterisks). Proliferative, EdU-positive cells in the vestibulocochlear ganglion (arrows) are confined to the periphery of the ganglion and do not co-express Sox3. Scale bar in **A**: 25  $\mu$ m (for all panels).



In order to confirm these results, another marker of proliferating cells was examined in otic vesicle, using immunohistochemistry for Proliferating Cell Nuclear Antigen (PCNA) at different stages between stage 20 to stage 40 (immunostaining and sections courtesy of G. Schlosser based on specimens described in Wullimann et al., 2005). At stage 20, most otic placode cells (ectodermal thickenings area) are immunopositive for PCNA (Fig. 3.7 A). Subsequently, the otic placode invaginates to form the otic cup at stage 23 and showed a strong PCNA staining, indicating that most cells are still in proliferation (Fig. 3.7 B). The otic cup then pinches off and invaginates to form the otic vesicle between stage 26 and 30 (Fig. 3.7 C-D). At stage 26, PCNA staining is still strong in the otic epithelium, while from stage 30 on PCNA staining becomes reduced and downregulated in the ventromedial side of the otic vesicle and only a few cells in this domain retain high PCNA-levels. This indicates that many cells in this region have left the cell cycle and form the vestibulocochlear ganglion cells (Fig. 3.7 D-F). In addition, PCNA immunohistochemistry showed positive staining in the vestibulocochlear ganglion from stage 35 on being confined to its periphery, in particular on its ventral side (Fig. 3.7 E-F).

To gain some insight into differences along the anteroposterior axis, the distribution of proliferative and non-proliferative progenitors was studied by using double staining for EdU and Sox3 at different levels of the otic vesicle in a stage 31 *Xenopus* embryo (Fig. 3.8). At all levels, only Sox3-immunopositive cells located near the dorsal and ventral border of the ventromedial Sox3-positive domain are proliferative as indicated by EdU staining (Fig. 3.8 A-I, M). However, the dorsoventral extent of this region of Sox3-immunopositive cells changes along the anteroposterior axis and reached its largest extent approximately at the center of the otic vesicle (Fig. 3.8 B, E, H).

Due to the lack of an antibody that recognizes Neurog1 in *Xenopus*, I was unable to investigate the precise relation of the Sox3-immunopositive region to regions of neuronal specification as defined by Neurog1 (Ma et al., 1998; Alsina et al., 2004;

Nieber et al., 2009; Riddiford et al., 2016). To clarify the approximate spatial relationship between areas of proliferative and non-proliferative progenitors and *Neurog1* expression in the otic vesicle, the expression of *Neurog1* was revealed by wholemount in situ hybridization in stage 28 *Xenopus* embryos followed by vibratome sectioning (Fig. 3.8 J-L). Comparison between Sox3 and *Neurog1* sections show that *Neurog1* expression partly overlaps with the ventromedial region of Sox3-immunostaining. However, *Neurog1* expression extends further dorsal than Sox3 in the posterior part of the otic vesicle (Fig. 3.8 M-O).

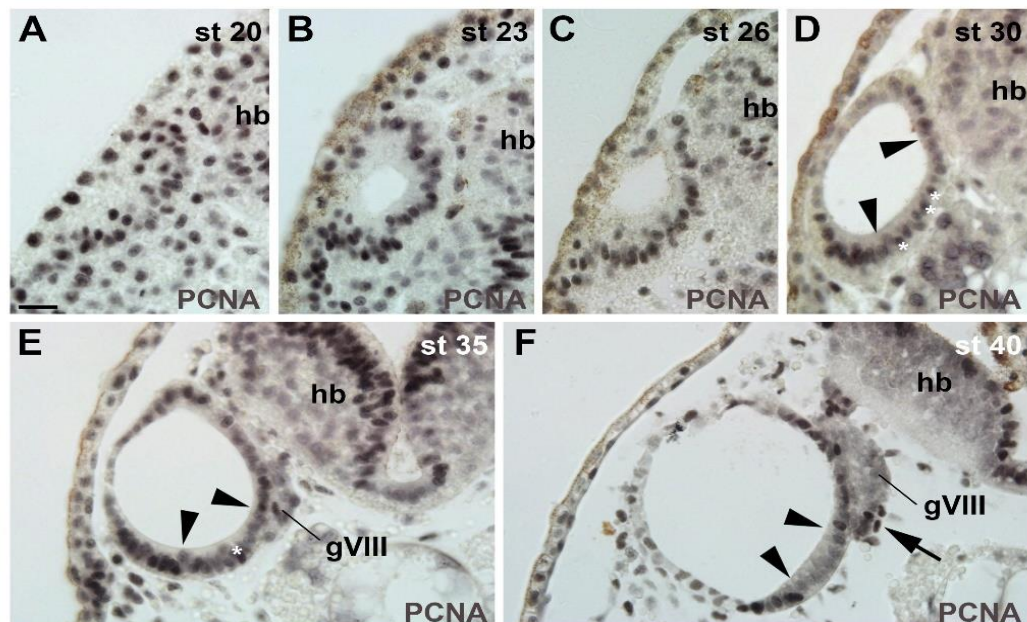


**Fig. 3.7. Time course of proliferation in the otic vesicle.** Distribution of PCNA-immunopositive, proliferative cells in transverse sections through the center of the left otic vesicle of *Xenopus* embryos from stage 20 to 40 (dorsal to the top, medial to the right). GVIII: vestibulocochlear ganglion; hb: hindbrain. Invagination of the otic vesicle is completed between stage 26 and 30. From stage 30 on, PCNA staining becomes reduced on the ventromedial side of the otic vesicle (between arrowheads) with only a few cells in this domain retaining high PCNA-levels (asterisks). PCNA-positive cells in the vestibulocochlear ganglion (which becomes evident after stage 30) are confined to its periphery, in particular on its ventral side (arrow). Scale bar in A: 25  $\mu$ m (for all panels). Figure courtesy of G. Schlosser based on PCNA-immunostained specimens described in Wullimann et al., (2005).

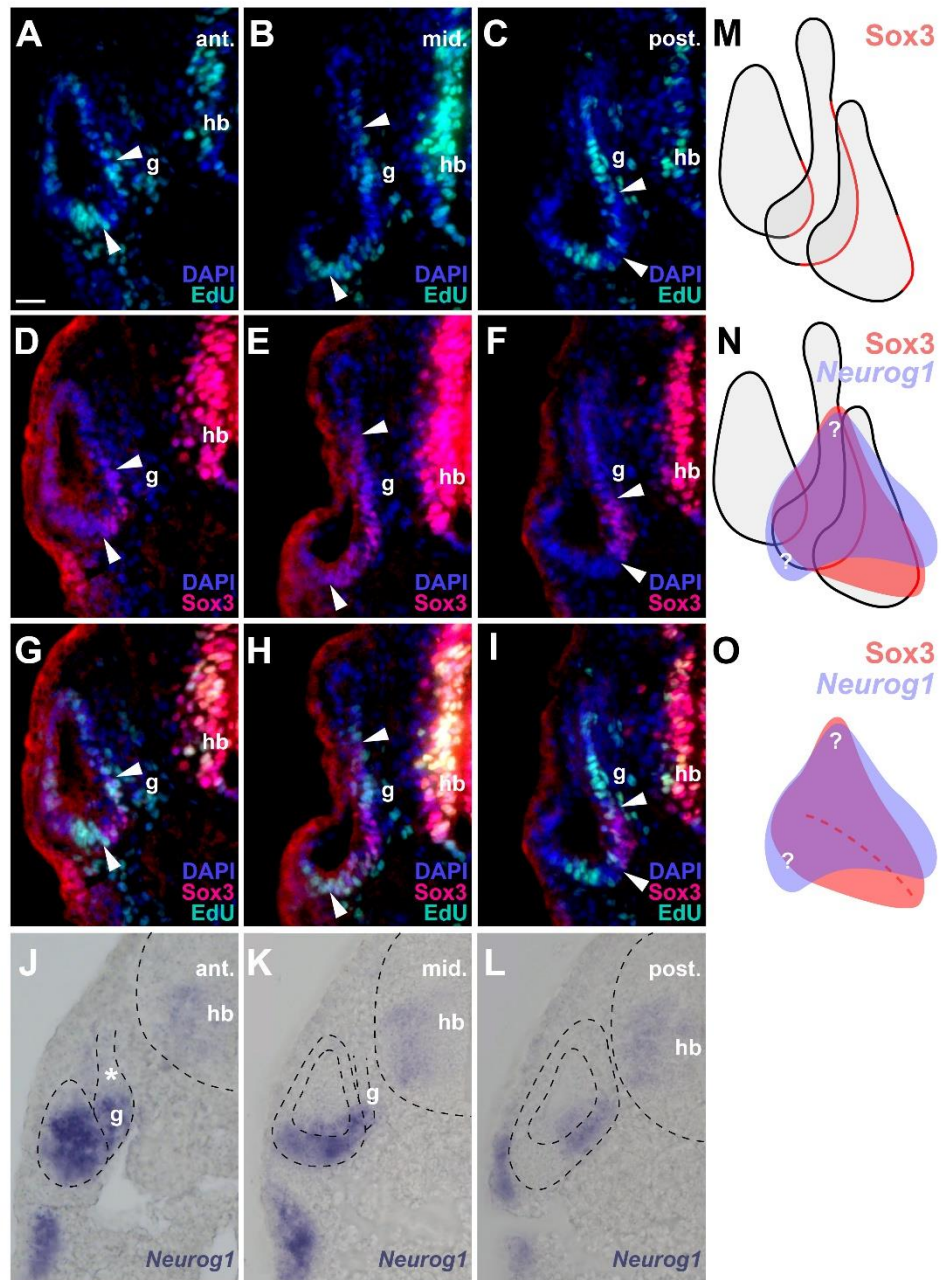


**Fig. 3.8. Distribution of proliferative and non-proliferative progenitors at different levels of the otic vesicle at stages 28-31.** A-I: Distribution of proliferative (EdU-positive) cells and Sox3-immunopositive sensorineural progenitors in four approximately equidistant transverse sections of the left otic vesicle of a stage 31 *Xenopus* embryo (dorsal to the top, medial to the right). Different channels of same section shown in each column (A, D, G; B, E, H; C, F, I). Extent of region containing Sox3-immunopositive cells indicated by arrowheads. G: vestibulocochlear ganglion; hb: hindbrain. Levels: ant.: anterior; mid.: midline; post.: posterior. J-L: Distribution of *Neurog1* expression in the left otic vesicle of a stage 28 *Xenopus* embryo showing three

approximately equidistant transverse vibratome sections (**J-L**). Note that at anterior levels, *Neurog1* is expressed throughout the ventral and ventromedial otic epithelium, while it is confined to the mid-dorsa/ventral part of the medial otic epithelium further posterior. In the vestibulocochlear ganglion, *Neurog1* is expressed only in the distal part next to the otic epithelium but is absent from the proximal part (asterisk). **M-O**: Schematic illustrations of extent of Sox3- and *Neurog1*-positive areas throughout the otic vesicle. Extent of Sox3 area is projected onto outline of otic vesicle for the three sections shown in **A-I** (red lines in **M**, red colored area in **N, O**). Only Sox3-positive cells located near the dorsal and ventral border of this area are proliferative as indicated by EdU staining. Note that the region of Sox3-immunopositive cells reaches its largest dorsoventral extent approximately at the midline of the otic vesicle. The approximate relation of the *Neurog1*-expressing area relative to the Sox3-positive area was inferred from vibratome sections (**J-L**) and is indicated in blue in **N** and **O**. Hatched line indicates the position of the ventralmost extent of the vestibulocochlear ganglion, which corresponds to the border between superior and inferior parts of the Sox3-domain in subsequent stages. Note that Sox3 is only partly overlapping with *Neurog1*. Question marks indicate uncertainties about the extent of Sox3+/*Neurog1*- and Sox3-/*Neurog1*+ areas in the anterior. Scale bar in **A**: 25  $\mu\text{m}$  (for all panels).

This dorsal part of the *Neurog1*-positive domain and Sox3-negative region approximately corresponds to the area, where the basal lamina is disrupted and most cell delamination occurs suggesting that neuronal progenitors maintain *Neurog1* but downregulate Sox3 prior to delamination (compare Fig. 3.8 A-O with Fig. 3.1 E-I). Anteriorly, *Neurog1* possibly extends further ventrolaterally than Sox3 immunostaining in a region corresponding to the ventral area of cell delamination described above, but this needs to be confirmed. Conversely, the posteroventral part of the medial otic epithelium which are immunopositive for Sox3, do not express *Neurog1* (and will probably contribute to the developing sensory areas Fig. 3.8 K-L and N-O). Schematic illustrations of the approximate relation of the *Neurog1*-expressing area relative to the Sox3-positive area are shown in Fig. 3.8 N-O, but the precise spatial relationships need to be confirmed in further studies.

### 3.4 Neuronal and sensory differentiation in the otic vesicle

Here the spatial and temporal pattern of differentiation of sensory cells (hair cells and supporting cells) and neurons was analysed by studying the distribution of Sox3-immunopositive sensorineural progenitors in relation to Islet1/2-immunopositive cells in the *Xenopus laevis* otic vesicle at stage 26 until stage 40. Islet-1 and Islet-2 are LIM/homeodomain proteins expressed in several populations of differentiated neurons, including motor neurons and sensory neurons (Lee and Pfaff, 2003; Ma et al., 2008; Lee et al., 2012). In particular, Islet-1 was previously shown to be a marker of inner ear derived differentiated sensory neurons and of presumptive sensory epithelia in other vertebrates (Li et al., 2004; Radde-Gallwitz et al., 2004).

As described above, at stage 26 Sox3 expression is already found in the ventromedial side of otic vesicle, where it continues to be present at least until stage 40. In contrast, Islet-1/2 immunostaining is not yet observed in the otic vesicle at stage 26 (Fig. 3.9 A-C). From stage 29 on, strongly Islet1/2 positive cells are evident in the peripheral cells of the vestibulocochlear ganglion (Fig. 3.9 D-L, Fig. 3.10). Islet1/2-positive cells were confined to cells in the core of the ganglion, while cells in its periphery do not stain for Islet1/2. This pattern indicates that Islet1/2 is not expressed in proliferating cells, which I have shown to be localized on the outside of the ganglion (see section 3.3).

In addition, there was co-localization between Sox3 and Islet-1/2 antibodies in the ventromedial side of the otic epithelium from stage 33 on, but Islet-1/2 was present at much lower levels in this domain than in the ganglion (Fig. 3.9. G-L, Fig. 3.10). While Islet1/2 is not expressed in the dorsalmost and ventralmost Sox3-immunopositive cells, which I have shown to be proliferative, it is expressed in most of the remaining population (Fig 3.9 G-J, Fig. 3.10), presumably defining the developing sensory areas.



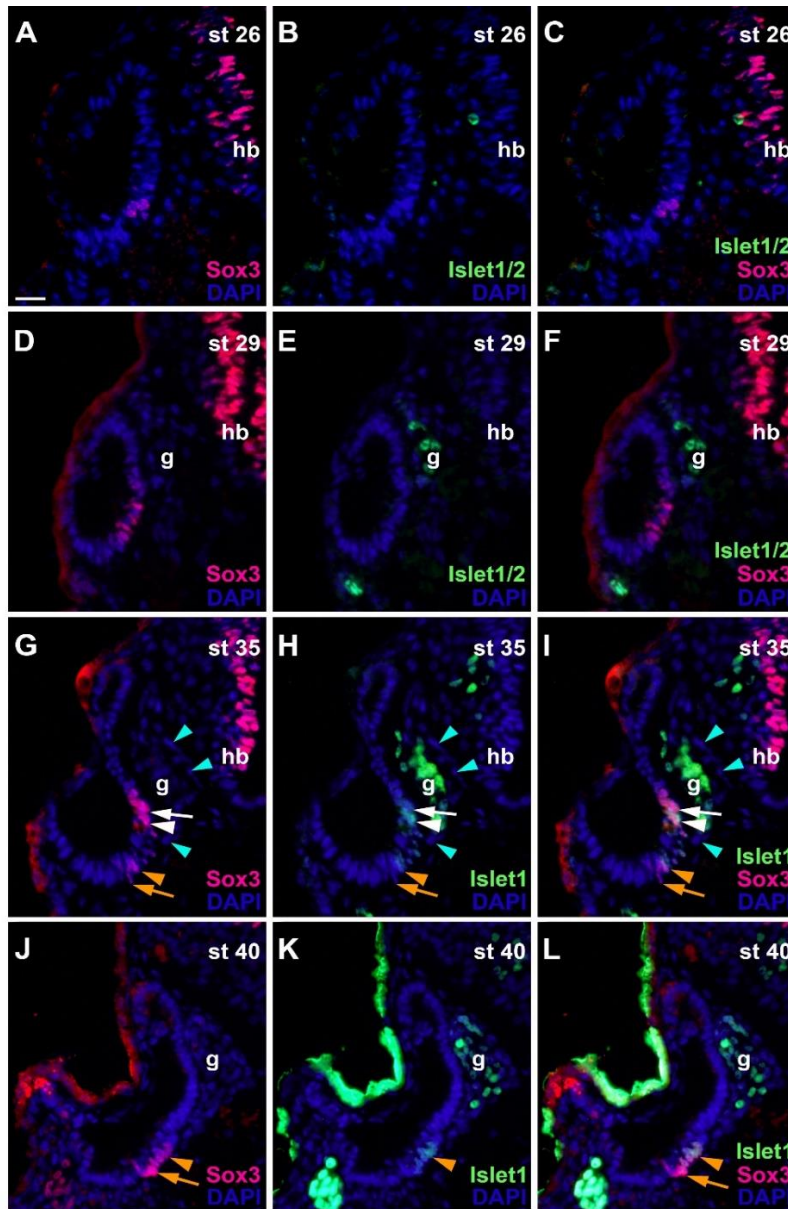


**Fig. 3.9. Changing distribution of sensorineural progenitors and differentiating neurons during development of the otic vesicle.** Distribution of Sox3-immunopositive sensorineural progenitors in relation to Islet1/2-immunopositive differentiating neurons in transverse sections through the center of the left otic vesicle of *Xenopus* embryos from stage 26 to 40 (dorsal to the top, medial to the right). Different channels of same section shown in **A-C**; **D-F**; **G-I**; and **H-K**. G: vestibulocochlear ganglion; hb: hindbrain. From stage 29 on, strongly Islet1/2 positive cells are evident in the vestibulocochlear ganglion. Note the absence of Islet1/2 staining in the peripheral cells of the ganglion (mint arrowheads). In addition, a subset of Sox3-positive cells in the otic epithelium shows weak Islet1/2 staining (arrowheads), whereas other Sox3-positive cells do not express Islet1/2 (arrows) (upper domain for stage 40 is only visible in more anterior section). Scale bar in **A**: 25  $\mu$ m (for all panels).

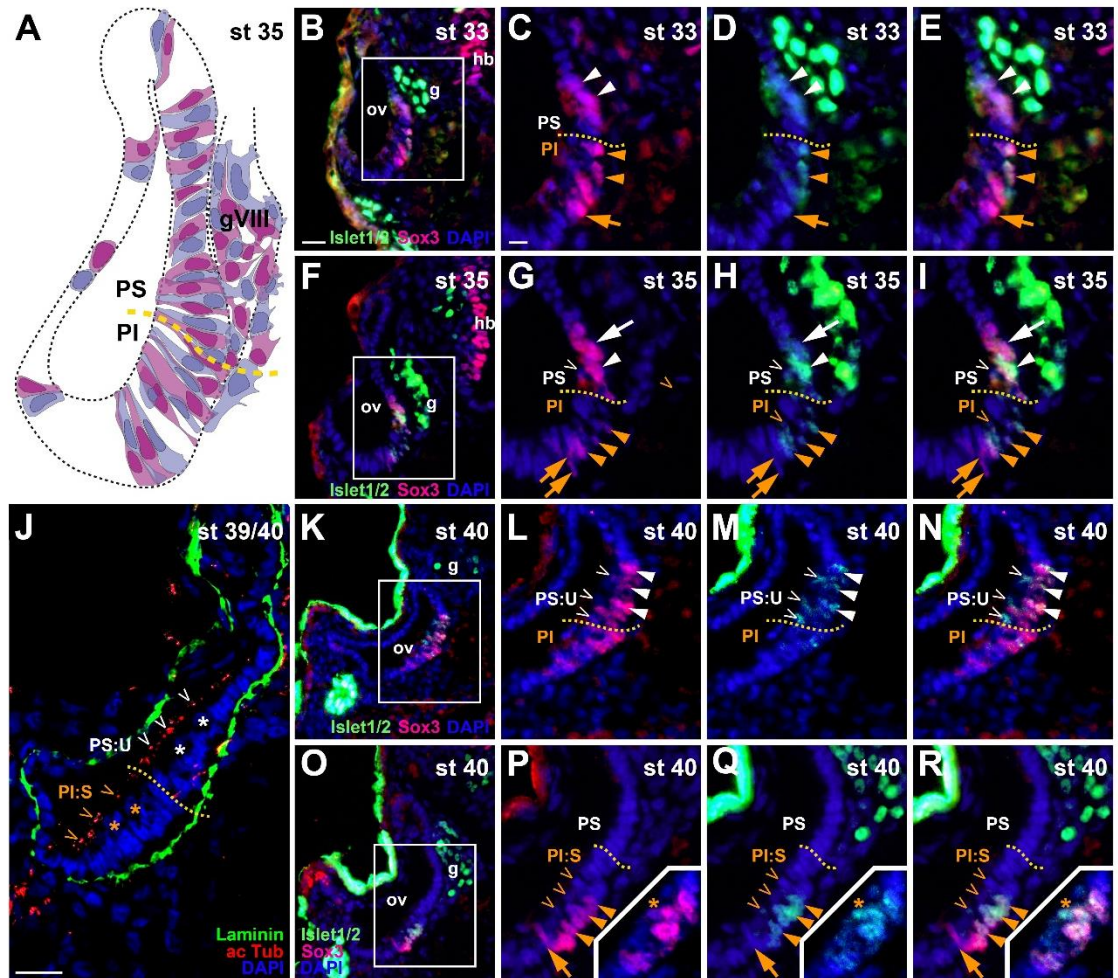


**Fig. 3.10. Dorso-ventral separation of the sensorineural area of the otic vesicle during stages 33-40.** **A:** Overview of cell distribution in stage 35 otic vesicle based on reconstructions from mGFP staining of a confocal z-stack (see Fig. 3). Hatched yellow line indicates approximate border between upper (PS) and lower (PI) part of the otic vesicle. **B-I, K-R:** Distribution of Sox3-immunopositive sensorineural progenitors and Islet1/2-immunopositive cells in transverse sections through the center of the left otic vesicle of *Xenopus* embryos from stage 33 to 40 (dorsal to the top, medial to the right). Overviews shown in **B** (stage 33), **F** (stage 35), **K** (stage 40, anterior half), **O** (stage 40, posterior half) with details of boxed areas shown in adjacent panels. From stage 33 on, the domain of Sox3-immunopositive cells in the ventromedial part of the otic epithelium separates into an upper domain (located in the pars superior of the otic vesicle: white arrows/arrowheads) and a lower domain (located in pars inferior: orange arrows/arrowheads). A subset of Sox3-positive cells in the otic epithelium shows weak Islet1/2 staining (arrowheads), whereas other Sox3-positive cells do not express Islet1/2 (arrows). At stage 40 Sox3-Islet1/2 double stained cells (arrowheads) appear to form a layer of supporting cells located basal to a layer of putative hair cells (open arrowheads),

which are not immunopositive for Sox3 and Islet1/2. Inserts in **P-R** show adjacent section with one putative hair cell (asterisk) expressing Islet1/2 but not Sox3, suggesting that Sox3 is downregulated before Islet1/2 in these cells. **J**: Distribution of hair cells as revealed by immunostaining of kinocilia with acetylated tubulin at stage 39/40 (open arrowheads; asterisks indicate nuclei of hair cells) (kinocilia shown as large red dots; small red dots may represent primary cilia) The utricular macula (U) in the pars superior (PS) can be distinguished from the saccular macula (S) in the pars inferior (PI). G: vestibulocochlear ganglion; hb: hindbrain, PS: pars superior; PI: pars inferior; S: saccular macula; U: utricular macula). Scale bars: **B**: 25  $\mu\text{m}$  (for **B, F, K, O**). **C**: 10  $\mu\text{m}$  (for **C-E, G-I, L-N, P-R**). **J**: 25  $\mu\text{m}$ .

A division between an upper and lower part of Sox3- and Islet1/2-doublestained cells separated by immunonegative cells was first observed at stage 33 and becomes more pronounced at stage 35, providing the first indication of a subdivision of the common sensorineural area (Fig. 3.9 G-J, Fig. 3.10 A-I). From stage 35 on, the epithelium on both sides of the dividing line starts to become bilayered. Cells with larger nuclei, which remain Sox3- and Islet1/2-positive, are positioned basally and cells with smaller nuclei, which are Sox3- and Islet1/2-negative, are positioned apically (Fig. 3.10 F-I). This suggests that sensory areas with apically located hair cells and basal supporting cells start to form. At stage 40, the distinction between the two layers becomes much clearer and the extent of the sensory areas, which will form the utricular macula in the superior part and the saccular macula in the inferior part of the otic vesicle, has increased (Fig. 3.10 O-R).

Since acetylated tubulin antibodies can be used to determine the distribution of primary cilia and kinocilia. I used them to confirm the distribution of hair cells in these two maculae (Fig. 3.10 J). Immunostaining of hair cell kinocilia revealed these as large dots (while primary cilia appeared as very small dots) located in areas of thickened epithelium near the lumen of the otic vesicle. These findings suggest that the utricular macula (U) in the pars superior (PS) separates from the saccular macula (S) in the pars inferior (PI) in the otic vesicle from stage 33 on (Fig. 3.10 O-R). Most of the putative hair cells in the sensory maculae show neither immunostaining for Sox3 nor for Islet1/2. However, a minority of hair cells is



Islet1/2- but not Sox3-positive, suggesting that Sox3 is downregulated before Islet1/2 in hair cell precursors (Fig. 3.10 K-R).

### **3.5 Summary**

Using immunostaining and confocal microscopy, I here provide the first detailed description of otic neurogenesis in *Xenopus laevis*. I show that the otic vesicle comprises a pseudostratified epithelium with apicobasal polarity (apical enrichment of Par3, aPKC, phosphorylated Myosin light chain, N-cadherin) and interkinetic nuclear migration (apical localization of mitotic, pH3-positive cells). A Sox3-immunopositive neurosensory area in the ventromedial otic vesicle gives rise to neuroblasts, which delaminate through breaches in the basal lamina between stages 27 and 39. Delaminated cells congregate to form the vestibulocochlear ganglion, whose peripheral cells continue to proliferate (as judged by EdU incorporation), while central cells differentiate into Islet1/2-immunopositive neurons from stage 29 on and send out neurites at stage 31. The central part of the neurosensory area retains Sox3 but stops proliferating from stage 33, forming the first sensory areas (utricle/sacculus).

## **Chapter-4 Eya1 localization in the developing otic vesicle and in other cranial placodes**

*Eya1* is expressed during early embryogenesis in the developing kidney, muscles and ear as well as in other placode-derived sense organs and cranial ganglia (Barui and Datta, 2019; David et al., 2001; Grifone, 2007; Izzedine et al., 2003; Li et al., 2010; Schlosser and Northachutt, 2004; Schlosser, 2003, 2010; Schlosser et al., 2008). It plays very important roles during development of these organs, for example the kidney and many different placodes and its mutation causes Branchio-Oto-Renal syndrome with anomalies in branchial areas, ears and kidney.

Previous studies have shown that the transcription factor Six1 and its cofactor Eya1 are key factors of inner ear development and function together to regulate the differentiation of neurons from the otic vesicle (Xu et al., 1999; Laclef et al., 2003; Zheng et al., 2003; Li et al., 2003; Zou et al., 2004). In *Eya1*<sup>-/-</sup>, *Six1*<sup>-/-</sup> or *Eya1*<sup>+/-</sup>; *Six1*<sup>-/-</sup> null mutants, *Neurog1* and *NeuroD1* expression was reduced and vestibulocochlear ganglion cells failed to form (Zou et al., 2004; Ahmed et al., 2012), while overexpression of both *Eya1* and *Six1* convert non-neuronal epithelial cells into neurons (Ahmed et al., 2012). However, Eya1 and Six1 affect multiple cellular processes including cell proliferation, apoptosis, as well as sensory and neuronal differentiation (reviewed in Silver and Rebay, 2005; Schlosser, 2010) and their mode of action during otic neurogenesis is still poorly understood. To further clarify the role of Eya1 for otic neurogenesis, I will therefore first provide a detailed description of Eya1 in the developing otic vesicle of *Xenopus* (this chapter) followed by loss and gain of function studies (chapter 5).

### **4.1 Eya1 antibody specificity**

Before clarifying the distribution of Eya1 protein in the placodes of *Xenopus laevis*, the specificity of two Eya1 peptide antibodies raised in guinea pig was validated by two methods. First, a western blot experiment has been done (courtesy of G.

Schlosser) verifying the specific binding of both types of guinea pig antibodies after in vitro transcription and translation (TNT) of *Eya1* plasmid. Both antibodies detected *Eya1* as a specific band at 66 KD (Fig. 4.1 A). There was no band for control TNTs which did not contain *Eya1* plasmids (Fig. 4.1 A).

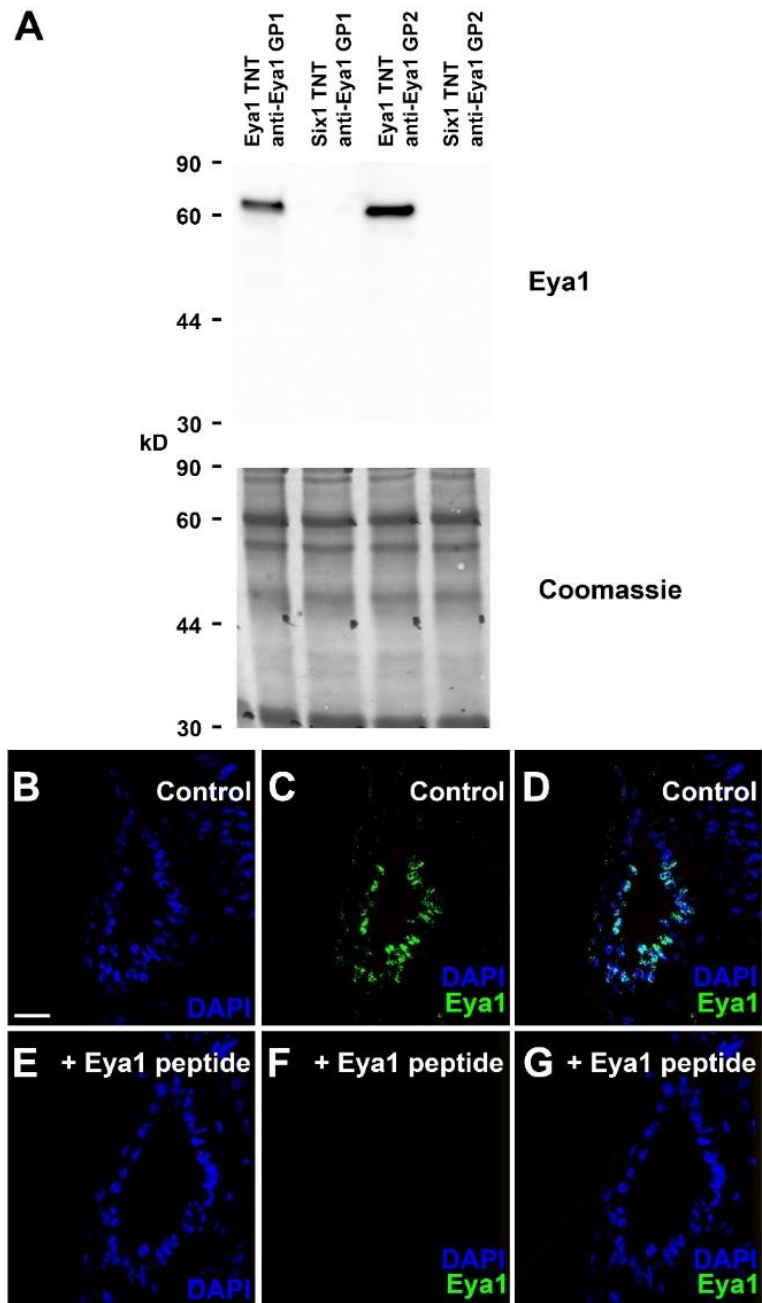


**Fig. 4. 1. Specificity of Eya1 antibodies.** **A:** Western blot to evaluate specificity of antibodies anti-Eya1 GP1 and anti-Eya1 GP2 raised in guinea pigs (GP). The antibodies recognize the Eya1 protein produced by in vitro transcription and translation (TNT) of *Eya1* plasmids but do not cross react with proteins in TNT reactions that do not contain *Eya1* (Six1 TNT). Coomassie staining demonstrates equal loading of all lanes. **B-G:** Peptide competition assay for anti-Eya1 GP1 antibody. Transverse sections through the left otic vesicle of a *Xenopus* embryos at stage 26 analyzed in single confocal planes (dorsal to the top, medial to the right). Different channels of same section shown in **B-D** and **E-G**. Eya1 immunostaining as evident in control embryos (**B-D**) is blocked after addition of Eya1 peptide (5 µg peptide/1 µg Eya1 antibody; **E-G**). Scale bar in **B**: 25 µm (for **B-G**).

In addition, a peptide competition assay has been done for the anti-Eya1 GP1 antibody to determine whether it specifically detects Eya1 in immunohistochemistry on cryosections (Fig. 4.1 B-G). Before proceeding to immunostaining, antibodies were incubated with a solution containing the Eya1 peptide against which the antibody had been raised. In control experiments, antibodies not pre-incubated with peptide were used. Peptide competition assays were done at two different concentrations of blocking peptide, at a peptide: antibody ratio of 5:1 and 10:1 (5 or 10 µg of blocking peptide, respectively for 1 µg of antibody) and at two different stages (stage 20 and 26). Confocal microscopy was used to determine the staining by anti-Eya1 GP1.

Control sections showed nuclear distribution of Eya1 in the otic placode or vesicle as well as in many other cranial placodes, somites and pharyngeal pouches (shown for the otic vesicle at stage 26 in Fig. 4.1 B-D; for stage 20 and other tissues see Appendix. Fig.B1). In sections that were treated with blocking peptide at any of the two dilutions tested (5:1 or 10:1), this nuclear staining has disappeared from all of these domains (shown for the otic vesicle at stage 26 in Fig 4.1. E-G; for stage 20 and other tissues (see Appendix. Fig.B1). Another peptide competition assay with anti-Eya1 GP2 antibody showed similar results (data not shown). Taken together with the western blot, this suggests that both antibodies specifically detect Eya1 in immunostaining and anti-Eya1 GP1 was subsequently used for immunostaining.

## 4.2 Eya1 distribution in the developing otic vesicle

Although *Eya1* expression has been studied in many vertebrates at the mRNA level, we currently know little about the distribution of Eya1 protein and its subcellular distribution. Since there are no commercially available antibodies which recognize *Xenopus* Eya1, the current study used the antibody anti-Eya1 GP1 previously generated by immunisation of guinea pigs with the Eya1 peptide RLSGSGDSPSGTGLDNSHINS (Ahrens and Schlosser, 2005). After carefully validating the specificity of this antibody for immunohistochemistry (see section 4.1), it was used to document Eya1 protein distribution during *Xenopus* development in detail with a special focus on otic placode and vesicle development. Eya1 localization has been studied in the developing otic placode and vesicle at stages 21, 26, 28, 32, 35 and 40. Images were taken by Olympus SZX7 stereomicroscope and confocal microscopy to reveal the distribution of Eya1 (Figs. 4.2-4).

At stage 21, the otic vesicle (vOt) is starting to invaginate as evident by the circular arrangement of Eya1 expression (Fig. 4.2 A- B). Ventral to the otic vesicle, the prospective middle lateral line placode (pM) also shows Eya1 expression (Fig. 4.2 A-B). At stage 26 to stage 28, Eya1 is strongly distributed in nuclei of the entire otic vesicle (vOt) except for dorsal and dorsolateral regions. The otic vesicle has almost completely invaginated at stage 26 and has separate from the surface ectoderm at stage 28 presenting an oval shape (Fig. 4.2 C-F). The middle lateral line placode (pM), which is located ventral to the otic vesicle also strongly expresses Eya1 during these stages (Fig. 4.2 C-F).

At stage 32, the otic vesicle (vOt) was completely separated from the ectoderm (Fig. 4.2 G-H). Eya1 was still expressed in the entire otic vesicle but was enriched in its ventral and medial part (Fig. 4.2 G-H). By this stage, a separate middle lateral line placode (pM) can still be distinguished ventrally of the otic vesicle and shows Eya1 expression (Fig. 4. 2 G-H). Interestingly, Eya1-immunostaining started then

to decrease in a ventromedial region of the otic epithelium from stage 35 on (Fig. 4.2 I-L), while it was still strongly expressed in adjacent regions of the ventromedial area of the otic epithelium (upper and lower regions) (Fig. 4.2 I-L). This region of decreased Eya1 staining in the ventromedial otic epithelium persists in subsequent stages and approximately corresponds to the region of putative sensory areas, where EdU-negative but Sox3- and weakly Islet1/2-positive cells are found (see chapter 3 and below).

At stages 35 and 40 (Fig. 4.2 I-L), this region of reduced Eya1-staining (putative sensory areas) becomes bilayered. While most cells in the basal layer (putative supporting cells) retain weak Eya1-immunostaining, only a few cells in the apical layer adjacent to the lumen (putative hair cells) express Eya1 weakly and many of the apical cells did not show any staining of Eya1. At stage 40, Eya1 immunostaining remains at a low level in some areas of the otic vesicle (vOt), especially in the developing sensory areas and it has completely disappeared from its lateral side and is now restricted to the upper and lower medial area of the otic vesicle epithelium (Fig. 4.2 K-L). Eya1 is still expressed strongly in upper and lower medial side of the otic placode epithelium adjacent to the putative sensory areas and weakly in the middle lateral line placode (pM) located ventrally and posterior to the otic vesicle (Fig 4.2. K-L).

From stages 32, staining of Eya1 is also seen in the vestibulocochlear ganglion (Fig.4.2 G-J). While there was a weak expression of Eya1 in the center of the vestibulocochlear ganglion stronger Eya1 staining is observed on its periphery, where proliferating cells are localized (Figs. 4.2, G-J, 4.3, 4.4).

To clarify the spatial relationship of Eya1 immunostaining in the otic vesicle with proliferating and non-proliferating progenitors and differentiating neurons, I compared Eya1 immunostaining with EdU and/or PCNA, Sox3 and Islet1/2 distribution at different antero-posterior levels of the otic vesicle (anterior, anterior middle, posterior middle and posterior) and in the vestibulocochlear ganglion at

stages 35 and 40 (Figs. 4.3, 4.4). EdU- and/or PCNA-positive proliferating cells extend through the entire otic vesicle anteriorly (Figs. 4.3, A, 4.4, A). However, in the central and posterior part of the otic vesicle, there is a gap in the ventromedial region of the otic vesicle epithelium, indicating reduced proliferation in this domain (Figs. 4.3, B-E, 4.4, B- C; see also chapter 3). Eya1 immunostaining was likewise found in the entire otic vesicle at an anterior level but was decreased in the ventromedial region (Figs. 4.3, F-H, 4.4, D-G). Sox3-immunopositive sensorineural progenitors cells, which also weakly expressed Islet1/2 were found in the ventromedial region, where PCNA, EdU and Eya1 were decreased, (Figs, 4.3, I-L, 4.4, I-L). Remarkably, at stage 40 the region of Sox3 staining extended more dorsally in the anterior half of the otic vesicle, while it was more ventrally confined in the posterior half (Fig. 4.4 I-L). At both stage 35 and 40, while there was a weak expression of Eya1 in the central cells of the vestibulocochlear ganglion, which are positive for Islet1/2, stronger Eya1 staining is observed on its periphery, where proliferating (EdU- and or – PCNA-positive) cells are localized (Figs. 4.2, G-J, 4.3, 4.4). These findings suggest that strong Eya1 expression is confined to proliferative cells both in the otic epithelium and in the vestibulocohlear ganglion, while weak Eya1 staining persists in the the non-proliferative Sox3-immunopositive cells of the putative sensory areas. The relationship to Sox3-immunopositive cells was subsequently confirmed by double-staining as described in section 4.5 below.

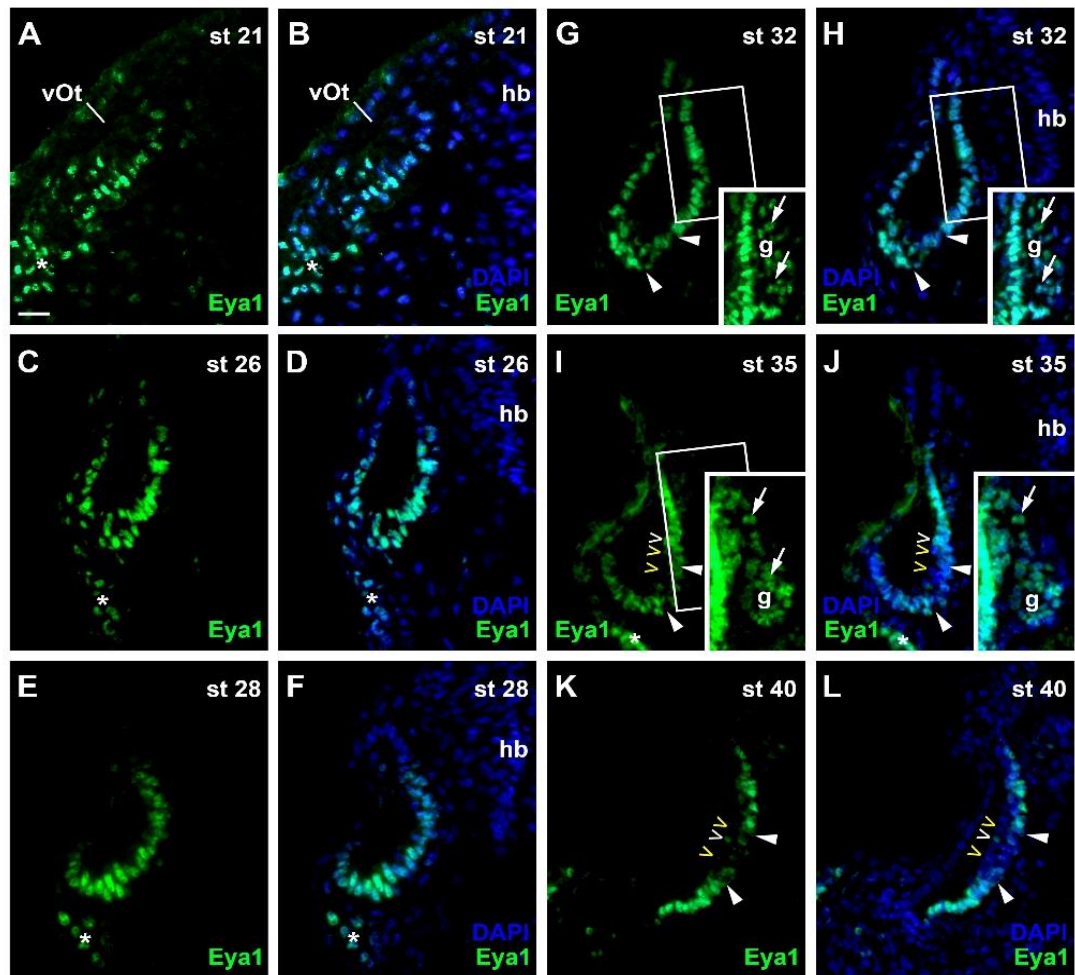


**Fig. 4.2. Changing distribution of Eya1 protein during development of the otic vesicle.** Distribution of Eya1-immunopositive cells in transverse sections through the center of the left otic vesicle of *Xenopus* embryos from stage 21 to 40 (dorsal to the top, medial to the right). For each stage, Eya1 staining is shown alone (left panel) as well as superimposed onto DAPI staining (right panel). Insets in **G**, **H** and **I** show boxed areas of same or adjacent section at higher magnification and with increased brightness (boxed area not shown in **J** for clarity). **A**, **B**: At stage 21, Eya1 is expressed in the invaginating otic vesicle and in the adjacent posterior placodal area (asterisk). **C-F**: At stages 26 (**C**, **D**) to 28 (**E**, **F**), Eya1 immunostaining persists throughout the otic vesicle except for dorsal and dorsolateral regions. **G-J**: From stage 32 (**G**, **H**) on, additional weak Eya1 staining is found throughout the vestibulocochlear ganglion (arrows in insets, which show boxed regions with increased brightness), while strong Eya1-immunostaining persists in the otic epithelium and in peripheral cells of the ganglion. From stage 32 on, Eya1-immunostaining decreases in a ventromedial region of the otic epithelium (flanked by arrowheads), while it remains high in adjacent regions. From stage 35 (**I**, **J**) onwards, hair cells (open arrowheads) become apparent as a separate layer. While most hair cells do not express Eya1 (yellow open arrowheads), a few hair cells show weak Eya1 staining (white open arrowheads). **K**, **L**: At stage 40 Eya1 is still weakly expressed in the vestibulocochlear ganglion (not shown here; see Fig. 4.4). In the otic epithelium Eya1 levels are low in the developing sensory areas (between arrowheads) but Eya1 remains strongly expressed in adjacent regions. **G**: vestibulocochlear ganglion; **hb**: hindbrain; **vOt**: otic vesicle. Scale bar in **A**: 25  $\mu$ m (for all panels).



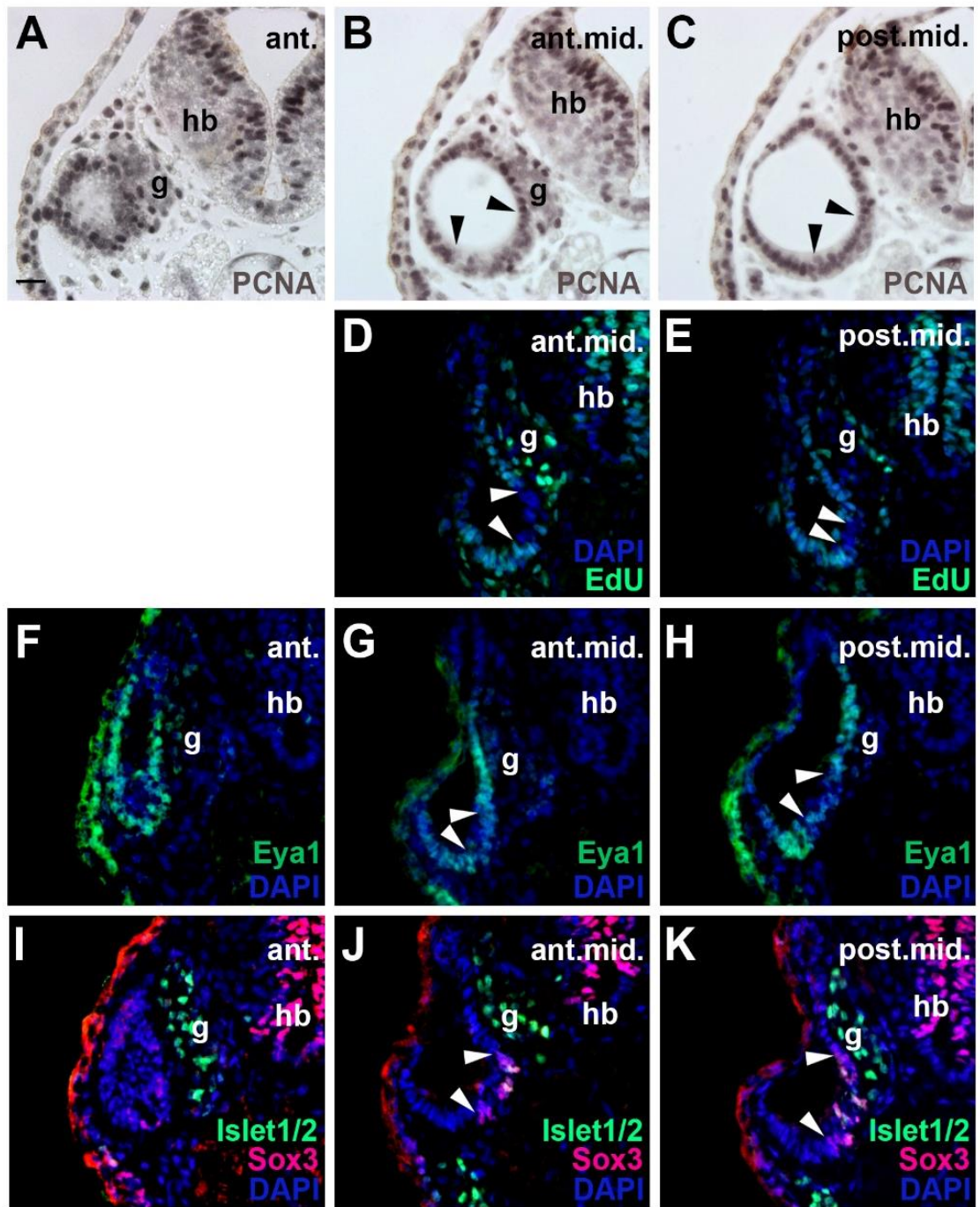


**Fig. 4.3. Distribution of Eya1 in relation to progenitor and differentiation markers at different levels of the otic vesicle at stage 35.** Distribution of proliferation markers (A-C: PCNA; D, E; EdU), Eya1-immunopositive cells (F-H), as well as Sox3-immunopositive sensorineural progenitors and Islet1/2-immunopositive differentiating neurons (I-K) in transverse sections in three approximately equidistant transverse sections of the left otic vesicle of a stage 35 *Xenopus* embryo (dorsal to the top, medial to the right). Note the decline of proliferation and Eya1 immunostaining in the ventromedial region (between arrowheads), where Sox3-immunopositive cells are located. G: vestibulocochlear ganglion; hb: hindbrain. Levels: ant.: anterior; ant.mid.: anterior of midline; post.mid.: posterior of midline. Note that shape of the otic vesicle is better preserved in PCNA stained sections (A-C) due to Bouin fixation than in sections stained for Eya1, Sox3, or Islet1/2, which were fixed with PFA (D-I). Scale bar in A: 25  $\mu$ m (for all panels). PCNA sections courtesy of G. Schlosser.

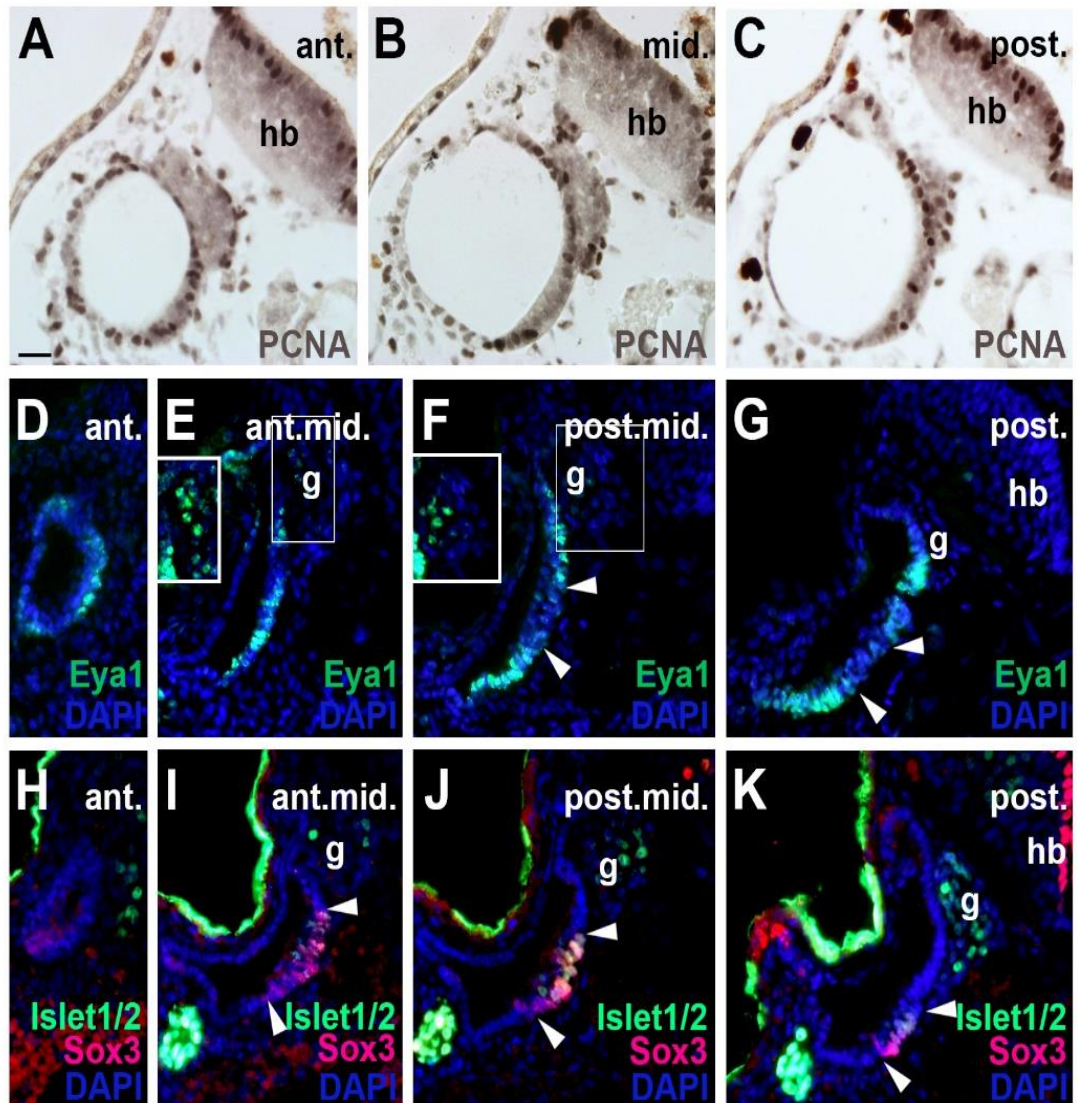


**Fig. 4.4. Distribution of Eya1 protein at different levels of the otic vesicle at stage 40.** Distribution of PCNA-immunopositive proliferation markers (A-C), Eya1-immunopositive cells (D-G), as well as Sox3-immunopositive sensorineural progenitors and Islet1/2-immunopositive differentiating neurons (H-K) in transverse sections in three (A-C) or four (D-K) approximately equidistant transverse sections of the left otic vesicle of a stage 40 *Xenopus* embryo (dorsal to the top, medial to the right). For PCNA one section is shown through the midline of the otic vesicle (B), whereas for the other markers two sections – one slightly anterior (E, I) and one slightly posterior of the midline (F, J) – are shown. Note the decreased proliferation and Eya1 immunostaining in the ventromedial region (between arrowheads), where Sox3-immunopositive cells are located. G: vestibulocochlear ganglion; hb: hindbrain. Levels: ant.: anterior; ant.mid.: anterior of midline; mid.: midline; post.mid.: posterior of midline; post.: posterior. Note that shape of the otic vesicle is better preserved in PCNA stained sections (A-C) due to Bouin fixation than in sections stained for Eya1, Sox3, or Islet1/2, which were fixed with PFA (D-I). Scale bar in A: 25  $\mu$ m (for all panels). PCNA sections courtesy of G. Schlosser.

### 4.3 Subcellular localization of Eya1

In order to analyze the distribution of Eya1 in the epithelium of the otic vesicle and vestibulocochlear ganglion in more detail, I next evaluated Z-stack images of the otic vesicle that were taken by confocal microscopy at 0.1  $\mu\text{m}$  intervals at various stages of development (stage 26, 29, 35, 40) (Figs. 4.5-8).

At stage 26, Eya1 immunopositive cells in the ventromedial region of the otic vesicle show predominantly nuclear Eya1 distribution (Fig. 4.5 A-D<sub>3</sub>). Eya1 localization changes during division of cells to a predominantly cytoplasmic distribution (Fig. 4.5 B<sub>1</sub>-D<sub>3</sub>). Furthermore, a few epithelium cells of the otic vesicle show cytoplasmic distribution of Eya1, which is often apically enriched (Fig. 4.5 B<sub>1</sub>-D<sub>3</sub>).

At stages 29 and 35, most cells in the otic epithelium continue to show nuclear distribution of Eya1 (Figs. 4.6, A-G<sub>3</sub>, 4.7, A-F<sub>3</sub>). However, at stage 35 levels of nuclear Eya1 are reduced in the region of the putative sensory areas in the ventromedial otic epithelium (Fig. 4.7 A-F<sub>3</sub>; see section 4.5 below). Moreover, cytoplasmic Eya1 staining is found in cells with basal protrusions, which are probably delaminating from the otic epithelium and in cells presumably migrating towards the vestibulocochlear ganglion (Figs. 4.6, B<sub>1</sub>-G<sub>3</sub>, 4.7, B<sub>1</sub>-D<sub>3</sub>, F<sub>1-3</sub>). In addition, there was clearly cytoplasmic distribution of Eya1 on the apical side of the otic vesicle epithelium (white arrows) and in dividing cells (Figs. 4.6, B<sub>1</sub>-G<sub>3</sub>, 4.7, B<sub>1</sub>-F<sub>3</sub>).

Furthermore, differentiating sensory neurons have already migrated out of the otic epithelium at these stages (stages 29, 35) to form the vestibulocochlear ganglion and Eya1 is also found in these cells (Figs. 4.6, E<sub>1</sub>-G<sub>3</sub>, 4.7, B<sub>1</sub>-F<sub>3</sub>). Whereas nuclear distribution of Eya1 was mostly restricted to the peripheral cells in the vestibulocochlear ganglion (Figs. 4.6, E<sub>1</sub>-G<sub>3</sub>, 4.7, B<sub>1</sub>-F<sub>3</sub>), there was mostly cytoplasmic localization in the center of the ganglion including in the processes that

extended to form the axon or dendrites of the differentiated sensory neurons located in the center (Figs. 4.6, E<sub>1</sub>-G<sub>3</sub>, 4.7, B<sub>1</sub>-F<sub>3</sub>).

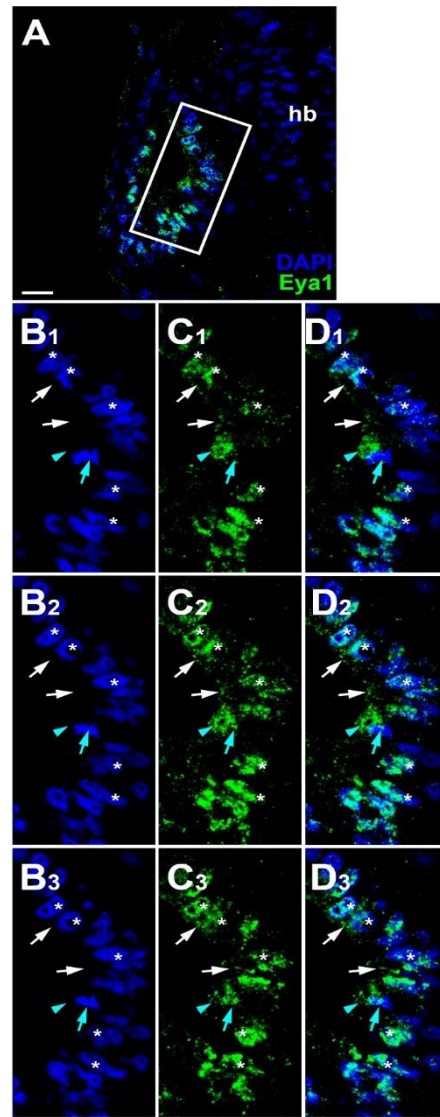


**Fig. 4.5. Subcellular localization of Eya1 protein in otic vesicle and vestibulocochlear ganglion at stage 26.** Immunostaining for Eya1 in a transverse section through the center of the left otic vesicle of *Xenopus* embryos at stage 26 analyzed by confocal microscopy (dorsal to the top, medial to the right). **A:** Overview showing the same confocal plane as **B<sub>2</sub>-C<sub>2</sub>**. **B<sub>1</sub>-D<sub>3</sub>:** Magnified views of the boxed area shown in different channels (columns B-D) and in three different confocal planes (rows 1-3). White asterisks show nuclear Eya1 staining, while white arrows show cytoplasmic staining in the otic epithelium. Mint arrowheads indicate cytoplasmic Eya1 staining in a dividing cell of the otic epithelium with the mint arrow indicating the division plane. Note that Eya1 shows mostly nuclear but also some cytoplasmic localization in the otic epithelium. Hb: hindbrain. Scale bar in **A:** 25  $\mu$ m.



At stage 40, strong nuclear localization of Eya1 persists in cells flanking the developing sensory areas in the superior and inferior part of the otic vesicle dorsally and ventrally, while the nuclei in the basal layer of these sensory area remain only weakly Eya1 positive and only a few nuclei in the apical layer show weak Eya1 staining (Fig. 4.8).

Interestingly, a similar pattern of Eya1 localization is observed in lateral line neuromasts. Sections through the periphery and center of a neuromast show a strong nuclear expression of Eya1 in a ring of supporting cells of neuromast cells (Fig. 4.8 F-H, N-P). These cells are probably highly proliferative as judged from PCNA-staining (Fig. 4.8 A-B, I-J, F-H, N-P). Similar to the otic vesicle epithelium, nuclear Eya1 staining was weaker in the centrally and basally localized supporting cells, while only a few of the apically localized hair cells expressed Eya1 very weakly (Fig.4.8 F-H, N-P).

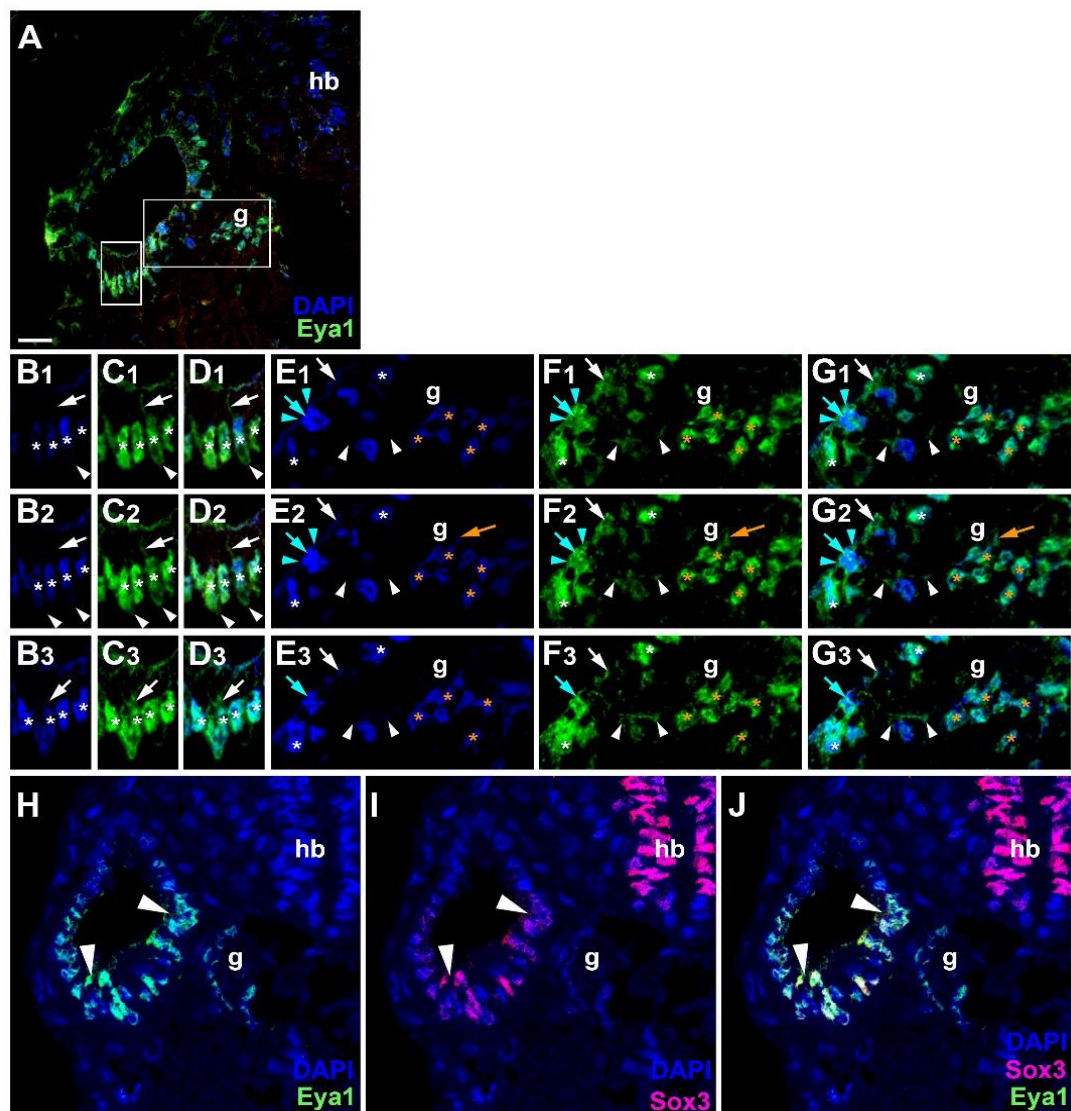


**Fig.4.6. Subcellular localization of Eya1 protein in otic vesicle and vestibulocochlear ganglion at stage 29.** **A- G:** Immunostaining for Eya1 in a transverse section through the center of the left otic vesicle of *Xenopus* embryos at stage 29 analyzed by confocal microscopy (dorsal to the top, medial to the right). **A:** Overview showing the same confocal plane as **B<sub>2</sub>-G<sub>2</sub>**. **B-G:** Magnified views of the small (**B-D**) and large (**E-G**) boxed areas shown in different channels (columns B-G) and in three different confocal planes (rows 1-3). Nuclear staining indicated by asterisks; cytoplasmic staining indicated by arrows. White asterisks show nuclear Eya1 staining in the otic epithelium; orange asterisk indicate Eya1-immunopositive nuclei in periphery of the vestibulocochlear ganglion. White arrows show cytoplasmic staining in the otic epithelium; orange arrows show cytoplasmic Eya1 staining in the ganglion. White arrowheads highlight Eya1-positive protrusions of delaminating cells. Mint arrowheads indicate cytoplasmic Eya1 staining in a dividing cell of the otic epithelium with the mint arrow indicating the division plane. Note that at this stage cells have begun to delaminate from the otic epithelium to form the vestibulocochlear ganglion. Eya1 shows mostly nuclear but also some cytoplasmic localization in the otic epithelium and vestibulocochlear ganglion. **H-J:** Immunostaining for Eya1 and Sox3 in a single confocal plane of another transverse section through the center of the left otic vesicle at stage 29. Note that the Eya1 domain includes but extends further dorsally and ventrolaterally than the Sox3 immunopositive domain (between arrowheads). **G:** vestibulocochlear ganglion; **hb:** hindbrain. Scale bar in **A:** 25  $\mu$ m (for **A, H-J**).

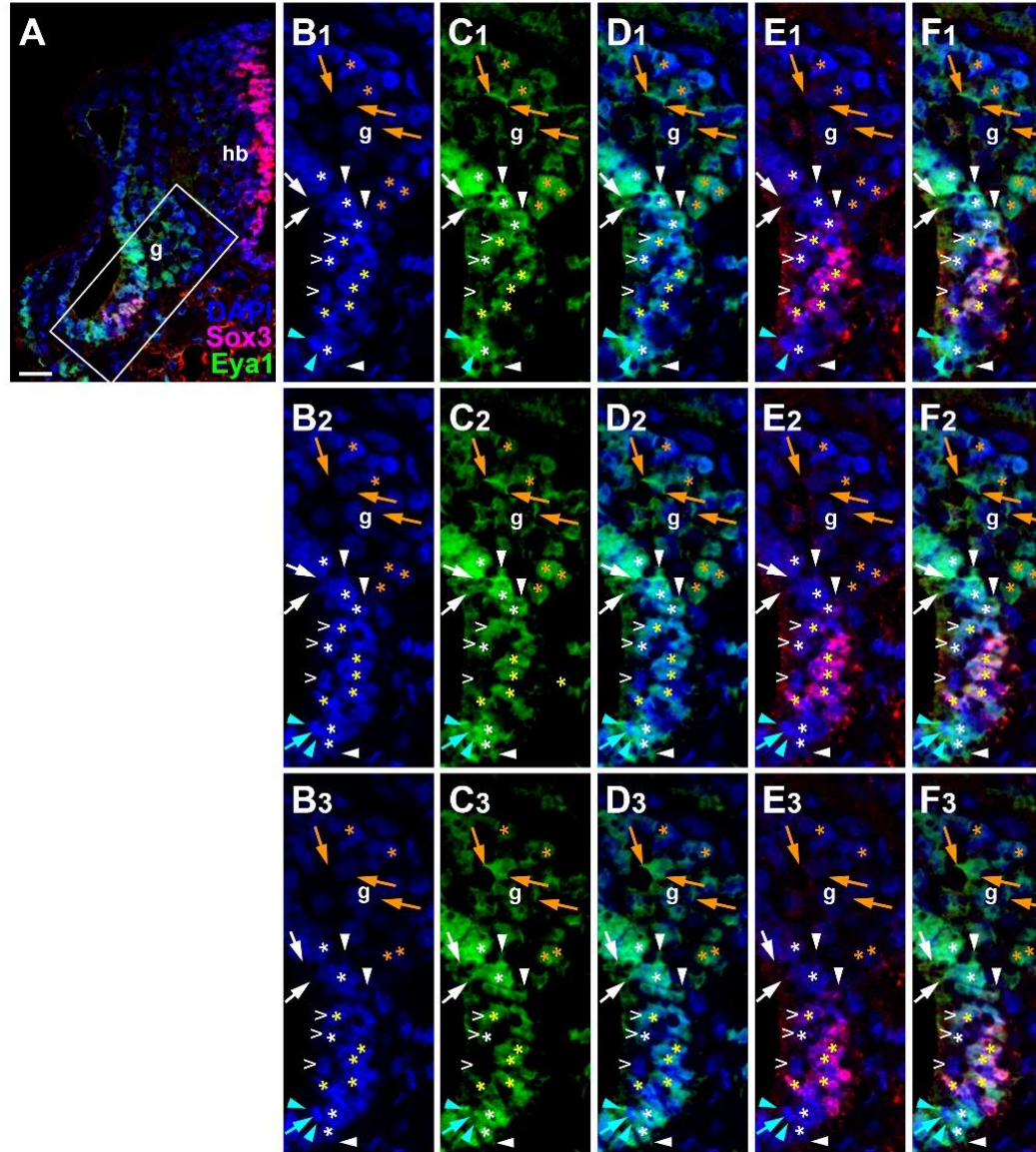


**Fig. 4.7. Subcellular localization of Eya1 protein in otic vesicle and vestibulocochlear ganglion at stage 35.** Immunostaining for Eya1 and Sox3 in a transverse section through the center of the left otic vesicle of *Xenopus* embryos at stage 35 analyzed by confocal microscopy (dorsal to the top, medial to the right). **A:** Overview showing the same confocal plane as **B<sub>2</sub>-F<sub>2</sub>**. **B-F:** Magnified views of the boxed area shown in different channels (columns B-F) and in three different confocal planes (rows 1-3). Putative hair cells indicated by white open arrowheads. Nuclear staining indicated by asterisks; cytoplasmic staining indicated by arrows. White asterisks show nuclear Eya1 staining in the otic epithelium; yellow asterisks indicate nuclei that are immunopositive for both Eya1 and Sox3. Orange asterisk indicate Eya1-immunopositive nuclei in the vestibulocochlear ganglion. White arrows show cytoplasmic staining in the otic epithelium; orange arrows show cytoplasmic Eya1 staining in the ganglion. White

arrowheads highlight Eya1-positive protrusions of delaminating cells. Mint arrowheads indicate cytoplasmic Eya1 staining in a dividing cell of the otic epithelium with the mint arrow indicating the division plane. Note that Eya1 shows mostly nuclear but also some cytoplasmic localization in the otic epithelium. Sox3-immunopositive nuclei also co-express Eya1, but at lower levels than adjacent cells. A subset of putative hair cells shows weak nuclear Eya1 staining and a subset of the latter also is weakly Sox3-immunopositive. In the vestibulocochlear ganglion, nuclear Eya1 is mostly found in cells located at the periphery (probably corresponding to proliferative cells), while in the center of the ganglion, Eya1 is mostly cytoplasmic. G: vestibulocochlear ganglion; hb: hindbrain. Scale bar in A: 25  $\mu$ m.

#### **4.4 Eya1 distribution in relation to Sox3-immunopositive progenitor cells**

Double immunostaining between Eya1 and Sox3 antibodies shows co-localization of both proteins in the nuclei of cells in the ventromedial region of the otic epithelium at stage 29 (Fig. 4.6 H-J). However, Eya1 expression extends further dorsally and ventrolaterally than the Sox3 immunopositive domain (Fig. 4.6 H-J). This suggests that Eya1 expression precedes Sox3 upregulation in proliferative progenitor cells. In addition, nuclear distribution of Eya1 was present mostly in peripheral vestibulocochlear ganglion cells where Sox3 expression was absent (Fig. 4.6 H-J).

At stage 35, overlap between Eya1 and Sox3 continues on the ventromedial side of the otic vesicle (Fig. 4.7 F<sub>1</sub>-F<sub>3</sub>), which has formed two layers. The cells in the basal layer (putative supporting cells) present a nuclear expression of Sox3 and also co-express Eya1 at weak levels, while Eya1 is expressed at higher levels in nuclei of adjacent (presumably proliferative) cells. Only a few of the cells in the apical layer (putative hair cells) show weak nuclear Eya1 staining and only rarely do these also show weak Sox3-immunostaining (Fig. 4.7 B-F). This suggests that hair cells arise from Sox3<sup>+</sup>/Eya1<sup>+</sup> progenitors and downregulate first Sox3 and then Eya1. Similarly, the persistence of Eya1 but not of Sox3 in the vestibulocochlear ganglion suggests that Sox3 is downregulated before Eya1 during neurogenesis



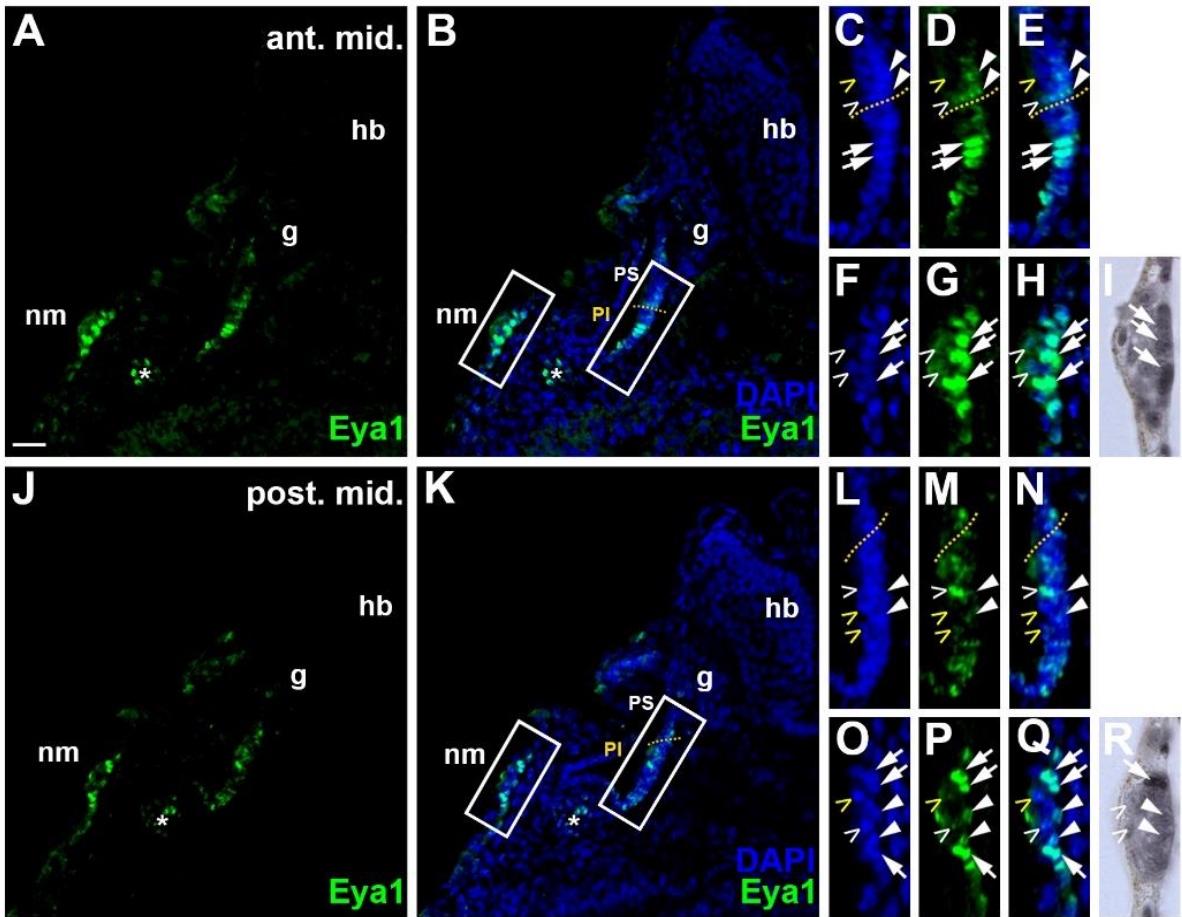


**Fig. 4.8. Subcellular localization of Eya1 protein in otic vesicle and vestibulocochlear ganglion at stage 40.** Immunostaining for Eya1 in transverse sections anterior (ant.mid., **A-H**) and posterior of the midline (post. mid., **J-Q**) of the left otic vesicle of *Xenopus* embryos at stage 40 analyzed by confocal microscopy (dorsal to the top, medial to the right). Overviews of single confocal planes shown in different channels in **A, B** and **J, K**. The approximate dividing line between pars superior (PS) and pars inferior (PI) is shown by a hatched orange line. Otic epithelium and a lateral line neuromast are boxed in **B** and **K** and shown in magnified views in different channels to the right (upper panels: otic epithelium; lower panels: neuromast). Section is through the periphery of the neuromast in **A-H** and through its center in **L-Q**. **I** and **R** show PCNA staining through the periphery and center of a neuromast, respectively (PCNA sections courtesy of G. Schlosser). Open arrowheads indicate hair cells, filled arrowheads indicate supporting cells and arrows indicate other, highly proliferative progenitor cells. Eya1 immunopositive hair cells are indicated by white open arrowheads, other hair cells by yellow arrowheads. Note that Eya1 is strongly expressed in nuclei of progenitors and maintained at weak levels in supporting cells, while only a subset of hair cells express Eya1 very weakly, suggesting that it is downregulated in these cells. Asterisk indicates the ganglion of the glossopharyngeal and middle lateral line nerve. G: vestibulocochlear ganglion; hb: hindbrain; nm: neuromast. Scale bar in **A**: 25  $\mu$ m (for **A, B, J, K**).

#### 4.5 Eya1 distribution in other placodes

Because Eya1 plays a central role for the development of cranial placodes, but the distribution of Eya1 protein during placode development is still unclear, the distribution of Eya1 in the various cranial placodes will be documented here for representative stages (stage 12, 13, 15, 18, 20, 23, 24, 26, 28, 29/30, 32, 35, 37/38 and 40 (Appendix C).

At early stages 12 and 13, no Eya1 expression was detected (data not shown). In neural plate and neural fold stage embryos (stage 15) (Fig. C1), Eya1 was mostly expressed in nuclei of the presomitic mesoderm and some endodermal cells (Fig. C1 A-F'). No nuclear staining was detected in the preplacodal ectoderm (PPE), a wedge-shaped ectodermal thickening intercalated between the neural crest and the epidermis, which is the region of origin for cranial placodes. However, Eya1 staining was found weakly in the cytoplasm of the PPE, distinguishing it from the adjacent neural crest which is devoid of any Eya1 expression (Fig. C 1 A-F').

At stage 20 (Fig. C 2-4), the neural tube has closed, and the brain can be distinguished in anterior transverse sections (Fig. C2 A-C'). The PPE has now given rise to distinct cranial placodes, all of which show nuclear (as well as some cytoplasmic) staining for Eya1 in the inner ectodermal layer. At anterior levels, the olfactory and profundal and trigeminal placodes can be clearly recognized (Fig. C2 A-F'). Located anterior to optic vesicle (ov), the olfactory placode (pOl) shows nuclear staining of Eya1 (Fig. C2 A-C'). In addition, Eya1 is expressed already in the profundal (pPr) and trigeminal placodes (Pv) (Fig. C2 D-F'). Eya1 positive cells are seen to migrate away from these placodes to form the profundal and trigeminal ganglia. While Eya1 was mildly expressed in the adenohipophyseal placode (pAH), it was completely absent from the optic vesicle (ov) (Figs. C2, A-F'', C3. A-C''). The lens placode cannot yet be recognized as a distinct thickening at this stage but the ectoderm overlying the central part of the optic vesicle (not shown) does not show Eya1 expression suggesting that Eya1 is absent from the

prospective lens placode. The outer ectodermal layer of the embryo sometimes shows weak Eya1 expression, which is not restricted to nuclei. In addition, there are scattered Eya1 immunopositive nuclei in the outer layer, which probably label a subset of epidermal cell types, possibly the multiciliated cells (Fig. C2 C') (Schlosser et al., 2008).

Posterior to the eye, a posterior placodal area (pPa) can be recognized in stage 20 (Fig. C3). Eya1 expression was widely expressed in the posterior placodal area (pPa), which it is known to give rise to lateral line (LL), otic (pOt) and epibranchial placodes (EB) (Schlosser and Ahrens, 2004) (Fig. C3 A- C''). Whereas the posterior placodal area has not yet subdivided into different placodes at stage 20, some of its subdomains can already be recognized. Ventral to the otic vesicle, the prospective middle lateral line placode (pM) also shows Eya1 expression (Fig. C3 D- F'). Neural crest streams extend ventrally at this stage and show no Eya1 expression (Fig. C3 D- F'). However, nuclear Eya1 staining is observed in the pharyngeal pouches. In the trunk, Eya1 is expressed in the nuclei and cytoplasm of somite cells (Fig. C4 A- C').

There are no major changes in Eya1 expression at stage 23, except for a stronger expression of Eya1 in the developing anterior pituitary derived from the adenohypophyseal placode (Fig. C4 D- F).

At stage 26, Eya1 continues to be expressed in the nuclei of most placodes (Fig. C5-7 D). The olfactory placode shows strong Eya1 expression (Fig. C5 A-C). Eya1 distribution is also evident in the profundal (pPr) and trigeminal placodes (pV) located on the dorsal (profundal placode) and posterior border (trigeminal placode) of the optic vesicle (Figs. C5, D-F', C6, A-C'). Eya1 positive cells continue to migrate away from these placodes to form the profundal and trigeminal ganglia. In addition, the facial epibranchial (epVII) and anteroventral lateral line placode (pAV) can now be recognized posterior to the optic vesicle with strong expression of Eya1 (Figs. C5, D-F, D''-F'', C6, A-C''). Immediately anterior to the otic

vesicle, *Eya1* distribution is expressed in the anterodorsal lateral line placode (pAD), which is still connected to a small part of the otic vesicle that has not yet invaginated (app). A strong nuclear distribution of *Eya1* was clear in otic vesicle (vOt), and middle lateral line (pM), (ventral to the otic vesicle) (Fig. C6, D-F').

Three further epibranchial placodes can be identified by their high signal of *Eya1* expression at this stage: a glossopharyngeal placode (epIX), adjacent to the second pharyngeal pouch); the first vagal placode (epX1) at the level of the otic vesicle; and the second vagal placode (epX2) in postotic sections (Figs. C6, D''-F'', C7, A-F'). The posterior poster lateral line placode (pP), which is located immediately dorsal to the second vagal placode also shows strong *Eya1* signal (Fig. C7 D-F').

At stage 32, olfactory placode (pOl) and adenohipophyseal placode (AH) continue to show strong *Eya1* expression (Fig. C8 A-I'). *Eya1* expression was also found in a small remnant of the profundal placode cells (pPr) dorsal to the optic vesicle (ov) (Fig. C8 G-I'). At the level of the central optic vesicle, the profundal ganglion (gPr) is now distinguishable as an aggregate of condensed cells and expresses *Eya1* (Fig. C9 A-C'). The anteroventral lateral line placode (pAV) was recognized ventrally of the optic vesicle and shows *Eya1* expression (Fig. C9 A-C''). In addition, the facial epibranchial placode (epVII) located ventrally of the optic vesicle and associated with the first pharyngeal pouch shows distribution of *Eya1* (Fig. C9 A-C'). However, *Eya1* is still absent from the retina that formed from the optic vesicle and from the lens placode (Fig. C9 A-C'). At the posterior border of the retina, *Eya1* is expressed strongly in cells migrating away from the trigeminal placode (pV) to form the trigeminal ganglion (Fig. C9 D-F').

In addition, *Eya1* is strongly expressed in a thickened ectodermal area that forms the anterodorsal lateral line placode (pAD) (Fig. C10 A-C'). There was also a weak signal of *Eya1* expression in the glossopharyngeal placode (Fig. C10 A-C') located adjacent to the second pharyngeal pouch (app). Also, *Eya1* was still expressed in the epithelium of otic vesicle (vOt) and middle lateral line placode (pM) (Figs. C10,

D-F', C11, A-C'). A weak signal of Eya1 is seen in the first vagal epibranchial placode (epX1) (Fig. C11, A-C'). At trunk levels Eya1 is still strongly expressed in somite cells (som) and the posterior lateral line placode (pP) (dorsal part) and the ventrally adjacent second vagal epibranchial placode (Fig. C11, D-F').

At stage 40, Eya1 is still expressed in the olfactory epithelium (eOl) derived from the olfactory placode (pOl) (Fig. C12 A-C'). Also, distribution of Eya1 was obvious in the remnant of the anterodorsal lateral line (pAD) (Fig. C13 A-F'). The sensory ridge of the supraorbital lateral line (so) which extends from the anterodorsal lateral line placode (pAD) shows a strong staining of Eya1 expression (Figs. C12, D-I', C13, A-C'). In addition, Eya1 was found in the sensory ridge of the infraorbital lateral line (io) that also elongated from the anterodorsal lateral line (pAD) (Figs. C12, D-I', 1.13, A-F'). The anteroventral lateral line placode (pAV) has now also elongated to form a sensory ridge in the ventral head ectoderm which continues to show Eya1 expression (Figs. C12, G-I, C13, A-C').

Furthermore, Eya1 was found in the primordium of the adenohypophysis (AH) (Fig. C12 G'-I'). Eya1 is still absent from retina and the lens, which has developed from the lens placode (Figs. C12, D-I, C13, A-C). Although profundal and trigeminal placodes have disappeared in this stage and Eya1 expression has been lost from the profundal ganglion, a few cells of the trigeminal ganglion (gV) still show Eya1 expression (Fig. C13 A-C'). A small remnant of the facial epibranchial placode (epVII) was determined by Eya1 staining (Fig. C13 A-C'). Additionally, the size of the Eya1 expressing glossopharyngeal placode (epIX) was decreased at stage 40 (Fig. C13 D-F'). There is also decreased Eya1 expression in some areas of the otic vesicle (vOt) as described in detail above (section 4.2), while it is still expressed in the middle lateral line placode (pM) (Fig. C14 A-I'). Eya1 staining is still recognized in a small area of the first vagal placode (epX1) and a weak signal of Eya1 is evident in the first and second hypobranchial placode (hp1, hp2) that is adjacent ventral of the second and third pharyngeal pouch (Fig. C14 D-I'). Also, Eya1 was strongly expressed in a small area located dorsally to the posterior lateral

line identified as supratemporal placode (pST) by Schlosser and Northcutt, 2000 (Fig. C15 A-C'). By stage 40, the posterior lateral line (pP) is still present and expresses Eya1 (Fig. C15 A-C'). In addition, a high level of Eya1 expression appeared in the primordium of the middle trunk line (m) that extends caudally from the posterior lateral line placode (Fig. C15 D-F'). Additionally, Eya1 expression was also detectable in a few cells located ventrally in the primordium of the ventral trunk line (v) (Fig. C15 D-F'). Somite cells have downregulated Eya1 expression at stage 40 with exception of a group of strongly Eya1 immunopositive nuclei at their ventrolateral border, which are the migratory hypaxial muscle precursors (David et al., 2001) (Fig. C15 A-F').

#### 4.6 Summary

To begin to understand the role of Eya1 for otic neurogenesis, the distribution of Eya1 protein was analysed in the developing otic vesicle using a *Xenopus*-specific Eya1 peptide antibody raised in guinea-pigs (Ahrens and Schlosser, 2005). This antibody specifically recognizes Eya1 protein and allowed me to characterize the subcellular localization of Eya1 proteins, their levels of expression as well as their distribution in relation to progenitor and neuronal differentiation markers during otic neurogenesis. This analysis showed that Eya1 protein localizes to both nuclei and cytoplasm in the otic epithelium, with levels of nuclear Eya1 declining in differentiating (Islet1/2+) vestibulocochlear ganglion neurons and in the developing sensory areas. The different levels and subcellular localization of Eya1 in progenitors and differentiating cells probably has important functional implications since previous studies revealed strongly dosage-dependent effects of Eya1 with high levels promoting a progenitor state and low levels promoting neuronal differentiation (Schlosser et al., 2008; Zou et al., 2008; Riddiford et al., 2017).

## Chapter-5 The function of *Eya1* in otic neurogenesis

*Eya1* and its binding partner, the transcription factor *Six1*, have been shown to be specifically required for the generation of sensory and neuronal cells from the otic vesicle and other placode-derived structures in amniotes and zebrafish (Xu et al., 1999; Zheng et al., 2003; Laclef et al., 2003; Zou et al., 2004; Bricaud and Collazo, 2006; Schlosser et al., 2008; Ahmed et al., 2012a; Ahmed et al., 2012b; Riddiford and Schlosser, 2016; Schlosser et al., 2008; Schlosser, 2010). In *Xenopus laevis*, *Six1* and *Eya1* knockdown leads to smaller otic vesicles and a reduction of expression of many markers of neurogenesis and placodal ectoderm such as *Neurog1*, *Atoh1*, *Pou4f1*, *Gfi1*, *NeuroD*, *Delta1*, *Sox3* and *Sox2* (Li et al, 2010; Riddiford and Schlosser, 2016; Schlosser et al., 2008). However, the specific deficiencies in otic neurogenesis after *Eya1* loss of function have not yet been studied in *Xenopus* and will be the focus of this chapter.

### 5.1 Efficacy and specificity of *Eya1* Morpholinos

Two *Eya1* morpholino antisense oligonucleotides (MO), *Eya1*MO1 (5'-TACTATGTGGACTGGTTA-GATCCTG-3') and *Eya1*MO2 (5'-ATATTTGTTCTGTCAGTGGCAAGTC-3') were used in this study, the effectivity and specificity of which was previously verified by their ability to block *Eya1* protein synthesis in vitro and by rescue experiments (Schlosser et al., 2008). To confirm that these *Eya1* MOs effectively blocked *Eya1* protein synthesis in vivo, a western blot (immunoblot) was performed after extracting proteins from *Xenopus* embryos.

Unfortunately, the *Eya1* antibody was unable to detect native *Eya1* protein in immunoblots after extraction of proteins from twenty uninjected embryos at stage 14, suggesting that the quantity of native *Eya1* proteins in vivo is not enough. Therefore, twenty embryos were injected with *Eya1* (500 pg) and *H2B-GFP* mRNAs (250 pg) and proteins extracted at stage 14. Both *Eya1* and GFP bands

were detectable in these protein extracts (Fig. 5.1). In the western blot, the efficacy of Eya1 MOs was verified by a strong reduction in Eya1 protein after coinjection of Eya1-MO1 and Eya1-MO2 (1 ng each) (Fig. 5.1).

To check whether Eya1 MOs effectively block Eya1 protein synthesis in the otic vesicle, embryos were injected with a mixture of Eya1-MO1 and Eya1-MO2 (1ng each) and co-injected with mGFP as a lineage tracer at the two cells stage, then embryos were collected at stage 26 following double immunostaining (Fig. 5.2 A-F). Injection of Eya1 MO resulted in a strong reduction of Eya1 protein, which was completely eliminated in some sections of otic vesicle at stage 26 (Fig. 5.2 A-F). In contrast, Eya1 expression was found strongly in nuclei of the otic epithelial cells on the uninjected side (Fig. 5.2. A-C) or after injection of control MO (Fig. 5.2 G-I). This suggests that the Eya1 MOs indeed block protein synthesis of Eya1 in the otic vesicle.

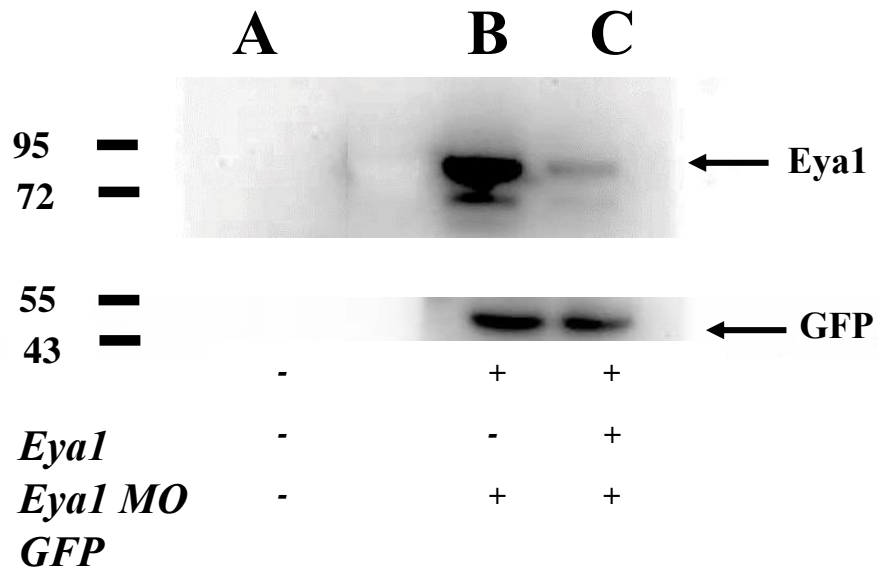


**Fig. 5.1. Specificity of Eya1 morpholinos.** Western blot to evaluate effectivity of Eya1 MOs in blocking *Eya1* translation in vivo. GFP was used as loading control. Eya1 was revealed with GP1 Eya1 antibody; GFP with Rabbit GFP antibody. Lane (A): Eya1 protein was not detected in uninjected embryos. Lane (B): Eya1 protein was detected after injection of *Eya1* mRNA. Lane (C) : Coinjection of *Eya1* MO1+2 reduced synthesis of Eya1 protein from injected *Eya1* mRNA. In B, C lanes, approximately equal intensity of GFP signal was recognized.



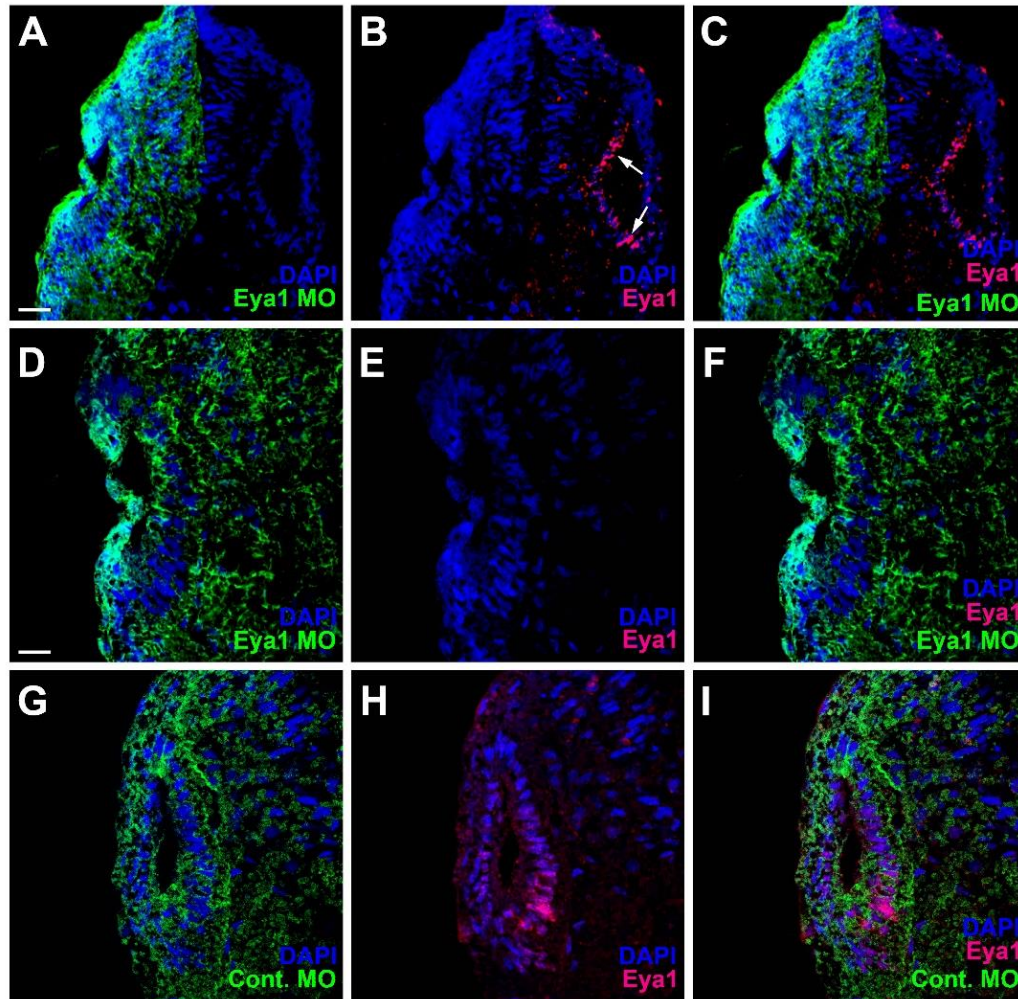


**Fig. 5.2. Effective reduction of otic Eya1 immunostaining by Eya1 morpholinos.** **A-F:** Transverse section through the central otic vesicles of a stage 26 *Xenopus* embryo injected with Eya1 MO (dorsal to the top, medial to the right). Different channels are shown in the three columns. In **A-C** the injected side is on the left, the uninjected side on the right. **D-F** show higher magnification views of the injected side. **G-I** show magnified otic vesicles in embryos injected with control MOs. Note that in Eya1 MO-injected embryos (**A-F**), Eya1-immunopositive cells, which are clearly visible in the otic vesicle on the uninjected side (arrows), are absent from the otic vesicle on the injected side suggesting that Eya1 MOs completely block Eya1 protein synthesis, while control MOs have no effect (**G-I**). Scale bars: **A:** 50  $\mu\text{m}$  (for **A-C**); **D:** 25  $\mu\text{m}$  (for **D-I**).

## **5.2 Role of *Eya1* for progenitor formation and neuronal differentiation in the otic vesicle**

### **5.2.1 The effect of *Eya1* knockdown on otic neurogenesis**

To elucidate the role of *Eya1* for otic neurogenesis, embryos were injected with *Eya1* MO1+2 (1 ng each) and co-injected with mGFP as a lineage tracer, which also allowed to visualize the shape of cells in the otic epithelium. This was followed by double immunostaining for GFP and one of the following markers: pH3, EDU, Sox3 and Islet1/2. To rule out unspecific side effects of MO injection (Corey and Abrams, 2001; Gentsch et al., 2018; Eisen and Smith, 2008), a Control MOs (1 ng) was co-injected with mGFP in another subset of embryos. Loss and gain of function experiments were analyzed in sections for at least three embryos for each marker.

To test whether proliferation of cells in the otic epithelium was affected after *Eya1* knockdown, the pH3 antibody was used to detect mitotic cells in stage 26 (Fig. 5.3 A). Injection of *Eya1* MOs significantly reduced the percentage of pH3-positive cells (Figs. 5.3 A, and Table 5.1) in comparison with otic vesicles from uninjected embryos or embryos after injection of control MO, while there was no significant change in the percentage of pH3-immunopositive cells after injection of control MO compared to wild type (Figs. 5.3 A and Table 5.1). This shows that cell proliferation in the otic vesicle is decreased after *Eya1* knockdown.

The effect of *Eya1* knockdown on markers of otic neurogenesis (EdU, Sox3 and Islet1/2) was then analyzed in more detail in transverse sections through the otic vesicle of stage 35 *Xenopus* embryos and compared with otic vesicles of embryos injected with control MOs (Fig. 5.3 B-M) or with the otic vesicle on the uninjected side of the same embryos (Fig. 5.3). The number of proliferating progenitor cells in the otic epithelium was still reduced at stage 35 after *Eya1* knockdown as indicated by reduced EdU staining although there were residual EdU immunopositive cells in some regions of the otic epithelium (Figs. 5.3, B-C, 5.4, A-B). The number of Sox3-immunopositive sensorineural progenitors in the

ventromedial region of the otic epithelium was also reduced after *Eya1* knockdown (Figs. 5.3, F-G, 5.4, C-D). Furthermore, *Islet1/2*-immunopositive differentiating neurons in the vestibulocochlear ganglion were clearly reduced (Figs. 5.3, J-K, 5.4, E-F). *Islet1/2* was also reduced in the developing sensory areas of the otic epithelium (putative supporting cells) (Fig. 5.4 G-H). In contrast, there was no change in the expression of *EdU*, *Sox3* and *Islet1/2* in the otic vesicle after injection of control MOs (Fig. 5.3 D-E, H-I, L-M).

**Table. 5.1. Percentage of mitotic (pH3 positive) nuclei during otice vesicle development after *Eya1* gain and loss of function.**

	Embryos	DAPI nuclei	pH3	%
Wild type	1	317	7	0.02208
	2	358	5	0.01396
	3	466	6	0.0128
<i>GR-Eya1</i> mRNA	1	375	51	0.136
	2	261	30	0.1149
	3	294	37	0.1258
Control MO	1	393	5	0.012
	2	376	6	0.015
	3	268	8	0.02
<i>Eya1</i> MO1+2	1	389	1	0.0025
	2	371	1	0.002
	3	422	4	0.009

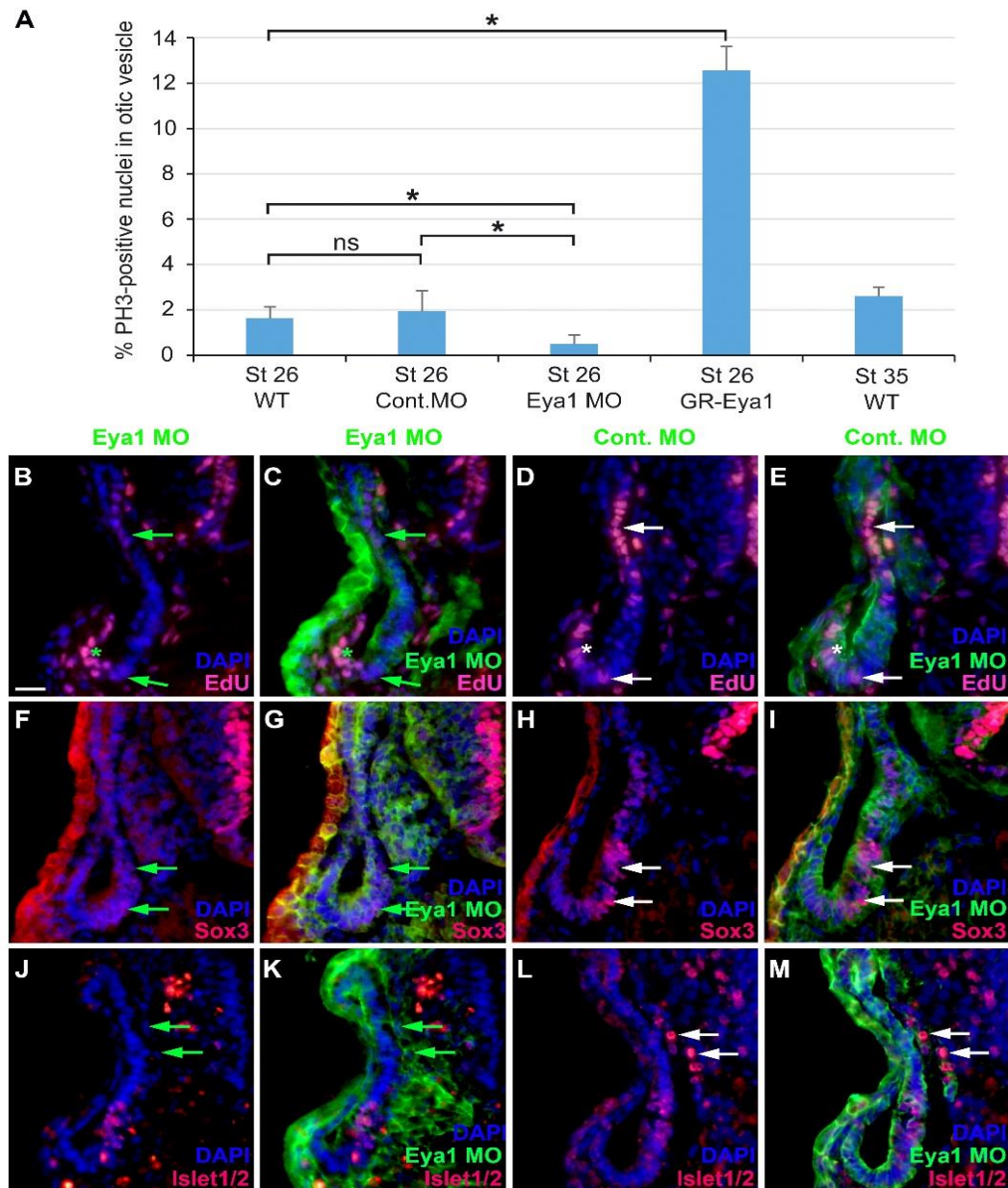


**Fig. 5.3. Role of *Eya1* in otic neurogenesis in comparisons of embryos injected with *Eya1* MOs or Control MOs.** **A:** pH3-immunopositive (mitotic) cells in the stage otic vesicle are unchanged after injection of Control MO (ns: not significant) but are significantly reduced after *Eya1* MO injection and significantly increased after GR-*Eya1* injection and DEX treatment at stage 19 compared to untreated (asterisk:  $p < 0.05$ , t test;  $n=3$  for each condition; standard deviations are indicated). **B-M:** Changes of EdU-positive proliferative progenitors (**B-E**), and Sox3- (**F-I**) and Islet1/2-immunopositive cells (**J-M**) in transverse sections through the central otic vesicle of stage 35 *Xenopus* embryos injected with *Eya1* MOs (left two columns; different channels of same section) or control MOs (right two columns; different channels of same section) (dorsal to the top, medial to the right). Reductions of EdU labelling and Sox3- or Islet1/2-immunoreactive cells in otic vesicle of *Eya1* MO injected embryos are indicated by green arrows (compare to white arrows for otic vesicle in Control MO injected embryos). Residual EdU labelling in otic vesicle of *Eya1* MO injected embryo is indicated by a green asterisk (compare to white asterisk for otic vesicle in Control MO injected embryo). Scale bar in **B**: 25  $\mu\text{m}$  (for **B-M**).



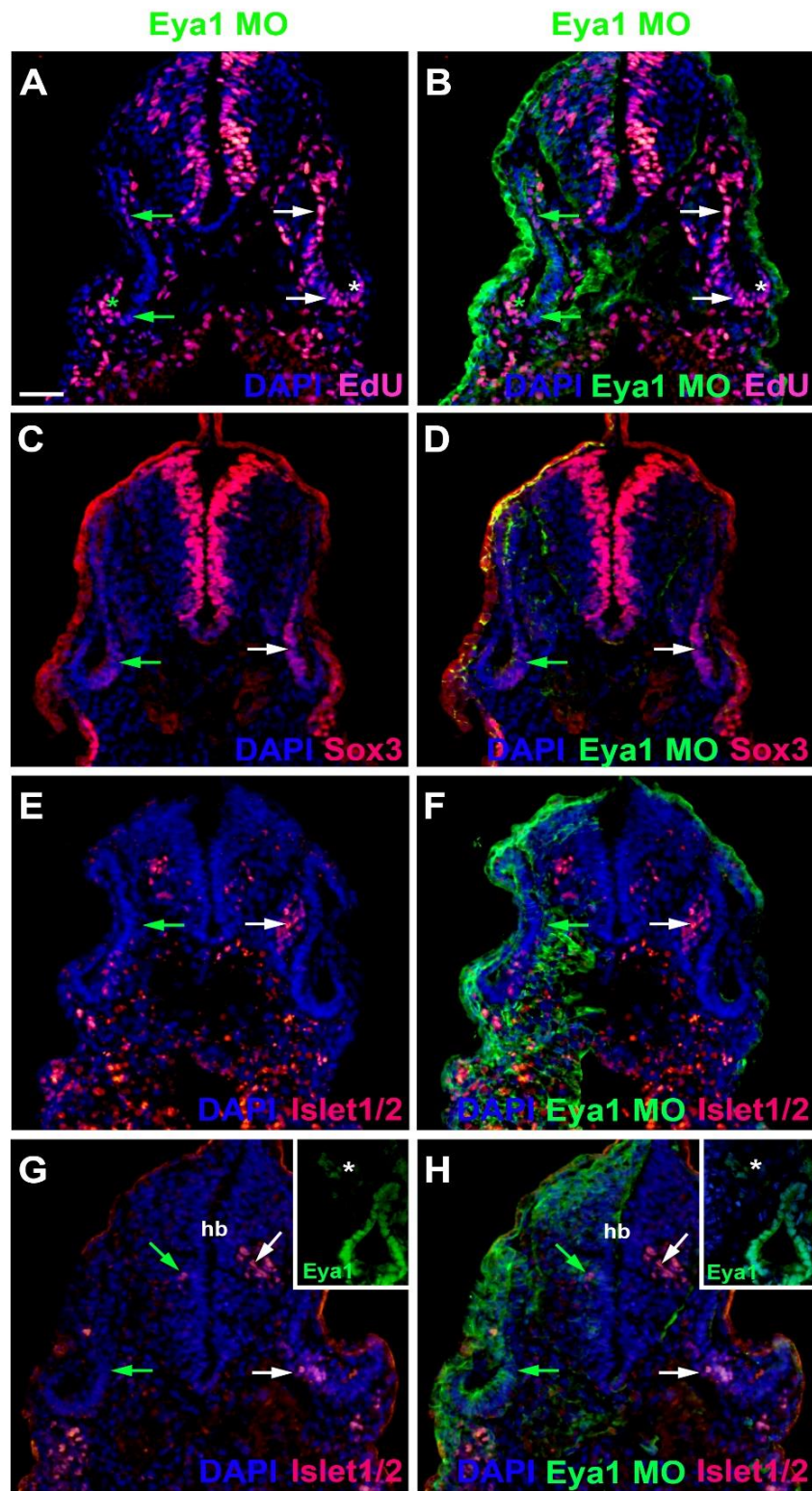


**Fig. 5.4. Role of Eya1 in otic neurogenesis in embryos injected with Eya1 MOs: Comparison of injected and uninjected sides.** Changes of EdU-positive proliferative progenitors (A, B), and Sox3- (C, D) and Islet1/2-immunopositive cells (E-H) in transverse sections through the central otic vesicles of stage 35

*Xenopus* embryos injected with Eya1 MO (dorsal to the top, medial to the right). Different channels of the same section are shown in the first and second column. In each panel, the injected side is on the left and the uninjected side is on the right. Reductions of EdU labelling and Sox3- or Islet1/2- immunoreactive cells in otic vesicle of Eya1 MO injected embryos indicated by green arrows (compare to white arrows for otic vesicle on uninjected side of same embryos). Residual EdU labelling in otic vesicle of Eya1 MO injected embryo indicated by green asterisk (compare to white asterisk for otic vesicle on uninjected side of same embryos). **E, F** and **G, H** show sections through two different embryos, one showing reduction of Islet1/2 in the vestibulocochlear ganglion (**E, F**), the other showing Islet1/2 reduction in the otic epithelium and the motorneurons of the hindbrain (**G, H**). The latter also are Eya1-immunopositive as shown in the insets (marked by asterisks). Scale bar in **A**: 50  $\mu\text{m}$  (for all panels).

Previous studies demonstrated that Eya1 and Six1 interact directly during otic vesicle neurogenesis and co-regulate many genes (Li et al., 2003; Ahmed et al., 2012a, b; Schlosser et al., 2008; Riddiford et al., 2016). If Eya1 exerts its effect on otic neurogenesis mainly due to its cooperation with Six1, it should be possible to mimic the effects of Eya1 knockdown by overexpressing a dominant-negative construct interfering with Six1 function. To test this hypothesis, it was decided to check expression of markers for otic neurogenesis after injection of the dominant-negative Six1 construct EnR-Six1 (Brugmann et al., 2004). This construct combines the Six domain and homeodomain of Six1 with the Engrailed repressor (EnR) domain and represses Six1 target genes in a cofactor-independent manner (Brugmann et al., 2004). To avoid perturbation of early embryonic development and to enable specific activation of this dominant-negative construct during the time window of otic neurogenesis, a hormone-inducible form of this construct (GR-EnR-Six1) was generated by adding the human glucocorticoid receptor (GR) as an upstream cassette. Embryos were then injected at the two cell stage with GR-EnR-Six1 and mGFP and incubated in dexamethasone (DEX) from stage 18 on to activate nuclear translocation of GR-EnR-Six1. Next, embryos were collected at stage 35, cryosectioned and double immunostained for GFP and for EdU, Sox3 or Islet1/2 (Fig. 5.5).

Transverse sections through the otic vesicles of these GR-Six1-EnR injected *Xenopus* embryos show a mild reduction of EdU-positive proliferative progenitor cells in injected side of the otic vesicle epithelium compared to uninjected side (Fig. 5.5 A-C). However, there was no obvious change in the expression of Sox3 between injected side and uninjected side (Fig. 5.5 D-F). The number of Islet1/2 positive differentiating neurons in the vestibulocochlear ganglion was also slight reduced compared to control otic vesicle (Fig. 5.5 G-I).

These findings show only relatively mild effects of GR-EnR-Six1 compared to Eya1 MO injections, but partly mimic the effect of Eya1 knockdown on EdU and Islet1/2.

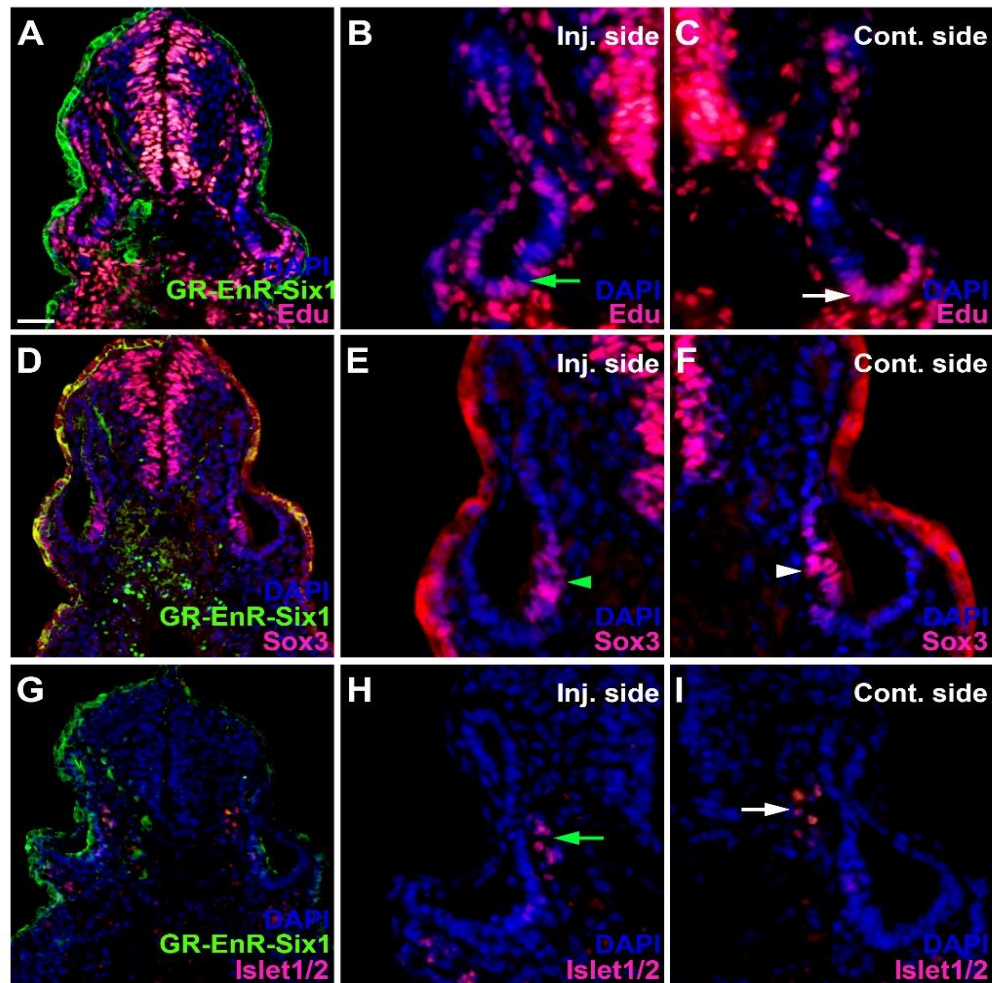


**Fig. 5.5. Role of Eya1/Six1 in otic neurogenesis as revealed by injection of the dominant negative construct GR-EnR-Six1.** Changes of EdU-positive proliferative progenitors (A-C), and Sox3- (D-F) and Islet1/2-immunopositive cells (G-I) in transverse sections through the central otic vesicles of stage 35 *Xenopus* embryos injected with GR-EnR-Six1 and induced with DEX at stage 18 (dorsal to the top, medial to the right). The first columns show an overview (injected side to the left), while the second and third columns higher magnification views of the otic vesicle on the injected and uninjected sides, respectively. There are only mild differences between injected and injected sides. Green arrows indicate a slight reduction of EdU-staining on the injected side compared to control side (white arrows), while no differences in Sox3-immunostaining could be observed between injected (green arrowheads and uninjected sides (white arrowheads). Islet1/2-immunostaining was slightly reduced on the injected side (green arrows) compared to the uninjected side (white arrows) in some embryos, while in other embryos (not shown) it was slightly increased on the injected side. Scale bar in A: 50  $\mu$ m (for all panels).



### 5.2.2 The effect of *Eya1* overexpression on otic neurogenesis

To complement our loss of function studies, we overexpressed GR- *Eya1* and GR- *Six1* individually by mRNA injection and co-injected mGFP. Then embryos were DEX-incubated from stage 17-19 and embryos were collected at stage 35, followed by cryosections and double immunostaining for GFP and for pH3, EdU, Sox3 or Islet1/2.

To gain insight into the effect of *Eya1* overexpression on proliferation, embryos that had been injected with GR-*Eya1* were incubated in DEX from stage 17-19 (neural tube stage) up to stage 26. Nuclei immunopositive for pH3 (mitotic cells) were counted and their proportion of total nuclei (stained with DAPI) was calculated (Fig. 5.4 A and Table 5.1). There was a significant increase of mitotic cells in the otic vesicle after *Eya1* overexpression compared to wild type embryos indicating that cell proliferation in the otic vesicle is increased after *Eya1* overexpression (Fig. 5.3 A and Table 5.1).

Injection of GR-*Eya1* mRNAs also expanded the distribution of EdU in the otic vesicle on the injected side in comparison with the otic vesicle on the uninjected side (Fig. 5.6 A-C). In one of the GR-*Eya1* injected embryos, EdU staining was elevated in the ventromedial part of the otic epithelium, but appeared to be reduced elsewhere. This confirms the results obtained after pH3 staining suggesting an increase of proliferation after GR-*Eya1* injection (Fig 5.3 A). Overexpression of GR-*Six1* similarly led to an increase in EdU-positive proliferative progenitors in the otic vesicle on the injected side in one embryo (Fig. 5.6 D-F), but to a decrease in another embryo (not shown).

Although *Eya1* overexpression did not notably affect Sox3 immunostaining in the injected otic vesicle epithelium, GR-*Six1* injection showed a decrease in the Sox3 distribution on the injected side (green arrows- Fig. 5.6 G-L). Finally, overexpression of GR-*Eya1* or GR-*Six1* typically caused a slight reduction in

Islet1/2 immunopositive cells in the vestibulocochlear ganglion on the injected side (Fig. 5.6 M-R). However, in one embryo, Islet1/2 expression was slightly increased in the vestibulocochlear ganglion after GR-Six1 injection (data not shown).

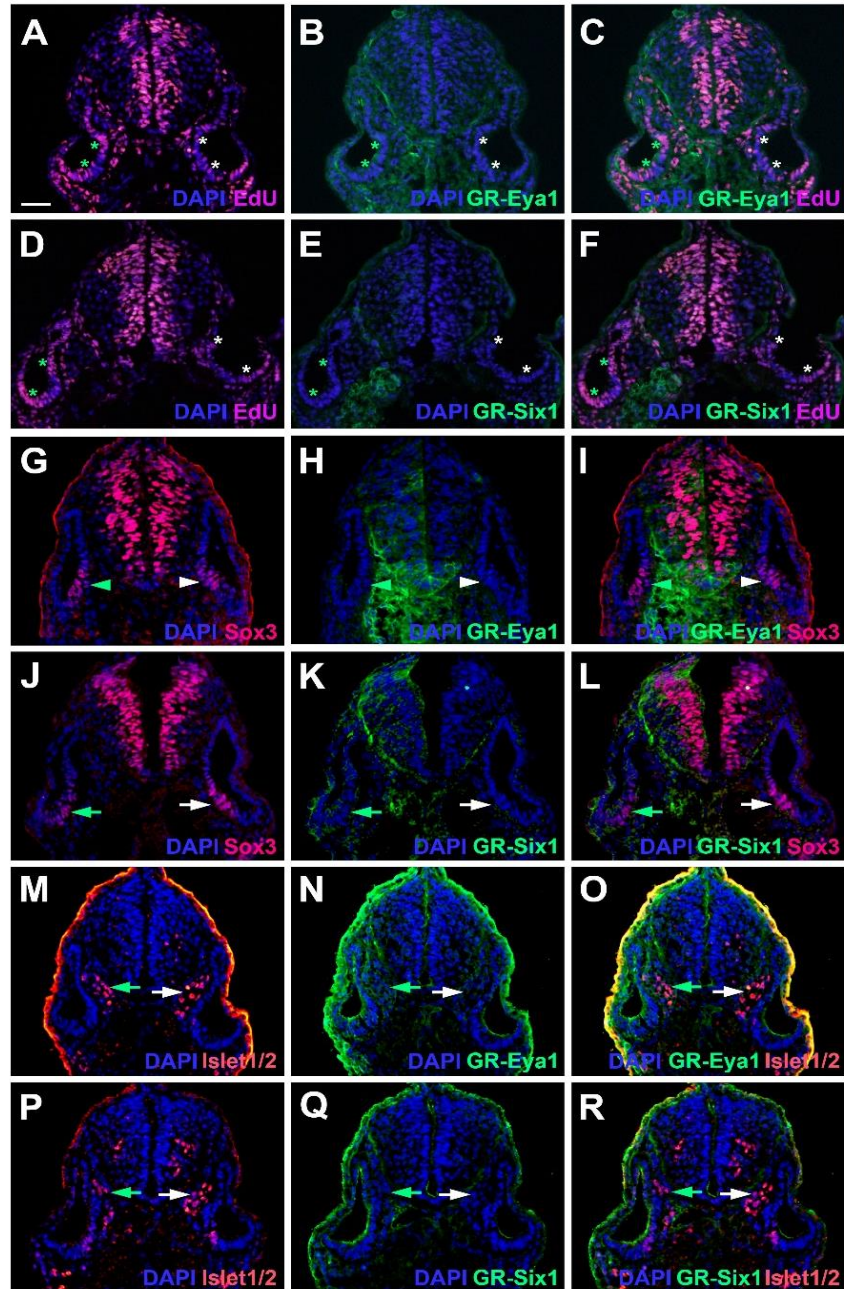


**Fig. 5.6. Role of Eya1/Six1 in otic neurogenesis as revealed by overexpression of GR-Eya1 or GR-Six1.** Changes of EdU-positive proliferative progenitors (A-F), and Sox3- (G-L) and Islet1/2-immunopositive cells (M-R) in transverse sections through the central otic vesicles of stage 28 (Sox3) and 35 (EdU, Islet1/2) *Xenopus* embryos injected with GR-Eya1 (A-C, G-I, M-O) or GR-Six1 (D-F, J-L, P-R) and DEX-induced at stage stage 17/19 (dorsal to the top, medial to the right). Different channels of the same section

are shown in the first, second and third column. In each panel, the injected side is on the left and the uninjected side is on the right. Increased EdU labelling in the otic vesicle on the injected side (after GR-Eya1 or GR-Six1 injection) is indicated by green asterisks (compare to white asterisk for otic vesicle on uninjected side). Reductions of Sox3- (after GR-Six1 injection) and Islet1/2-immunoreactive cells (after GR-Eya1 and GR-Six1 injection) in otic vesicle on the injected side are indicated by green arrows (compare to white arrows for otic vesicle on uninjected side of same embryos). In other embryos (not shown), numbers of Islet1/2-immunopositive cells were slightly increased after GR-Six1 injection. Scale bar in **A**: 50  $\mu\text{m}$  (for all panels).

These results indicate that Six1 and Eya1 have overall similar effects on otic neurogenesis when overexpressed and are sufficient to promote progenitor proliferation, which typically interferes with neuronal differentiation. The seemingly paradoxical finding that Islet1/2 in the vestibulocochlear ganglion may be increased or decreased after Six1 overexpression and that EdU staining in the otic vesicle may occasionally be decreased rather than increased after Eya1 or Six1 overexpression is in line with previous reports that *Islet2* as well as *Neurog1/2* expression in cranial placodes can be either increased or decreased after overexpression of Eya1 or Six1 (Schlosser et al., 2008; Riddiford et al., 2016, 2017). These opposite phenotypes may result from the fact that Eya1 and Six1 are required for both progenitor proliferation and neuronal or sensory differentiation but promote progenitor proliferation at high doses (thereby inhibiting differentiation), while they promote differentiation at low doses (Schlosser et al., 2008; Zou et al., 2008; Riddiford et al., 2017), as will be discussed in more detail in chapter 6.

### **5.3 Role of Eya1 for apicobasal cell polarity in the otic vesicle**

Because changes in the distribution of cell polarity proteins accompany and possibly help to regulate the transition between epithelial progenitors and delaminating neurons in the *Xenopus* otic vesicle (see chapter 3), I next analysed whether knockdown or overexpression of Eya1 also affected the distribution of cell polarity proteins. Again, two different morpholinos antisense oligonucleotides

(*Eya1* Mo1 and *Eya1* Mo2) or mRNAs encoding GR-*Eya1* were injected into one out of two cells of embryos of *Xenopus laevis* and the otic vesicle was then analyzed in transverse sections at stage 26 to explore the effect of *Eya1* gain and loss of function on atypical protein kinase C (aPKC), Partitioning defective 3 homolog (PAR3), Myosin light chain (MLC) and N-cadherin. Co-injected mGFP was used to identify the injected side and to visualize cell membranes in the otic epithelium. Images were taken by using confocal microscopy (Figs. 5.7-5.10).

### **5.3.1 The effect of *Eya1* knockdown on cell polarity proteins**

To investigate how *Eya1* knockdown affects aPKC, PAR3, MLC and N-cadherin, different doses of MOs (1 ng, 2 ng and 10 ng) were injected. No difference was observed between these different doses. To rule out unspecific side effects of MO injection, a control morpholino was co-injected with mGFP in another subset of embryos.

At stage 26, *Xenopus* embryos injected with *Eya1*MO show a mild reduction of Par3 and aPKC expression but not of MLC on the apical side next to the lumen of the otic vesicle epithelium compared to embryos injected with control MOs or compared to the uninjected side (Figs. 5.7 A-F and 5.8 A-L). At higher magnification, PAR3 distribution can be seen to be irregular and delocalized from the apical membrane compared to embryos injected with control MO that show Par3 localized strictly to the apical membrane (Fig. 5.8 A-D, I-L). In addition, Par3 and MLC distribution in cytoplasmic and perinuclear regions was increased compared to the uninjected side of the same embryo or to embryos injected with Control MO (Figs. 5.7 A-B, E-F and 5.8 A-D, I-L).

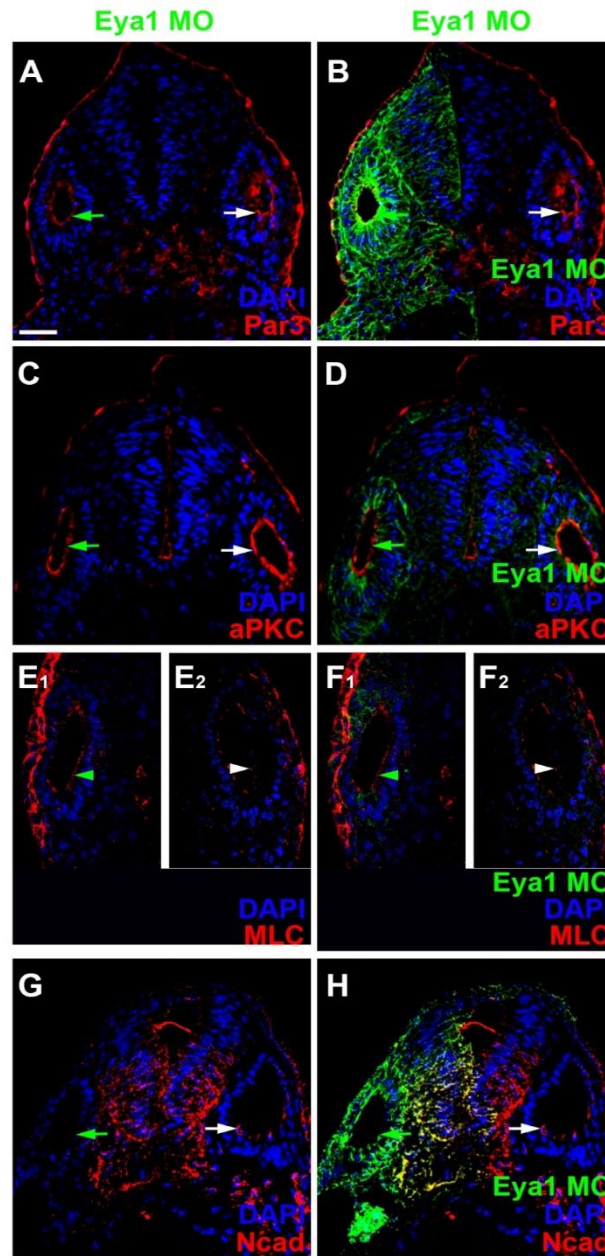


**Fig. 5.7. Role of Eya1 in otic cell polarity in embryos injected with Eya1 MOs: Comparison of injected and uninjected sides.** Changes of Par3 (A, B) aPKC- (C, D) MLC (E, F) and N-Cadherin (G, H) immunostaining in transverse sections through the central otic vesicle of stage 26 *Xenopus* embryos injected with Eya1 (dorsal to the top, medial to the right). Different channels of the same section are shown in the first and second column. In each panel, the injected side is on the left and the uninjected side is on the right. Note that Par3, aPKC and MLC remain apically localized after Eya1 MO injection, although apical protein levels of Par3 and aPKC (green arrows) but not MLC (green arrowhead) are often reduced compared on the injected side compared to the uninjected side of the same embryo (white arrows and arrowhead). However, apicolateral staining of N-cadherin is completely abolished after Eya1 MO injections (green arrow) on the injected side (compare to uninjected side, white arrow). Scale bar in A: 50  $\mu$ m (for all panels).



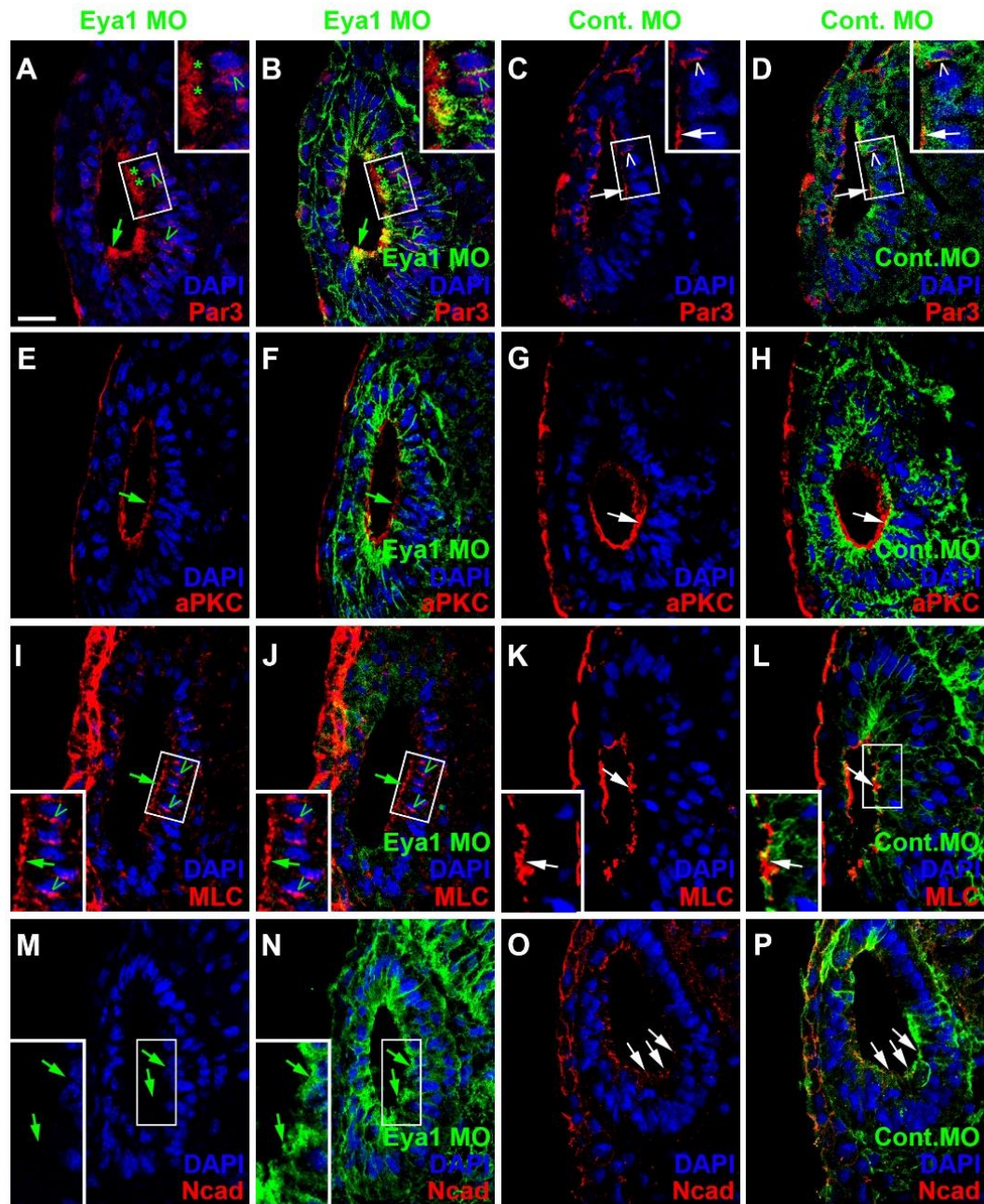


**Fig. 5.8. Role of Eya1 in otic cell polarity in comparisons of embryos injected with Eya1 MOs or Control MOs.** Changes of Par3- (A-D), aPKC- (E-H) MLC (I-L) and N-Cadherin (M-P) immunostaining in transverse sections through the central otic vesicle of stage 26 *Xenopus* embryos injected with Eya1 (left two columns; different channels of same section) or control MOs (right two columns; different channels of same section) (dorsal to the top, medial to the right). The latter show a normal pattern of protein distribution (see Fig. 2). Boxed areas are shown at higher magnification in insets. Protein distribution in the apical and apicolateral membrane (arrows), cytoplasm (asterisks) and between nuclei and membrane (open arrowheads) are indicated. Green symbols indicate

protein distribution in *Eya1* MO injected embryos and white symbols in Control MO injected embryos. Note that Par3, aPKC and MLC remain apically localized after *Eya1* MO injection, although apical protein levels of Par3 and aPKC are often reduced compared to embryos injected with Control MO. Apicolateral staining of N-cadherin is completely abolished after *Eya1* MO injections but not affected after injection with Control MOs. Increasing cytoplasmic and perinuclear distribution of Par3 and MLC is observed in embryos injected with *Eya1* MO as compared to Control MO injected embryos. Scale bar in **A**: 25  $\mu\text{m}$  (for all panels).

To test whether the reduction of apical polarity proteins after *Eya1* MO injection is cell-autonomous, double immunostaining was used to detect aPKC and myc after coinjection of *Eya1*MO1+2 with *myc-GFP*. Different intensities of Myc staining suggested different intensities of *Eya1*MO distribution in epithelial cells of otic vesicle. Embryos, which showed clear mosaic distribution of myc-immunostaining in the otic vesicle were selected and were analyzed for aPKC distribution on the injected side (Fig.5.9 A-C). aPKC was completely reduced on the apical membrane of epithelial cells showing high myc-staining (Fig.5-9 A, C). However, residual aPKC staining was found on the apical surface of adjacent cells showing no myc staining (Figs. 5.9 A, C, 5.7 C-D) suggesting that aPKC is reduced cell-autonomously in those cells, in which *Eya1* is lost.

Most strikingly, knockdown of *Eya1* led to the complete absence of N-cadherin expression on the apical and apicolateral sides of the otic epithelial cells (Figs. 5.7 G-H and 5.8 M-N) in comparison with otic vesicles on the control side (Fig 6.5. A-D) or after injection of control MO (Figs. 5.7 G-H and 5.8 O-P). This suggests that *Eya1* is required to maintain proper apicobasal polarity and apicolateral N-cadherin localization in the otic epithelium while its downregulation may promote N-cadherin depletion (and possibly favor delamination from the otic epithelium).

To test whether these effects of *Eya1* knockdown could be reproduced also by dominant-negative Six1 (see section 5.2.1), embryos were again injected with the dominant negative construct GR-EnR-Six1 and incubated in DEX to activate nuclear translocation at stage 18. Embryos were then collected at stage 26 for

cryosections and immunostaining. Transverse sections through the otic vesicle of a stage 26 *Xenopus* embryo show no clear difference in the distribution of aPKC (other markers were not analyzed due to time constraints) between the injected side and uninjected side (Fig. 5.10 A-C). This raises the possibility that the effects of Eya1 on cell polarity proteins may be mediated in a Six1-independent pathway, but this hypothesis needs to be tested in further studies (for further discussion see chapter 6).

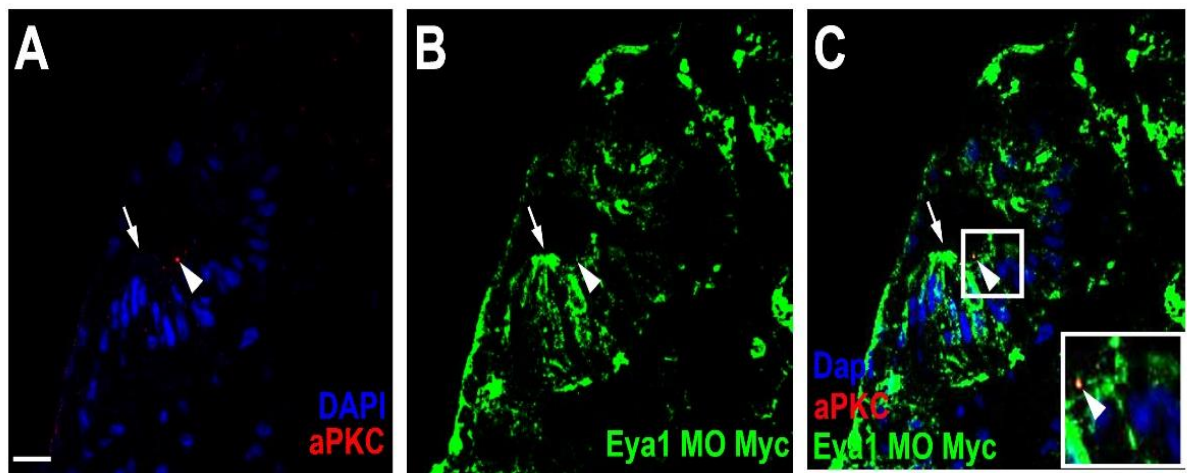


**Fig. 5.9. Role of Eya1 in otic cell polarity in embryos injected with Eya1 MOs and co-injected with Myc-GFP.** Changes of aPKC-immunostaining in transverse sections through the central otic vesicle of a stage 26 *Xenopus* embryo injected with Eya1 Mo-Myc (dorsal to the top, medial to the right) in (A-C). The white arrows are shown distribution of aPKC in epithelial cells receiving a large amount of Eya1 morpholino. Boxed areas are shown at higher magnification in insets. **A- C:** Nuclei are stained with DAPI (blue) and injected side is determined by Myc staining (**B-C**) in epithelial cells of otic vesicle (**B, C**: green). aPKC (**A, C**: red) expression is found weakly in apical membrane. Merged channels. **C:** aPKC disappeared in epithelial cells receiving a large amount of Eya1 morpholino (white arrowhead). White arrowhead points to residual aPKC distribution is observed in epithelial cells that received a small amount of Eya1 morpholino (white box; insert shows area in white box at higher magnification). Scale bars: **A:** 50  $\mu\text{m}$  (for **A-C**).



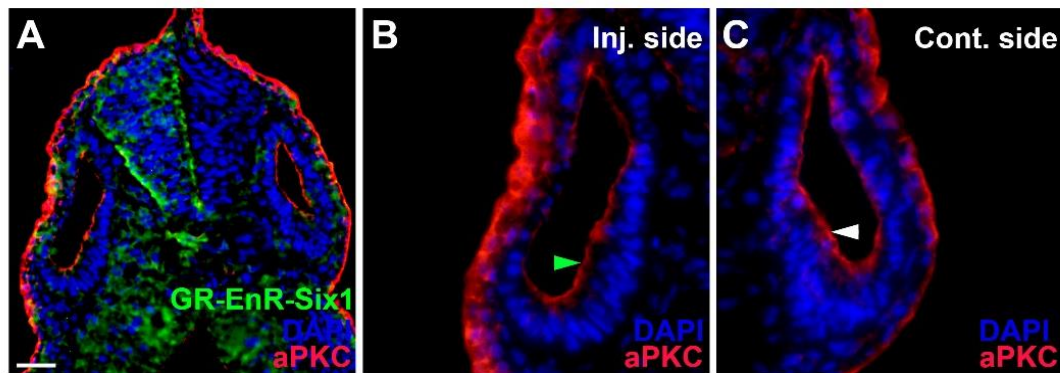


**Fig. 5.10. Role of *Eya1/Six1* in otic neurogenesis as revealed by injection of the dominant negative construct GR-EnR-Six1.** Changes of aPKC-immunostaining in transverse sections through the central otic vesicle of a stage 26 *Xenopus* embryo injected with GR-EnR-Six1 and induced with DEX at stage 17/18 (dorsal to the top, medial to the right). **A** shows an overview (injected side to the left), while **B** and **C** show higher magnification views of the otic vesicle on the injected and uninjected sides, respectively. No major differences of Par3 distribution between injected (green arrowheads) and injected (white arrowheads) sides were observed. Scale bar in **A**: 50  $\mu$ m (for all panels).

### 5.3.2 The effect of *Eya1* overexpression on cell polarity proteins

For *Eya1* overexpression, *GR-Eya1* mRNA was co-injected with *mGFP* mRNA into one cell at the two-cell stage, and nuclear translocation of *Eya1* was activated by DEX treatment from stage 19 (neural tube stage). Cell polarity, proteins Par3, aPKC, MLC and N-cadherin were then analyzed by using double immunostaining with mGFP.

Overexpression of *Eya1* led to no clear changes in the distribution of cell polarity proteins (Par3, aPKC, MLC) or N-Cadherin (*Six1* overexpression was not analysed) (Fig. 5.11) when compared to uninjected otic vesicles (see Fig. 5.7, right sides).

However, some subtle differences in the distribution of cell polarity proteins were noted after *Eya1* overexpression. The distribution of Par3 and aPKC on the apical membrane of the epithelial cells of otic vesicle was more irregular and less clearly apically confined than in uninjected otic vesicles (Fig 5.11 A-F). Similarly, MLC distribution appeared more diffuse and delocalized after the overexpression of *Eya1* (Fig 5.11 G-I).

These results show that *Eya1* overexpression causes only minor, if any changes in the distribution of cell polarity proteins compared to uninjected embryos.

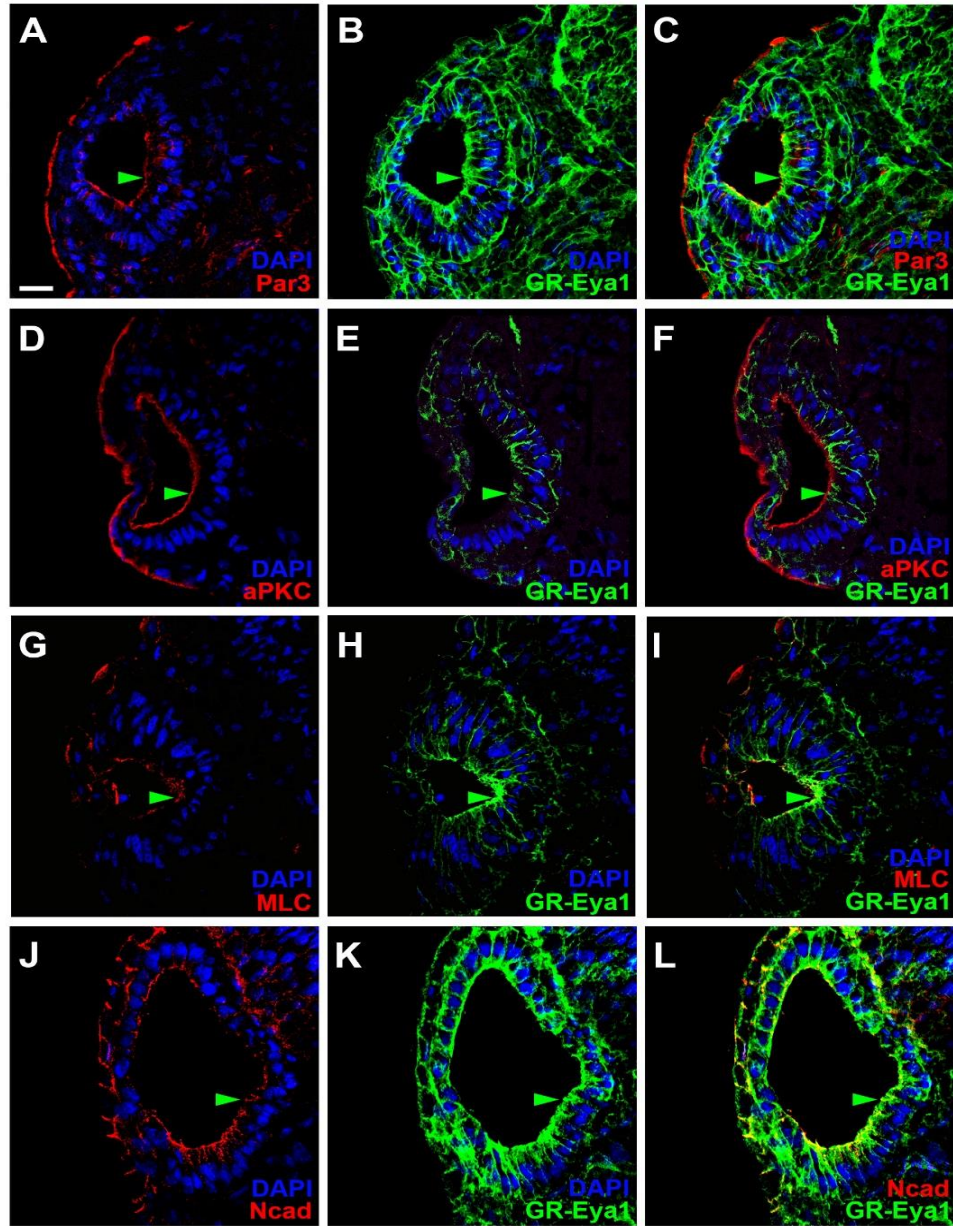


**Fig. 5.11. Role of Eya1 in otic cell polarity as revealed by overexpression of GR-Eya1.** Changes of Par3 (A-C), aPKC- (D-F) MLC (G-I) and N-Cadherin (J-L) immunostaining in transverse sections through the central otic vesicle of stage 26 *Xenopus* embryos injected with GR-Eya1 and DEX-induced at stage 19 (dorsal to the top, medial to the right). Different channels of the same section are shown in the first, second and third column. There are no major changes in protein distribution compared to uninjected embryos (see Fig. 2). Apical or apicolateral localization of all markers highlighted by green arrowheads. Scale bar in A: 25  $\mu$ m (for all panels).

## 5.4 Summary

To characterize the role of Eya1 for otic neurogenesis, I analysed the consequences of Eya1 knockdown or overexpression for cell proliferation and the distribution of progenitors and differentiating neurons as well as for cell polarity proteins in the otic vesicle. Eya1 knockdown significantly reduced the percentage of pH3-immunopositive cells in the otic vesicle at stage 26 and led to a decrease in EdU-staining, indicating that proliferation of otic progenitors is reduced. The number of Sox3-immunopositive cells in the ventromedial otic epithelium and of Islet1/2-immunopositive cells in the ganglion and in the otic epithelium was also reduced. Eya1 MO injection also resulted in some reduction or redistribution of cell polarity proteins and shown irregular and delocalization distribution of PAR3 and aPKC proteins. Most strikingly, apicolateral staining for N-Cadherin was completely abolished in the otic epithelium after Eya1 MO injection. None of these changes were observed after injections of Control MO. This indicates that Eya1 is required for proliferation, formation of Sox3-positive progenitors and the differentiation of sensory neurons in the otic epithelium.

It further suggests that Eya1 is required to maintain proper apicobasal polarity and apicolateral N-cadherin in the otic epithelium while its downregulation may promote N-cadherin depletion and possibly delamination.

## Chapter-6 Discussion

### 6.1 Time course of otic vesicle development

The present study provides the first detailed description of otic neurogenesis in *Xenopus laevis*. Different antibodies were used in this study in order to determine the time course of neuronal differentiation and migration outside of the otic vesicle. Although the development of the otic vesicle is similar in different vertebrates, there are differences in the time of neuronal differentiation of otic vesicle (Alsina et al., 2009; Baker and Bronner-Fraser, 2001; Bailey and Streit, 2005; Maier et al., 2014) (Figs. 1.4, 6.1).

In *Xenopus* like in other vertebrates, all cranial placodes emerge from a crescent-shaped region surrounding the anterior neural plate and located between the neural plate and the epidermis, this region is called preplacodal region (PPR) (or panplacodal primordium) (see Figs. 1.4, 6.1) (Akimenko et al., 1994; Esteve and Bovolenta, 1999; McLarren et al., 2003; Sahly et al., 1999; Sato et al., 2010; Schlosser and Ahrens, 2004; Schlosser and Northcutt, 2000). The PPR subsequently segregates and gives rise to different placodes (Schlosser et al., 2010). In the posterior PPR, initially a common precursor for otic, lateral line and epibranchial placodes forms, the so-called posterior placodal area which is defined by Pax2/8-expression (Alsina and Whitfield, 2017; Schlosser, 2010). At stage 21 in *Xenopus* (after neural tube closure), 10 somites in chick and E8.5 in mouse, the otic placode then begins to separate from the posterior placodal area (Figs. 1.4, 6.1). In zebrafish at the 10 somite stage, the otic placode can be seen as a compacted mass of unorganised ectodermal cells (Fig. 6.1). In most of the vertebrates, the otic placode invaginates to form first the otic cup, containing a cavity and then the otic vesicle, while the otic placode in zebrafish forms the otic vesicle by cavitation (Figs. 1.4, 6.1).

When the otic vesicle is completely detached from the ectoderm, a common neurosensory area containing progenitors for the sensory and supporting cells of the inner ear and for the sensory neurons of the vestibulocochlear ganglion and defined by Sox2 and/or Sox3 expression forms in zebrafish, chick and mammals (Ma et al. 1998; Adam et al. 1998; Andermann, Ungos, and Raible 2002; Alsina et al. 2004; Satoh and Fekete 2005; Pujades et al. 2006; Raft et al. 2007; Millimaki et al. 2007; Millimaki, Sweet, and Riley 2010; Sapede, Dyballa, and Pujades 2012). The results of the present study indicate that Sox3 marks a common neurosensory area in the *Xenopus* otic vesicle, possibly in conjunction Sox2 which is expressed in partly overlapping domains but extends more dorsally (see sections 6.4 and 6.5 for further discussion).

Similar to other vertebrates, in *Xenopus* neurons begin to delaminate from this neurosensory area even before invagination is complete and form the sensory neurons of the ganglion of the eighth (VIII) cranial nerve (vestibulocochlear ganglion) (Freyer and Morrow, 2010; Maier et al., 2014; Sadaghiani and Thiebaud, 1987; Schlosser and Northcutt, 2000; Schlosser and Ahrens, 2004; Schlosser et al., 2008; Schlosser, 2010, 2014; Sullivan et al., 2019) (Figs. 1.4, 6.1).

Delamination of neurons from the sensorineural area in the ventromedial otic vesicle in *Xenopus* was observed between stage 27 and stage 35. During these stages, cells are seen to form basal protrusions, which mirror deformations and disruption in the basal lamina similar to what has been observed in other vertebrates (Carney and Silver, 1983; Hemond and Morest, 1991; Meier, 1979; Whitehead and Morest, 1985a, b) and suggesting that the basal lamina gets displaced and dissolved by cellular protrusions. Based on Islet1/2 expression and acetylated tubulin staining, the first neurons of the vestibulocochlear ganglion differentiate at stage 29 and send out their first neurites at stage 31. The first hair cells in the developing sensory areas differentiate from the sensorineural area at about the same time (stage 32; Quick and Serrano, 2005), followed by the separation into multiple sensory areas from stage 33 on. Therefore, in *Xenopus* otic neurogenesis proceeds in

parallel with the differentiation of the first otic hair cells. This time course resembles zebrafish, but is different from amniotes, where most neurons delaminate before the onset of hair cell differentiation (Fig. 6.1) (Haddon and Lewis 1996; Adam et al. 1998; Pujades et al. 2006; Raft et al. 2007). At stage 39, the basal lamina had largely reformed on the medial side of the otic epithelium, suggesting that delamination of cells has largely stopped.

These findings confirm and extend previous observations, showing that the basal lamina initially completely surrounds the entire otic vesicle but is disrupted on the medial ventral side of the otic vesicle during neuron delamination (Graziadei and Graziadei, 1979; Hemond and Morest, 1991; Hilfer and Randolph, 1993; Meier, 1978). These breaks in the basal lamina suggest that breakdown of the basal lamina plays a role in the migration of neurons from otic vesicle to the vestibulocochlear ganglion (VCG).

Several mechanisms, including release of enzymes from migrating neurons and mechanical forces have previously been suggested to explain the breakdown of the basal lamina in the region of neuronal migration (Hemond and Morest, 1991; Hilfer and Randolph, 1993). In the current study, reconstruction of the shapes of otic epithelial cells after injection of memGFP together with immunostaining with a laminin antibody allowed to further characterize the interplay between delaminating neurons and the basal lamina. Fragments of the basal lamina were found to be attached to protrusions of migrating neurons supporting the idea that there is a mechanical force generated by the epithelial cells migrating out of the otic vesicle, while disruptions of the basal lamina in the vicinity of the protrusions suggest that the latter may release degrading enzymes, similar to what has been observed in other vertebrates (Carney and Silver, 1983; Hemond and Morest, 1991; Hilfer and Randolph, 1993; Meier, 1979; Whitehead and Morest, 1985a,b).

Event	Pre-placodal region (PPR)	Otic placode	Otic cup	Otic vesicle	Migration of neuroblasts into vestibulocochlear ganglion	Differentiation of ganglion cells (first neurites)	Sensory areas begin to separate	First hair cells differentiate	Development of otolith organs and semicircular canals are completed
<i>Xenopus</i>	<b>NF 14</b> (Schlosser and Ahrens, 2004)	<b>NF 21</b> (Schlosser and Northcutt, 2000)	<b>NF 22/23</b> (Schlosser and Northcutt, 2000)	<b>NF 28</b> (Schlosser and Northcutt, 2000)	<b>NF 27-39</b> This study	<b>NF 29/32</b> This study	<b>NF 33</b> This study	<b>NF 31</b> (Quick and Serrano, 2005)	<b>NF 47</b> (Quick and Serrano, 2005)
<i>Zebrafish</i>	<b>10 hpf (1 som)</b> (Akimenko et al., 1994; Sahly et al., 1999)	<b>14 hpf (10 som)</b> (Haddon and Lewis, 1996)	-	<b>19.5 hpf (21 som)</b> (Haddon and Lewis, 1996)	<b>17 hpf to 42hpf</b> (Haddon and Lewis, 1996; Vemaraju et al., 2012)	<b>24/30 hpf</b> (Haddon and Lewis, 1996)	<b>24 hpf</b> (Haddon and Lewis, 1996)	<b>24 hpf</b> (Haddon and Lewis, 1996)	<b>72 hpf</b> (Haddon and Lewis, 1996)
<i>Chick</i>	<b>HH 7 (23-26h; 1 som)</b> (Esteve and Bovolenta, 1999; McLarren et al., 2003)	<b>HH 10 (33-38 h; 10 som)</b> (Hilfer et al., 1989)	<b>HH 12 (45-49 h; 16 som)</b> (Hilfer et al., 1989; Wu and Oh, 1996)	<b>HH 17 (52-64 h)</b> (Wu and Oh, 1996)	<b>HH 16-28 (51 h – 6 d)</b> (D’Amico-Martel and Noden, 1983; Hemond and Morest, 1991; Bell et al., 2008)	<b>HH 26 (5 d)</b> (Bartolami et al., 1991)	<b>HH 19- 24 (3-4.5 d)</b> (Wu and Oh, 1996; Oh et al., 1996)	<b>HH 26 (5 d)</b> (Bartolami et al., 1991; Oh et al., 1996)	<b>HH 30 (6.5-7 d)</b> (Bissonnette and Fekete, 1996)
<i>Mouse</i>	<b>E8</b> (Sato et al., 2010)	<b>E8.5</b> (Anniko and Wikstrom, 1984)	<b>E9</b> (Anniko and Wikstrom, 1984)	<b>E9.5</b> (Anniko and Wikstrom, 1984)	<b>E9-E11.5</b> (Carney and Silver, 1983; Wikstrom and Anniko, 1987; Ma et al., 1998; Raft et al., 2004)	<b>E11.5</b> (Carney and Silver, 1983)	<b>E11.5</b> (Morsli et al., 1998; Raft et al., 2007)	<b>E11.5</b> (Shailam et al., 1999)	<b>E13 to E17</b> (Morsli et al., 1998)

**Fig.6.1. Schematic diagram of inner ear development from the otic placode to the otocyst stage in *Xenopus*, chick, zebrafish and mouse.**



## **6.2 The otic epithelium as a pseudostratified epithelium with apicobasal polarity**

In pseudostratified epithelia (PSE) nuclei are found in different positions at a single layer of the columnar epithelium (Smart, 1972). Pseudostratified epithelia are highly proliferative tissues serving as embryonic precursors of many organs including the central nervous system and many placodes (Ichikawa et al., 2013; Norden, 2017; Strzyz et al., 2015). All pseudostratified epithelia show apico-basal polarity but the shapes of the epithelial cells range from flat or squamous, to cuboidal or columnar cells (Meier, 1978a; Drubin and Nelson, 1996; Strzyz et al., 2015; Norden, 2017).

In pseudostratified epithelia, nuclei are more densely packed (Norden, 2017; Sauer, 1935). Moreover, in PSEs such as the neuroepithelium or otic epithelium in amniotes, nuclei transfer to the apical surface for mitosis in a process known as interkinetic nuclear migration (Kosodo, 2012; Rahilly, 1963; Tsue et al., 1994; Strzyz et al., 2015). During interkinetic nuclear migration, the nuclei of the epithelial cells migrate apically during the G2 phase of the cell cycle and basally during the G1 phase. (Hildebrand 2005; Spear and Erickson, 2012; Yu et al. 2011). Previous studies demonstrated that microtubules are required for apical movement during division in elongated cells such as radial glial cells, while actin is required in shorter epithelia such as retinal epithelial cells (Norden et al., 2009; Tsai et al., 2010; Kosodo et al., 2011; Leung et al., 2011; Strzyz et al., 2015; Norden, 2017; Spear and Erickson, 2012). Both actin/myosin and microtubule have also been implicated in basal nuclear movements (Spear and Erickson, 2012).

In the present study, pH3-immunopositive mitotic cells in the *Xenopus* otic vesicle were found to be located adjacent to the apical surface of the columnar epithelial cells of the otic vesicle epithelium. Taken together with the varying positions of the nuclei and the cell shapes as reconstructed from mGFP, this indicates that the *Xenopus* otic vesicle epithelium forms a pseudostratified columnar epithelium

undergoing interkinetic nuclear migration, confirming previous studies in other vertebrates (Rahilly, 1963; Meier, 1978; Christophorou et al., 2010; Mreier, 1978, a, b; Sai and Ladher, 2015).

This study is the first study to describe in detail the distribution of several proteins associated with apical-basal polarity and cell adhesion in the PSE of the *Xenopus* otic vesicle. By immunostaining, the distribution of aPKC, PAR3 and MLC, was shown to be enriched on the apical surface (Jung et al., 2011) and N-cadherin on the apicolateral side of the epithelial cells of the otic vesicle at early embryonic stages (stage 26) before the onset of neuronal differentiation and migration. Other vertebrates show a similar expression of the aPKC, MLC and N-cadherin proteins on the apical surface and apicolateral side of the epithelial cells of otic vesicle (Barrionuevo et al., 2008; Jung et al., 2011; Matsumata et al., 2005; Novince et al., 2003; Sai and Ladher, 2015). A nonmuscle myosin heavy chain (MYH9) was expressed on the luminal edges and apicolateral side of the otic vesicle epithelium and cochlear duct development in the mammalian inner ear (Mhatre et al., 2004). Conversely, a phosphorylated myosin light chain was detected on both apical and basal side of otic epithelial cells in the chick otic placode (Sai and Ladher, 2008).

In *Xenopus*, the apical distribution of aPKC and N-cadherin in the otic vesicle was maintained at a later stage (stage 35). On the contrary, PAR3 and MLC disappeared from the apical side of the epithelial cells of the otic vesicle \*and only weak staining of MLC remained on the apicolateral side of the epithelial cells\* in stage 35. Although PAR6, PAR3 and atypical protein kinase C (aPKC) bind together and form a complex that is required to maintain cells polarity, it was reported previously that PAR3, PAR6 and aPKC also can act independently (Ali et al., 2016; Iden et al., 2006). The observation that PAR3 and aPKC overlap on the apical side of the otic vesicle at early (stage 26) but not later stages (stage 35), suggests that these two proteins may initially act as part of a common complex but may subsequently act independently.

Surprisingly, we also found some localization of PAR3, aPKC and MLC to the periphery of the nuclei and to the adjacent cell membrane. This raises the possibility that these proteins may play a role in the mechanism driving interkinetic nuclear migration (IKNM). As mentioned above, previous studies suggested that IKNM is mediated by actin and myosin in short pseudostratified epithelia such as the otic epithelium, while it involves microtubule-dependent processes in pseudostratified epithelia with longer cells (Norden et al., 2009; Tsai et al., 2010; Kosodo et al., 2011; Leung et al., 2011; Strzyz et al., 2015; Norden, 2017). Cell polarity proteins have so far not been implicated in this process, but our data suggest that they may play a role, for example in anchoring cytoskeletal proteins to both the nucleus and the cell membrane or in regulating their dynamics as has been shown in other contexts (Etienne-Manneville and Hall, 2003; Suzuki and Ohno, 2006; Hapak et al., 2018). However, this hypothesis still needs to be tested experimentally.

We also report here for the first time that the distribution of cell polarity proteins changes in the otic vesicle, when cells begin to delaminate. Both PAR3 and aPKC are then becoming localized to basal protrusions as well as to cell membranes and cytoplasm of vestibulocochlear ganglion cells including their axon and dendrite forming processes. Some basally distributed MLC was also observed in a distinctive region on the ventromedial side of the otic epithelium. Since PAR3 and aPKC have been implicated in neuronal cell migration and neurite outgrowth in the vertebrate nervous system (Shi et al., 2003; Du et al., 2010; Solecki et al., 2004, 2009; Solecki, 2012; Moore et al., 2013; Chen and Zhang, 2013; Ramahi and Solecki, 2014; Hapak et al., 2018), this suggests that besides playing a role in apicobasal polarity of otic epithelial cells, aPKC, PAR3 and possibly other cell polarity proteins may relocate to the leading edge of migrating otic neurons, where they may be required for delamination, migration and neurite outgrowth of vestibulocochlear ganglion cells. Of course, this hypothesis needs to be further tested in functional studies.

The distribution of N-cadherin in the otic vesicle is complementary to regions of cell re-arrangements or delamination already at stage 26. While there is strong apicolateral N-cadherin staining in most parts of the otic epithelium, N-cadherin is absent laterally, where epithelial cells are rearranged and dorsal and ventral epithelia fuse during invagination of the otic vesicle. In addition, N-cadherin is reduced ventromedially, where cells prepare to delaminate from the otic vesicle to form the vestibulocochlear ganglion (VCG). At stage 35, N-cadherin show only weak staining in the cytoplasm of ganglion cells and did not associate with VCG membranes. These findings suggest that there is a change in the distribution of N-cadherin from apical and apicolateral sides to the cytoplasm once differentiating neurons leave the otic vesicle and migrate to form the vestibulocochlear ganglion. This suggests that downregulation of N-cadherin may promote the delamination of neuroblast from the otic epithelium, similar to their role for neural crest cells (NCC), where downregulation of N-cadherin initiates the epithelial-to-mesenchymal transition (EMT) and delamination from the neuroepithelium and causes de-epithelialization and decreased cell adhesion (Clay and Halloran, 2011; Taneyhill and Schiffmacher, 2017). Whereas overexpression of N-cadherin prevents neural crest delamination, blocking N-cadherin results in precocious migration (Nakagawa and Takeichi, 1998; Bronner-Fraser et al., 1992; Shoval et al., 2007; Taneyhill and Schiffmacher, 2017). Only at later stages, is N-cadherin then required for proper neural crest migration (Piloto and Schilling, 2010; Theveneau et al., 2010, 2013; Powell et al., 2015).

Taken together with previous studies, the apical localization of aPKC, PAR3, MLC and N-cadherin in the otic vesicle observed in the current study and the change in their distribution during the migration of neurons to form the vestibuloacoustic ganglion (VCG) raises the possibility that the re-distribution of cell polarity proteins and of N-cadherin may play some causal role in regulating the transition from epithelial cells to delaminating neurons in the otic epithelium. However, this needs to be confirmed in functional studies.

### **6.3 Distribution of Eya1 during development of the otic vesicle in *Xenopus***

Eya1 genes play a very important role in cranial sensory neurogenesis (Borsani et al., 1999; Li et al., 2003; Schlosser and Ahrens, 2004; Schlosser et al., 2008; Schlosser, 2010; Silver and Rebay, 2005; Xu et al., 1997a; Xu et al., 1997b; Zhang et al., 2004; Zou et al., 2004) and in otic placode development (Li et al., 2010; Sullivan et al., 2019; Xu et al., 1999; Zou et al., 2004; Zheng et al., 2003). However, only the distribution of Eya1 mRNA during sensory neurogenesis has been described so far, while protein distribution has not been characterized.

To further clarify the function of Eya1 for placodal neurogenesis, this study has analyzed the expression of the Eya1 protein in all cranial placodes from the end of gastrulation to early larval stages in *Xenopus laevis*. It then analyzed the subcellular distribution of Eya1 protein during development of the otic placode and vesicle in detail using confocal microscopy. In order to determine the location of Eya1 protein in cranial neurogenic placodes of *Xenopus laevis*, a specific guinea pig anti-*Xenopus*-Eya1 antibodies was used. Specificity of this antibody was verified in Western Blots and in peptide competition assays.

#### **6.3.1 Distribution of Eya1 in different cranial placodes**

The GP anti Eya1 antibody used in the present study allowed me for the first time to describe the localization of Eya1 protein during development of cranial neurogenic placodes at different stages. While Bane et al. (2005) previously reported Eya1 immunostaining in the anterior side of otocyst at stage 37, 41 and 44 in *Xenopus laevis*, the specificity of the antibody used in this study has not been verified in *Xenopus* and neither the subcellular localization of Eya1 nor its wider distribution have been described.

In the present study, nuclear expression of Eya1 was detected already at early stages (stage 15) in the neural plate, neural fold, mesoderm, and endoderm but only a weak

cytoplasmic and no nuclear expression of Eya1 was found in the preplacodal ectoderm (PPE). In contrast, Eya1 mRNA expression was found to be strongly upregulated in the PPE already at the end of gastrulation (stage 13) (Schlosser and Ahrens, 2004). This suggests a significant delay in the accumulation of Eya1 protein compared to Eya1 mRNA in the PPE and indicates that nuclear enrichment of Eya1 in the developing placodes only occurs after stage 15 and, thus, at neural fold stages.

After cranial placodes became distinct at stage 20/23, a nuclear distribution of Eya1 was observed in the following cranial placodes: olfactory (pOl), profundal (pPr) and trigeminal placodes (pV), adenohipophyseal placode (pAH), otic placode (pOt) and middle lateral line placode (pM). Also, there was some Eya1 expression in the developing pharyngeal pouches. In later stages (stage 26-35), Eya1 expression continued to be nuclear in these and other placodes except for the lens placode, which does not express any Eya1. In the present study, at stage 40 Eya1 was found to be still expressed in some placodes but reduced in other placodes, for example, the glossopharyngeal placode (epIX) and the lateral side of the otic vesicle. In addition, new Eya1 staining has appeared in the second hypobranchial placode (hp2), supratemporal placode (pST) and the primordium of the ventral trunk line (v).

The distribution of *Xenopus* Eya1 protein in all ectodermal placodes except the lens placode described here is in line with previous studies describing the distribution of Eya1 mRNA expressed in *Xenopus*, zebrafish, and mammals (David et al., 2001; Sahly et al., 1999; Schlosser and Ahrens, 2004; Xu et al., 1997a; Zou et al., 2004). Previous in situ hybridization experiments in *Xenopus* revealed Eya1 mRNA expression from the late gastrula to tadpole stages in different placodes including adenohipophyseal and all neurogenic placodes (David et al., 2001; Li et al., 2010; Schlosser, 2003; Schlosser and Ahrens, 2004; Schlosser et al., 2008; Sullivan et al., 2019). In other vertebrates (mice and zebrafish), Eya1 mRNA expression was documented in all neurogenic placodes, excluding profundal and trigeminal

placodes. In contrast to *Xenopus*, Eya1 is also found in the lens placodes of the mouse (David et al., 2001; Ishihara et al., 2008; Kozlowski et al., 2005; Nica et al., 2006; Sahly et al., 1999; Xu et al., 1997a; Zou et al., 2004). Taken together, this suggests that the pattern of Eya1 expression is widely conserved in vertebrates.

### **6.3.2 Distribution of Eya1 in the developing otic vesicle**

Using the specific Eya1 antibody, it is shown here that Eya1 protein is initially distributed throughout the otic placode, but becomes reduced in the lateral and dorsal part of the otic vesicle after invagination. Eya1 is predominantly nuclear in the otic epithelium and its distribution largely mimics the distribution of Six1 (e.g. Schlosser and Ahrens, 2004; Schlosser et al., 2008). It has previously been shown that binding of Eya1 protein to the Six1 transcription factor results in nuclear translocation of Eya1, where Eya1 then acts as a transcriptional coactivator of Six1 (Ohto et al. 1999; Zhang et al., 2004). However, nuclear distribution of Eya1 was previously reported only for the olfactory placode in mice (Purcell et al., 2005).

Together the Six1-Eya1 protein complex then promotes both the proliferation of sensory and neuronal progenitors and the subsequent differentiation of neurons and sensory cells in the otic vesicle and in derivatives of other cranial placodes (Li et al. 2003; Zheng et al., 2003; Laclef et al., 2003; Zou et al., 2006, 2008; Schlosser et al. 2008; Ahmed et al., 2012a, b; Riddiford et al., 2016, 2017; Li et al., 2020). Previous studies proposed that this occurs in a dosage-dependent manner with high levels of Eya1/Six1 promoting progenitors and low levels promoting differentiation (Schlosser et al., 2008; Zou et al., 2008; Riddiford et al., 2017). Using the specific Eya1 antibody in combination with EdU-incorporation and Sox3- and Islet1/2-immunostaining, I now show that the distribution of Eya1 protein in progenitors and differentiating neurons of the developing inner ear is consistent with this hypothesis.

High levels of nuclear Eya1 are found only in proliferating (EdU+, Islet1/2-) progenitor cells of the otic epithelium flanking the neurosensory area (including the Sox3+ cells at its dorsal and ventral border) and in the proliferating (EdU+, Islet1/2-) peripheral cells of the vestibulocochlear ganglion as summarized in Figure. 6.2. In contrast, lower levels of nuclear Eya1 are found in the relatively quiescent (EdU-) supporting cells of the sensory areas, which co-express Sox3 and low levels of Islet1/2 protein, while nuclear Eya1 staining disappears as soon as neurons and hair cells differentiate. Levels of nuclear Eya1, thus, decline along the trajectory from progenitors to differentiating cells in both the neuronal and sensory lineages.

In addition to nuclear staining, the present study finds Eya1 in the cytoplasm, in particular in delaminating neuroblasts and in the differentiating (Islet1/2 +) neurons of the vestibulocochlear ganglion, where it shows a similar distribution than Par3 and aPKC. In the cytoplasm, Eya proteins have been previously shown to act as phosphatases, which may bind to and dephosphorylate other proteins independently of Six1 thereby affecting their activity and localization (Rebay, 2016; Merk et al., 2020; Roychoudhoury and Hegde, 2021). During the development of mouse embryonic lung, Eya1 expression was found apically enriched in lung epithelium, where it was reported to dephosphorylate aPKC and affect the balance between symmetric and asymmetric cell divisions (El-Hashash et al., 2011). Although, this study was later retracted (El Hashash et al., 2017), another recent study confirmed that Eya1 can dephosphorylate aPKC in cerebellar neurons thereby affecting the balance between symmetric and asymmetric cell divisions (Merk et al., 2020). Whether cytoplasmic Eya1 may have a similar role during otic development will be further discussed in section 6.6 below.

#### **6.4 Otic neurogenesis in *Xenopus***

Double immunostaining for EdU and Sox3 or Islet1/2 and Sox3 allowed us to document the progression of neuronal differentiation and sensory area formation in the *Xenopus* otic vesicle as summarized in Figure. 6.2. When neurogenesis starts in



*Xenopus* around stages 26-28, EDU/PCNA-immunopositive proliferative cells are found scattered along the medial wall of the otic vesicle but absent from its lateral side. Sox3-immunopositive cells are found in proliferating cells throughout the region where the basal lamina is interrupted and/or neuroblasts are delaminating.

At later stages (stage 33, 35), Sox3-immunopositive sensorineural progenitors cells were still found in the ventromedial region but most of these have now stopped proliferating as indicated by decreased EdU and PCNA staining and probably define the region of the prospective sensory areas (see section 6.5). However, proliferative Sox3-immunopositive cells are still found at the dorsal and ventral border of this ventromedial region, where neuroblasts continue to delaminate (Fig. 6.2). In the developing vestibulocochlear ganglion, peripheral cells continue to proliferate, while Sox3 expression is absent.

These findings are in line with previous studies in different vertebrates, which have shown that Sox3 and/or Sox2 plays a central role for regulating neurogenesis of the otic vesicle (Abelló et al., 2010; Nechiporuk et al., 2007; Neves et al., 2007; Padanad and Riley, 2011; Sun et al., 2007). In the otic vesicles of teleosts, chickens, and mice both Sox3 and Sox2 expression have been determined in the neurogenic domain and play a crucial role as upstream regulators of neuronal differentiation (Collignon et al., 1996; Köster et al., 2000; Rex et al., 1994; Neves et al., 2012). For example, Abelló et al. (2010) demonstrated that the ectopic expression of Sox3 promoted neurogenesis in the non-neurogenic domain of the otic epithelium. However, these proteins must be downregulated for neuronal differentiation to proceed since high levels of Sox3 or Sox2 prevent neuronal differentiation (Bylund et al., 2003; Graham et al., 2003; Evsen et al., 2013).

Whereas in zebrafish and chick, neuronal differentiation in the otic vesicle is promoted by Sox3 (Neves et al. 2007; Abello et al. 2010; Evsen et al. 2013; Gou, Vemaraju, et al. 2018), Sox2 is required for neuronal differentiation in mammals (Kiernan et al. 2005; Puligilla et al. 2010; Steevens et al. 2017). Whether Sox2 may

play a similar role in *Xenopus* or may act redundantly with Sox3 in otic neurogenesis still needs to be clarified. While Sox2 expression in the otic vesicle of *Xenopus* has not been described in detail, previous studies indicate that it is expressed more broadly during these stages and extends further dorsally than Sox3 (David et al., 2001; Schlosser and Ahrens, 2004; Park and Saint-Jeannet, 2010). This pattern suggests that Sox2 expression may be maintained in delaminating neuroblasts (and possibly the proliferative peripheral ganglion cells) longer than Sox3 or may be expressed in neuronal progenitors that do not express Sox3, but this needs to be confirmed in further studies.

Downstream of Sox3 and Sox2, several neuronal determination (proneural) and differentiation genes were previously shown to be important for neurogenesis in otic vesicles of different vertebrates (Bertrand et al., 2002; Maier et al., 2014; Schlosser et al., 2008; Zou et al., 2004). Knockout mutations of proneural genes such as *Neurog1* or *Neurog2* leads to block in neuronal or sensory differentiation in the cranial ganglia derived from the profundal/trigeminal, epibranchial, otic, and lateral line placodes in mice and zebrafish (Andermann et al., 2002; Bermingham et al., 1999; Cau et al., 1997, 2002; Chen et al., 2002; Guillemot et al., 1993; Murray et al., 2003). Conversely, overexpression of proneural proteins such as *Ascl1*, *Neurog1/2* or *NeuroD2* can convert ventral non-neural ectoderm into neurons in *Xenopus* embryos (Lee et al., 1995; Ma et al., 1996; Perron et al., 1999; Talikka et al., 2002).

A central role for the determination of neurons derived from the otic vesicle is played by the neuronal determination gene *Neurog1*, which is expressed throughout the neurogenic epithelium of the otic vesicle and activates the transcription of *NeuroD1*, which is expressed in postmitotic cells and governs neuronal differentiation in the otic vesicle (Abelló, 2007; Bell et al., 2008; Bertrand et al., 2002; Lassiter et al., 2014; lee et al., 1995; Raft et al., 2007; Ma et al., 1998; Maier et al., 2014).

While expression of *Neurog1* and *NeuroD1* in the otic vesicle has also been described for *Xenopus* (Schlosser et al., 2008; Nieber et al., 2009; Riddiford et al., 2016), there is no a specific antibody that recognizes Neurog1 protein in the frog. Therefore, I have combined in situ hybridization for Neurog1 with immunostaining for Sox3 to reveal the degree of overlap between Neurog1 expression and Sox3 in the otic vesicle. While Sox3 is overlapping with Neurog1 expression, cells in the dorsal part of the *Neurog1* expression domain, where most neuroblasts are delaminating and the basal lamina is maximally disrupted, do not express Sox3 and the latter is also completely absent from the vestibulocochlear ganglion. This conforms to the model that Sox3 is important to initiate neuronal determination by neuronal determination genes such as *Neurog1*, but that downregulation of Sox3 expression is required to allow the differentiation of neurons (Fig. 6.2). Conversely, Sox3 positive immunostaining extended more ventrally in the posterior region of the vesicle than *Neurog1* expression, suggesting this region participates in the developing sensory areas and has stopped to produce neurons (see section 6.5).

Proneural proteins such as Neurog1 are known to act in cooperation with other bHLH proteins to specify sensory and neuronal cell types specific for individual placodes, including LIM-type (e.g., *Islet1*) and POU-type (e.g., *Brn3a* and *Brn3c*) homeodomain proteins (Alsina, 2020; Lee and Pfaff, 2003; Ma et al., 2008; Lee et al., 2012). *Islet1/2* has been previously shown to be expressed in the differentiating neurons of the chicken inner ear (Adam et al., 1998; Begbie et al., 2002; Camarero et al., 2001; Deng et al., 2014; Durruthy-Durruthy et al., 2014; Li et al., 2004), and has been implicated in specification and maintenance of these neurons (Li et al., 2004). In the present study, immunostaining for the LIM/homeodomain proteins *Islet1* and/or *Islet2* was used as one of the earliest markers for the differentiation of cells delaminating from the otic vesicle and forming the vestibulocochlear ganglion. *Islet1/2*-immunopositive differentiating neurons were found in the central region of the vestibulocochlear ganglion from stage 29 on, but were notably absent from the peripheral, proliferative (EdU+ and PCNA+) cells, confirming that *Islet1/2* is only expressed in postmitotic cells (Fig. 6.2).

Using the acetylated tubulin antibody to label neurites of differentiated neurons (Chu and Klymkowsky, 1989; Gilmour et al., 2002; Lopez-Verrilli et al., 2013). The first indication of neurites in otic vesicle derived neurons was observed at stage 31 indicating that the neurons of the vestibulocochlear ganglion send out neurites immediately after the onset of differentiation.

### **6.5 Early development of sensory areas in the otic vesicle in *Xenopus***

The domain of Sox3 immunostaining in the medial wall of the otic vesicle extends more ventral than Neurog1 expression and Sox3 is maintained in this ventromedial domain (mostly in non-proliferative cells including putative supporting cells) even at stage 40, when the delamination of neuroblasts has been completed. From stage 33 on, this ventromedial region becomes thickened and bilayered indicating the formation of the first sensory area, which begins to separate into a dorsal and ventral part from stage 35 on (Fig. 6.2). These will subsequently give rise to the utricular and saccular maculae, respectively and probably contribute to the formation of additional sensory areas at later stages (Quick and Serrano, 2005).

The distribution of Sox3 in regions of neuronal delamination as well as in the developing sensory areas suggests that Sox3 marks a common neurosensory area in the *Xenopus* otic vesicle, possibly in conjunction with Sox2 which is expressed in partly overlapping domains but extends more dorsally (see section 6.4). A similar neurosensory area containing progenitors for the sensory and supporting cells of utricular and saccular macula and for the sensory neurons of the vestibulocochlear ganglion has been described in zebrafish, chick and mammals (Ma et al. 1998; Adam et al. 1998; Andermann, Ungos, and Raible 2002; Alsina et al. 2004; Satoh and Fekete 2005; Pujades et al. 2006; Raft et al. 2007; Millimaki et al. 2007; Millimaki et al., 2010; Sapede et al., 2012). Subsequently, Sox3 persists together with Islet1/2 in the putative supporting cells, located basally in the developing sensory areas, while both Sox3 and Islet1/2 are downregulated in the developing hair cells located apically (Fig. 6.2). Similar transitory expression of Islet1 in the

supporting cells but not hair cells has been described in other vertebrates (Li et al., 2004; Radde-Gallwitz et al., 2004; Neves et al., 2007). My data suggest that Sox3 is then downregulated first, followed by Islet1/2 downregulation during hair cell differentiation.

However, while Sox3 precedes Sox2 expression and promotes neural differentiation in chick and zebrafish embryos, only Sox2 is maintained in their developing sensory areas and promotes sensory differentiation (Neves et al. 2007; Abello et al. 2010; Evsen et al. 2013; Gou, Vemaraju, et al. 2018). In mammals, the neurosensory area expresses only Sox2, which is required for both neuronal and sensory differentiation (Kiernan et al. 2005; Puligilla et al. 2010; Steevens et al. 2017). Since persistent expression of Sox2 and/or Sox3 blocks neuronal or sensory differentiation, these transcriptions must be downregulated before sensory neurons or hair cells differentiate in all vertebrates (Dabdoub et al. 2008; Evsen et al. 2013; Puligilla and Kelley 2017). Taken together, these comparisons suggest that either Sox3 or Sox2 or both play a central role for the formation of sensory and neuronal progenitors in the developing inner ear of all vertebrates but that their respective role for sensori- or neurogenesis has changed during vertebrate evolution with Sox3 presumably adopting a more central role for sensorigenesis in *Xenopus* .

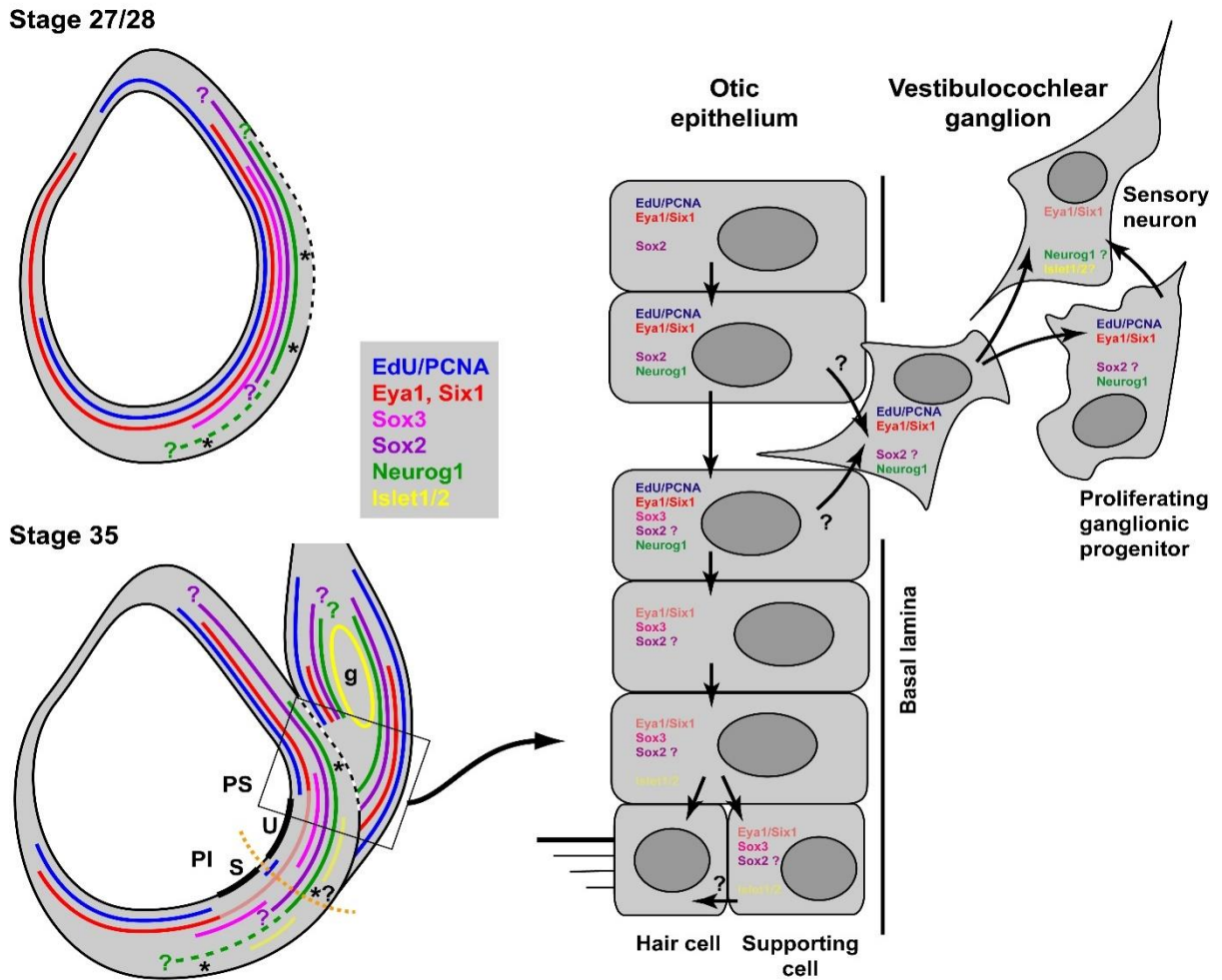


**Fig.6.2. Neurogenesis and sensory area formation in the otic vesicle of *Xenopus laevis*.** Schematic diagrams of central sections through otic vesicles are shown with proliferation zones (EdU/PCNA) and approximate extent of marker expression domains in the otic vesicle and the vestibulocochlear ganglion (g) indicated by colored lines. Faint red and yellow colors indicate domains of weak Eya1 and Islet1/2 expression, respectively. Data from previous publications suggest that Six1 is expressed is similar to Eya1, while Sox2 is expressed broadly in the medial otic epithelium but is absent from its ventral most part (Pandur et al., 2000; David et al., 2001; Schlosser and Ahrens, 2004; Park and Saint-Jeannet, 2010). All other data are based on the current study. Question marks indicate that the precise position of the expression boundaries are not known for Neurog2 and Sox2. The hatched part of the line for Neurog1 indicates that its expression extends more ventrally in the anterior otic vesicle. The broken white line indicates the extent of the breach in the basal lamina. Thick black lines indicate the developing sensory areas (maculae) of the saccule (S) in the pars inferior (PI) and of the utricle (U) in the pars superior (PS) of the otic vesicle. Asterisks indicate areas of neuronal delamination. These extend broadly throughout the ventromedial part of the otic vesicle at early stages but probably become restricted to the ventral and dorsal borders of this domain at stage 35. See text for details

## 6.6 Role of *Eya1* in otic neurogenesis in *Xenopus*

### 6.6.1 Role of *Eya1* for proliferation, progenitor maintenance and neuronal differentiation

In mouse, the disruption of *Eya1* arrested development of the ear at otic vesicle stage and prevented formation of the vestibulocochlear ganglion (Xu et al., 1999; Zheng et al., 2003). Similarly, microinjection of *Eya1* morpholino caused several abnormalities in the otic vesicle of zebrafish: the otic vesicle became smaller and abnormally shaped and the number of hair cells in the saccular and utricular maculae of the inner ear was reduced (Kozłowski et al., 2005). In turn, the expression of *Neurog1* and *NeuroD1* was reduced in neuroblast precursors in the ventral otic vesicle and sensory neurons of the VIIIth ganglion in mice and *Xenopus* (Zou et al., 2004;). In *Xenopus*, injection of either *Six1*-MO or *Eya1*-MO, led to reduction of expression of the progenitor marker *Sox3* as well as the neuronal differentiation markers *N-tubulin* and *NeuroD1* in all cranial placodes (Schlosser et al., 2008; Riddiford et al., 2017). These results confirmed that *Eya1* or/and *Six1* are very important in maintaining the sensory neurons and regulating the differentiation of neurons. Conversely, gain of *Eya1* function in *Xenopus* led to ectopic ectodermal expression of *NeuroD1* (Schlosser et al., 2008). Gain of *Eya1* or *Six1* function in mammals increased *NeuroD1* expression in the otocyst and promoted neuronal differentiation and hair cell formation in cochlear nonsensory epithelial cells (Ahmed et al., 2012, a, b, Wong et al., 2013).

However, *Eya1* and *Six1* play an important role not only for neuronal differentiation processes but also for proliferation and maintenance of neuronal progenitors expressing *SoxB1* genes that act to maintain cells in a proliferative progenitor state (Ahmed et al., 2012a; 2012b; Schlosser et al., 2008; Zou et al., 2004). In *Xenopus*, mice and chicks, *Six1*, *Eya1* and *Sox2* or *Sox3* showed overlapping expression on the ventral side of the otic placode (Zou et al., 2008; Schlosser et al., 2008). Injection of *Eya1*-MO in *Xenopus* led to reduction of

expression of the progenitor markers *Sox2* and *Sox3* in all cranial placodes (Schlosser et al., 2008). Moreover, *Eya1* mutation in mice led to reduced *Sox2* levels in the otic vesicle suggesting that *Eya1* is necessary for the normal distribution of *Sox2* in the ventral side of the otic vesicle epithelium and for the maintenance on the prosensory and nonsensory cells in the cochlea (Zou et al., 2008). In gain of function studies, *Eya1* and *Six1* previously have been shown to induce the activation of *SoxB1* genes (Chen et al., 2009; Schlosser et al., 2008; Schlosser, 2010; Wegner and Solt, 2005; Zou et al., 2004, 2008; Riddiford and Schlosser, 2016). Additionally, it has been well documented that *Six1* and *Eya1* activate progenitors at high doses and neuronal differentiation or maturation at low doses (Schlosser et al., 2008; Zou et al., 2008; Riddiford and Schlosser, 2017). In vertebrates, the knockdown of *Six1* or *Eya1* showed reduction of cell proliferation in multiple cranial placodes (Schlosser et al., 2008; Zheng et al., 2003; Zou et al., 2006). Conversely, the number of pH3-positive cells in cranial placodes significantly increased in *Six1* and *Eya1* gain of function experiments (Schlosser et al., 2008).

Taken together, these previous studies indicate that *Eya1* and *Six1* are required to both maintain progenitor cells and to regulate neuronal differentiation in a dosage-dependent way, with high levels of *Eya1/Six1* promoting progenitors and low levels promoting differentiation sensory and neuronal differentiation.

The loss of function experiments conducted in the present study specifically analyzed the function of *Eya1* for the developing *Xenopus* otic placode and vesicle, which have not previously been described. The findings reported here suggest that *Eya1* is indeed essential for maintaining proliferation (pH3; EdU) and *Sox3*-immunostaining in the developing neurosensory area of the otic vesicle, similar to its role in other cranial placodes or in otic vesicles of other vertebrates. *Eya1* most likely acts as a transcriptional coactivator of *Six1* in this context, since *Eya1* and *Six1* are co-localized in the nuclei of the medial otic epithelium; both proteins have previously been shown to cooperate in the direct activation of *Sox2* and *Sox3*; and



Eya1 and Six1 are jointly required for *Sox2* expression in the neurosensory area of the mouse (Schlosser et al., 2008; Riddiford et al., 2016, 2017; Xu et al., 2021). Similarly, the reduction of Islet1/2-positive sensory neurons that is reported here after Eya1 knockdown has been shown to be mirrored by a similar reduction after Six1 knockdown in a previous study, which also identified *Islet2* as a putatively direct transcriptional target of Six1 and Eya1 (Riddiford et al., 2016). In addition, *Eya1* loss of function significantly reduced the percentage of mitotic cells in the otic vesicle as indicated by pH3 immunostaining. Taken together this suggests that Eya1 and Six1 directly transcriptionally activate genes promoting neuronal differentiation (possibly at lower doses) as well as those promoting progenitor status (possibly at higher doses).

To confirm our Eya1 loss of function studies, I also injected mRNA encoding the inducible dominant negative GR-EnR-Six1 construct and induced its nuclear translocation by dexamethasone after completion of gastrulation. This is expected to block transcriptional activation of Six1-target genes and should, therefore, largely mimic the effect of Eya knockdown for those target genes, which are activated by the Six1-Eya coactivator complex. Indeed, proliferation (EdU incorporation) and Islet1/2-immunostaining were mildly reduced in some embryos similar to what was observed after Eya1 knockdown, whereas *Sox3* was unaffected. Although these experiments partly mimicked the Eya1 knockdown phenotype, the effects were much milder. There may be several explanations for this observation. First, dexamethasone-treatment may not result in sufficient nuclear translocation of GR-EnR-Six1 resulting in low efficiency of this dominant-negative protein. Second, Eya1 may be required as a Six1 coactivator prior to the stage, when nuclear translocation of GR-EnR-Six1 was activated (stage 18). And third, Eya1 may affect otic development at least partially in a Six1-independent pathway. Additional experiments will be needed to decide between these different and not mutually exclusive possibilities.

In contrast to the loss of function experiments, the gain of function studies reported here show that cell proliferation in the otic epithelium (pH3, EdU) is increased after *Eya1* or *Six1* overexpression. However, *Islet1/2* immunostaining in the vestibulocochlear ganglion may be decreased or increased after *Eya1* and *Six1* overexpression. This confirms previous reports that *Islet2* as well as *Neurog1/2* expression in cranial placodes may be either increased or decreased after overexpression of *Eya1* or *Six1* (Schlosser et al., 2008; Riddiford et al., 2016, 2017). These seemingly paradoxical findings may result from the dosage dependent effects of *Eya1/Six1* on progenitor proliferation and neuronal or sensory differentiation. In promoting proliferation and upregulating *Sox2/3* in the neurosensory area, high levels of *Eya1/Six1* expand the pool of neuronal progenitors, which are, however, blocked from differentiation by high levels of *Sox2/3*. Maintenance of high levels of *Eya1/Six1* should therefore repress neuronal differentiation resulting in reduced numbers of *Islet1/2* cells in the ganglion. Should, however, levels of *Eya1* and/or *Six1* subsequently decline sufficiently in the otic vesicle, the expanded progenitor pool may contribute to increased numbers of *Islet1/2* cells. The precise levels of *Eya1* and/or *Six1* and their dynamics after overexpression may, therefore determine, whether neuronal differentiation is increased or decreased.

### **6.6.2 Role of *Eya1* for apicobasal cell polarity**

The present study is the first study that reports the effect of *Eya1* gain and loss function on the distribution of cell polarity proteins (aPKC, PAR3, MLC) and N-cadherin in the otic vesicle. The distribution of all of these proteins was found to be significantly altered after injection of either *Eya1-MO* or *GR-Eya1* mRNA.

The findings reported here indicate that in addition to its effects on proliferation and neuronal differentiation, knockdown of *Eya1* also affects the distribution of cell polarity proteins and N-cadherin in the developing otic vesicle (possibly with indirect effects on the balance between progenitors and differentiating cells). Apical

protein levels of Par3 and aPKC were reduced and cytoplasmic localization of Par3 and MLC were increased, while N-cadherin disappeared completely from the apicolateral membrane. However, injection of the dominant-negative GR-EnR-Six1 construct did not result in clear differences in the distribution of Par3 protein (see discussion in 6.6.1).

Conversely, Eya1 overexpression led to irregular and delocalized distribution of aPKC, PAR3, MLC in the otic vesicle epithelium. Similar to previous findings after Eya1 gain of function, several morphological defects were observed such as malformations of the otic vesicle and disordered tissue surrounding the vesicle (Li et al., 2010).

The downregulation of N-cadherin after Eya1 knockdown is particularly noteworthy since it suggests that Eya1 may be required for N-cadherin localization to adherens junctions and thereby may be required to maintain epithelial integrity of the pseudostratified otic epithelium, while conversely the reduction of Eya1 levels may promote delamination. Consistent with this hypothesis, it is shown here that areas of neuroblast delamination in the normal otic vesicle show reduced apicolateral N-cadherin staining. This is reminiscent of the downregulation of N-cadherin in regions of neural crest delamination (Nakagawa and Tekeichi, 1998; Akitaya and Bronner-Fraser, 1992; Davidson and Keller, 1999; Daddy et al., 2012; Rogers et al., 2013). Such downregulation of N-cadherin has been previously shown to be required for initial delamination of the neural crest as discussed in section 6.2.

If N-cadherin plays a similar role in the otic vesicle, one role of Eya1 may be to maintain N-cadherin in the otic epithelium thereby maintaining an epithelial phenotype, while downregulation of Eya1 may permit delamination. However, this proposal needs to be confirmed in further studies.

The present study leaves open, whether Eya1 affects the distribution of cell polarity proteins and N-cadherin via transcriptional regulation of the genes encoding these proteins or by direct protein-protein interactions in the cytoplasm, where the phosphatase activity of Eya1 may play a role in dephosphorylation of protein interaction partners, which in turn may affect their subcellular localization (Rebay, 2016; Merk et al., 2020; Roychoudhoury and Hegde, 2021). The latter scenario receives some support from the observation that cytoplasmic Eya1 protein is present in basal protrusions of delaminating cells and in the developing neurites of ganglion cells, where it may interact with Par3 and aPKC. Dephosphorylation of aPKC by Eya1, has already been shown to inactivate the cell polarity complex in cerebellar neurons leading to changes in microtubule orientation and distribution of Numb protein (Merk et al., 2020). In the cerebellum, this affects the balance between symmetric and asymmetric cell divisions (with Eya1 promoting symmetric divisions resulting in two proliferative progenitors) and, therefore, helps to regulate the transition between proliferating progenitors and differentiating neurons (Merk et al., 2020). However, whether changes in cell polarity similarly affect the balance between progenitors and differentiating neurons in the otic epithelium still needs to be investigated.

Nevertheless, the present study shows that Eya1 is required for the proper distribution and stabilization of cell polarity proteins during otic vesicle epithelium development and neuronal differentiation (whether by transcriptional regulation or direct protein-protein interactions). Taken together with previous studies that show the important role of Eya1 and Six1 for both the maintenance of proliferative progenitors and for neuronal differentiation in the otic and other placodes, this raises the possibility that by modulating apicobasal cell polarity during otic development changing levels of Eya1 may affect the proportion of symmetric versus asymmetric cell divisions, which in turn may affect the balance between proliferating progenitors and differentiating neurons (Schlosser et al., 2008; Schlosser, 2010; Zheng et al., 2003; Zou et al., 2006). However, this hypothesis needs to be tested in further functional studies.

## 6.7 Outlook

The present study determines the time course of progenitor formation, neuronal delamination and differentiation in the otic vesicle of *Xenopus laevis*. It also describes for the first time the subcellular localization of Eya1 during development of the otic vesicle and investigates the role of Eya1 for otic neurogenesis.

The Eya1 gain and loss of function experiments reported here show clearly that Eya1 is required for the proliferation of sensorineural progenitors as well as the for differentiation of neurons in the otic vesicle. In addition, they reveal a requirement of Eya1 for the proper distribution of cell polarity proteins (Par3, aPKC, MLC) and N-cadherin in the otic vesicle. Taken together with previous reports of dosage dependent requirement of Eya1 for progenitor maintenance (high doses) and neuronal differentiation (low doses) (Schlosser et al., 2008; Zou et al., 2008; Riddiford et al., 2017), these findings suggest that declining levels of Eya1 in the otic epithelium may help to regulate the transition from proliferating progenitors to the delaminating and differentiating sensory neurons. They further raise the possibility that the dosage-dependent effects of Eya1 in otic neurogenesis may at least partly be mediated via its effect on cell polarity proteins, with high levels of Eya1 maintaining apicobasal cell polarity and N-cadherin localization to adherens junctions, while low levels may promote loss of apicobasal polarity and N-cadherin resulting in delamination of neuroblasts. The effects of Eya1 on cell polarity may also affect the balance between progenitors and differentiating neurons by modulating the proportion of symmetric versus asymmetric cell divisions. However, additional knockout or knockdown experiments need to be done, to test these various possible mechanisms.

## References

- Abdelhak, S., Kalatzis, V., Heilig, R., Compain, S., Samson, D., Vincent, C., Levi-Acobas, F., Cruaud, C., Le Merrer, M., Mathieu, M., 1997a. Clustering of mutations responsible for branchio-oto-renal (BOR) syndrome in the eyes absent homologous region (eyaHR) of EYA1. *Human molecular genetics* 6, 2247-2255.
- Abdelhak, S., Kalatzis, V., Heilig, R., Compain, S., Samson, D., Vincent, C., Weil, D., Cruaud, C., Sahly, I., Leibovici, M., 1997b. A human homologue of the *Drosophila* eyes absent gene underlies branchio-oto-renal (BOR) syndrome and identifies a novel gene family. *Nature genetics* 15, 157.
- Abello, G., Khatri, S., Giráldez, F., Alsina, B., 2007. Early regionalization of the otic placode and its regulation by the Notch signaling pathway. *Mechanisms of development* 124, 631-645.
- Abello, G., Khatri, S., Radosevic, M., Scotting, P., Giraldez, F., Alsina, B., 2010. Independent regulation of Sox3 and Lmx1b by FGF and BMP signaling influences the neurogenic and non-neurogenic domains in the chick otic placode. *Developmental biology* 339, 166-178.
- Abu-Elmagd, M., Ishii, Y., Cheung, M., Rex, M., Le Rouëdec, D., Scotting, P.J., 2001. cSox3 expression and neurogenesis in the epibranchial placodes. *Developmental biology* 237, 258-269.
- Adam, J., Myat, A., Le Roux, I., Eddison, M., Henrique, D., Ish-Horowicz, D., Lewis, J., 1998. Cell fate choices and the expression of Notch Delta and Serrate homologues in the chick inner ear: parallels with *Drosophila* sense-organ development. *Development*, 125, pp. 4645-4654.
- Ahmed, M., Wong, E.Y., Sun, J., Xu, J., Wang, F., Xu, P.-X., 2012a. Eya1-Six1 interaction is sufficient to induce hair cell fate in the cochlea by activating Atoh1 expression in cooperation with Sox2. *Developmental cell* 22, 377-390.
- Ahmed, M., Xu, J., Xu, P.-X., 2012b. EYA1 and SIX1 drive the neuronal developmental program in cooperation with the SWI/SNF chromatin-remodeling complex and SOX2 in the mammalian inner ear. *Development* 139, 1965-1977.
- Ahrens, K., Schlosser, G., 2005. Tissues and signals involved in the induction of placodal Six1 expression in *Xenopus laevis*. *Developmental biology* 288, 40-59.

Akimenko, M.A., Ekker, M., Wegner, J., Lin, W., Westerfield, M., 1994. Combinatorial expression of three zebrafish genes related to distal-less: part of a homeobox gene code for the head. *The Journal of neuroscience : the official journal of the Society for Neuroscience* 14, 3475-3486.

Akitaya, T., Bronner-Fraser, M., 1992. Expression of cell adhesion molecules during initiation and cessation of neural crest cell migration. *Developmental dynamics : an official publication of the American Association of Anatomists* 194, 12-20.

Alexandre, P., Reugels, A.M., Barker, D., Blanc, E., Clarke, J.D.J.N.n., 2010. Neurons derive from the more apical daughter in asymmetric divisions in the zebrafish neural tube. 13, 673.

Ali, F., Hindley, C., McDowell, G., Deibler, R., Jones, A., Kirschner, M., Guillemot, F., Philpott, A., 2011. Cell cycle-regulated multi-site phosphorylation of Neurogenin 2 coordinates cell cycling with differentiation during neurogenesis. *Development* 138, 4267-4277.

Ali, F.R., Cheng, K., Kirwan, P., Metcalfe, S., Livesey, F.J., Barker, R.A., Philpott, A., 2014. The phosphorylation status of *Ascl1* is a key determinant of neuronal differentiation and maturation in vivo and in vitro. *Development* 141, 2216-2224.

Ali, N.J., Gomes, M.D., Bauer, R., Brodesser, S., Niemann, C., Iden, S., 2016. Essential role of polarity protein Par3 for epidermal homeostasis through regulation of barrier function, keratinocyte differentiation, and stem cell maintenance. *Journal of Investigative Dermatology* 136, 2406-2416.

Alsina, B., 2020. Mechanisms of cell specification and differentiation in vertebrate cranial sensory systems. *Current opinion in cell biology* 67, 79-85.

Alsina, B., Abelló, G., Ulloa, E., Henrique, D., Pujades, C., Giraldez, F., 2004. FGF signaling is required for determination of otic neuroblasts in the chick embryo. *Developmental biology* 267, 119-134.

Alsina, B., Giraldez, F., Pujades, C., 2009. Patterning and cell fate in ear development. *International Journal of Developmental Biology* 53, 1503-1513.

Alsina, B., Whitfield, T.T., 2017. Sculpting the labyrinth: morphogenesis of the developing inner ear, *Seminars in cell & developmental biology*, Elsevier, pp. 47-59.

Amaya, E., Offield, M.F., Grainger, R.M., 1998. Frog genetics: *Xenopus tropicalis* jumps into the future. *Trends in Genetics* 14, 253-255.

Andermann, P., Ungos, J., Raible, D.W., 2002. Neurogenin1 defines zebrafish cranial sensory ganglia precursors. *Developmental biology* 251, 45-58.

Assémat, E., Bazellières, E., Pallesi-Pocachard, E., Le Bivic, A., Massey-Harroche, D., 2008. Polarity complex proteins. *Biochimica et Biophysica Acta (BBA)-Biomembranes* 1778, 614-630.

Atwood, S.X., Chabu, C., Penkert, R.R., Doe, C.Q., Prehoda, K.E.J.J.o.c.s., 2007. Cdc42 acts downstream of Bazooka to regulate neuroblast polarity through Par-6–aPKC. *Development* 135, 3200-3206.

Bailey, A.P., Streit, A., 2005. Sensory organs: making and breaking the pre-placodal region. *Current topics in developmental biology* 72, 167-204.

Baker, C., Stark, M.R., Marcelle, C., Bronner-Fraser, M., 1999. Competence, specification and induction of Pax-3 in the trigeminal placode. *Development* 126, 147-156.

Baker, C.V., Bronner-Fraser, M., 2001. Vertebrate cranial placodes I. Embryonic induction. *Developmental biology* 232, 1-61.

Baker, C.V., O'Neill, P., McCole, R.B., 2008. Lateral line, otic and epibranchial placodes: developmental and evolutionary links? *Journal of Experimental Zoology Part B: Molecular and Developmental Evolution* 310, 370-383.

Baker, N.E., Brown, N.L., 2018. All in the family: proneural bHLH genes and neuronal diversity. *Development* 145, dev159426.

Bane, B.C., Van Rybroek, J.M., Kolker, S.J., Weeks, D.L., Manaligod, J.M., 2005. EYA1 expression in the developing inner ear. *Annals of Otology, Rhinology & Laryngology* 114, 853-858.

Barald, K.F., Kelley, M.W., 2004. From placode to polarization: new tunes in inner ear development. *Development* 131, 4119-4130.

Barber, P., 1982. Neurogenesis and regeneration in the primary olfactory pathway of mammals. *Bibliotheca anatomica*, 12-25.



Barrionuevo, F., Naumann, A., Bagheri-Fam, S., Speth, V., Taketo, M.M., Scherer, G., Neubüser, A., 2008. Sox9 is required for invagination of the otic placode in mice. *Developmental biology* 317, 213-224.

Bartolami, S., Goodyear, R., Richardson, G.J.J.o.C.N., 1991. Appearance and distribution of the 275 kD hair-cell antigen during development of the avian inner ear. 314, 777-788.

Barui, A., Datta, P., 2019. Biophysical factors in the regulation of asymmetric division of stem cells. *Biological Reviews* 94, 810-827.

Begbie, J., Ballivet, M., Graham, A., 2002. Early steps in the production of sensory neurons by the neurogenic placodes. *Molecular and cellular neurosciences* 21, 502-511.

Bell, D., Streit, A., Gorospe, I., Varela-Nieto, I., Alsina, B., Giraldez, F., 2008. Spatial and temporal segregation of auditory and vestibular neurons in the otic placode. *Developmental biology* 322, 109-120.

Benton, R., Johnston, D.S., 2003. A conserved oligomerization domain in *Drosophila* Bazooka/PAR-3 is important for apical localization and epithelial polarity. *Current Biology* 13, 1330-1334.

Bermingham, N.A., Hassan, B.A., Price, S.D., Vollrath, M.A., Ben-Arie, N., Eatock, R.A., Bellen, H.J., Lysakowski, A., Zoghbi, H.Y., 1999. Math1: an essential gene for the generation of inner ear hair cells. *Science (New York, N.Y.)* 284, 1837-1841.

Bertrand, N., Castro, D.S., Guillemot, F., 2002. Proneural genes and the specification of neural cell types. *Nature Reviews Neuroscience* 3, 517.

Biggs, L.C., Mikkola, M.L., 2014. Early inductive events in ectodermal appendage morphogenesis, *Seminars in cell & developmental biology*, Elsevier, pp. 11-21.

Bilder, D., Schober, M., Perrimon, N., 2003. Integrated activity of PDZ protein complexes regulates epithelial polarity. *Nature cell biology* 5, 53.

Bissonnette, J.P., Fekete, D.M.J.J.o.C.N., 1996. Standard atlas of the gross anatomy of the developing inner ear of the chicken. 368, 620-630.

Bok, J., Raft, S., Kong, K.-A., Koo, S.K., Dräger, U.C., Wu, D.K., 2011. Transient retinoic acid signaling confers anterior-posterior polarity to the inner ear. *Proceedings of the National Academy of Sciences* 108, 161-166.

Bonini, N.M., Bui, Q.T., Gray-Board, G.L., Warrick, J.M., 1997. The *Drosophila* eyes absent gene directs ectopic eye formation in a pathway conserved between flies and vertebrates. *Development* 124, 4819-4826.

Borsani, G., DeGrandi, A., Ballabio, A., Bulfone, A., Bernard, L., Banfi, S., Gattuso, C., Mariani, M., Dixon, M., Donnai, D., 1999. EYA4, a novel vertebrate gene related to *Drosophila* eyes absent. *Human molecular genetics* 8, 11-23.

Bricaud, O., and Collazo, A. (2006). The transcription factor six1 inhibits neuronal and promotes hair cell fate in the developing zebrafish (*Danio rerio*) inner ear. *J. Neurosci.* 26(41), 10438-10451.

Bronner-Fraser, M., Wolf, J. J., & Murray, B. A., 1992. Effects of antibodies against N-cadherin and N-CAM on the cranial neural crest and neural tube. *Developmental Biology*, 153, 291–301.

Brownell, A.G., Slavkin, H.C., 1980. Role of basal lamina in tissue interactions. *Kidney and Blood Pressure Research* 3, 193-204.

Brugmann, S.A., Moody, S.A., 2005. Induction and specification of the vertebrate ectodermal placodes: precursors of the cranial sensory organs. *Biology of the Cell* 97, 303-319.

Brugmann, S.A., Pandur, P.D., Kenyon, K.L., Pignoni, F., Moody, S.A., 2004. Six1 promotes a placodal fate within the lateral neurogenic ectoderm by functioning as both a transcriptional activator and repressor. *Development* 131, 5871-5881.

Buck, A.K., Herrmann, K., Zum Büschenfelde, C.M., Juweid, M.E., Bischoff, M., Glatting, G., Weirich, G., Möller, P., Wester, H.-J., Scheidhauer, K.J.C.c.r., 2008. Imaging bone and soft tissue tumors with the proliferation marker [18F] fluorodeoxythymidine. 14, 2970-2977.

Bultje, R.S., Castaneda-Castellanos, D.R., Jan, L.Y., Jan, Y.-N., Kriegstein, A.R., Shi, S.-H.J.N., 2009. Mammalian Par3 regulates progenitor cell asymmetric division via notch signaling in the developing neocortex. 63, 189-202.

Bylund, M., Andersson, E., Novitsch, B.G., Muhr, J., 2003. Vertebrate neurogenesis is counteracted by Sox1–3 activity. *Nature neuroscience* 6, 1162.

Camarero, G., Avendano, C., Fernandez-Moreno, C., Villar, A., Contreras, J., de Pablo, F., Pichel, J.G., Varela-Nieto, I., 2001. Delayed inner ear maturation and neuronal loss in postnatal Igf-1-deficient mice. *The Journal of neuroscience : the official journal of the Society for Neuroscience* 21, 7630-7641.

Carlsson, R., Engvall, E., Freeman, A., Ruoslahti, E., 1981. Laminin and fibronectin in cell adhesion: enhanced adhesion of cells from regenerating liver to laminin. *Proceedings of the National Academy of Sciences* 78, 2403-2406.

Carney, P.R., Silver, J., 1983. Studies on cell migration and axon guidance in the developing distal auditory system of the mouse. *Journal of Comparative Neurology* 215, 359-369.

Carpenter, E., 1937. The head pattern in *Amblystoma* studied by vital staining and transplantation methods. *Journal of Experimental Zoology* 75, 103-129.

Cau, E., Casarosa, S., Guillemot, F., 2002. Mash1 and Ngn1 control distinct steps of determination and differentiation in the olfactory sensory neuron lineage. *Development* 129, 1871-1880.

Cau, E., Gradwohl, G., Fode, C., Guillemot, F., 1997. Mash1 activates a cascade of bHLH regulators in olfactory neuron progenitors. *Development (Cambridge, England)* 124, 1611-1621.

Chalmers, A.D., Pambos, M., Mason, J., Lang, S., Wylie, C., Papalopulu, N.J.D., 2005. aPKC, Crumbs3 and Lgl2 control apicobasal polarity in early vertebrate development. *Development* 132, 977-986.

Charville, G.W., Rando, T.A., 2013. The mortal strand hypothesis: non-random chromosome inheritance and the biased segregation of damaged DNA, *Seminars in cell & developmental biology*, Elsevier, pp. 653-660.

Chen, B., Kim, E.-H., Xu, P.-X., 2009. Initiation of olfactory placode development and neurogenesis is blocked in mice lacking both Six1 and Six4. *Developmental biology* 326, 75-85.

Chen, J., Zhang, M.J.E.c.r., 2013. The Par3/Par6/aPKC complex and epithelial cell polarity. *Developmental biology* 319, 1357-1364.

Chen, P., Johnson, J.E., Zoghbi, H.Y., Segil, N., 2002. The role of Math1 in inner ear development: Uncoupling the establishment of the sensory primordium from hair cell fate determination. *Development (Cambridge, England)* 129, 2495-2505.

Chen, R., Amoui, M., Zhang, Z., Mardon, G., 1997. Dachshund and eyes absent proteins form a complex and function synergistically to induce ectopic eye development in *Drosophila*. *Cell* 91, 893-903.

Chen, S., Chen, J., Shi, H., Wei, M., Castaneda-Castellanos, D.R., Bultje, R.S., Pei, X., Kriegstein, A.R., Zhang, M., Shi, S.-H., 2013. Regulation of microtubule stability and organization by mammalian Par3 in specifying neuronal polarity. *Developmental cell* 24, 26-40.

Chen, Y., Shi, L., Zhang, L., Li, R., Liang, J., Yu, W., Sun, L., Yang, X., Wang, Y., Zhang, Y., 2008. The molecular mechanism governing the oncogenic potential of SOX2 in breast cancer. *Journal of Biological Chemistry* 283, 17969-17978.

Christophorou, N.A., Bailey, A.P., Hanson, S., Streit, A., 2009. Activation of Six1 target genes is required for sensory placode formation. *Developmental biology* 336, 327-336.

Christophorou, N.A., Mende, M., Lleras-Forero, L., Grocott, T., Streit, A., 2010. Pax2 coordinates epithelial morphogenesis and cell fate in the inner ear. *Developmental biology* 345, 180-190.

Chu, D.T., Klymkowsky, M.W., 1989. The appearance of acetylated  $\alpha$ -tubulin during early development and cellular differentiation in *Xenopus*. *Developmental biology* 136, 104-117.

Clay, M.R., Halloran, M.C., 2011. Regulation of cell adhesions and motility during initiation of neural crest migration. *Current opinion in neurobiology* 21, 17-22.

Collignon, J., Sockanathan, S., Hacker, A., Cohen-Tannoudji, M., Norris, D., Rastan, S., Stevanovic, M., Goodfellow, P.N., Lovell-Badge, R., 1996. A comparison of the properties of Sox-3 with Sry and two related genes, Sox-1 and Sox-2. *Development* 122, 509-520.

Coopman, P., Djiane, A.J.C., sciences, m.l., 2016. Adherens Junction and E-Cadherin complex regulation by epithelial polarity. *73*, 3535-3553.

Corey, D.R., Abrams, J.M., 2001. Morpholino antisense oligonucleotides: tools for investigating vertebrate development. *Genome biology* 2, reviews1015. 1011.

Costa, M.R., Wen, G., Lepier, A., Schroeder, T., Götz, M.J.D., 2008. Par-complex proteins promote proliferative progenitor divisions in the developing mouse cerebral cortex. 135, 11-22.

Dabdoub, A., Puligilla, C., Jones, J. M., Fritsch, B., Cheah, K. S., Pevny, L. H., et al., 2008. Sox2 signaling in prosensory domain specification and subsequent hair cell differentiation in the developing cochlea. *Proc. Natl. Acad. Sci. U.S.A.* 105, 18396–18401. doi: 10.1073/pnas.0808175105.

D'amico-Martel, A., Noden, D.M.J.A.J.o.A., 1983. Contributions of placodal and neural crest cells to avian cranial peripheral ganglia. 166, 445-468.

David, R., Ahrens, K., Wedlich, D., Schlosser, G., 2001. *Xenopus* Eya1 demarcates all neurogenic placodes as well as migrating hypaxial muscle precursors. *Mechanisms of development* 103, 189-192.

Davidson, L., Keller, R.J.D., 1999. Neural tube closure in *Xenopus laevis* involves medial migration, directed protrusive activity, cell intercalation and convergent extension. 126, 4547-4556.

Davies, S.N., Kitson, D.L., Roberts, A., 1982. The development of the peripheral trigeminal innervation in *Xenopus* embryos. *Development* 70, 215-224.

de Matos Simões, S., Blankenship, J.T., Weitz, O., Farrell, D.L., Tamada, M., Fernandez-Gonzalez, R., Zallen, J.A., 2010. Rho-kinase directs Bazooka/Par-3 planar polarity during *Drosophila* axis elongation. *Developmental cell* 19, 377-388.

Deng, M., Yang, H., Xie, X., Liang, G., Gan, L., 2014. Comparative expression analysis of POU4F1, POU4F2 and ISL1 in developing mouse cochleovestibular ganglion neurons. *Gene expression patterns : GEP* 15, 31-37.

Dhallan, R.S., Yau, K.-W., Schrader, K.A., Reed, R.R., 1990. Primary structure and functional expression of a cyclic nucleotide-activated channel from olfactory neurons. *Nature* 347, 184.

Dhouailly, D., 2009. A new scenario for the evolutionary origin of hair, feather, and avian scales. *Journal of anatomy* 214, 587-606.

Diogo, R., Kelly, R.G., Christiaen, L., Levine, M., Ziermann, J.M., Molnar, J.L., Noden, D.M., Tzahor, E., 2015. A new heart for a new head in vertebrate cardiopharyngeal evolution. *Nature* 520, 466.

Doe, C.Q., Bowerman, B., 2001. Asymmetric cell division: fly neuroblast meets worm zygote. *Current opinion in cell biology* 13, 68-75.

Drubin, D.G., Nelson, W.J., 1996. Origins of cell polarity. *Cell* 84, 335-344.

Du, D., Xu, F., Yu, L., Zhang, C., Lu, X., Yuan, H., Huang, Q., Zhang, F., Bao, H., Jia, L., Wu, X., Zhu, X., Zhang, X., Zhang, Z., Chen, Z., 2010. The tight junction protein, occludin, regulates the directional migration of epithelial cells. *Developmental cell* 18, 52-63.

Durruthy-Durruthy, R., Gottlieb, A., Hartman, B.H., Waldhaus, J., Laske, R.D., Altman, R., Heller, S., 2014. Reconstruction of the mouse otocyst and early neuroblast lineage at single-cell resolution. *Cell* 157, 964-978.

Dutta, S., Ganguli, R., Samanta, B., 2005. Investigation of two neural network methods in an automatic mapping exercise. *Journal of Applied GIS* 1, 1-19.

Dvorakova, M., Macova, I., Bohuslavova, R., Anderova, M., Fritsch, B., Pavlinkova, G., 2019. Early ear neuronal development, but not olfactory or lens development, can proceed without SOX2. *Developmental biology* 457,43-65.

Eagleson, G., Ferreiro, B., Harris, W.A., 1995. Fate of the anterior neural ridge and the morphogenesis of the *Xenopus* forebrain. *Journal of neurobiology* 28, 146-158.

Eisen, J.S., Smith, J.C., 2008. Controlling morpholino experiments: don't stop making antisense. *Development* 135, 1735-1743.

El-Hashash, A.H., Al Alam, D., Turcatel, G., Bellusci, S., Warburton, D., 2011. Eyes absent 1 (*Eya1*) is a critical coordinator of epithelial, mesenchymal and vascular morphogenesis in the mammalian lung. *Developmental biology* 350, 112-126.

El-Hashash, A.H., Turcatel, G., Al Alam, D., Buckley, S., Tokumitsu, H., Bellusci, S., Warburton, D.J.D., 2017. Retraction: *Eya1* controls cell polarity, spindle orientation, cell fate and Notch signaling in distal embryonic lung epithelium. *Development*. 144, 3849.

Eriksson, P., 2019. Critical thermal minimum of the embryonic development in the common frog (*Rana temporaria*). Master's thesis. Faculty of Natural Resources and Agricultural Sciences. Swedish University of Agricultural Sciences.

Esteve, P., Bovolenta, P., 1999. *cSix4*, a member of the six gene family of transcription factors, is expressed during placode and somite development. *Mech. Dev.*, 85 (1999), pp. 161-165.

Etienne-Manneville, S., Hall, A., 2003. Cell polarity: Par6, aPKC and cytoskeletal crosstalk. *Current opinion in cell biology* 15, 67-72.

Evsen, L., Sugahara, S., Uchikawa, M., Kondoh, H., Wu, D.K., 2013. Progression of neurogenesis in the inner ear requires inhibition of Sox2 transcription by neurogenin1 and neurod1. *The Journal of neuroscience : the official journal of the Society for Neuroscience* 33, 3879-3890.

Farkas, L.M., Huttner, W.B.J.C.o.i.c.b., 2008. The cell biology of neural stem and progenitor cells and its significance for their proliferation versus differentiation during mammalian brain development. 20, 707-715.

Favaro, R., Valotta, M., Ferri, A.L., Latorre, E., Mariani, J., Giachino, C., Lancini, C., Tosetti, V., Ottolenghi, S., Taylor, V., 2009. Hippocampal development and neural stem cell maintenance require Sox2-dependent regulation of Shh. *Nature neuroscience* 12, 1248.

Fode, C., Gradwohl, G., Morin, X., Dierich, A., LeMeur, M., Goridis, C., Guillemot, F., 1998. The bHLH protein NEUROGENIN 2 is a determination factor for epibranchial placode-derived sensory neurons. *Neuron* 20, 483-494.

Fornaro, M., Geuna, S., Fasolo, A., Giacobini-Robecchi, M., 2001. Evidence of very early neuronal migration from the olfactory placode of the chick embryo. *Neuroscience* 107, 191-197.

Francisco-Cruz, A., Parra, E.R., Tetzlaff, M.T., Wistuba, I.I., 2020. Multiplex immunofluorescence assays, *Biomarkers for Immunotherapy of Cancer*, Springer, pp. 467-495.

Freter, S., Fleenor, S.J., Freter, R., Liu, K.J., Begbie, J., 2013. Cranial neural crest cells form corridors prefiguring sensory neuroblast migration. *Development* 140, 3595-3600.

Freter, S., Muta, Y., Mak, S.-S., Rinkwitz, S., Ladher, R.K., 2008. Progressive restriction of otic fate: the role of FGF and Wnt in resolving inner ear potential. *Development* 135, 3415-3424.

Freyer, L., Morrow, B.E., 2010. Canonical Wnt signaling modulates Tbx1, Eya1, and Six1 expression, restricting neurogenesis in the otic vesicle. *Developmental Dynamics* 239, 1708-1722.

Fritsch, B., Beisel, K., Jones, K., Farinas, I., Maklad, A., Lee, J., Reichardt, L., 2002. Development and evolution of inner ear sensory epithelia and their innervation. *Journal of neurobiology* 53, 143-156.

Fritsch, B., Beisel, K.W., Hansen, L.A., 2006. The molecular basis of neurosensory cell formation in ear development: a blueprint for hair cell and sensory neuron regeneration? *Bioessays* 28, 1181-1193.

Fritsch, B., Eberl, D.F., Beisel, K.W., 2010. The role of bHLH genes in ear development and evolution: revisiting a 10-year-old hypothesis. *Cellular and molecular life sciences* 67, 3089-3099.

Gallagher, B.C., Henry, J.J., Grainger, R.M., 1996. Inductive Processes Leading to Inner Ear Formation during *Xenopus* Development. *Developmental biology* 175, 95-107.

Gálvez, H., Abelló, G., Giraldez, F., 2017. Signaling and transcription factors during inner ear development: the generation of hair cells and otic neurons. *Frontiers in Cell and Developmental Biology* 5, 21.

Gentsch, G.E., Spruce, T., Monteiro, R.S., Owens, N.D., Martin, S.R., Smith, J.C., 2018. Innate immune response and off-target mis-splicing are common morpholino-induced side effects in *Xenopus*. *Developmental cell* 44, 597-610. e510.

Gilmour, D.T., Maischein, H.-M., Nüsslein-Volhard, C., 2002. Migration and function of a glial subtype in the vertebrate peripheral nervous system. *Neuron* 34, 577-588.

Goldstein, B., Macara, I.G., 2007. The PAR proteins: fundamental players in animal cell polarization. *Developmental cell* 13, 609-622.



Gompel, N., Cubedo, N., Thisse, C., Thisse, B., Dambly-Chaudière, C., Ghysen, A., 2001. Pattern formation in the lateral line of zebrafish. *Mechanisms of development* 105, 69-77.

Goodman, C., Doe, C., 1993. The development of *Drosophila melanogaster*, *Embryonic Development of the Drosophila Central Nervous System*, Cold Spring Harbor Laboratory Press Cold Spring Harbor, NY, pp. 1131-1206.

Gou, Y., Vemaraju, S., Sweet, E.M., Kwon, H.-J., Riley, B.B., 2018. *sox2* and *sox3* Play unique roles in development of hair cells and neurons in the zebrafish inner ear. *Developmental biology* 435, 73-83.

Graham, A., Begbie, J., 2000. Neurogenic placodes: a common front. *Trends in neurosciences* 23, 313-316.

Graham, A., Blentic, A., Duque, S., Begbie, J., 2007. Delamination of cells from neurogenic placodes does not involve an epithelial-to-mesenchymal transition. *Development* 134, 4141-4145.

Graham, V., Khudyakov, J., Ellis, P., Pevny, L., 2003. SOX2 functions to maintain neural progenitor identity. *Neuron* 39, 749-765.

Graziadei, P., Graziadei, G.M., 1979. Neurogenesis and neuron regeneration in the olfactory system of mammals. I. Morphological aspects of differentiation and structural organization of the olfactory sensory neurons. *Journal of neurocytology* 8, 1-18.

Grifone, R., Demignon, J., Giordani, J., Niro, C., Souil, E., Bertin, F., Laclef, C., Xu, P.-X., Maire, P., 2007. *Eya1* and *Eya2* proteins are required for hypaxial somitic myogenesis in the mouse embryo. *Developmental biology* 302, 602-616.

Groves, A.K., Bronner-Fraser, M., 2000. Competence, specification and commitment in otic placode induction. *Development* 127, 3489-3499.

Guillemot, F., Lo, L.C., Johnson, J.E., Auerbach, A., Anderson, D.J., Joyner, A.L., 1993. Mammalian achaete-scute homolog 1 is required for the early development of olfactory and autonomic neurons. *Cell* 75, 463-476.

Gutjahr, M.C., Rossy, J., Niggli, V., 2005. Role of Rho, Rac, and Rho-kinase in phosphorylation of myosin light chain, development of polarity, and spontaneous

migration of Walker 256 carcinosarcoma cells. *Experimental cell research* 308, 422-438.

Haddon, C., Lewis, J., 1996. Early ear development in the embryo of the zebrafish, *Danio rerio*. *Journal of Comparative Neurology* 365, 113-128.

Hammond, K.L., van Eeden, F.J., Whitfield, T.T., 2010. Repression of Hedgehog signalling is required for the acquisition of dorsolateral cell fates in the zebrafish otic vesicle. *Development* 137, 1361-1371.

Hapak, S.M., Rothlin, C.V., Ghosh, S., 2018. PAR3–PAR6–atypical PKC polarity complex proteins in neuronal polarization. *Cellular and molecular life sciences* 75, 2735-2761.

Harris, T.J., Peifer, M., 2004. Adherens junction-dependent and-independent steps in the establishment of epithelial cell polarity in *Drosophila*. *The Journal of cell biology* 167, 135-147.

Harris, T.J., Tepass, U.J.N.r.M.c.b., 2010. Adherens junctions: from molecules to morphogenesis. 11, 502-514.

Hartman, B.H., Reh, T.A., Bermingham-McDonogh, O., 2010. Notch signaling specifies prosensory domains via lateral induction in the developing mammalian inner ear. *Proceedings of the National Academy of Sciences* 107, 15792-15797.

Hartsock, A., Nelson, W.J.J.B.e.B.A.-B., 2008. Adherens and tight junctions: structure, function and connections to the actin cytoskeleton. 1778, 660-669.

Hemond, S.G., Morest, D.K., 1991. Ganglion formation from the otic placode and the otic crest in the chick embryo: mitosis, migration, and the basal lamina. *Anatomy and embryology* 184, 1-13.

Hemond, S.G., Morest, D.K.J.A., embryology, 1991. Ganglion formation from the otic placode and the otic crest in the chick embryo: mitosis, migration, and the basal lamina. 184, 1-13.

Hildebrand, J. D., 2005. Shroom regulates epithelial cell shape via the apical positioning of an actomyosin network. *J. Cell Sci.* 118, 5191–5203.

Hildebrand, J. D. 2005. Shroom regulates epithelial cell shape via the apical positioning of an actomyosin network. *J. Cell Sci.* 118, 5191–5203.

Hilfer, S.R., Randolph, G.J., 1993. Immunolocalization of basal lamina components during development of chick otic and optic primordia. *The Anatomical Record* 235, 443-452.

Holmberg, J., Hansson, E., Malewicz, M., Sandberg, M., Perlmann, T., Lendahl, U., Muhr, J., 2008. SoxB1 transcription factors and Notch signaling use distinct mechanisms to regulate proneural gene function and neural progenitor differentiation. *Development* 135, 1843-1851.

Horikoshi, Y., Suzuki, A., Yamanaka, T., Sasaki, K., Mizuno, K., Sawada, H., Yonemura, S., Ohno, S. *J. J. o. c. s.*, 2009. Interaction between PAR-3 and the aPKC–PAR-6 complex is indispensable for apical domain development of epithelial cells. 122, 1595-1606.

Hrynyk, M.A., Brunetti, C., Kerr, L., Metcalfe, C.D., 2018. Effect of imidacloprid on the survival of *Xenopus* tadpoles challenged with wild type frog virus 3. *Aquatic Toxicology* 194, 152-158.

Hutterer, A., Betschinger, J., Petronczki, M., Knoblich, J.A., 2004. Sequential roles of Cdc42, Par-6, aPKC, and Lgl in the establishment of epithelial polarity during *Drosophila* embryogenesis. *Developmental cell* 6, 845-854.

Ichikawa, T., Nakazato, K., Keller, P.J., Kajiura-Kobayashi, H., Stelzer, E.H., Mochizuki, A., Nonaka, S., 2013. Live imaging of whole mouse embryos during gastrulation: migration analyses of epiblast and mesodermal cells. *PloS one* 8, e64506.

Iden, S., Rehder, D., August, B., Suzuki, A., Wolburg-Buchholz, K., Wolburg, H., Ohno, S., Behrens, J., Vestweber, D., Ebnet, K., 2006. A distinct PAR complex associates physically with VE-cadherin in vertebrate endothelial cells. *EMBO reports* 7, 1239-1246.

Ishihara, T., Sato, S., Ikeda, K., Yajima, H., Kawakami, K., 2008. Multiple evolutionarily conserved enhancers control expression of *Eya1*. *Developmental dynamics: an official publication of the American Association of Anatomists* 237, 3142-3156.

IUCN RED LIST CATEGORIES AND CRITERIA, 2019. International Union for Conservation of Nature and Natural Resources,[ <https://www.iucnredlist.org/> ] Accessed 15/8/2019.

Izumikawa, M., Minoda, R., Kawamoto, K., Abrashkin, K.A., Swiderski, D.L., Dolan, D.F., Brough, D.E., Raphael, Y., 2005. Auditory hair cell replacement and hearing improvement by *Atoh1* gene therapy in deaf mammals. *Nature medicine* 11, 271.

Izzedine, H., Bodaghi, B., Launay-Vacher, V., Deray, G., 2003. Eye and kidney: from clinical findings to genetic explanations. *Journal of the American Society of Nephrology* 14, 516-529.

Jiang, L., Bi, D., Ding, H., Wu, X., Zhu, R., Zeng, J., Yang, X., Kan, X., 2019. Systematic Identification and Evolution Analysis of Sox Genes in *Coturnix japonica* Based on Comparative Genomics. *Genes* 10, 314.

Jidigam, V.K., Srinivasan, R.C., Patthey, C., Gunhaga, L., 2015. Apical constriction and epithelial invagination are regulated by BMP activity. *Biology open* 4, 1782-1791.

Jossin, Y., Cooper, J.A., 2011. Reelin, Rap1 and N-cadherin orient the migration of multipolar neurons in the developing neocortex. *Nature neuroscience* 14, 697.

Jung, B., Köhler, A., Schambony, A., Wedlich, D., 2011. PAPC and the Wnt5a/Ror2 pathway control the invagination of the otic placode in *Xenopus*. *BMC developmental biology* 11, 36.

Kalatzis, V., Sahly, I., El-Amraoui, A., Petit, C., 1998. *Eya1* expression in the developing ear and kidney: towards the understanding of the pathogenesis of Branchio-Oto-Renal (BOR) syndrome. *Developmental dynamics: an official publication of the American Association of Anatomists* 213, 486-499.

Kamachi, Y., Kondoh, H., 2013. Sox proteins: regulators of cell fate specification and differentiation. *Development* 140, 4129-4144.

Kay, B.K., Peng, H.B., 1992. *Xenopus laevis*: practical uses in cell and molecular biology. Academic press.

Kemphues, K., 2000. PARsing embryonic polarity. *Cell* 101, 345-348.

Khokha, M.K., Chung, C., Bustamante, E.L., Gaw, L.W., Trott, K.A., Yeh, J., Lim, N., Lin, J.C., Taverner, N., Amaya, E., 2002. Techniques and probes for the study of *Xenopus tropicalis* development. *Developmental dynamics: an official publication of the American Association of Anatomists* 225, 499-510.

Kiernan, A.E., 2013. Notch signaling during cell fate determination in the inner ear, *Seminars in cell & developmental biology*, Elsevier, pp. 470-479.

Kiernan, A.E., Pelling, A.L., Leung, K.K., Tang, A.S., Bell, D.M., Tease, C., Lovell-Badge, R., Steel, K.P., Cheah, K.S., 2005. Sox2 is required for sensory organ development in the mammalian inner ear. *Nature* 434, 1031.

Kishi, M., Mizuseki, K., Sasai, N., Yamazaki, H., Shiota, K., Nakanishi, S., Sasai, Y., 2000. Requirement of Sox2-mediated signaling for differentiation of early *Xenopus* neuroectoderm. *Development* 127, 791-800.

Klein, S., Graziadei, P., 1983. The differentiation of the olfactory placode in *Xenopus laevis*: a light and electron microscope study. *Journal of Comparative Neurology* 217, 17-30.

Knoblich, J.A., 2010. Asymmetric cell division: recent developments and their implications for tumour biology. *Nature reviews Molecular cell biology* 11, 849.

Kosodo, Y., 2012. Interkinetic nuclear migration: beyond a hallmark of neurogenesis. *Cellular and Molecular Life Sciences* 69, 2727-2738.

Kosodo, Y., Suetsugu, T., Suda, M., Mimori-Kiyosue, Y., Toida, K., Baba, S.A., Kimura, A., Matsuzaki, F., 2011. Regulation of interkinetic nuclear migration by cell cycle-coupled active and passive mechanisms in the developing brain. *The EMBO journal* 30, 1690-1704.

Köster, R.W., Kühnlein, R.P., Wittbrodt, J., 2000. Ectopic Sox3 activity elicits sensory placode formation. *Mechanisms of development* 95, 175-187.

Kozlowski, D.J., Murakami, T., Ho, R.K., Weinberg, E.S.J.B., *biology*, c., 1997. Regional cell movement and tissue patterning in the zebrafish embryo revealed by fate mapping with caged fluorescein. *75*, 551-562.

Kozlowski, D.J., Whitfield, T.T., Hukriede, N.A., Lam, W.K., Weinberg, E.S., 2005. The zebrafish dog-eared mutation disrupts *eya1*, a gene required for cell

survival and differentiation in the inner ear and lateral line. *Developmental biology* 277, 27-41.

Krahn, M.P., Egger-Adam, D., Wodarz, A., 2009. PP2A antagonizes phosphorylation of Bazooka by PAR-1 to control apical-basal polarity in dividing embryonic neuroblasts. *Developmental cell* 16, 901-908.

Kumar, J., 2009. The sine oculis homeobox (SIX) family of transcription factors as regulators of development and disease. *Cellular and molecular life sciences* 66, 565.

Kuwabara, T., Hsieh, J., Muotri, A., Yeo, G., Warashina, M., Lie, D.C., Moore, L., Nakashima, K., Asashima, M., Gage, F.H., 2009. Wnt-mediated activation of NeuroD1 and retro-elements during adult neurogenesis. *Nature neuroscience* 12, 1097.

Laclef, C., Souil, E., Demignon, J., Maire, P., 2003. Thymus, kidney and craniofacial abnormalities in Six 1 deficient mice. *Mechanisms of development* 120, 669-679.

Lanford, P.J., Shailam, R., Norton, C.R., Ridley, T., Kelley, M.W., 2000. Expression of Math1 and HES5 in the cochleae of wildtype and Jag2 mutant mice. *Journal of the Association for Research in Otolaryngology* 1, 161-171.

Lassiter, R.N., Stark, M.R., Zhao, T., Zhou, C.J., 2014. Signaling mechanisms controlling cranial placode neurogenesis and delamination. *Developmental biology* 389, 39-49.

Laudet, V., Stehelin, D., Clevers, H., 1993. Ancestry and diversity of the HMG box superfamily. *Nucleic acids research* 21, 2493-2501.

Lee, J.E., Hollenberg, S.M., Snider, L., Turner, D.L., Lipnick, N., Weintraub, H., 1995. Conversion of *Xenopus* ectoderm into neurons by NeuroD, a basic helix-loop-helix protein. *Science (New York, N.Y.)* 268, 836-844.

Lee, S., Cuvillier, J.M., Lee, B., Shen, R., Lee, J.W., Lee, S.-K.J.P.o.t.N.A.o.S., 2012. Fusion protein Isl1-Lhx3 specifies motor neuron fate by inducing motor neuron genes and concomitantly suppressing the interneuron programs. 109, 3383-3388.

Lee, S.-K., Pfaff, S.L.J.N., 2003. Synchronization of neurogenesis and motor neuron specification by direct coupling of bHLH and homeodomain transcription factors. *38*, 731-745.

Lele, Z., Folchert, A., Concha, M., Rauch, G.-J., Geisler, R., Rosa, F., Wilson, S.W., Hammerschmidt, M., Bally-Cuif, L.J.D., 2002. Parachute/n-cadherin is required for morphogenesis and maintained integrity of the zebrafish neural tube. *129*, 3281-3294.

Leung, L., Klopper, A.V., Grill, S.W., Harris, W.A., Norden, C., 2011. Apical migration of nuclei during G2 is a prerequisite for all nuclear motion in zebrafish neuroepithelia. *Development (Cambridge, England)* *138*, 5003-5013.

Li, H., Liu, H., Sage, C., Huang, M., Chen, Z.Y., Heller, S.J.J.o.C.N., 2004. Islet,1 expression in the developing chicken inner ear. *477*, 1-10.

Li, J., Zhang, T., Ramakrishnan, A., Fritsch, B., Xu, J., Wong, E.Y., Loh, Y.-H.E., Ding, J., Shen, L., Xu, P.-X.J.N.a.r., 2020. Dynamic changes in cis-regulatory occupancy by Six1 and its cooperative interactions with distinct cofactors drive lineage-specific gene expression programs during progressive differentiation of the auditory sensory epithelium. *48*, 2880-2896.

Li, X., Ohgi, K.A., Zhang, J., Krones, A., Bush, K.T., Glass, C.K., Nigam, S.K., Aggarwal, A.K., Maas, R., Rose, D.W., 2003. Eya protein phosphatase activity regulates Six1–Dach–Eya transcriptional effects in mammalian organogenesis. *Nature* *426*, 247.

Li, Y., Manaligod, J.M., Weeks, D.L., 2010. EYA1 mutations associated with the branchio-oto-renal syndrome result in defective otic development in *Xenopus laevis*. *Biology of the Cell* *102*, 277-292.

Liu, Q., Chen, P., Wang, J., 2014. Molecular mechanisms and potentials for differentiating inner ear stem cells into sensory hair cells. *Developmental biology* *390*, 93-101.

Lopez, Verrilli, M.A., Picou, F., Court, F.A., 2013. Schwann cell-derived exosomes enhance axonal regeneration in the peripheral nervous system. *Glia* *61*, 1795-1806.

Lyu, Q., Zheng, H.S., Laprocina, K., Huang, C.-C.J.J.J.o.v.e.J., 2020. Microwaving and fluorophore-tyramide for multiplex immunostaining on mouse adrenals—using un-conjugated primary antibodies from the same host species.

Ma, Q., Anderson, D.J., Fritsch, B., 2000. Neurogenin 1 null mutant ears develop fewer, morphologically normal hair cells in smaller sensory epithelia devoid of innervation. *Journal of the Association for Research in Otolaryngology* 1, 129-143.

Ma, Q., Chen, Z., del Barco Barrantes, I., de la Pompa, J.L., Anderson, D.J., 1998. neurogenin1 is essential for the determination of neuronal precursors for proximal cranial sensory ganglia. *Neuron* 20, 469-482.

Ma, Q., Kintner, C., and Anderson, D.J., 1996. Identification of neurogenin, a Vertebrate Neuronal Determination Gene. *Cell* 87, 43-52.

Ma, Y.-C., Song, M.-R., Park, J.P., Ho, H.-Y.H., Hu, L., Kurtev, M.V., Zieg, J., Ma, Q., Pfaff, S.L., Greenberg, M.E.J.N., 2008. Regulation of motor neuron specification by phosphorylation of neurogenin 2. *Development* 135, 65-77.

Macara, I.G., 2004. Parsing the polarity code. *Nature reviews Molecular cell biology* 5, 220.

Maier, E.C., Saxena, A., Alsina, B., Bronner, M.E., Whitfield, T.T., 2014. Sensational placodes: Neurogenesis in the otic and olfactory systems. *Developmental biology* 389, 50-67.

Manni, L., Lane, N.J., Joly, J.S., Gasparini, F., Tiozzo, S., Caicci, F., Zaniolo, G., Burighel, P., 2004. Neurogenic and non-neurogenic placodes in ascidians. *Journal of Experimental Zoology Part B: Molecular and Developmental Evolution* 302, 483-504.

Maroon, H., Walshe, J., Mahmood, R., Kiefer, P., Dickson, C., Mason, I., 2002. Fgf3 and Fgf8 are required together for formation of the otic placode and vesicle. *Development* 129, 2099-2108.

Martin-Belmonte, F., Perez-Moreno, M., 2012. Epithelial cell polarity, stem cells and cancer. *Nature Reviews Cancer* 12, 23.

Masserdotti, G., Gillotin, S., Sutor, B., Drechsel, D., Irmeler, M., Jørgensen, H.F., Sass, S., Theis, F.J., Beckers, J., Berninger, B., 2015. Transcriptional mechanisms of proneural factors and REST in regulating neuronal reprogramming of astrocytes. *Cell stem cell* 17, 74-88.

Matsumata, M., Uchikawa, M., Kamachi, Y., Kondoh, H., 2005. Multiple N-cadherin enhancers identified by systematic functional screening indicate its Group



B1 SOX-dependent regulation in neural and placodal development. *Developmental biology* 286, 601-617.

McCabe, K.L., Bronner-Fraser, M., 2009. Molecular and tissue interactions governing induction of cranial ectodermal placodes. *Developmental biology* 332, 189-195.

McLarren, K.W., Litsiou, A., Streit, A., 2003. DLX5 positions the neural crest and preplacode region at the border of the neural plate. *Developmental biology* 259, 34-47.

Meier, S., 1978a. Development of the embryonic chick otic placode. I. Light microscopic analysis. *The Anatomical Record* 191, 447-458.

Meier, S., 1978b. Development of the embryonic chick otic placode. II. Electron microscopic analysis. *The Anatomical Record* 191, 459-477.

Meier, S., 1979. Development of the chick embryo mesoblast. Formation of the embryonic axis and establishment of the metameric pattern. *Developmental biology* 73, 24-45.

Merk, D.J., Zhou, P., Cohen, S.M., Pazyra-Murphy, M.F., Hwang, G.H., Rehm, K.J., Alfaro, J., Zhao, X., Park, E., Xu, P.-X.J.b., 2019. The *Eya1* phosphatase mediates Shh-driven symmetric cell division of cerebellar granule cell precursors. 668277.

Merk, D.J., Zhou, P., Cohen, S.M., Pazyra-Murphy, M.F., Hwang, G.H., Rehm, K.J., Alfaro, J., Reid, C.M., Zhao, X., Park, E., Xu, P.X., Chan, J.A., Eck, M.J., Nazemi, K.J., Harwell, C.C., Segal, R.A., 2020. The *Eya1* Phosphatase Mediates Shh-Driven Symmetric Cell Division of Cerebellar Granule Cell Precursors. *Developmental neuroscience* 42, 170-186.

Metcalf, W.K., 1989. Organization and development of the zebrafish posterior lateral line, The mechanosensory lateral line, Springer, pp. 147-159.

Meulemans, D., Bronner-Fraser, M.J.I.j.o.b.s., 2007. The amphioxus SoxB family: implications for the evolution of vertebrate placodes. 3, 356.

Mhatre, A.N., Li, J., Kim, Y., Coling, D.E., Lalwani, A.K., 2004. Cloning and developmental expression of nonmuscle myosin IIA (Myh9) in the mammalian inner ear. *Journal of neuroscience research* 76, 296-305.

Mikkola, M.L., 2007. Genetic basis of skin appendage development, *Seminars in cell & developmental biology*, Elsevier, pp. 225-236.

Millimaki, B.B., Sweet, E.M., Dhasan, M.S., Riley, B.B., 2007. Zebrafish *atoh1* genes: classic proneural activity in the inner ear and regulation by Fgf and Notch. *Development* 134, 295-305.

Millimaki, B.B., Sweet, E.M., Riley, B.B., 2010. Sox2 is required for maintenance and regeneration, but not initial development, of hair cells in the zebrafish inner ear. *Developmental biology* 338, 262-269.

Miyamoto, Y., Sakane, F., Hashimoto, K.J.C.a., migration, 2015. N-cadherin-based adherens junction regulates the maintenance, proliferation, and differentiation of neural progenitor cells during development.

Moore, R., Theveneau, E., Pozzi, S., Alexandre, P., Richardson, J., Merks, A., Parsons, M., Kashef, J., Linker, C., Mayor, R., 2013. Par3 controls neural crest migration by promoting microtubule catastrophe during contact inhibition of locomotion. *Development (Cambridge, England)* 140, 4763-4775.

Morais-de-Sá, E., Mirouse, V., St Johnston, D.J.C., 2010. aPKC phosphorylation of Bazooka defines the apical/lateral border in *Drosophila* epithelial cells. 141, 509-523.

Murray, R.C., Navi, D., Fesenko, J., Lander, A.D., Calof, A.L., 2003. Widespread defects in the primary olfactory pathway caused by loss of Mash1 function. *The Journal of neuroscience : the official journal of the Society for Neuroscience* 23, 1769-1780.

Musharraf, A., Kruspe, D., Tomasch, J., Besenbeck, B., Englert, C., Landgraf, K., 2014. BOR-syndrome-associated *Eya1* mutations lead to enhanced proteasomal degradation of *Eya1* protein. *PloS one* 9, e87407.

Nakagawa, S., Takeichi, M., 1998. Neural crest emigration from the neural tube depends on regulated cadherin expression. *Development*, 125:2963-2971.

Nance, J., Zallen, J.A., 2011. Elaborating polarity: PAR proteins and the cytoskeleton. *Development* 138, 799-809.

Nechiporuk, A., Linbo, T., Poss, K.D., Raible, D.W., 2007. Specification of epibranchial placodes in zebrafish. *Development* 134, 611-623.

Neves, J., Abelló, G., Petrovic, J., Giraldez, F.J.D., growth, differentiation, 2013. Patterning and cell fate in the inner ear: a case for *notch* in the chicken embryo. 55, 96-112.

Neves, J., Kamaid, A., Alsina, B., Giraldez, F., 2007. Differential expression of *Sox2* and *Sox3* in neuronal and sensory progenitors of the developing inner ear of the chick. *Journal of Comparative Neurology* 503, 487-500.

Neves, J., Uchikawa, M., Bigas, A., Giraldez, F., 2012. The prosensory function of *Sox2* in the chicken inner ear relies on the direct regulation of *Atoh1*. *PLoS one* 7, e30871.

Nica, G., Herzog, W., Sonntag, C., Nowak, M., Schwarz, H., Zapata, A.G., Hammerschmidt, M., 2006. *Eya1* is required for lineage-specific differentiation, but not for cell survival in the zebrafish adenohypophysis. *Developmental biology* 292, 189-204.

Nieber, F., Pieler, T., Henningfeld, K.A., 2009. Comparative expression analysis of the neurogenins in *Xenopus tropicalis* and *Xenopus laevis*. *Developmental Dynamics* 238, 451-458.

Nieuwkoop, P., Faber, J., 1967. *Normal Table of Xenopus Laevis (Daudin)*. 2nd. edn. Utrecht: Hubrecht Lab, Amsterdam: North-Holland Publishing Co.

Noatynska, A., Tavernier, N., Gotta, M., Pintard, L., 2013. Coordinating cell polarity and cell cycle progression: what can we learn from flies and worms? *Open biology* 3, 130083.

Norden, C., 2017. Pseudostratified epithelia - cell biology, diversity and roles in organ formation at a glance. *Journal of cell science* 130, 1859-1863.

Norden, C., Young, S., Link, B.A., Harris, W.A., 2009. Actomyosin is the main driver of interkinetic nuclear migration in the retina. *Cell* 138, 1195-1208.

Nornes, H., Dressler, G., Knapik, E., Deutsch, U., Gruss, P., 1990. Spatially and temporally restricted expression of Pax2 during murine neurogenesis. *Development* 109, 797-809.

Northcutt, J., Foegeding, E., Edens, F., 1994. Water-holding properties of thermally preconditioned chicken breast and leg meat. *Poultry Science* 73, 308-316.

Northcutt, R.G., 1992. The phylogeny of Octavolateralis Ontogenies: a reaffirmation of Garstang's phylogenetic hypothesis, *The evolutionary biology of hearing*, Springer, pp. 21-47.

Northcutt, R.G., 1996. The origin of craniates: neural crest, neurogenic placodes, and homeobox genes. *Israel Journal of Zoology* 42, S273-S313.

Northcutt, R.G., 1997. Animal behaviour: Swimming against the current. *Nature* 389, 915.

Northcutt, R.G., 2004. Taste buds: development and evolution. *Brain, behavior and evolution* 64, 198-206.

Northcutt, R.G., Brändle, K., Fritsch, B., 1995. Electrosensory and mechanosensory lateral line organs arise from single placodes in axolotls. *Developmental biology* 168, 358-373.

Northcutt, R.G., Brändle, K.J.J.o.C.N., 1995. Development of branchiomic and lateral line nerves in the axolotl. 355, 427-454.

Northcutt, R.G., Gans, C., 1983. The genesis of neural crest and epidermal placodes: a reinterpretation of vertebrate origins. *The Quarterly review of biology* 58, 1-28.

Novince, Z., Azodi, E., Marrs, J., Raymond, P., Liu, Q., 2003. Cadherin expression in the inner ear of developing zebrafish. *Gene expression patterns* 3, 337-339.

Ohto, H., Kamada, S., Tago, K., Tominaga, S.-I., Ozaki, H., Sato, S., Kawakami, K., 1999. Cooperation of six and eya in activation of their target genes through nuclear translocation of Eya. *Molecular and cellular biology* 19, 6815-6824.

O'Rahilly, R., 1963. The early development of the otic vesicle in staged human embryos. *Development* 11, 741-755.

Orten, D.J., Fischer, S.M., Sorensen, J.L., Radhakrishna, U., Cremers, C.W., Marres, H.A., Van Camp, G., Welch, K.O., Smith, R.J., Kimberling, W.J., 2008. Branchio-oto-renal syndrome (BOR): novel mutations in the EYA1 gene, and a review of the mutational genetics of BOR. *Human mutation* 29, 537-544.

Padanad, M.S., Riley, B.B., 2011. Pax2/8 proteins coordinate sequential induction of otic and epibranchial placodes through differential regulation of foxi1, sox3 and fgf24. *Developmental biology* 351, 90-98.

Panaliappan, T.K., Wittmann, W., Jidigam, V.K., Mercurio, S., Bertolini, J.A., Sghari, S., Bose, R., Patthey, C., Nicolis, S.K., Gunhaga, L., 2018. Sox2 is required for olfactory pit formation and olfactory neurogenesis through BMP restriction and Hes5 upregulation. *Development* 145, dev153791.

Pandur, P.D., Moody, S.A., 2000. Xenopus Six1 gene is expressed in neurogenic cranial placodes and maintained in the differentiating lateral lines. *Mechanisms of development* 96, 253-257.

Pappu, K.S., Mardon, G., 2004. Genetic control of retinal specification and determination in *Drosophila*. *International Journal of Developmental Biology* 48, 913-924.

Park, B.Y., Saint-Jeannet, J.P., 2010. *Developmental Biology, Induction and Segregation of the Vertebrate Cranial Placodes*, Morgan & Claypool Life Sciences  
Perron, M., Furrer, M.P., Wegnez, M., Théodore, L., 1999. Xenopus elav-like genes are differentially expressed during neurogenesis. *Mechanisms of development* 84, 139-142.

Petronczki, M., Knoblich, J.A., 2001. DmPAR-6 directs epithelial polarity and asymmetric cell division of neuroblasts in *Drosophila*. *Nature cell biology* 3, 43.

Petrovic, J., Formosa-Jordan, P., Luna-Escalante, J.C., Abelló, G., Ibañes, M., Neves, J., Giraldez, F., 2014. Ligand-dependent Notch signaling strength orchestrates lateral induction and lateral inhibition in the developing inner ear. *Development* 141, 2313-2324.

Pevny, L., Placzek, M., 2005. SOX genes and neural progenitor identity. *Current opinion in neurobiology* 15, 7-13.

Pieper, M., Ahrens, K., Rink, E., Peter, A., Schlosser, G., 2012. Differential distribution of competence for panplacodal and neural crest induction to non-neural and neural ectoderm. *Development* 139, 1175-1187.

Pieper, M., Eagleson, G.W., Wosniok, W., Schlosser, G., 2011. Origin and segregation of cranial placodes in *Xenopus laevis*. *Developmental biology* 360, 257-275.

Pike, S., Matthes, M.S., McSteen, P., Gassmann, W., 2019. Using *Xenopus laevis* Oocytes to Functionally Characterize Plant Transporters. *Current protocols in plant biology* 4, e20087.

Piloto, S., & Schilling, T., F., 2010. *Ovo1* links Wnt signaling with Ncadherin localization during neural crest migration. *Development*, 137, 1981–1990.

Pohl, E., Aykut, A., Beleggia, F., Karaca, E., Durmaz, B., Keupp, K., Arslan, E., Onay, M.P., Yigit, G., Özkinay, F., 2013. A hypofunctional PAX1 mutation causes autosomal recessively inherited otofaciocervical syndrome. *Human genetics* 132, 1311-1320.

Powell, D. R., Williams, J. S., Hernandez-Lagunas, L., Salcedo, E., O'brien, J. H., & Artinger, K. B., 2015. *Cdon* promotes neural crest migration by regulating N-cadherin localization. *Developmental Biology*, 407, 289–299

Pozzoli, O., Bosetti, A., Croci, L., Consalez, G.G., Vetter, M.L.J.D.b., 2001. *Xebf3* is a regulator of neuronal differentiation during primary neurogenesis in *Xenopus*. 233, 495-512.

Pujades, C., Kamaid, A., Alsina, B., Giraldez, F., 2006. BMP-signaling regulates the generation of hair-cells. *Developmental biology* 292, 55-67.

Puligilla, C., Dabdoub, A., Brenowitz, S.D., Kelley, M.W., 2010. *Sox2* induces neuronal formation in the developing mammalian cochlea. *The Journal of neuroscience : the official journal of the Society for Neuroscience* 30, 714-722.

Puligilla, C., Kelley, M.W., 2017. Dual role for *Sox2* in specification of sensory competence and regulation of *Atoh1* function. *Developmental neurobiology* 77, 3-13.

Punzo, C., Kurata, S., Gehring, W.J., 2001. The eyeless homeodomain is dispensable for eye development in *Drosophila*. *Genes & development* 15, 1716-1723.

Purcell, P., Oliver, G., Mardon, G., Donner, A.L., Maas, R.L., 2005. Pax6-dependence of *Six3*, *Eya1* and *Dach1* expression during lens and nasal placode induction. *Gene expression patterns* 6, 110-118.

Pyron, R.A., Wiens, J.J., 2011. A large-scale phylogeny of Amphibia including over 2800 species, and a revised classification of extant frogs, salamanders, and caecilians. *Molecular phylogenetics and evolution* 61, 543-583.

Quick, Q.A., Serrano, E.E., 2005. Inner ear formation during the early larval development of *Xenopus laevis*. *Developmental dynamics : an official publication of the American Association of Anatomists* 234, 791-801.

Radde.Gallwitz, K., Pan, L., Gan, L., Lin, X., Segil, N., Chen, P.J.J.o.C.N., 2004. Expression of *Islet1* marks the sensory and neuronal lineages in the mammalian inner ear. *Development* 138, 412-421.

Radosevic, M., Robert-Moreno, À., Coolen, M., Bally-Cuif, L., Alsina, B., 2011. *Her9* represses neurogenic fate downstream of *Tbx1* and retinoic acid signaling in the inner ear. *Development* 138, 397-408.

Raft, S., Koundakjian, E.J., Quinones, H., Jayasena, C.S., Goodrich, L.V., Johnson, J.E., Segil, N., Groves, A.K., 2007. Cross-regulation of *Ngn1* and *Math1* coordinates the production of neurons and sensory hair cells during inner ear development. *Development* 134, 4405-4415.

Raft, S., Nowotschin, S., Liao, J., Morrow, B.E., 2004. Suppression of neural fate and control of inner ear morphogenesis by *Tbx1*. *Development* 131, 1801-1812.

Raible, D.W., Kruse, G.J., 2000. Organization of the lateral line system in embryonic zebrafish. *Journal of Comparative Neurology* 421, 189-198.

Ramahi, J.S., Solecki, D.J., 2014. The PAR polarity complex and cerebellar granule neuron migration. *Advances in experimental medicine and biology* 800, 113-131.

Rebay, I., 2016. Multiple Functions of the *Eya* Phosphotyrosine Phosphatase. *Molecular and cellular biology* 36, 668-677.

Rex M., Uwanogho D., Cartwright E., Pearl G., Sharpe P.T., Scotting P.J., 1994.

Riddiford, N., Schlosser, G., 2016. Dissecting the pre-placodal transcriptome to reveal presumptive direct targets of *Six1* and *Eya1* in cranial placodes. *Elife* 5, e17666.

Riddiford, N., Schlosser, G., 2017. Six1 and Eya1 both promote and arrest neuronal differentiation by activating multiple Notch pathway genes. *Developmental biology* 431, 152-167.

Rogers, C.D., Archer, T.C., Cunningham, D.D., Grammer, T.C., Casey, E.M.S., 2008. Sox3 expression is maintained by FGF signaling and restricted to the neural plate by Vent proteins in the *Xenopus* embryo. *Developmental biology* 313, 307-319.

Rogers, C.D., Saxena, A., Bronner, M.E., 2013. Sip1 mediates an E-cadherin-to-N-cadherin switch during cranial neural crest EMT. *The Journal of cell biology* 203, 835-847.

Rolls, M.M., Albertson, R., Shih, H.-P., Lee, C.-Y., Doe, C.Q., 2003. *Drosophila* aPKC regulates cell polarity and cell proliferation in neuroblasts and epithelia. *The Journal of cell biology* 163, 1089-1098.

Ross, S.E., Greenberg, M.E., Stiles, C.D., 2003. Basic helix-loop-helix factors in cortical development. *Neuron* 39, 13-25.

Rouso, D.L., Pearson, C.A., Gaber, Z.B., Miquelajauregui, A., Li, S., Portera-Cailliau, C., Morrisey, E.E., Novitch, B.G.J.N., 2012. Foxp-mediated suppression of N-cadherin regulates neuroepithelial character and progenitor maintenance in the CNS. *74*, 314-330.

Roychoudhury, K., Hegde, R.S., 2021. The Eyes Absent Proteins: Unusual HAD Family Tyrosine Phosphatases. *International journal of molecular sciences* 22.

Sabherwal, N., Tsutsui, A., Hodge, S., Wei, J., Chalmers, A.D., Papalopulu, N., 2009. The apicobasal polarity kinase aPKC functions as a nuclear determinant and regulates cell proliferation and fate during *Xenopus* primary neurogenesis. *Development* 136, 2767-2777.

Sadaghiani, B., Thiébaud, C.H., 1987. Neural crest development in the *Xenopus laevis* embryo, studied by interspecific transplantation and scanning electron microscopy. *Developmental biology* 124, 91-110.

Sahly, I., Andermann, P., Petit, C., 1999. The zebrafish *eya1* gene and its expression pattern during embryogenesis. *Development genes and evolution* 209, 399-410.



Sai, X., Ladher, R.K., 2008. FGF signaling regulates cytoskeletal remodeling during epithelial morphogenesis. *Current Biology* 18, 976-981.

Sai, X., Ladher, R.K., 2015. Early steps in inner ear development: induction and morphogenesis of the otic placode. *Frontiers in pharmacology* 6, 19.

Saint-Jeannet, J.-P., Moody, S.A., 2014. Establishing the pre-placodal region and breaking it into placodes with distinct identities. *Developmental biology* 389, 13-27.

Sánchez-Guardado, L.Ó., Puellas, L., Hidalgo-Sánchez, M., 2014. Fate map of the chicken otic placode. *Development* 141, 2302-2312.

Sapède, D., Dyballa, S., Pujades, C., 2012. Cell lineage analysis reveals three different progenitor pools for neurosensory elements in the otic vesicle. *The Journal of neuroscience : the official journal of the Society for Neuroscience* 32, 16424-16434.

Sarkar, A., Hochedlinger, K., 2013. The sox family of transcription factors: versatile regulators of stem and progenitor cell fate. *Cell stem cell* 12, 15-30.

Sato, S., Ikeda, K., Shioi, G., Ochi, H., Ogino, H., Yajima, H., Kawakami, K.J.D.b., 2010. Conserved expression of mouse *Six1* in the pre-placodal region (PPR) and identification of an enhancer for the rostral PPR. *Development* 138, 158-171.

Satoh, T., Fekete, D.M., 2005. Clonal analysis of the relationships between mechanosensory cells and the neurons that innervate them in the chicken ear. *Development* 132, 1687-1697.

Sauer, F. C., 1935. Mitosis in the neural tube. *J. Comp. Neurol.* 62, 377-405.

Schlosser, G., 2002a. Development and evolution of lateral line placodes in amphibians I. *Development. Zoology* 105, 119-146.

Schlosser, G., 2002b. Development and evolution of lateral line placodes in amphibians.-II. Evolutionary diversification. *Zoology* 105, 177-193.

Schlosser, G., 2003. Hypobranchial placodes in *Xenopus laevis* give rise to hypobranchial ganglia, a novel type of cranial ganglia. *Cell and tissue research* 312, 21-29.

Schlosser, G., 2006. Induction and specification of cranial placodes. *Developmental biology* 294, 303-351.

Schlosser, G., 2010. Making senses: development of vertebrate cranial placodes, *International review of cell and molecular biology*, Elsevier, pp. 129-234.

Schlosser, G., 2014. Early embryonic specification of vertebrate cranial placodes. *Wiley Interdisciplinary Reviews: Developmental Biology* 3, 349-363.

Schlosser, G., Ahrens, K., 2004. Molecular anatomy of placode development in *Xenopus laevis*. *Developmental biology* 271, 439-466.

Schlosser, G., Awtry, T., Brugmann, S.A., Jensen, E.D., Neilson, K., Ruan, G., Stammler, A., Voelker, D., Yan, B., Zhang, C., 2008. *Eya1* and *Six1* promote neurogenesis in the cranial placodes in a *SoxB1*-dependent fashion. *Developmental biology* 320, 199-214.

Schlosser, G., Kintner, C., Northcutt, R.G., 1999. Loss of ectodermal competence for lateral line placode formation in the direct developing frog *Eleutherodactylus coqui*. *Developmental biology* 213, 354-369.

Schlosser, G., Northcutt, R.G., 2000. Development of neurogenic placodes in *Xenopus laevis*. *Journal of Comparative Neurology* 418, 121-146.

Schwarzer, S., Spieß, S., Brand, M., Hans, S., 2017. *Dlx3b/4b* is required for early-born but not later-forming sensory hair cells during zebrafish inner ear development. *Biology open* 6, 1270-1278.

Shi, S.-H., Jan, L.Y., Jan, Y.-N., 2003. Hippocampal neuronal polarity specified by spatially localized *mPar3/mPar6* and *PI 3-kinase* activity. *Cell* 112, 63-75.

Shoval, I., Ludwig, A., & Kalcheim, C., 2007. Antagonistic roles of fulllength *N-cadherin* and its soluble *BMP* cleavage product in neural crest delamination. *Development*, 134, 491–501.

Silver, S.J., Davies, E.L., Doyon, L., Rebay, I., 2003. Functional dissection of eyes absent reveals new modes of regulation within the retinal determination gene network. *Molecular and cellular biology* 23, 5989-5999.

Silver, S.J., Rebay, I., 2005. Signaling circuitries in development: insights from the retinal determination gene network. *Development* 132, 3-13.

Sive, H., Bradley, L., 1996. A sticky problem: the *Xenopus* cement gland as a paradigm for anteroposterior patterning. *Developmental dynamics: an official publication of the American Association of Anatomists* 205, 265-280.

Slavkin, H.C., Brownell, A.G., Bringas, P., MacDougall, M., Bessem, C., 1983. Basal lamina persistence during epithelial-mesenchymal interactions in murine tooth development in vitro. *J Craniofac Genet Dev Biol* 3, 387-407.

Smart, I.H., 1972. Proliferative characteristics of the ependymal layer during the early development of the mouse diencephalon, as revealed by recording the number, location, and plane of cleavage of mitotic figures. *Journal of anatomy* 113, 109-129.

Solecki, D.J., 2012. Sticky situations: recent advances in control of cell adhesion during neuronal migration. *Current opinion in neurobiology* 22, 791-798.

Solecki, D.J., Govek, E.-E., Hatten, M.E.J.J.o.N., 2006. mPar6 $\alpha$  controls neuronal migration. 26, 10624-10625.

Solecki, D.J., Model, L., Gaetz, J., Kapoor, T.M., Hatten, M.E., 2004. Par6 $\alpha$  signaling controls glial-guided neuronal migration. *Nature neuroscience* 7, 1195.

Solecki, D.J., Trivedi, N., Govek, E.-E., Kerekes, R.A., Gleason, S.S., Hatten, M.E., 2009. Myosin II motors and F-actin dynamics drive the coordinated movement of the centrosome and soma during CNS glial-guided neuronal migration. *Neuron* 63, 63-80.

Solomon, K.S., Kudoh, T., Dawid, I.B., Fritz, A., 2003. Zebrafish foxi1 mediates otic placode formation and jaw development. *Development* 130, 929-940.

Sox gene expression during neuronal development. *Biochem. Soc. Trans.*, 22 , p. 252S

Spear, P.C., Erickson, C.A., 2012. Interkinetic nuclear migration: a mysterious process in search of a function. *Development, growth & differentiation* 54, 306-316.

St Johnston, D., Ahringer, J., 2010. Cell polarity in eggs and epithelia: parallels and diversity. *Cell* 141, 757-774.

Steevens, A.R., Sookiasian, D.L., Glatzer, J.C., Kiernan, A.E., 2017. SOX2 is required for inner ear neurogenesis. *Scientific reports* 7, 4086.

Streit, A., 2002. Extensive cell movements accompany formation of the otic placode. *Developmental biology* 249, 237-254.

Strzyz, P.J., Lee, H.O., Sidhaye, J., Weber, I.P., Leung, L.C., Norden, C., 2015. Interkinetic nuclear migration is centrosome independent and ensures apical cell division to maintain tissue integrity. *Developmental cell* 32, 203-219.

Sullivan, C.H., Majumdar, H.D., Neilson, K.M., Moody, S.A., 2019. Six1 and Irx1 have reciprocal interactions during cranial placode and otic vesicle formation. *Developmental biology* 446, 68-79.

Sun, S.-K., Dee, C.T., Tripathi, V.B., Rengifo, A., Hirst, C.S., Scotting, P.J., 2007. Epibranchial and otic placodes are induced by a common Fgf signal, but their subsequent development is independent. *Developmental biology* 303, 675-686.

Suzuki, A., Hirata, M., Kamimura, K., Maniwa, R., Yamanaka, T., Mizuno, K., Kishikawa, M., Hirose, H., Amano, Y., Izumi, N.J.C.B., 2004. aPKC acts upstream of PAR-1b in both the establishment and maintenance of mammalian epithelial polarity. *Developmental cell* 14, 1425-1435.

Suzuki, A., Ohno, S., 2006. The PAR-aPKC system: lessons in polarity. *Journal of cell science* 119, 979-987.

Suzuki, Y., Mizoguchi, I., Nishiyama, H., Takeda, M., Obara, N., 2003. Expression of Hes6 and NeuroD in the olfactory epithelium, vomeronasal organ and non-sensory patches. *Chemical senses* 28, 197-205.

Tabuse, Y., Izumi, Y., Piano, F., Kempfues, K.J., Miwa, J., Ohno, S.J.D., 1998. Atypical protein kinase C cooperates with PAR-3 to establish embryonic polarity in *Caenorhabditis elegans*. *Developmental cell* 125, 3607-3614.

Takeichi, M., Hatta, K., Nose, A., Nagafuchi, A., 1988. Identification of a gene family of cadherin cell adhesion molecules. *Cell Differentiation and Development* 25, 91-94.

Talikka, M., Perez, S.E., Zimmerman, K., 2002. Distinct patterns of downstream target activation are specified by the helix-loop-helix domain of proneural basic helix-loop-helix transcription factors. *Developmental biology* 247, 137-148.

Taneyhill, L.A., Schiffmacher, A.T., 2017. Should I stay or should I go? Cadherin function and regulation in the neural crest. *Genesis (New York, N.Y. : 2000)* 55.

Tepass, U.J.A.r.o.c., biology, d., 2012. The apical polarity protein network in *Drosophila* epithelial cells: regulation of polarity, junctions, morphogenesis, cell growth, and survival. 28, 655-685.

Theveneau, E., Marchant, L., Kuriyama, S., Gull, M., Moepps, B., Parsons, M., & Mayor, R., 2010. Collective chemotaxis requires contactdependent cell polarity. *Developmental Cell*, 19, 39–53.

Theveneau, E., Steventon, B., Scarpa, E., Garcia, S., Trepate, X., Streit, A., & Mayor, R., 2013. Chase-and-run between adjacent cell populations promotes directional collective migration. *Nature Cell Biology*, 15, 763–772

Toth, Z.E., Mezey, E.J.J.o.H., *Cytochemistry*, 2007. Simultaneous visualization of multiple antigens with tyramide signal amplification using antibodies from the same species. 55, 545-554.

Tsai, J.W., Lian, W.N., Kemal, S., Kriegstein, A.R., Vallee, R.B., 2010. Kinesin 3 and cytoplasmic dynein mediate interkinetic nuclear migration in neural stem cells. *Nature neuroscience* 13, 1463-1471.

Tsue, T.T., Watling, D.L., Weisleder, P., Coltrera, M.D., Rubel, E.W., 1994. Identification of hair cell progenitors and intermitotic migration of their nuclei in the normal and regenerating avian inner ear. *Journal of Neuroscience* 14, 140-152.

Van Wijhe, J., 1883. Ueber die Mesodermsegmente und die Entwicklung der Nerven des Selachierkopfes, *Versl. dk Akad. v. Wetensch* 18, 71.

Vemaraju, S., Kantarci, H., Padanad, M.S., Riley, B.B.J.P.G., 2012. A spatial and temporal gradient of Fgf differentially regulates distinct stages of neural development in the zebrafish inner ear. 8, e1003068.

Vicente-Manzanares, M., Horwitz, A.R., 2010. Myosin light chain mono- and di-phosphorylation differentially regulate adhesion and polarity in migrating cells. *Biochemical and biophysical research communications* 402, 537-542.

von Kupffer C., 1895. Studien zur vergleichenden Entwicklungsgeschichte des Kopfes der Kranioten. III. Die Entwicklung der Kopfnerven von

Vorhagen, S., Niessen, C.M.J.E.c.r., 2014. Mammalian aPKC/Par polarity complex mediated regulation of epithelial division orientation and cell fate. 328, 296-302.

Vorhagen, S., Niessen, C.M.J.E.c.r., 2014. Mammalian aPKC/Par polarity complex mediated regulation of epithelial division orientation and cell fate. 328, 296-302.

Walters, B.J., Coak, E., Dearman, J., Bailey, G., Yamashita, T., Kuo, B., Zuo, J., 2017. In vivo interplay between p27Kip1, GATA3, ATOH1, and POU4F3 converts non-sensory cells to hair cells in adult mice. Cell reports 19, 307-320.

Wang, C., Gargollo, P., Guo, C., Tang, T., Mingin, G., Sun, Y., Li, X.J.D.b., 2011. Six1 and Eya1 are critical regulators of peri-cloacal mesenchymal progenitors during genitourinary tract development. 360, 186-194.

Wegner, M., 1999. From head to toes: the multiple facets of Sox proteins. Nucleic acids research 27, 1409-1420.

Wegner, M., 2010. All purpose Sox: The many roles of Sox proteins in gene expression. The international journal of biochemistry & cell biology 42, 381-390.

Wegner, M., Stolt, C.C., 2005. From stem cells to neurons and glia: a Soxist's view of neural development. Trends in neurosciences 28, 583-588.

White, J.G., Southgate, E., Thomson, J.N., Brenner, S., 1986. The structure of the nervous system of the nematode *Caenorhabditis elegans*. Philos Trans R Soc Lond B Biol Sci 314, 1-340.

Whitehead, M., Morest, D., 1985a. The development of innervation patterns in the avian cochlea. Neuroscience 14, 255-276.

Whitehead, M., Morest, D., 1985b. The growth of cochlear fibers and the formation of their synaptic endings in the avian inner ear: a study with the electron microscope. Neuroscience 14, 277-300.

Whitfield, T.T., 2002. Zebrafish as a model for hearing and deafness. Journal of neurobiology 53, 157-171.

Whitlock, K., Illing, N., Brideau, N., Smith, K., Twomey, S., 2006. Development of GnRH cells: setting the stage for puberty. *Molecular and cellular endocrinology* 254, 39-50.

Willardsen, M.I., Link, B.A.J.D.D., 2011. Cell biological regulation of division fate in vertebrate neuroepithelial cells. 240, 1865-1879.

Winklbauer, R., 1989. Development of the lateral line system in *Xenopus*. *Progress in neurobiology* 32, 181-206.

Winklbauer, R., Hausen, P., 1983. Development of the lateral line system in *Xenopus laevis*: II. Cell multiplication and organ formation in the supraorbital system. *Development* 76, 283-296.

Wodarz, A., Grawe, F., Knust, E.J.M.o.d., 1993. CRUMBS is involved in the control of apical protein targeting during *Drosophila* epithelial development. 44, 175-187.

Wodarz, A., Ramrath, A., Kuchinke, U., Knust, E.J.N., 1999. Bazooka provides an apical cue for Inscuteable localization in *Drosophila* neuroblasts. 402, 544-547.

Wong, E.Y., Ahmed, M., Xu, P.-X., 2013. EYA1–SIX1 complex in neurosensory cell fate induction in the mammalian inner ear. *Hearing research* 297, 13-19.

Wright, T.J., Mansour, S.L., 2003. Fgf3 and Fgf10 are required for mouse otic placode induction. *Development* 130, 3379-3390.

Wu, D.K., Oh, S.-H.J.J.o.N., 1996. Sensory organ generation in the chick inner ear. 16, 6454-6462.

Wu, W., Ren, Z., Li, P., Yu, D., Chen, J., Huang, R., Liu, H., 2015. Six1: A critical transcription factor in tumorigenesis. *International journal of cancer* 136, 1245-1253.

Xu, H., Dude, C.M., Baker, C.V., 2008. Fine-grained fate maps for the ophthalmic and maxillomandibular trigeminal placodes in the chick embryo. *Developmental biology* 317, 174-186.

Xu, J., Li, J., Zhang, T., Jiang, H., Ramakrishnan, A., Fritsch, B., Shen, L., Xu, P.-X.J.P.o.t.N.A.o.S., 2021. Chromatin remodelers and lineage-specific factors interact to target enhancers to establish proneurosensory fate within otic ectoderm. 118.

Xu, P.-X., 2013. The EYA-SO/SIX complex in development and disease. *Pediatric nephrology* 28, 843-854.

Xu, P.-X., Adams, J., Peters, H., Brown, M.C., Heaney, S., Maas, R., 1999. *Eya1*-deficient mice lack ears and kidneys and show abnormal apoptosis of organ primordia. *Nature genetics* 23, 113.

Xu, P.-X., Woo, I., Her, H., Beier, D.R., Maas, R.L., 1997a. Mouse *Eya* homologues of the *Drosophila* eyes absent gene require *Pax6* for expression in lens and nasal placode. *Development* 124, 219-231.

Xu, P.-X., Zheng, W., Laclef, C., Maire, P., Maas, R.L., Peters, H., Xu, X., 2002. *Eya1* is required for the morphogenesis of mammalian thymus, parathyroid and thyroid. *Development* 129, 3033-3044.

Xu, R.-H., Kim, J., Taira, M., Lin, J.-J., Zhang, C., Sredni, D., Evans, T., Kung, H., 1997b. Differential regulation of neurogenesis by the two *Xenopus* GATA-1 genes. *Molecular and Cellular Biology* 17, 436-443.

Yu, J., Lei, K., Zhou, M., Craft, C.M., Xu, G., Xu, T., Zhuang, Y., Xu, R., Han, M., 2011. KASH protein *Syne-2/Nesprin-2* and SUN proteins *SUN1/2* mediate nuclear migration during mammalian retinal development. *Human molecular genetics* 20, 1061-1073.

Zaouter, C., 2017. SOX transcription factors: multifaceted regulators of central nervous system development.

Zeng, C., Pan, F., Jones, L.A., Lim, M.M., Griffin, E.A., Sheline, Y.I., Mintun, M.A., Holtzman, D.M., Mach, R.H.J.B.r., 2010. Evaluation of 5-ethynyl-2'-deoxyuridine staining as a sensitive and reliable method for studying cell proliferation in the adult nervous system. 1319, 21-32.

Zhang, C., Basta, T., Jensen, E.D., Klymkowsky, M., 2003. The  $\beta$ -catenin/VegT-regulated early zygotic gene *Xnr5* is a direct target of SOX3 regulation. *Development* 130, 5609-5624.



Zhang, H., Macara, I.G., 2008. The PAR-6 polarity protein regulates dendritic spine morphogenesis through p190 RhoGAP and the Rho GTPase. *Developmental cell* 14, 216-226.

Zhang, Y., Knosp, B.M., Maconochie, M., Friedman, R.A., Smith, R.J., 2004. A comparative study of Eya1 and Eya4 protein function and its implication in branchio-oto-renal syndrome and DFNA10. *Journal of the Association for Research in Otolaryngology : JARO* 5, 295-304.

Zheng, W., Huang, L., Wei, Z.-B., Silvius, D., Tang, B., Xu, P.-X., 2003. The role of Six1 in mammalian auditory system development. *Development* 130, 3989-4000.

Zhong, W., Chia, W., 2008. Neurogenesis and asymmetric cell division. *Current opinion in neurobiology* 18, 4-11.

Zhou, C., Yang, X., Sun, Y., Yu, H., Zhang, Y., Jin, Y., 2016. Comprehensive profiling reveals mechanisms of SOX2-mediated cell fate specification in human ESCs and NPCs. *Cell research* 26, 171.

Zimmerman, J.E., Bui, Q.T., Steingrímsson, E., Nagle, D.L., Fu, W., Genin, A., Spinner, N.B., Copeland, N.G., Jenkins, N.A., Bucan, M., 1997. Cloning and characterization of two vertebrate homologs of the *Drosophila* eyes absent gene. *Genome research* 7, 128-141.

Zou, D., Erickson, C., Kim, E.-H., Jin, D., Fritsch, B., Xu, P.-X., 2008. Eya1 gene dosage critically affects the development of sensory epithelia in the mammalian inner ear. *Human molecular genetics* 17, 3340-3356.

Zou, D., Silvius, D., Fritsch, B., Xu, P.-X., 2004. Eya1 and Six1 are essential for early steps of sensory neurogenesis in mammalian cranial placodes. *Development* 131, 5561-5572.

Zou, D., Silvius, D., Rodrigo-Blomqvist, S., Enerbäck, S., Xu, P.-X., 2006. Eya1 regulates the growth of otic epithelium and interacts with Pax2 during the development of all sensory areas in the inner ear. *Developmental biology* 298, 430-441.

## **Appendix A: Solutions and buffers**

### **A.1 Stock Solutions for Microinjection & in vitro Fertilisation (IVF)**

#### **10 x MBS salts**

- 51.3 g NaCl
- 0.75 g KCl
- 2 g MgSO<sub>4</sub> x 7 H<sub>2</sub>O
- 23.8 g HEPES
- 2.0 g NaHCO<sub>3</sub>
- pH adjusted to 7.6 with NaOH pellets
- Adjusted to 1 litre with dH<sub>2</sub>O and autoclaved

#### **1 x MBSH**

- 100 ml 10 x MBS salts
- 7 ml 0.1 M CaCl<sub>2</sub>
- 4 ml 5 M NaCl
- Adjusted to 1 litre with dH<sub>2</sub>O

#### **1 x MBS**

- 100 ml 10 x MBS salts
- 7 ml 0.1 M CaCl<sub>2</sub>
- Adjusted to 1 litre with dH<sub>2</sub>O

#### **Cysteine**

- 4 g Cysteine
- Adjusted to 100 ml with dH<sub>2</sub>O
- Adjusted pH to 8.0 with NaOH pellets

#### **Phosphate Buffer (PB)**

- 28.48 g Na<sub>2</sub>HPO<sub>4</sub> x 2 H<sub>2</sub>O or 42.90 g Na<sub>2</sub>HPO<sub>4</sub> x 7 H<sub>2</sub>O
- 5.44 g KH<sub>2</sub>PO<sub>4</sub>
- Adjusted to 1 litre of dH<sub>2</sub>O
- pH: 7.38

#### **Phosphate Buffer Saline (PBS)**

- 26.8 g  $\text{Na}_2\text{HPO}_4 \times 7 \text{ H}_2\text{O}$
- 16 g NaCl
- Adjusted to 1 litre of  $\text{dH}_2\text{O}$
- Adjusted pH to 7.2 (With 10% HCl)

## **A.2 Solutions and Buffers for In situ Hybridization**

**Anti-digoxigenin Antibody, AP-coupled (Roche, Cat. No.-11093274910);** stored at  $4^\circ\text{C}$

**BCIP, 50 mg/ml (Roche, Cat. No.- 11383221001);** stored at  $-20^\circ\text{C}$

### **Boehringer Blocking Reagent (10% BBR)**

- 10 g Boehringer Blocking Reagent (Roche, Cat. No.- 11096176)
- 1x MAB, adjusted to 100 ml
- Stirred and heated to dissolve
- Autoclaved and stored at  $-20^\circ\text{C}$

### **DEPC- H<sub>2</sub>O**

- Prepared under fume hood!
- 1 ml DEPC (Diethylpyrocarbonate) added to 1 liter  $\text{dH}_2\text{O}$
- Mixed well, let evaporate under fume hood overnight or at least 1 hr
- Autoclaved and stored at RT

### **EDTA, 0.5 M**

- 73.05 g EDTA (Ethylenediaminetetraacetate) or 93.05 g Disodium EDTA\* $2\text{H}_2\text{O}$
- Dissolved in 400 ml  $\text{dH}_2\text{O}$ , adjust pH to approx.  $\text{pH}=8.0$  with NaOH pellets  
(will only dissolve EDTA at  $\text{pH}>7$ )
- Adjusted to 500 ml  $\text{dH}_2\text{O}$
- 0.5 ml DEPC added
- Mixed well and lid opened, let evaporate under fume hood overnight or at least 1 hr

- Autoclaved and stored at RT

### **EGTA, 0.2 M**

- 7.61 g EGTA
- Dissolved in 70 ml dH<sub>2</sub>O, pH adjusted to approx. pH=8.0 with NaOH pellets  
(will only dissolve EGTA at pH>7)
- Adjusted to 100 ml of dH<sub>2</sub>O
- 0.1 ml of DEPC added
- Mixed well and lid opened, let evaporate under fume hood overnight or at least 1 hr
- Autoclaved and stored at RT

### **Heat Inactivated Goat Serum (HIGS)**

- Normal Goat serum bottle of 5 ml
- Heated 30 min at 60° C and store at 4° C

### **Hybridization Buffer**

- 25 ml Formamide (Roche, Cat. No.- 11814320001)
- 12.5 ml 20x SSC
- 50 mg Torula yeast RNA (Roche, Cat. No.- 10109223001)
- 5 mg Heparin
- 1 ml 50x Denhart's solution (prepared with DEPC- H<sub>2</sub>O)
- 50 µl Tween 20
- 50 mg CHAPS
- 1 ml 0.5 M EDTA
- Filled up to 50 ml with DEPC-H<sub>2</sub>O
- Vortexed well until precipitate goes into solution and stored at -20° C

### **MAB 10x Buffer**

- 58 g of Maleic acid
- 43.8 g NaCl

- 400 ml dH<sub>2</sub>O added and pH adjusted to 7.5 with NaOH pellets (Approx. 39.5 g)
- Adjusted to 500 ml of dH<sub>2</sub>O
- Autoclaved and stored at 4°C

#### **MgCl<sub>2</sub> 1M Buffer**

- 20.33 g of MgCl<sub>2</sub>\*6 H<sub>2</sub>O
- Adjusted to 100 ml of dH<sub>2</sub>O
- Autoclaved and stored at RT

#### **MgSO<sub>4</sub> 1M Buffer**

- 12.04 g of MgSO<sub>4</sub>
- Adjusted to 100 ml of dH<sub>2</sub>O
- Add 0.1 ml DEPC
- Mixed well and lid opened, let evaporate under fume hood overnight or at least 1 hr
- Autoclaved and stored at RT

#### **MOPS 1M Buffer**

- 104.65 g MOPS
- 10.25 g NaOAc (Sodium Acetate)
- 50 ml EDTA, 0.5 M
- Dissolved in 300 ml dH<sub>2</sub>O, pH adjusted to pH=7.0 with NaOH pellets
- Adjusted to 500 ml of DEPC-H<sub>2</sub>O
- Not autoclaved and stored at 4°C.

#### **Sodium Acetate (NaOAc) 3M Solution**

- 123.04 g NaOAc
- Dissolve in 400 ml dH<sub>2</sub>O, adjust pH to pH=5.0 with Glacial Acetic Acid
- Add 500 ml of dH<sub>2</sub>O
- Add 0.5 ml DEPC
- Mixed well and lid opened, let evaporate under fume hood overnight or at least 1hr

- Autoclaved and stored at RT

**NBT 100 mg/ml (Roche, Cat. No.- 11383213001)**

- Stored at -20°C

**Ammonium Acetate (NH<sub>4</sub>OAc) 10M Buffer**

- 77 g NH<sub>4</sub>OAc

- Dissolved in 25 ml DEPC-H<sub>2</sub>O (Mix and Gently warm to <37°C)

- DEPC- H<sub>2</sub>O adjusted to 100 ml

- Not autoclaved and stored at RT

**Proteinase K, 25 mg/ml**

- 25 mg Proteinase K (Roche, Cat. No.- 03115836001)

- 1 ml DEPC-H<sub>2</sub>O and stored at -20° C

**RNA digoxigenin labeling kit:**

- SP6/T7 (Roche, Cat. No.- 11175025910); stored at -20° C

- T3 (Roche, Cat. No.- 11031163001); stored at -20° C

**RNase A 2mg/ml Solution**

- Filter tips used to prepare (to avoid RNase contamination of pipette)

- 25 mg RNaseA (Roche, Cat. No.- 10109142001)

- Added 12.5 ml dH<sub>2</sub>O and stored at -20° C

**RNase T1 Solution**

- This RNase comes in solution (Roche, Cat. No.- 10109193001); stored at 4° C

**SSC 20x Salt**

- 87.65 g NaCl

- 44.1 g Nacitrate\*2 H<sub>2</sub>O (Trisodium Citrate)
- Dissolve in 400 ml dH<sub>2</sub>O , pH adjusted to pH=7.0
- Adjusted to 500 ml of dH<sub>2</sub>O
- 0.5 ml DEPC added
- Mixed well and lid opened, let evaporate under fume hood overnight or at least 1hr
- Autoclaved and stored at RT

#### **TEA 1M Solution**

- 66.7 ml 100% TEA (Tri-Ethanol-Amine) Solution (7.5 M)
- 33.3 ml DEPC-H<sub>2</sub>O added and stored it at 4° C

#### **Tris. 1M Buffers**

- 60.55 g Tris Base
- Dissolved in 400 ml dH<sub>2</sub>O, adjust pH to pH=9.5
- Adjusted to 500 ml of dH<sub>2</sub>O
- Autoclaved and stored at RT

#### **1x PBS Solution**

- 100 ml of 10x PBS
- 900 ml of DEPC-H<sub>2</sub>O and stored at RT

#### **Ptw Buffer (1 Liter)**

- 1 liter of 1x PBS
- 1ml of Tween-20
- Mixed well and stored at RT

#### **Proteinase K (50ml)**

- 50 ml of Ptw
- 20 µl PK (25 mg/ml)
- Mixed well and stored at 4° C

**0.1 M TEA (200 ml)**

- 20 ml of 1 M TEA
- 180 ml of DEPC-H<sub>2</sub>O
- Mixed well inside the fume hood and stored at 4° C

**0.1 M TEA + Acetic Anhydride (200ml)**

- 20 ml of 1 M TEA
- 180 ml of DEPC-H<sub>2</sub>O
- Mixed well inside the fume hood and stored at 4° C

**RNase Solutions (10 ml)**

- 10 ml of 2x SSC
- 0.1ml of 2 mg/ml fresh RNase A
- 1 µl RNase T1
- Every time freshly prepared

**1x MAB Solutions (500 ml)**

- 50 ml of 10x MAB
- 450 ml of DEPC-H<sub>2</sub>O
- Mixed well and prepared freshly prior to the experiment

**MAB + BBR Solutions (10 ml)**

- 2 ml of 10% BBR
- 8 ml of 1x MAB
- Mixed well and prepared freshly prior to the experiment

**MAB + BBR + HIGS Solutions (15 ml)**

- 3 ml of 10% BBR
- 9 ml of 1x MAB



- 3 ml of HIGS
- Mixed well and prepared freshly prior to the experiment

**MAB + BBR + HIGS + Antibodies Solutions (5 ml)**

- 1 ml of 10% BBR
- 3 ml of 1x MAB
- 1 ml of HIGS
- 5 ml of Antibodies
- Mixed well and prepared freshly prior to the experiment

**Alkaline Phosphate (AP) Buffer (50 ml)**

- 5 ml 1M Tris, pH 9.5
- 2.5 ml 1M MgCl<sub>2</sub>
- 1 ml 5M NaCl
- 50 µl Tween-20
- 41.5 ml dH<sub>2</sub>O
- Mixed well and prepared freshly prior to the experiment
- 50 ml AP buffer + 500 µl levamisole (24 mg/ml)

**Dig Antibody Staining Solutions (10 ml)**

- 10 ml of AP buffer
- 4.5 µl NBT (100 mg/ml)
- 35 µl BCIP (50 mg/ml)
- Mixed well and prepared freshly prior to the experiment

**Refixing Solutions (10 ml) – Bouin Solution without Picric Acid**

- 2.5 ml Formaldehyde
- 7.0 ml dH<sub>2</sub>O
- 0.5 ml Glacial acetic acid
- Mixed well and prepared freshly prior to the experiment

### **Bleaching Solution (10 ml)**

- 8.65 ml dH<sub>2</sub>O
- 0.5 ml 20x SSC
- 0.35 ml H<sub>2</sub>O<sub>2</sub> (30%)
- 0.5 ml Formamide
- Mixed well and prepared freshly prior to the experiment

### **A.3 Vibratome buffer**

#### **Phosphate buffer (PB), 0.1M**

- 2.63g NaH<sub>2</sub>PO<sub>4</sub> dH<sub>2</sub>O
- 21.65g Na<sub>2</sub>HPO<sub>4</sub> d7H<sub>2</sub>O
- Dissolved in 800 ml dH<sub>2</sub>O, adjusted pH to pH=7.4
- dH<sub>2</sub>O adjusted to 1 l

### **A.4 Gel electrophoresis**

#### **50x TAE:**

- 242 g Tris
- dissolved in 800 ml H<sub>2</sub>O dest.
- 57.1 ml glacial acetic acid
- 18.6 g EDTA
- pH adjusted to 7.6-7.8 with glacial acetic acid
- dH<sub>2</sub>O adjusted to 1 l
- not autoclaved and stored at RT

### **A.5 Mini Prep TELT Buffer**

- TELT Buffer Solution Mix
- 2.5 ml 1M Tris, pH 7.5
- 6.25 ml 0.5 M EDTA, pH 8.0
- 39.05 ml 3.2 M LiCl

- 200 µl 100% Triton X-100
- 2 ml dH<sub>2</sub>O
- Autoclaved and stored at RT

#### **A. 6 Western Blot Buffer**

**Sol A:** 30% Acrylamide, 0.8% Bisacrylamide (Roth: Roiphorese Gel 30, 3029.1) and stored at 4°C

**Sol B:** 1.5 M Tris-HCl, pH 8.8, 3mM EDTA:

- 72,68 g Tris dissolved in 300 ml dH<sub>2</sub>O
- 2.4 ml 0.5M EDTA
- pH adjusted to pH=8.8
- dH<sub>2</sub>O adjusted to 400 ml
- filtrated and autoclaved and stored at 4°C

**Sol D:** 0.5M Tris-Hcl, pH 6.8, 4mM EDTA:

- 12.14g Tris dissolved in 150 ml dH<sub>2</sub>O
- 1.6 ml 0.5M EDTA
- pH adjusted to pH=6.8
- dH<sub>2</sub>O to 200 ml
- filtrated and autoclaved and stored at 4°C

**2x Sol E:** 6% SDS

- 0.25 ml Sol D
- 0.375 ml SDS (filtered)
- 0.125 ml 2M DTT
- 0.5 ml 87% glycerol (autoclaved)
- small quantity (0.2 mg or 25 µl of 1% bromophenol blue) of bromophenol blue and stored at -20°C

**Electrode buffer**

- 30 g Tris
- 144 g Glycine
- 50 ml 20% SDS
- dH<sub>2</sub>O dest. adjusted to 1 l
- stored at 4°C

**10x PBS**

- 400 g NaCl
- 10 g KCl
- 10 g KH<sub>2</sub>PO<sub>4</sub>
- 57.5 g Na<sub>2</sub>HPO<sub>4</sub> x 2H<sub>2</sub>O (or 86.8 g Na<sub>2</sub>HPO<sub>4</sub> x 7H<sub>2</sub>O)
- dissolved in 4 l H<sub>2</sub>O
- pH adjusted to pH=7.4
- dH<sub>2</sub>O adjusted to 5 l
- autoclaved and stored at room temperature

**PBST (PBS, 0.05 % Tween)**

- 5ml 20% Tween
- 200ml 10x PBS
- 1.8 l dH<sub>2</sub>O

**20 x Borate transfer buffer (BTB)**

- 49.46 g boric acid
- 14.8 g EDTA
- dissolved in 1.7 l dH<sub>2</sub>O
- pH adjusted to pH=8.8 with NaOH pellets
- dH<sub>2</sub>O adjusted to 2 l

**Coomassie solution**

- 0.2 % Coomassie Brilliant Blue R250
- 40% methanol
- 5% glacial acetic acid

**Differentiating solution**

- 40% methanol
- 5% glacial acetic acid

## Appendix B: Specificity of Eya1 antibodies

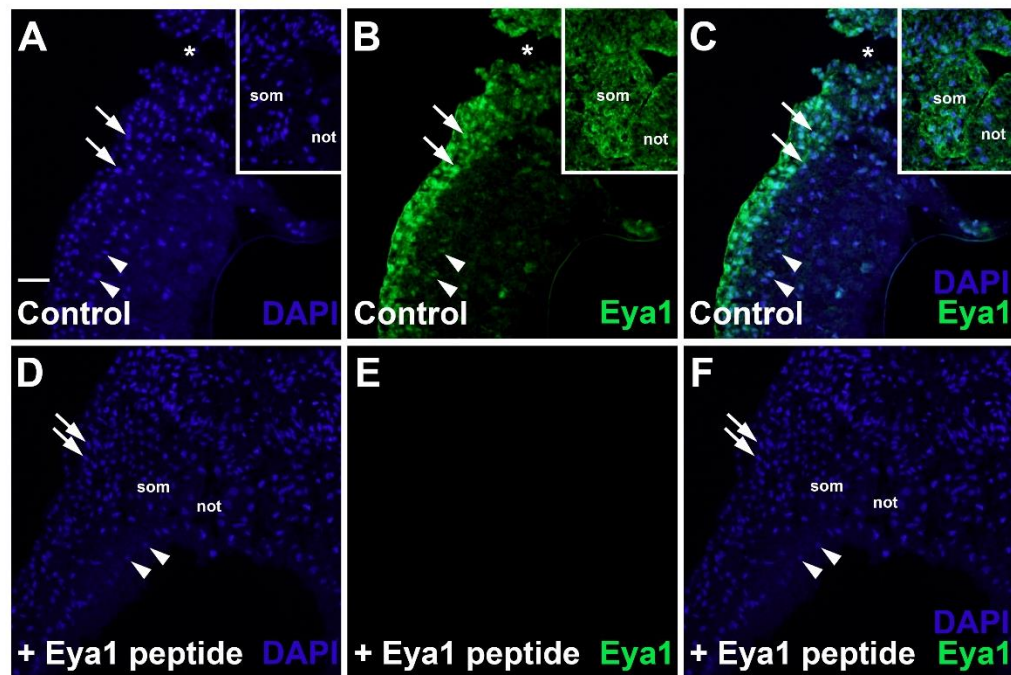


**Fig.B1. Specificity of Eya1 antibodies.** **A-F:** Peptide competition assay for anti-Eya1 GP1 antibody. Transverse sections through the left otic vesicle of a *Xenopus* embryos at stage 20 analyzed in single confocal planes (dorsal to the top, medial to the right). Different channels of same section shown in **A-C** and **D-F**. Arrows indicate nuclear expression in placodes, arrowheads indicate nuclear expression in pharyngeal endoderm. Insets in **A-C** show expression of Eya1 in nuclei and cytoplasm in somites in another section. Eya1 immunostaining as evident in control embryos (**A-C**) is blocked after addition of Eya1 peptide (5  $\mu\text{g}$  peptide/1  $\mu\text{g}$  Eya1 antibody; **D-F**). Not: notochord; som: somite. Scale bar in **A**: 50  $\mu\text{m}$  (for all panels).

## Appendix C: Eya1 distribution in cranial placodes

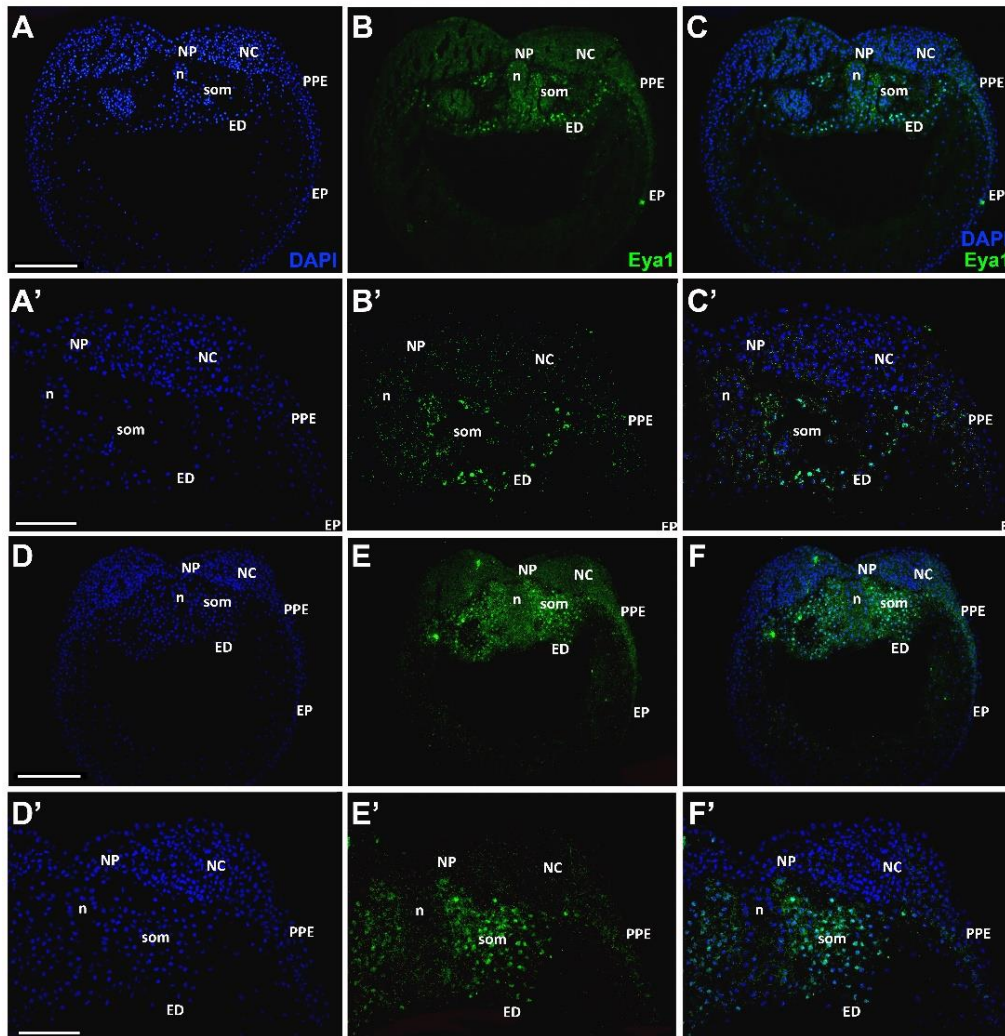


**Fig. C1. Eya1 distribution in transverse sections of *Xenopus laevis* at stage 15.** A-C, D-F: Overview of stage 15 embryo showing Eya1 immunostaining. A'-C', D'-F': Detail of Eya1 distribution in stage 15. Nuclei are stained with DAPI (A, A', D, D'). Eya1 (B, B', E, E': green) localizes to nuclei. C, C', F, F': Merged channels: Eya1 is expressed weakly in preplacodal ectoderm (PPE) in cytoplasm. Also, Eya1 expression is found in nuclei of the endoderm layer (ED), mesoderm layer (MS), somite cells (som) (white arrows) and neural crest (NC). Eya1 expression is undetectable in neural plate (NP), notochord (n) and epidermis layer (EP). Scale bars: A, D: 200  $\mu\text{m}$  (for A-C and D-F); A', D': 100  $\mu\text{m}$  (for A'-C' and D'-F)

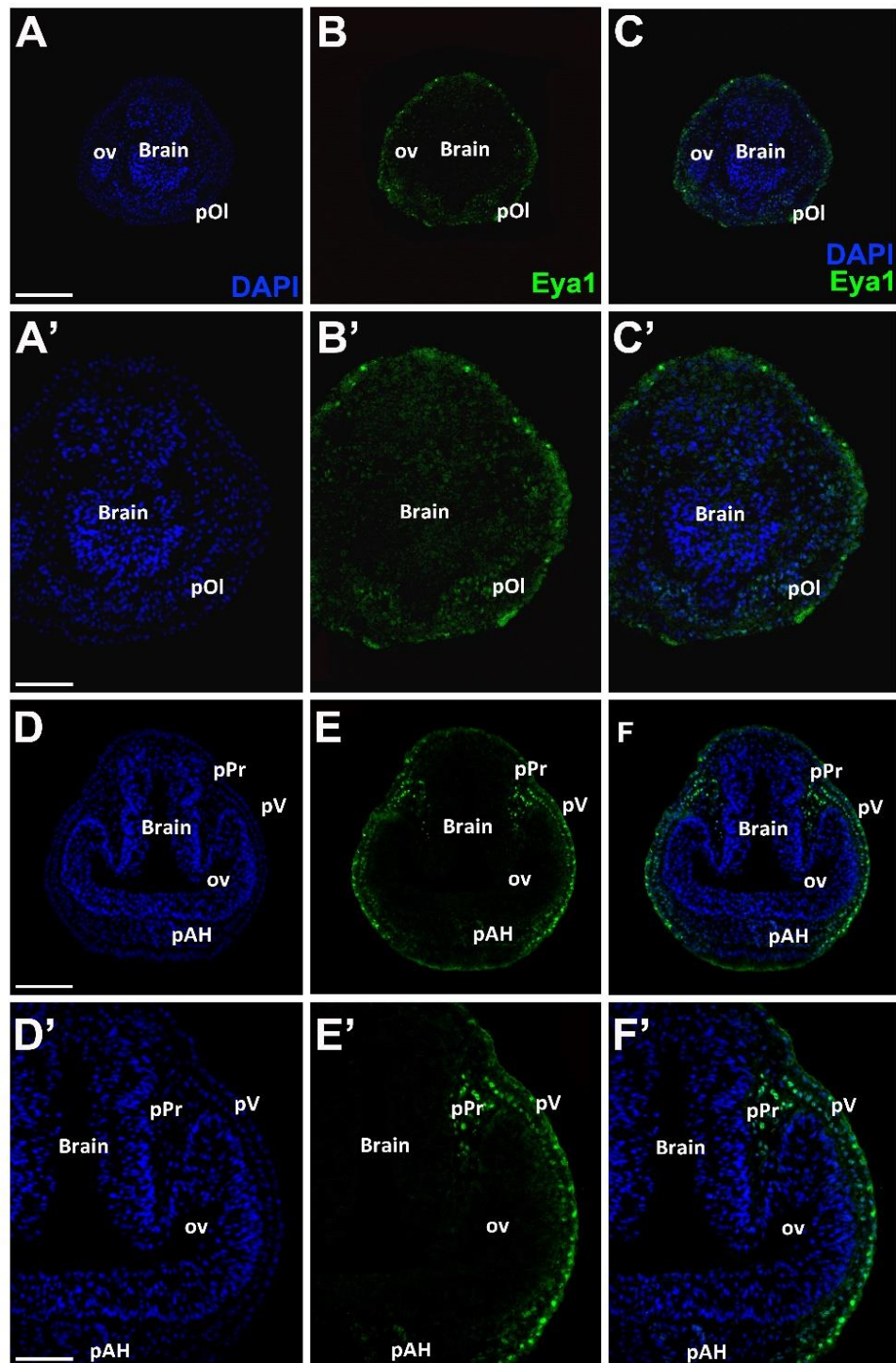


**Fig. C2. Eya1 distribution in transverse sections of *Xenopus laevis* at stage 20.** A-C, D-F: Overview of stage 20 embryo showing Eya1 immunostaining. A'-C', D'-F'': Detail of Eya1 distribution in placodes. Nuclei are stained with DAPI (A, A', D, D', D''). Eya1 (B, B', E, E', E'': green) localizes to nuclei. C, C', F, F', F'': Merged channels: Eya1 is expressed in olfactory placode (pOl), profundal placode (pPr), trigeminal placode (pV) and adenohypophyseal placode (pAH). Eya1 expression is undetectable in brain and optic vesicle (ov). Scale bars: A, D: 200  $\mu$ m (for A-C and D-F); A', D', D'': 100  $\mu$ m (for A'-C', D'-F', and, D''-F'')



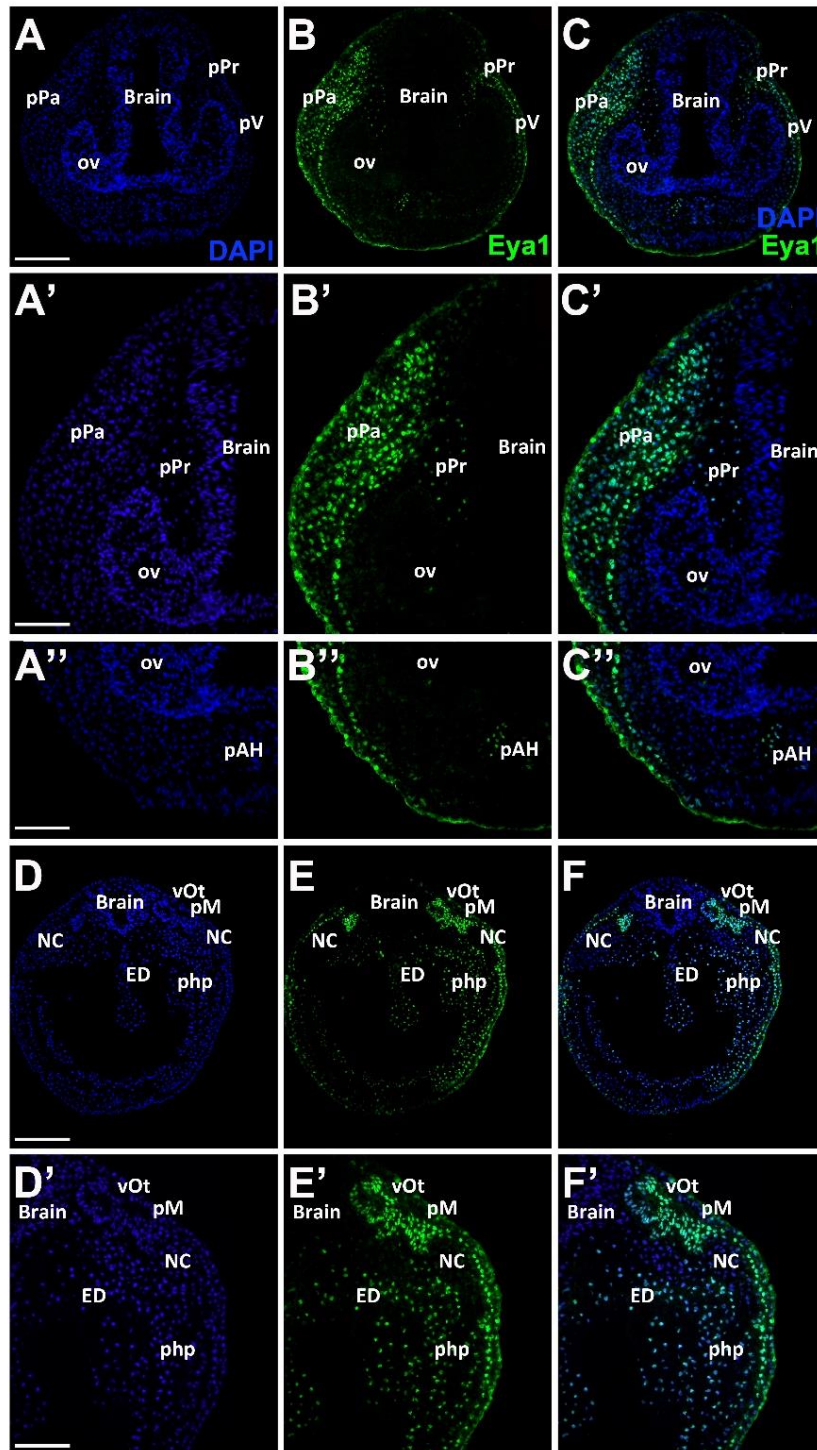


**Fig.C3. Eya1 distribution in transverse sections of *Xenopus laevis* at stage 20.** A-C, D-F: Overview of stage 20 embryo showing Eya1 immunostaining. A'-C'', D'-F': Detail of Eya1 distribution in placodes. Nuclei are stained with DAPI (A, A', A'', D, D'). Eya1 (B, B', B'', E, E': green) localizes to nuclei. C, C', C'', F, F': Merged

channels: Eya1 is expressed in posterior placodal area (pPa), profundal placode (pPr), trigeminal placode (pV), adenohipophyseal placode (pAH), otic vesicle (vOt), middle lateral line (PM) and endoderm (ED) including pharyngeal pouches (php). Eya1 expression is undetectable in brain, neural crest (NC) and optic vesicle (ov). Scale bars: **A, D**: 200  $\mu\text{m}$  (for **A-C** and **D-F**); **A', A'', D'**: 100  $\mu\text{m}$  (for **A'-C'**, **A''-C''** and **D'-F'**).

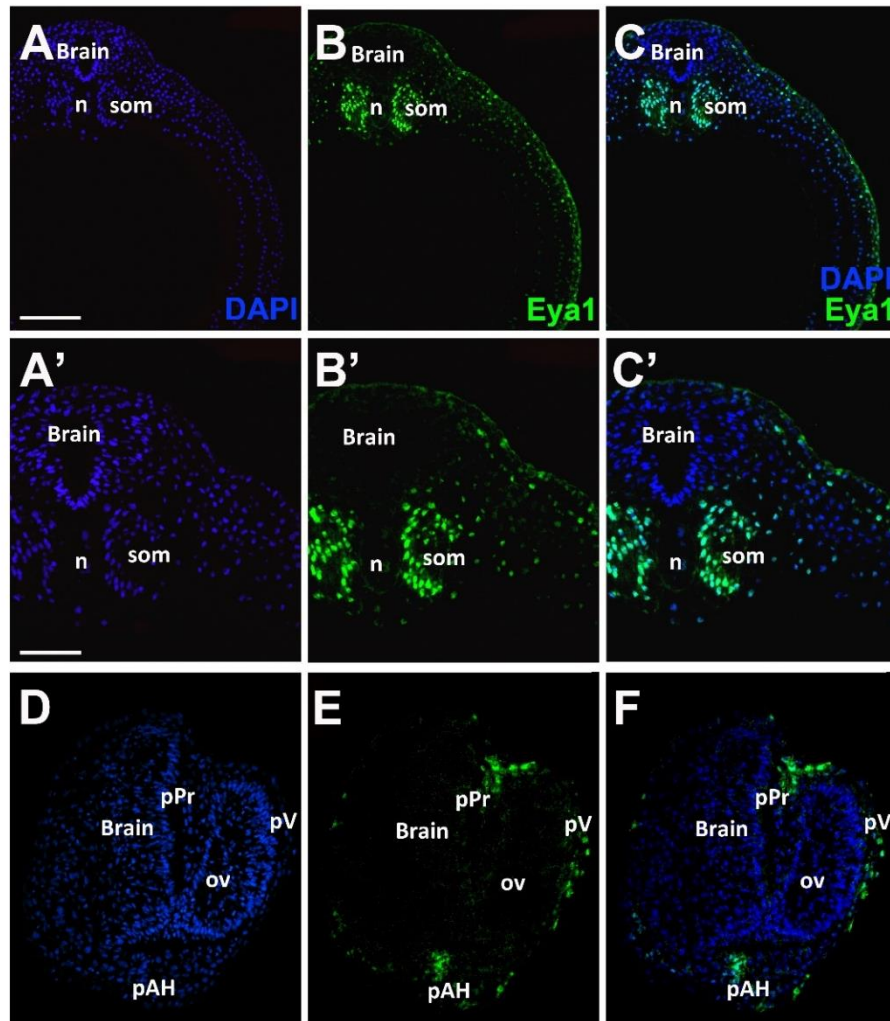


**Fig. C4. Eya1 distribution in transverse sections of *Xenopus laevis* at stages 20 and 23.** **A-C**: Overview of stage 20 embryo showing Eya1 immunostaining. **A'-C'**: Detail of Eya1 distribution in trunk sections. **D-F**: Overview of stage 23 embryo showing Eya1 expression in placodes. Nuclei are stained with DAPI (**A, A', D**). Eya1 (**B, B', E**: green) localizes to nuclei. **C, C', F**: Merged channels: Eya1 is expressed in somite cells (som), profundal placode (pPr), trigeminal placode (pV), adenohipophyseal placode (pAH). Eya1 expression is undetectable in brain, notochord (n) and optic vesicle (ov). Scale bars: **A, D**: 200  $\mu\text{m}$  (for **A-C** and **D-F**); **A'**: 100  $\mu\text{m}$  (for **A'-C'**).

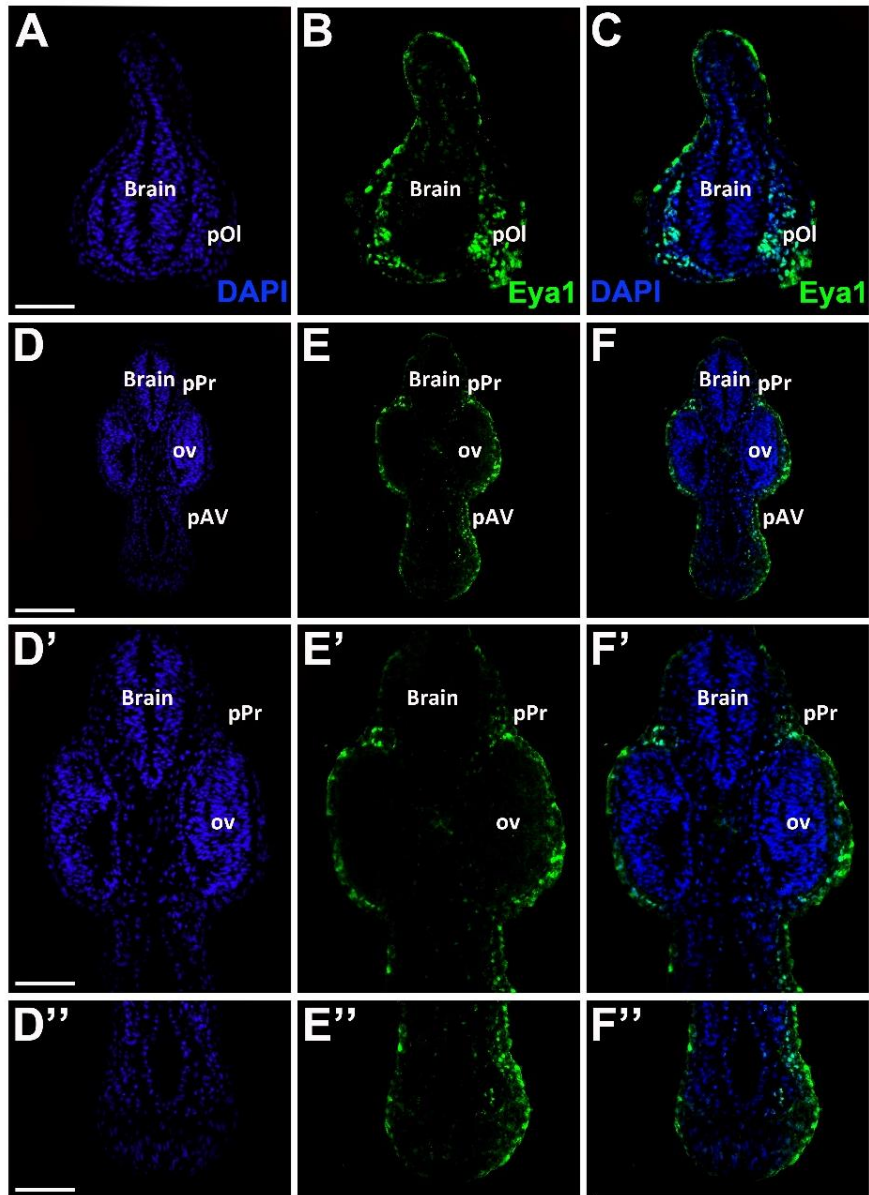


**Fig. C5. Eya1 distribution in transverse sections of *Xenopus laevis* at stage 26.** A-F'': Overview of stage 26 embryo showing Eya1 immunostaining. A'-C: Detail of Eya1 distribution in olfactory placode. Nuclei are stained with DAPI (A, D, D', D''). Eya1 (B, E, E', E'': green) localizes to nuclei. C, F, F', F'': Merged channels: Eya1 is expressed in olfactory placode (pOl), profundal placode (pPr) and anteroventral lateral line placode (pAV). Eya1 expression is undetectable in brain and optic vesicle (ov). Scale bars: A: 100  $\mu$ m (for A-C); D: 200  $\mu$ m (for D-F); D', D'': 100  $\mu$ m (for D-F'').

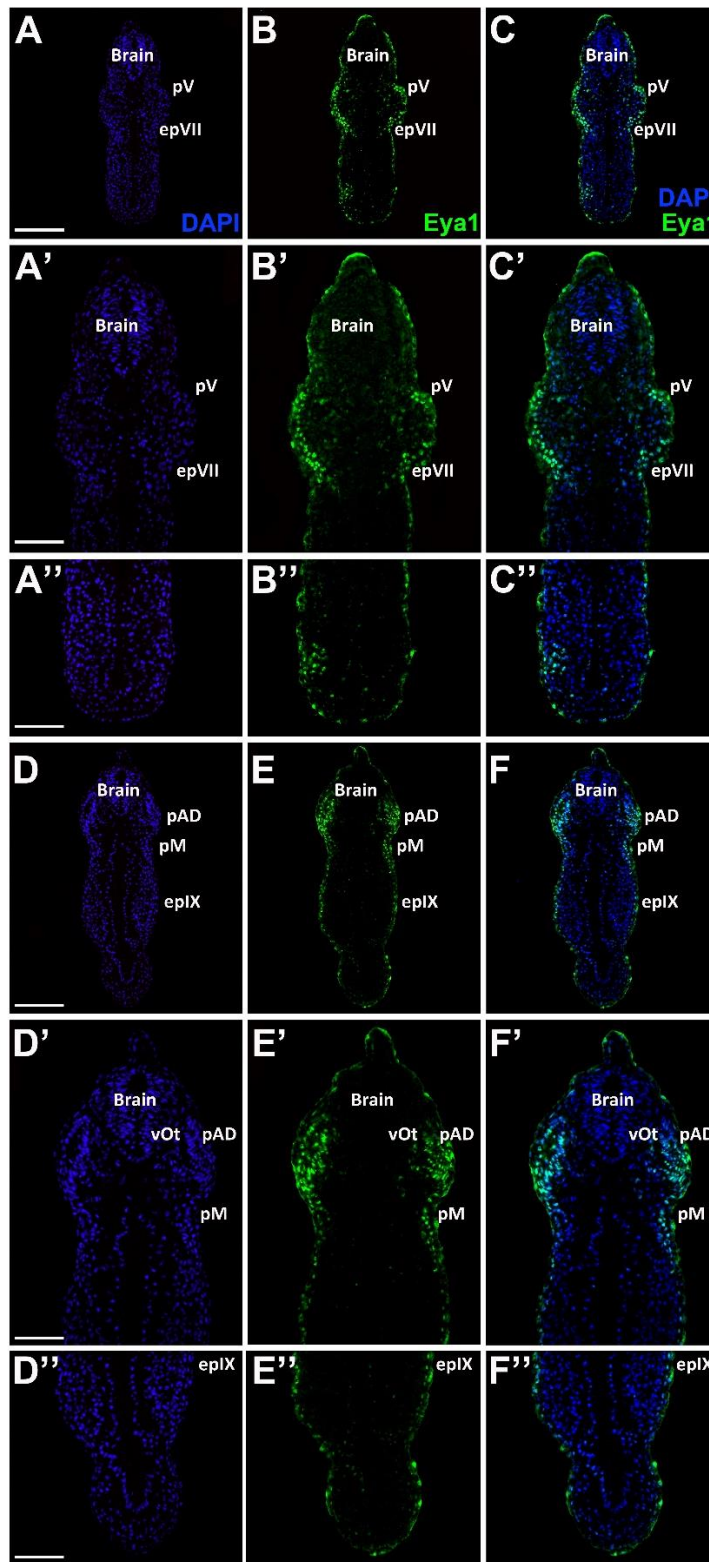


**Fig. C6.** *Eya1* distribution in transverse sections of *Xenopus laevis* at stage 26. A-C: Overview of stage 26 embryo showing *Eya1* immunostaining. A'-C'', D'-F'':

Detail of Eya1 distribution in placodes. Nuclei are stained with DAPI (**A, A', A'', D, D', D''**). Eya1 (**B, B', B'', E, E', E''**): green) localizes to nuclei. **C, C', C'', F, F', F''**: Merged channels: Eya1 is expressed in trigeminal placode (pV), the facial epibranchial placode (epVII), anterodorsal lateral line placode (pAD), middle lateral line placode (pM), otic vesicle (vOt) and a glossopharyngeal placode (epIX). Eya1 expression is undetectable in Brain. Scale bars: **A, D**: 200  $\mu\text{m}$  (for **A-C** and **D-F**); **A', A'', D', D''**: 100  $\mu\text{m}$  (for **A'-C', A''-C'', D'-F'** and **D''-F''**).



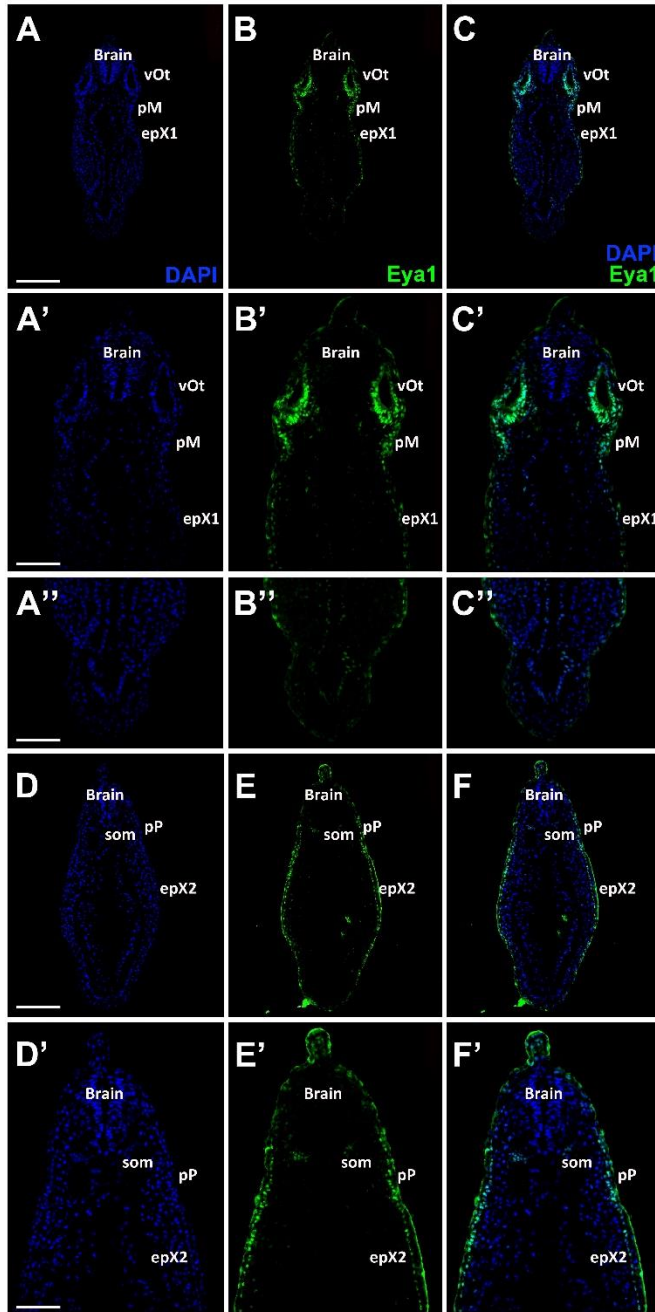


**Fig. C7. Eya1 distribution in transverse sections of *Xenopus laevis* at stage 26.** Overview of stage 26 embryo showing Eya1 immunostaining. **A'-C''**, **D'-F'**: Detail of Eya1 distribution in placodes and in trunk section. Nuclei are stained with DAPI (**A**, **A'**). Eya1 (**B**, **B'**: green) localizes to nuclei. **C**, **C'**: Merged channels: Eya1 is expressed in middle lateral line placode (pM), the first vagal placode (epX1), otic vesicle (vOt), posterior lateral line placode (pP), the second vagal placode (epX2) and somite cells (som). Eya1 expression is undetectable in brain. Scale bars: **A**, **D**: 200  $\mu$ m (for **A-C** and **D-F**); **A'**, **D'**: 100  $\mu$ m (for **A'-C''** and **D'-F'**).

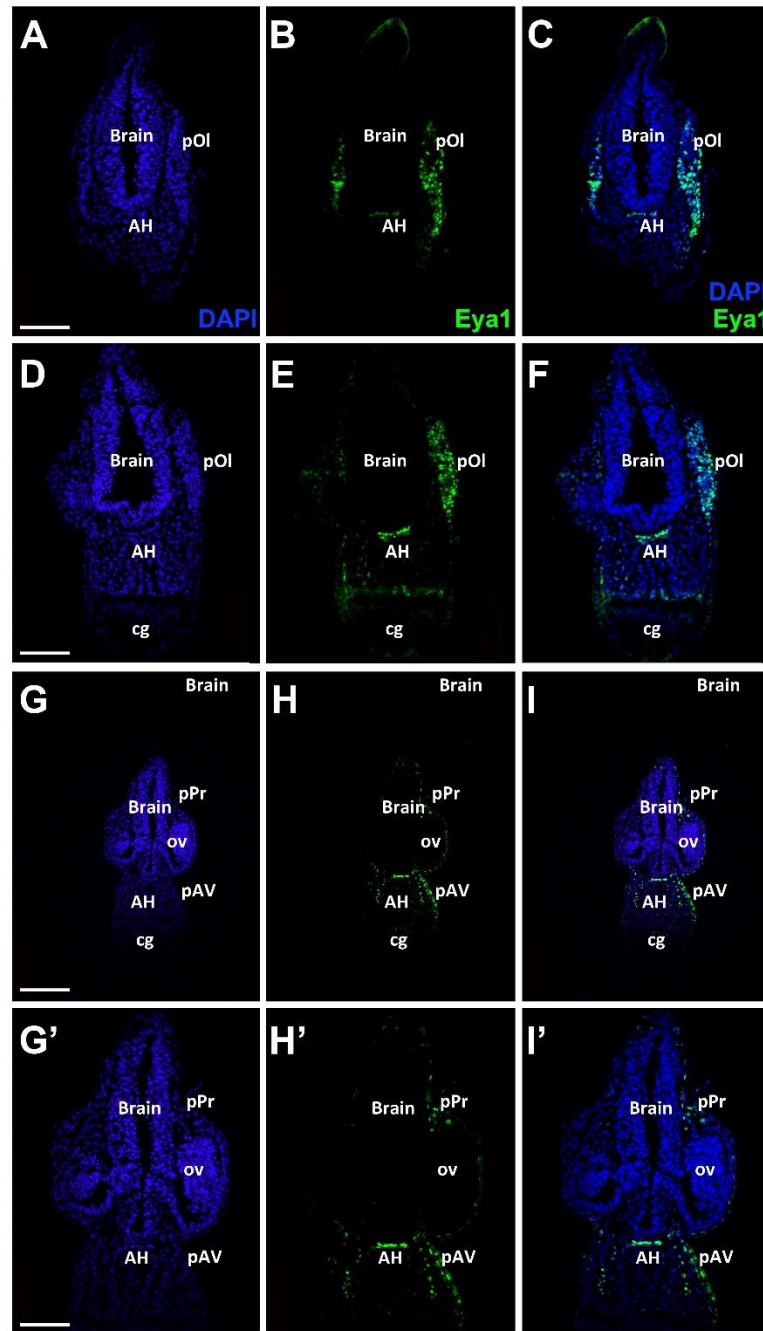


**Fig. C8. Eya1 distribution in transverse sections of *Xenopus laevis* at stage 32.** A-C, G-I: Overview of stage 32 embryo showing Eya1 immunostaining. D-F, G'-I': Detail of Eya1 distribution in placodes. Nuclei are stained with DAPI (A, D, G, G'). Eya1 (B, E, H', H'': green) localizes to nuclei. C, F, I, I': Merged channels: Eya1 is expressed in olfactory placode (pOl), adenohipophysis (AH), profundal placode (pPr) and anteroventral lateral line placode (pAV). Eya1 expression is undetectable in Brain, optic vesicle (ov) and segment gland (cg). Scale bars: A, G: 200  $\mu$ m (for A-C and G-I); D, G: 100  $\mu$ m (for D-F and G-I').

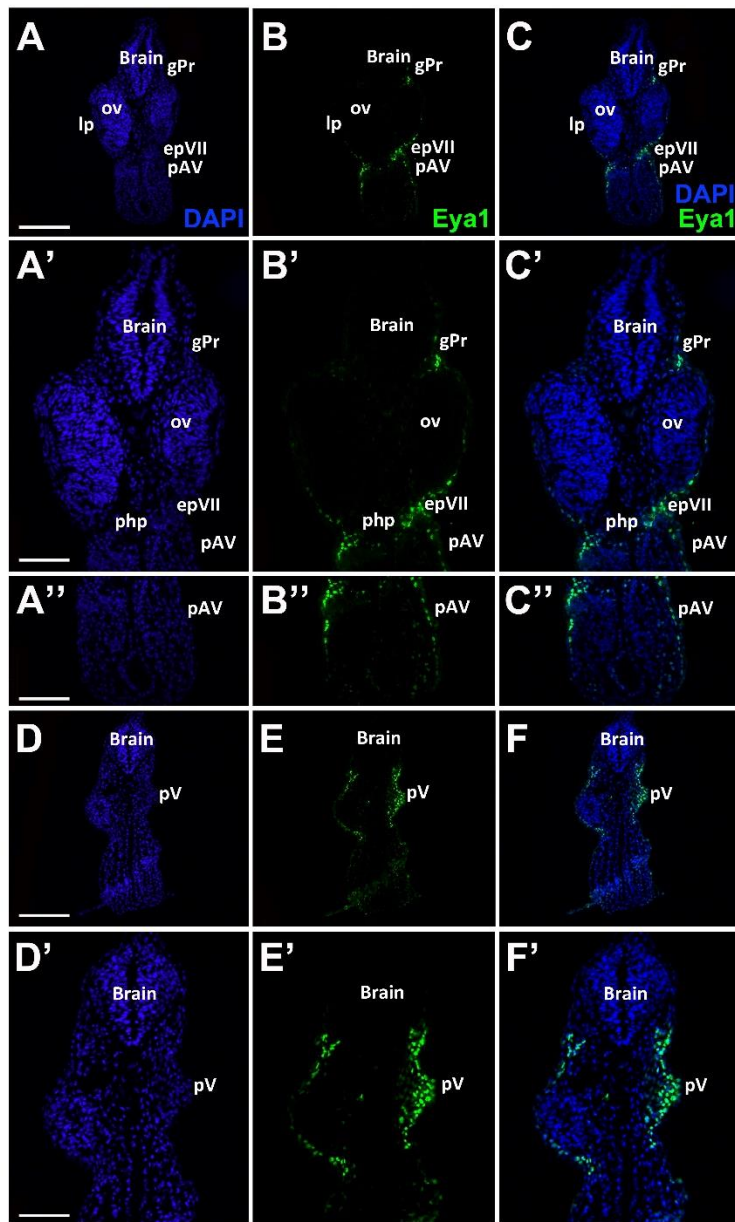


**Fig. C9. Eya1 distribution in transverse sections of *Xenopus laevis* at stage 32.** A-C, D-F: Overview of stage 32 embryo showing Eya1 immunostaining. A'-C'', D'-F': Detail of Eya1 distribution in placodes. Nuclei are stained with DAPI (A, A', A'', D, D'). Eya1 (B, B', B'', E, E': green) localizes to nuclei. C, C', C'', F, F': Merged channels: Eya1 is expressed in anteroventral lateral line placode (pAV), profundal ganglion (gPr), facial epibranchial placode (epVII), adenohipophysis or hypobranchial placode, pharyngeal pouch (php), (AH, php), and trigeminal placode (pV). Eya1 expression is undetectable in Brain, lens placode (lp) and optic vesicle (ov). Scale bars: A, D: 200  $\mu$ m (for A-C and D-F); A', D': 100  $\mu$ m (for A'-C'', D'-F').



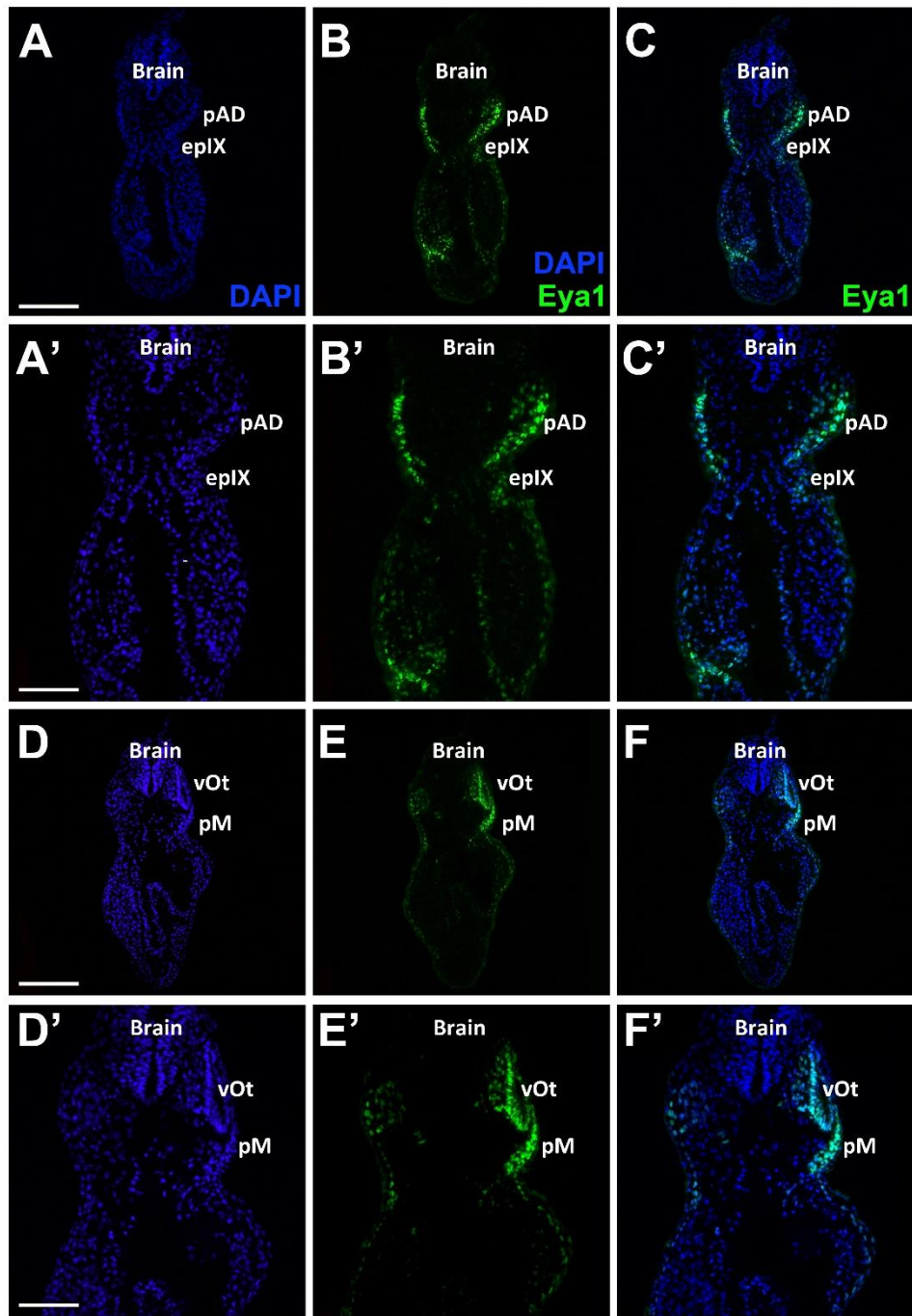


**Fig. C10.** Eya1 distribution in transverse sections of *Xenopus laevis* at stage 32. A-C, D-F: Overview of stage 32 embryo showing Eya1 immunostaining. A'-C', D'-

**F'**: Detail of Eya1 distribution in placodes. Nuclei are stained with DAPI (**A**, **A'**, **D**, **D'**). Eya1 (**B**, **B'**, **E**, **E'**: green) localizes to nuclei. **C**, **C'**, **F**, **F'**: Merged channels: Eya1 is expressed in anterodorsal lateral line placode (pAD), middle lateral line placode (pM), a glossopharyngeal placode (epIX) and otic vesicle (vOt). Eya1 expression is undetectable in brain. Scale bars: **A**, **D**, **G**: 200  $\mu\text{m}$  (for **A-C**, **D-F**); **A'**, **D'**: 100  $\mu\text{m}$  (for **A'-C'**, **D'-F'**).

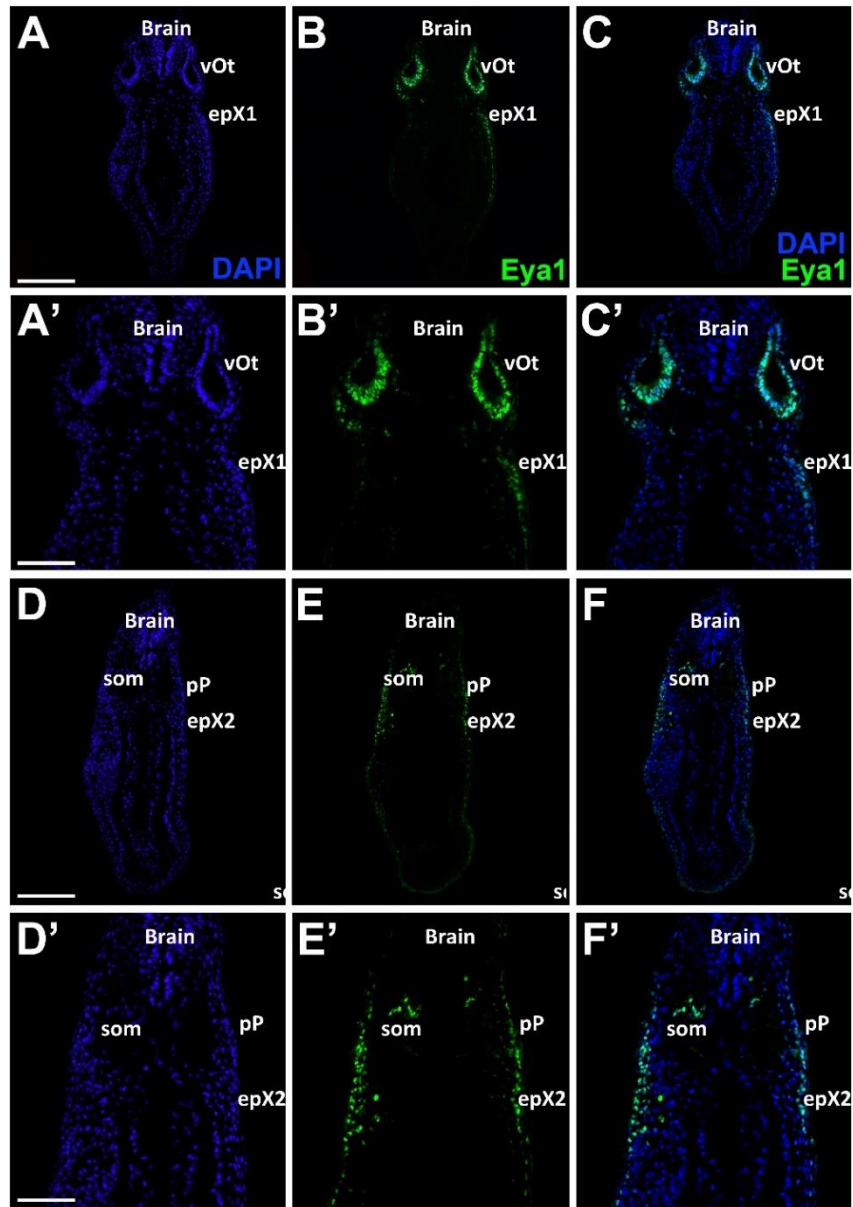


**Fig. C11. Eya1 distribution in transverse sections of *Xenopus laevis* at stage 32.** A-C, D-F: Overview of stage 32 embryo showing Eya1 immunostaining. A'-C', D'-F': Detail of Eya1 distribution in trunk section. Nuclei are stained with DAPI (A, A', D, D'). Eya1 (B, B', E, E': green) localizes to nuclei. C, C', F, F': Merged channels: Eya1 is expressed in the first vagal placode (epX1), otic vesicle (vOt), posterior lateral line placode (pP), the second vagal placode (epX2) and somite cells (som). Eya1 expression is undetectable in brain. Scale bars: A, D: 200  $\mu$ m (for A-C, D-F); A', D': 100  $\mu$ m (for A'-C', D'-F').

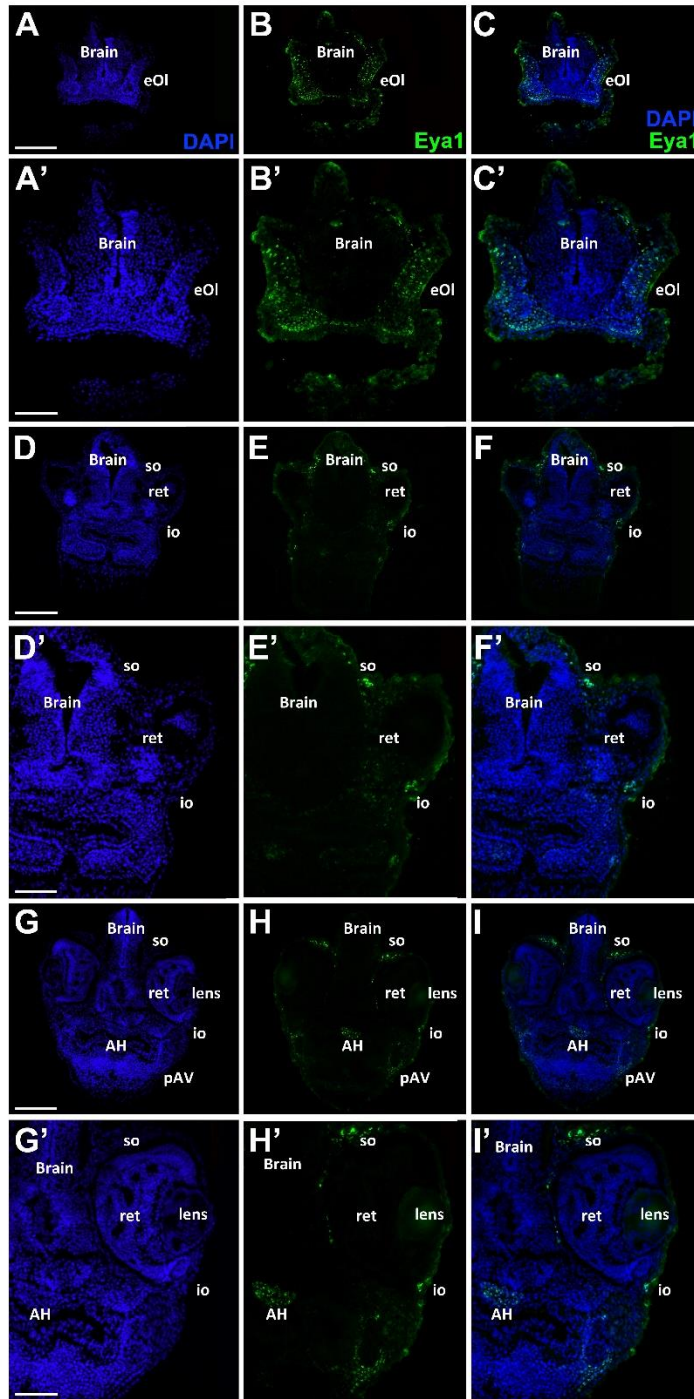


**Fig. C12. Eya1 distribution in transverse sections of *Xenopus laevis* at stage 40.**  
 A-C, D-F, G-I: Overview of stage 40 embryo showing Eya1 immunostaining. A'-

**C', D'-F', G'-I'**: Detail of Eya1 distribution in placodes. Nuclei are stained with DAPI (**A, A', D, D', G, G'**). Eya1 (**B, B', E, E', H, H'**: green) localizes to nuclei. **C, C', F, F', I, I'**: Merged channels: Eya1 is expressed in olfactory epithelium (eOl), adenohypophysis (AH), anteroventral lateral line placode (pAV), sensory ridge of supraorbital lateral line (so) and sensory ridge of infraorbital lateral line (io). Eya1 expression is undetectable in brain, lens and retina. Scale bars: **A, D, G**: 200  $\mu\text{m}$  (for **A-C, D-F** and **G-I**); **A', D', G'**: 100  $\mu\text{m}$  (for **A'-C', D'-F'** and **G'-I'**).

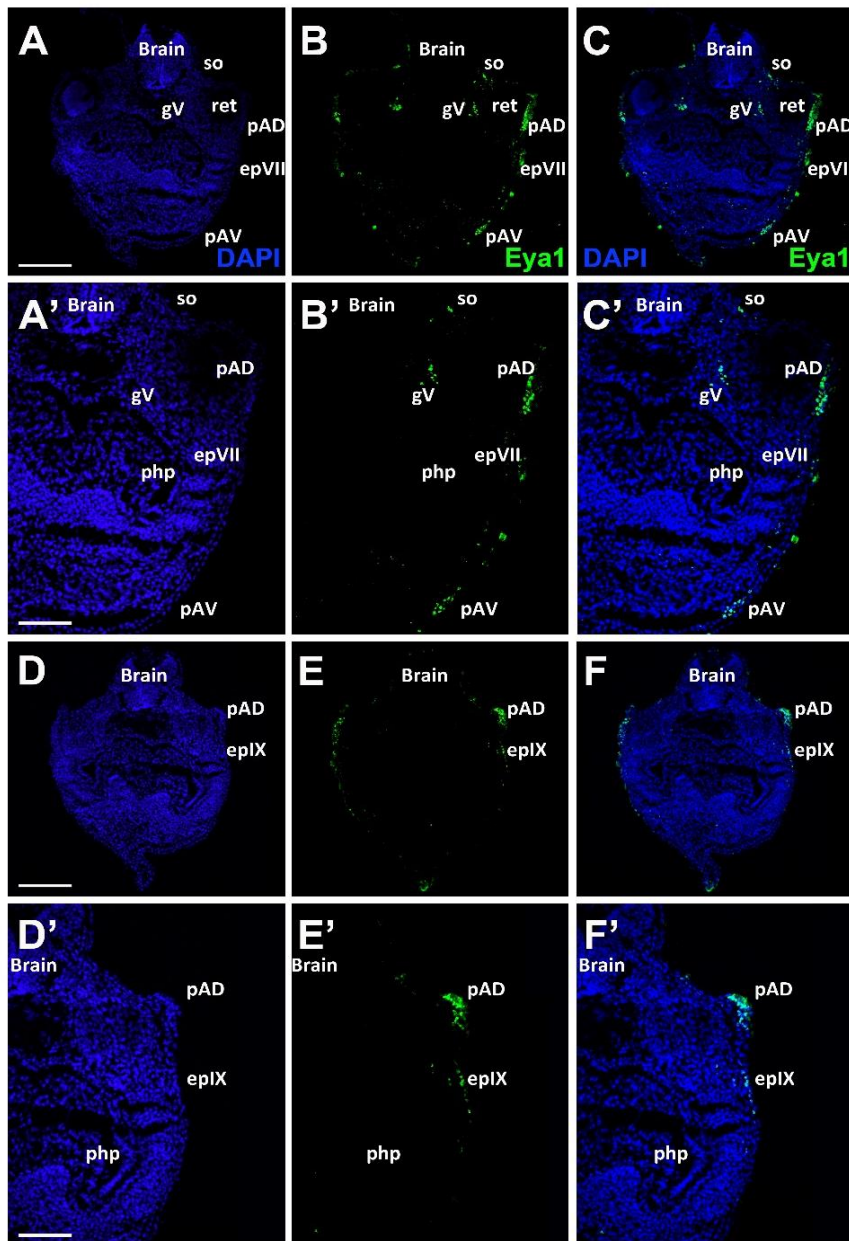


**Fig. C13. Eya1 distribution in transverse sections of *Xenopus laevis* at stage 40.** A-C, D-F: Overview of stage 40 embryo showing Eya1 immunostaining. A'-C', D'-F': Detail of Eya1 distribution in placodes. Nuclei are stained with DAPI (A, A', D, D'). Eya1 (B, B', E, E': green) localizes to nuclei. C, C', F, F': Merged channels: Eya1 is expressed in anterodorsal lateral line placode (pAD), anteroventral lateral line placode (pAV), sensory ridge of supraorbital lateral line (so), trigeminal ganglion (gV), the facial epibranchial placode, pharyngeal pouch (php), (epVII) and a glossopharyngeal placode (epIX). Eya1 expression is undetectable in brain and retina. Scale bars: A, D: 200  $\mu$ m (for A-C and D-F); A', D': 100  $\mu$ m (for A'-C' and D'-F')



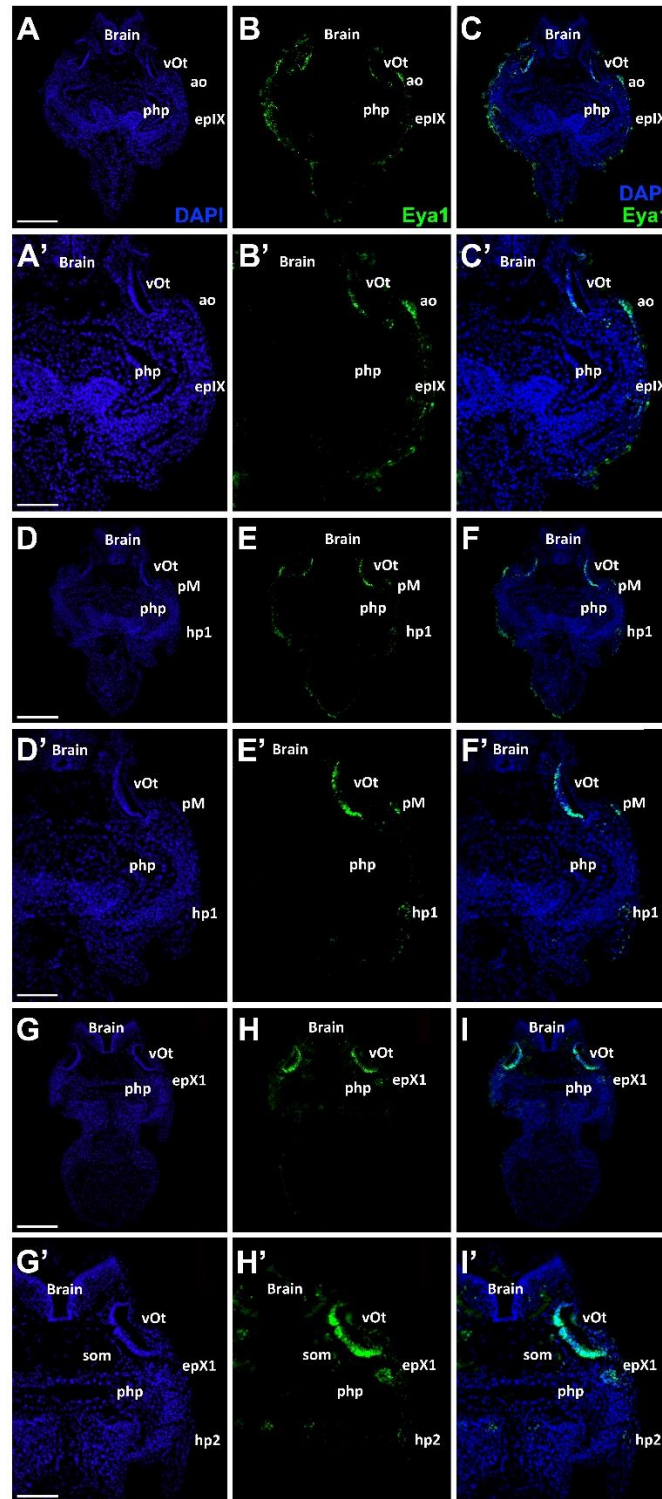


**Fig. C14.** *Eya1* distribution in transverse sections of *Xenopus laevis* at stage 40. **A-C, D-F, G-I:** Overview of stage 40 embryo showing *Eya1* immunostaining.

**A'-C', D'-F', G'-I'**: Detail of Eya1 distribution in placodes. Nuclei are stained with DAPI (**A, A', D, D', G, G'**). Eya1 (**B, B', E, H, H'**: green) localizes to nuclei. **C, C', F, F', I, I'**: Merged channels: Eya1 is expressed in otic vesicle (vOt), middle lateral line placode (pM), the first vagal epibranchial placode (epX1), first hypobranchial placode (hp1), second hypobranchial placode (hp2), pharyngeal pouch (php) and somite cells (som). Eya1 expression is undetectable in brain. Scale bars: **A, D, G**: 200  $\mu\text{m}$  (for **A-C, D-F** and **G-I**); **A', D', D'', G'**: 100  $\mu\text{m}$  (for **A'-C', D'-F'** and **G'-I'**).



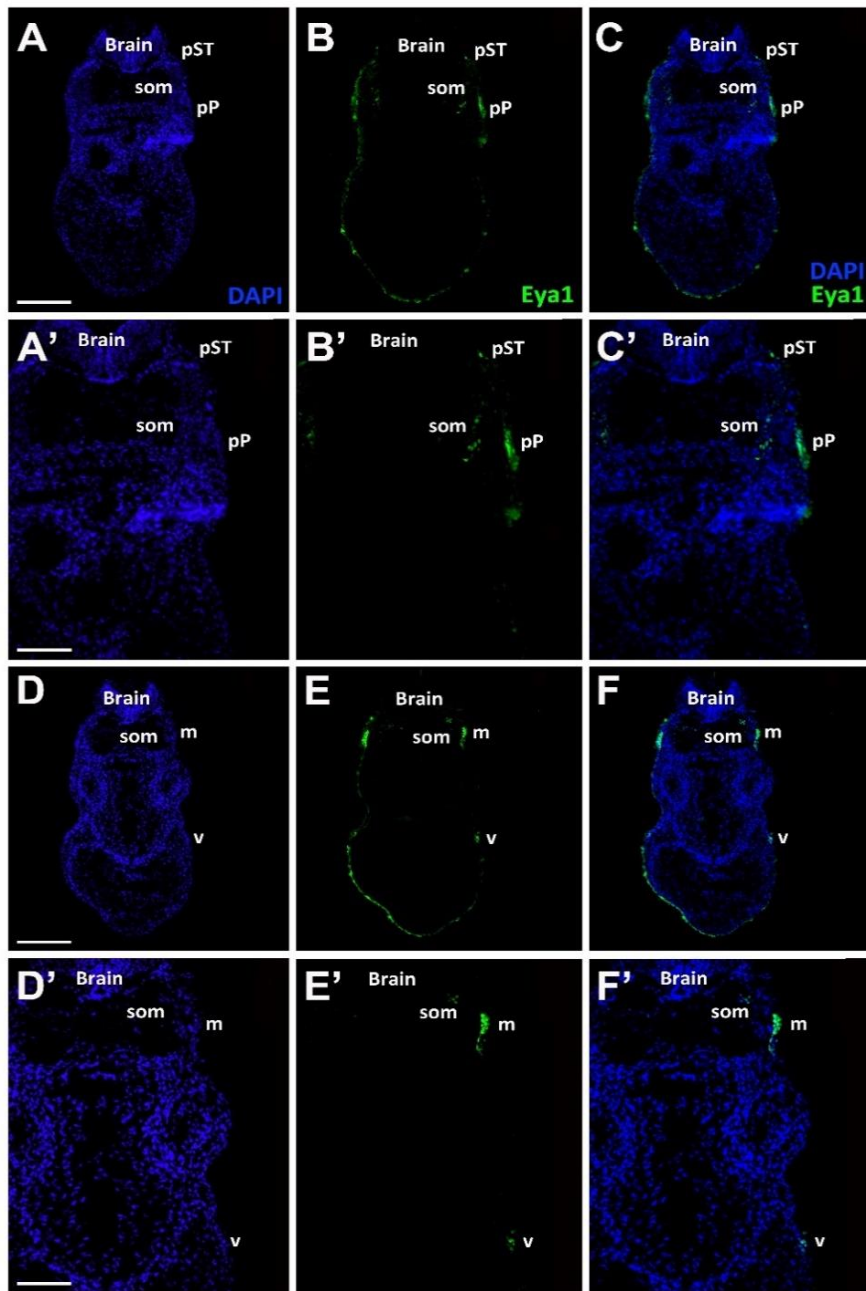


**Fig. C15. Eya1 distribution in transverse sections of *Xenopus laevis* at stage 40.** A-C, D-F: Overview of stage 40 embryo showing Eya1 immunostaining. A'-C', D'-F': Detail of Eya1 distribution in placodes. Nuclei are stained with DAPI (A, A', D, D'). Eya1 (B, B', E, E': green) localizes to nuclei. C, C', F, F': Merged channels: Eya1 is expressed in posterior lateral line placode (pP), supratemporal placode (pST), the middle trunk line (m) and the ventral trunk line (v). Eya1 expression is undetectable in brain. Scale bars: A, D: 200  $\mu$ m (for A-C and D-F); A', D': 100  $\mu$ m (for A'-C' and D'-F).

